EXPLORATIONS OF IRON-IRON HYDROGENASE ACTIVE SITE MODELS BY EXPERIMENT AND THEORY

A Dissertation

by

JESSE WAYNE TYE

Submitted to the Office of Graduate Studies of
Texas A&M University
in partial fulfillment of the requirements for the degree of

DOCTOR OF PHILOSOPHY

May 2006

Major Subject: Chemistry

EXPLORATIONS OF IRON-IRON HYDROGENASE ACTIVE SITE MODELS BY EXPERIMENT AND THEORY

A Dissertation

by

JESSE WAYNE TYE

Submitted to the Office of Graduate Studies of
Texas A&M University
in partial fulfillment of the requirements for the degree of

DOCTOR OF PHILOSOPHY

Approved by:

Co-Chairs of Committee,	Marcetta Y. Darensbourg
	Michael B. Hall
Committee Members,	Timothy R. Hughbanks
	Jerry W. Tsai
Head of Department,	Emile A. Schweikert

May 2006

Major Subject: Chemistry

ABSTRACT

Explorations of Iron-Iron Hydrogenase Active Site Models
by Experiment and Theory. (May 2006)
Jesse Wayne Tye, B.S., University of Kentucky
Co-chairs of Advisory Committee: Dr. Marcetta Y. Darensbourg
Dr. Michael B. Hall

This dissertation describes computational and experimental studies of synthetic complexes that model the active site of the iron-iron hydrogenase [FeFe]H_2ase enzyme.

Simple dinuclear iron dithiolate complexes act as functional models of the iron-iron hydrogenase enzyme by catalyzing isotopic exchange in D_2/H_2O mixtures. Density Functional Theory (DFT) calculations and new experiments have been performed that suggest reasonable mechanistic explanations for this reactivity. Evidence for the existence of an acetone derivative of the di-iron complex, as suggested by theory, is presented.

Bis-phosphine substituted dinuclear iron dithiolate complexes react with the electrophilic species, H^+ and Et^+ ($Et^+ = CH_3CH_2^+$) with differing regioselectivity; H^+ reacts to form a 3c-2e$^-$ Fe-H-Fe bond, while Et^+ reacts to form a new C-S bond. The instability of a bridging ethyl complex is attributed to the inability of the ethyl group, in contrast to a hydride, to form a stable 3c-2e$^-$ bond with the two iron centers.

Gas-phase density functional theory calculations are used to predict the solution-phase infrared spectra for a series of CO and CN-containing dinuclear iron complexes dithiolate. It is shown that simple linear scaling of the computed C-O and C-N stretching

frequencies yields accurate predictions of the experimentally determined ν(CO) and ν(CN) values.

An N-heterocyclic carbene containing [FeFe]H_2ase model complex, whose X-ray structure displays an apical carbene, is shown to undergo an unexpected simultaneous two-electron reduction. DFT shows, in addition to a one-electron Fe-Fe reduction, that the aryl-substituted N-heterocyclic carbene can accept a second electron more readily than the Fe-Fe manifold. The juxtaposition of these two one-electron reductions resembles the [FeFe]H_2ase active site with an FeFe di-iron unit joined to the electroactive 4Fe4S cluster.

Simple synthetic di-iron dithiolate complexes synthesized to date fail to reproduce the precise orientation of the diatomic ligands about the iron centers that is observed in the molecular structure of the reduced form of the enzyme active site. Herein, DFT computations are used for the rational design of synthetic complexes as accurate structural models of the reduced form of the enzyme active site.

DEDICATION

This dissertation is dedicated to my great aunt Estile Williams and

to the memory of my beloved grandmother Eva Harp.

ACKNOWLEDGMENTS

First of all, I thank my graduate research advisors, Dr. Marcetta Y. Darensbourg and Dr. Michael B. Hall, for providing me with this unique opportunity to study at the interface of theoretical and synthetic organometallic chemistry. I thank them for their extraordinary support in my search for a postdoctoral position. Finally, I thank them for encouraging and supporting my trip to the International Hydrogenase Conference in Reading, England.

I thank Dr. Timothy R. Hughbanks and Dr. Jerry W. Tsai for serving on my dissertation committee and Dr. Paul A. Lindahl for being on my literature seminar committee.

I thank my undergraduate research advisor at the University of Kentucky, Dr. Stephen M. Testa, for his amazing support. I thank Dr. Carolyn P. Brock and Dr. Folami T. Ladipo (University of Kentucky) for being excellent mentors and advocates for me.

I thank Jonghyuk Lee and Hsiao-Wan Wang for performing electrochemistry and Rosario Mejia-Rodriguez for synthesizing and characterizing the IMes complex.

I thank Bruce Neide, Dino Villagrán, Yubo Fan, Steve Jeffery, Daesung Chong and Sergey Ibragimov for being great personal friends during my time here.

I thank my wife, Melanie, for her unconditional love and endless support.

TABLE OF CONTENTS

CHAPTER Page

CHAPTER Page

LIST OF TABLES

LIST OF FIGURES

FIGURE Page

FIGURE Page

FIGURE Page

CHAPTER I

INTRODUCTION

This chapter provides a very broad overview and general review of the activation of dihydrogen by homogeneous catalysts and the hydrogenase enzymes. Each individual chapter will review the specific background on the iron-iron hydrogenase enzyme that is relevant for understanding that chapter.

Motivations for Studying H_2 Activation

Why activate H_2?

Dihydrogen has the potential to act as a "clean" alternative to fossil fuels.[1] The oxidation of dihydrogen, either electrochemically or via combustion, leads only to the production of water. One of the major drawbacks of solar, hydroelectric, and wind power is that periods of peak energy production do not necessarily coincide with periods of peak energy consumption. Solar, hydroelectric, and wind power, however, could be used to electrochemically generate H_2 that can be stored and later burned to produce thermal power or converted back to H^+ and e^- to produce electrical power.[2]

In many industrially important reactions, such as hydroformylation and hydrogenation, dihydrogen gas serves as reducing agent and/or hydrogen atom source. Even small improvements in the efficiency of these reactions translate into large monetary savings.

This dissertation follows the style and format of *Inorganic Chemistry*.

This review will focus on the homogeneous catalysis of H-H bond cleavage and formation by discrete transition metal complexes and enzymes. These topics have been the subject of a number of excellent reviews.[3-21] This review will not discuss in detail the electrochemical H^+ reduction or H_2 oxidation,[22-24] or the heterogeneous activation of H_2 by extended systems.[25-29]

Why is it so difficult to activate H_2?

The H_2 molecule is, in fact, so stable that it was used as an "inert" gas in early air-free chemistry. The following physical properties of H_2 combine to make it a very unreactive molecule: (1) The H-H bond is remarkably strong. (2) The H_2 molecule is completely non-polar. (3) The frontier molecular orbitals of H_2 do not permit most direct, concerted reactions between dihydrogen and other non-metals. (4) The H_2 molecule is a very poor acid.

The amount of energy required for homolytic cleavage of the H-H bond ($H_2 \rightarrow 2H^{\bullet}$) is +103.25(1) kcal/mol.[30] As shown in Table I-1, this value places the H-H bond

Table I-1. Bond Dissociation Energies for H-X Bonds

bond type	**average BDE**[a]
H–F	135(1)[b]
H–O	109.60(4)
H–H	103.25(1)
H–Cl	102.3(1)
H–C	98.3(8)
H–N	92(2)

[a] in kcal mol^{-1}. [b] Error in last digit is given parenthetically.

among the strongest single bonds.[31] Since most new H-X bonds will generally be weaker than the H-H bond, there is often little or no thermodynamic driving force for the cleavage of the H-H bond.

The polarity of the reacting molecules often enhances the rates of chemical reactions. Scheme I-1 contrasts the proton transfer reaction between the very polar

Scheme I-1

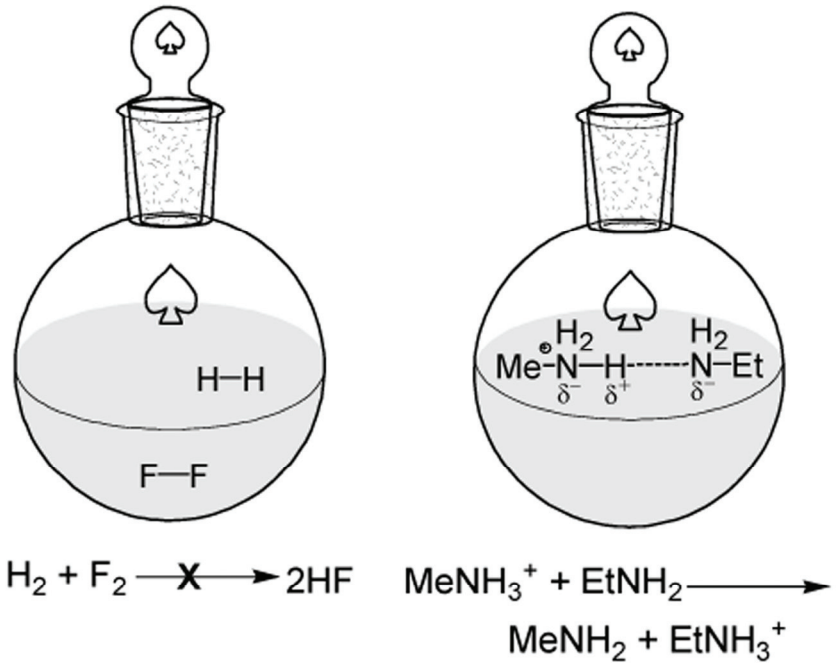

reactants $MeNH_3^+$ and $EtNH_2$ and the reaction between non-polar reactants H_2 and F_2 to produce HF. For the reaction between $MeNH_3^+$ and $EtNH_2$, the partially positively charged ammonium hydrogen atoms of $MeNH_3^+$ are attracted to the negatively charged nitrogen center of $EtNH_2$. The polarity of the reactants therefore helps to organize them

spatially for effective proton transfer between $MeNH_3^+$ and $EtNH_2$. No such strong intermolecular forces exist for the reaction between H_2 and F_2. Since the H_2 molecule is completely non-polar, it a poor target for attack by either electrophiles or nucleophiles, resulting in large activation energies for H_2 activation. Even when direct reaction with H_2 is thermodynamically feasible, the rates of reactions with H_2 are often extremely slow.

The analysis of the frontier molecular orbitals of dihydrogen also suggests that direct, concerted reactions between H_2 and most non-metals should have high activation energies. In frontier molecular orbital theory, a high activation energy is predicted when the symmetry of the HOMO of one reactant does not match the symmetry of the LUMO of the second reactant and vice versa. An illustrative example is the concerted addition of dihydrogen to ethylene to yield ethane ($C_2H_4 + H_2 \rightarrow C_2H_6$). Although the hydrogenation of ethylene is a thermodynamically favorable process ($\Delta H_{298} \approx -32$ kcal mol^{-1}),[32] mixtures of the two gases are stable indefinitely in the absence of an appropriate catalyst. The implied high activation energy for the reaction $C_2H_4 + H_2 \rightarrow C_2H_6$ may be explained in the context of frontier molecular orbital theory.[33] The frontier molecular orbitals of H_2 are the H-H bonding HOMO and H-H antibonding LUMO and the frontier molecular orbitals of ethylene are the C-C π bonding HOMO and C-C π antibonding LUMO. As shown in Figure I-1, the frontier molecular orbitals of H_2 and ethylene are inappropriate for a direct concerted reaction between these species to yield ethane. In the reaction of ethylene with dihydrogen, the HOMO of ethylene is not a match for the LUMO of dihydrogen (likewise, the HOMO of H_2 does not match the

LUMO of ethylene.) The direct reaction of H_2 with C_2H_4 is therefore expected to have a large activation barrier.

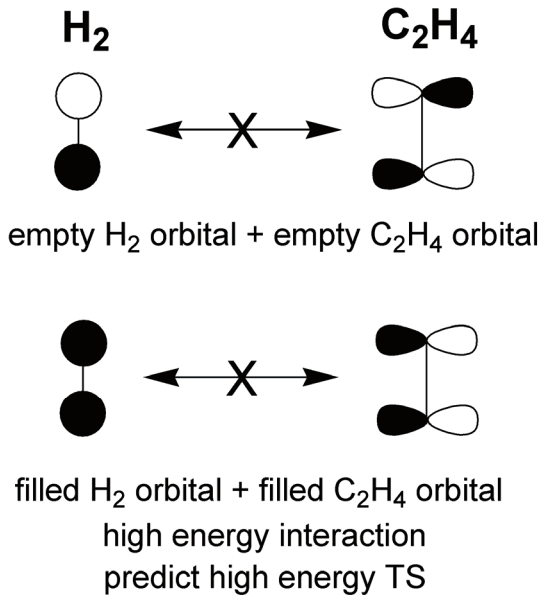

Figure I-1. The shapes of the frontier molecular orbitals of H_2 and C_2H_4 are inappropriate for a direct, concerted reaction. The interactions between the LUMO's of H_2 and C_2H_4 have no effect on the energy since they are interactions between empty orbitals. The interaction between the filled HOMO's of H_2 and C_2H_4 is inherently destabilizing, since the interaction is between two filled orbitals.

The uncatalyzed heterolytic cleavage of the H-H bond ($H_2 \rightarrow H^+ + H^-$) is also difficult. The strength of the H-H bond and its lack of polarity contribute to the poor kinetic and thermodynamic acidity of H_2. The pK_a values for a series of mono-protic "acids",

dissolved in either tetrahydrofuran or acetonitrile solvent, are given in Table I-2. Dihydrogen with an estimated pK_a of 49 in tetrahydrofuran solvent is among the weakest acids.

Table I-2. Proton Dissociation Constants for Several Compounds in Organic Solvents

acid	pKa	solvent	reference
H**H**	49	THF	34
Ph_3C**H**	44	THF	34
cyclohexane-O**H**	38	THF	34
Ph_2P**H**	35	THF	34
CH_3COO**H**	22.3	CH_3CN	35
$CH_3(C_6H_4)SO_3$**H**	8.0	CH_3CN	36
CF_3SO_3**H**	2.6	CH_3CN	36

Structure and Bonding of Metal-Bound Hydrogen Atoms

Why can metal centers react directly with H_2, while most non-metals cannot?

Metal centers have low energy d orbitals. The nodal character and energy of the d orbitals may permit a given transition metal center to react directly with H_2 in a concerted reaction with a low activation barrier. As shown in Figure I-2, for the reaction between H_2 and a d^6 ML_5 center, the symmetry of the LUMO of the metal complex matches the symmetry of the HOMO of H_2, and a filled orbital of the metal center matches the symmetry of the LUMO of H_2. In the transition state for H_2 binding to the metal center, there is a synergistic flow of electron density from H_2 to the metal center and from the metal center to the H_2 ligand. A low energy transition state is therefore

expected for addition of H_2 to the ML_5 fragment. (Contrast the reaction of ML_5, given in Figure I-2, with that of H_2 and C_2H_4 given in Figure I-1.

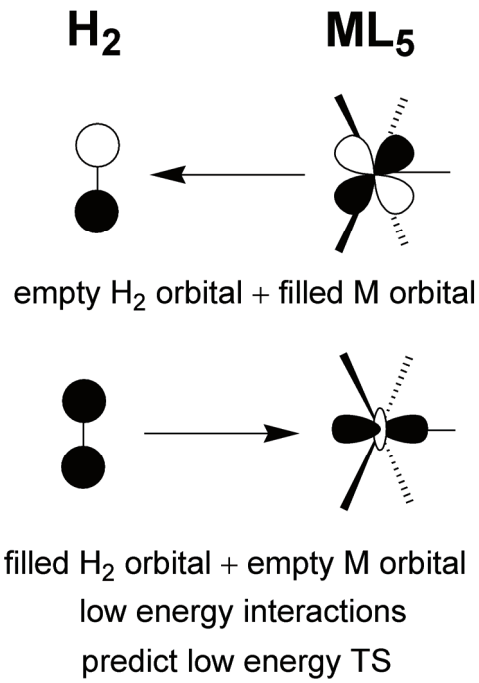

Figure I-2. The shapes of the frontier molecular orbitals of H_2 and ML_5 (left) are appropriate for a direct, concerted reaction. In the transition state for M-(η^2-H_2) bond formation, there is a synergistic flow of electron density from the HOMO of H_2 into the LUMO of ML_5, and from an occupied orbital of ML_5 to the LUMO of H_2.

The bonding of dihydrogen to a transition metal center may be qualitatively described using the Dewar-Chatt-Duncanson (DCD) bonding model.[37] (The qualitative ideas of the DCD bonding model are supported by *ab initio* quantum chemical

calculations.[38-42]) The DCD model partitions metal-H_2 bonding into two parts: $H_2(\sigma)\rightarrow M$ donation and $M\rightarrow H_2(\sigma^*)$ back-donation. Dihydrogen to metal donation ($H_2(\sigma)\rightarrow M$) consists of the transfer of electron density from the H-H bonding orbital to an empty orbital on the transition metal center. Metal to dihydrogen back-donation ($M\rightarrow H_2(\sigma^*)$) consists of the transfer of electron density from a filled orbital on the metal center to the H-H antibonding orbital of dihydrogen. It is noteworthy that both $H_2\rightarrow M$ donations and $M\rightarrow H_2$ back-donation weaken the H-H bond.

Seminal work: the discovery of metal-bound H_2 complexes

Since the H_2 molecule has a very strong H-H bond and possesses no nonbonding electrons or "lone pairs", it was generally believed that an intact dihydrogen molecule could not act as a ligand to a transition metal center. In the early 1980's, however, Kubas and coworkers reported evidence for the existence of a transition metal complex containing side-on bound H_2 as a ligand to a tungsten center.[43] They showed that the reaction of the coordinatively unsaturated tungsten complex $(PPr^i_3)_2W(CO)_3$ with H_2 gas resulted in the formation of a complex of the form, $(\eta^2\text{-}H_2)(PPr^i_3)_2W(CO)_3$ (η^2 reflects the fact that both hydrogen atoms of H_2 are bound to the W center) (Scheme I-2).

Scheme I-2

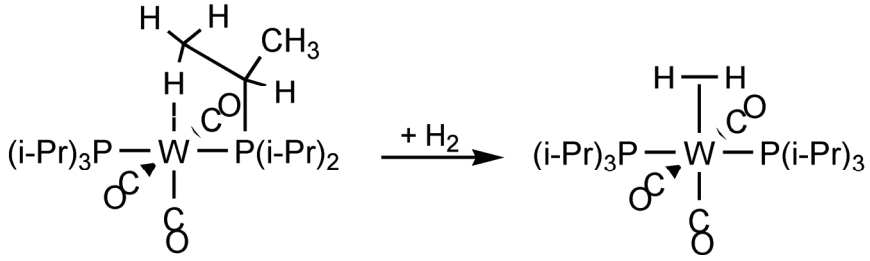

The molecular structure of $(\eta^2\text{-}H_2)(PPr^i_3)_2W(CO)_3$ as determined by single crystal neutron diffraction studies shows that the binding of H_2 to the tungsten has led to an increase in the H-H distance from 0.74 Å (free H_2) to 0.84 Å. The observed H-H distance suggests that coordination to the tungsten center has weakened the H-H bond. The metal-ligand distances and ligand-metal-ligand angles of the 6-coordinate $(\eta^2\text{-}H_2)(PPr^i_3)_2W(CO)_3$ complex are similar to those observed in the molecular structure of the 5-coordinate $(PPr^i_3)_2W(CO)_3$ derived from x-ray diffraction. The similarity between these two structures suggest that the complex is more accurately described as a six-coordinate tungsten(0) $\eta^2\text{-}H_2$ complex, and not a 7-coordinate tungsten(II) bis-hydride complex.

Scheme I-3

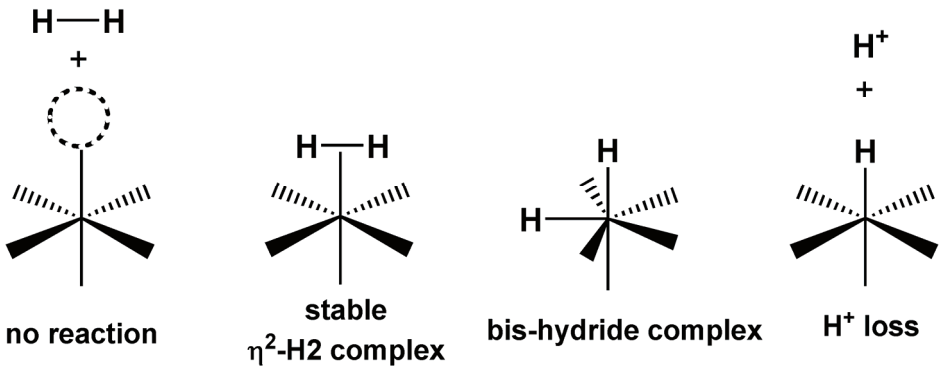

What are the possible consequences when H_2 approaches a coordinatively unsaturated transition metal center?

When a molecule of H_2 approaches a coordinatively unsaturated transition metal center, there are at least four possible outcomes (Scheme I-3): (1) There is no reaction whatsoever. (2) An essentially intact H_2 molecule is bound to the transition metal center. (3) The H-H bond is homolytically cleaved, resulting in a bis-hydride complex. (4) The H-H bond is heterolytically cleaved, resulting in the formation of a metal hydride with loss of H^+. Note: throughout this chapter, (η^2-H_2) indicates a dihydrogen ligand, $(H)_n$, (n = 1,2, ...) denotes n classical hydride ligands, and H_x (x = 1,2, ...) indicates an unspecified structural form.

There is often no reaction whatsoever between a coordinatively unsaturated metal complex and H_2. The first step in the activation of dihydrogen is the formation of a transition state, intermediate, or product structure in which an essentially intact H_2 molecule is bound side-on to the metal center.[44] In order for H_2 to bind to a coordinatively unsaturated metal complex, it must displace any intermolecular and/or intramolecular interactions that are stabilizing the "vacant" site. The formation of an η^2-H_2 complex, even transiently, is often a difficult task since intact H_2 is generally the most weakly binding ligand for a given complex.[45]

Once dihydrogen is bound to the metal center, the steric and electronic properties of the metal center and ligand set determine whether the complex will exist as a stable η^2-H_2 complex, or whether homolytic or heterolytic cleavage of the H-H bond will

result. Homolytic cleavage of the H-H bond to generate the corresponding bis hydride complex is favored for electron-rich metal centers and for ligands with a minimum of steric bulk. Heterolytic cleavage of the H-H bond to generate the corresponding hydride complex and release H^+ is favored for electron-poor metal centers.

The reactivity of dihydrogen can be explained qualitatively by the DCD bonding model. This model partitions metal-H_2 bonding into two parts: $H_2(\sigma)\rightarrow M$ donation and $M\rightarrow H_2(\sigma^*)$ back-donation. When attached to an electron-poor metal center, $H_2(\sigma)\rightarrow M$ donation dominates, leading to a weakening of the H-H bond and the depletion of electron density on the hydrogen atoms. Therefore, the bonding of dihydrogen to an electron-poor metal center increases its acidity relative to free H_2. When attached to an electron-rich metal center, $M\rightarrow H_2(\sigma^*)$ back-donation dominates, leading to a weakening of the H-H bond and the build-up of electron density on the hydrogen atoms.

Hall and coworkers have utilized *ab initio* electronic structure calculations to examine the factors that determine the structures of hydride and η^2-H_2 complexes.[46-49] For 114 polyhydride species, Hall and Bayse found that the most stable structure maximizes use of the n d and (n+1) s orbitals on the metal in the formation of the M-H bonds.[49] Hall and Lin examined factors which lead to oxidative addition to form a bis-hydride or association of an intact molecule of H_2 to form the corresponding η^2-H_2 complex. They conclude that a bis-hydride is preferred over an η^2-H_2 complex when twice the ionization enthalpy of an electron in the M-H bond is greater than sum of the ionization enthalpies of an electron in the H-H bond and one in the metal d orbital.[47]

Hall and Lin have also examined the periodic trends for the formation of stable η^2-H_2 complexes.[46] They conclude that for neutral phosphine complexes (i. e. $M(PH_3)_x$) a diagonal line passing through Ru and Ir divides the periodic table into bis-hydride complexes (left) from the η^2-H_2 complexes (right). For monocationic complexes, this line shifts to between Tc/Ru and Os/Ir. They find that the stability of η^2-H_2 complex relative to the corresponding bis-hydride complex is directly related to the number and type of π-accepting ligands. Successive replacement of PH_3 by CO shifts the dividing line to the left of the periodic table.

Morris has shown that the product of the reaction of a coordinatively unsaturated metal complex with H_2 correlates quantitatively with the electron density available at the H_2 binding site as determined by the ν(NN) stretching frequency and redox potential of the corresponding η^1-N_2 complex.[44,50,51] For η^1-N_2 complexes with ν(NN) values of less than 2050 cm^{-1} and $E_{1/2}$ values of less than 0.5 V, the reaction with H_2 led to H-H cleavage and only the dihydride form was observed. For η^1-N_2 complexes with ν(NN) values between 2050 and 2200 cm^{-1} and $E_{1/2}$ values between 0.5 and 2.0 V, the reaction with H_2 led to stable η^2-H_2 complexes. The η^2-H_2 complexes became increasingly acidic as ν(NN) and $E_{1/2}$ approached their threshold values of 2200 cm^{-1} and 2.0 V. For η^1-N_2 complexes with ν(NN) values greater than 2200 cm^{-1} and $E_{1/2}$ values of more than 2.0 V, H_2 did not react at all or was found to bind only transiently.

The steric bulk of the ligand set is also important in determining whether a given complex will exist in the η^2-H_2 form or the corresponding bis hydride form. The

higher formal oxidation state and higher coordination number of the bis hydride form leads to shorter metal-ligand distances and smaller ligand-metal-ligand angles than in the corresponding η^2-H_2 complex. The presence of bulky ligands, therefore disfavors the bis hydride form.

The work of Kubas, Heinekey, and their respective coworkers illustrates the importance of the steric properties of the ligand set in determining the relative energies of the bis hydride and η^2-H_2 forms (Scheme I-4). Although the PCy_3, $P(i\text{-}Pr)_3$, and PMe_3

Scheme I-4

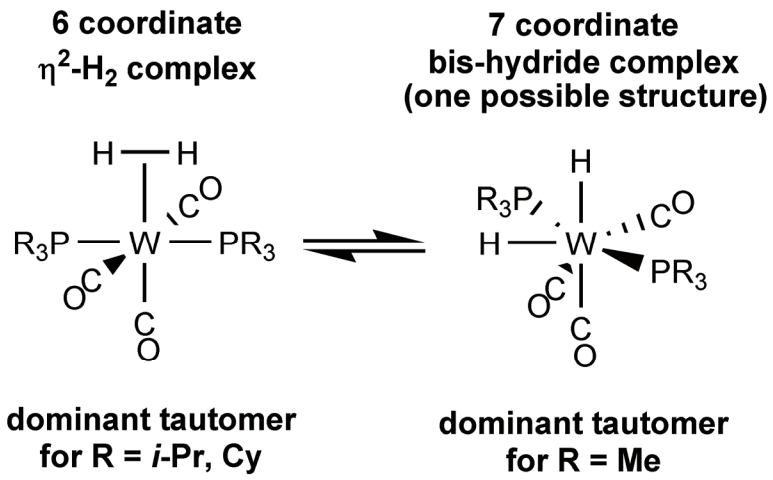

ligands are similar in their electron-donating ability, the PCy_3, and $P(i\text{-}Pr)_3$ ligands are much larger. For the PCy_3-, and $P(i\text{-}Pr)_3$-containing complex, the 6-coordinate (η^2-H_2)$W(CO)_3(PR_3)_2$ form is in dynamic equilibrium with the 7-coordinate $(H)_2W(CO)_3(PR_3)_2$ form with the η^2-H_2 form being the dominant tautomer.[52] The

corresponding PMe_3-containing complex exists exclusively as the bis hydride tautomer.[53]

Elongated η^2-H_2 complexes

Complexes with H-H distances between 1.0 and 1.5 Å are often referred to as elongated dihydrogen complexes. The properties of these complexes make it difficult to justify their classification as either "true" dihydrogen complexes (d_{H-H} < 1.0 Å), or cis dihydride complexes (d_{H-H} > 1.5 Å). Other authors further categorize these complexes as "true" elongated dihydrogen complexes (d_{H-H} < 1.0–1.3 Å) and compressed bis-hydrides (d_{H-H} < 1.3–1.5 Å).[44]

There is no consensus on the nature of elongated dihydrogen complexes and how they should best be described. While electronic structure calculations generally provide accurate H-H distances for true η^2-H_2 complexes and true cis dihydride complexes, they often fail to replicate the H-H distances observed in the molecular structures determined by single-crystal neutron diffraction for elongated dihydrogen complexes. Instead, these computations often predict that these complexes should exist as either a true η^2-H_2 complex, a true cis hydride complex, or an equilibrium mixture of the two species.

Lluch, Lledos, and coworkers have shown that the potential energy surface for elongation or contraction of the H-H distance is remarkably flat in the case of elongated dihydrogen complexes.[54-58] Heinekey, Lledos, and Lluch state, " ...the description of ... [certain elongated dihydrogen complexes]... as a dihydrogen or dihydride complex loses its significance, and it is more appropriate to describe it as a complex containing two H

atoms moving freely in a wide region of the coordination sphere of the metal."[20] They argue that the elongated dihydrogen complexes cannot, in general, be described by a single static structure.

The H-H distance in elongated dihydrogen complexes, as determined by the value of J_{HD}, is often dramatically affected by small changes in temperature.[59-61] This result provides strong experimental evidence that the potential energy surface is flat with respect to changes in the H-H distance.

Hall and coworkers used density functional theory calculations to assign the inelastic neutron scattering derived vibrational spectrum of the elongated dihydrogen complex, $(Tp^*)Rh(H)_2(\eta^2\text{-}H_2)$ (Tp^* = tris(3,5-dimethylpyrazolyl)hydroborate).[62] They conclude that the H-H distance derived from neutron diffraction for the $(Tp^*)Rh(H)_2(\eta^2\text{-}H_2)$ complex may in fact correspond to the average of the H-H distances of the tetrahydride and bis-hydride/h^2-H_2 species.

Experimental gauges of the H-H interaction and degree of activation

Ever since the discovery of the of the first η^2-H_2 complex by Kubas, there has been the lingering question: After coordination to a metal center, what remains of the H-H bond? A series of experimental methods for answering this question are presented below.

There are several experimental tools available for the determination of the H-H distance and the degree of the H-H bonding interaction. Neutron diffraction studies provide an accurate measure of the H-H distance. The measurement of the spin-lattice

proton relaxation time, T_1, for an η^2-H_2 complex or the proton-deuteron coupling constant, J_{HD}, for the corresponding isotopically substituted η^2-HD complex via ^{1}H-NMR spectroscopy provides a quantitative measure of the H-H distance. The frequency of the ν(HH) stretching band, as determined by Raman or infrared spectroscopy of η^2-H_2 complexes provides semi-quantitative information about the strength of the H-H interaction.

Neutron diffraction

The two main methods for the determination of the three-dimensional structures of molecules are single crystal x-ray diffraction and single crystal neutron diffraction studies.[63] Single crystal x-ray diffraction generally requires smaller crystals and is widely available. It is the method of choice for determining the three dimensional structure of most molecules. The constituent atoms of the molecule are located by the way in which their electron clouds scatter x-ray radiation. Since hydrogen atoms have only a single electron, they are difficult to locate accurately using x-ray diffraction. Neutrons are scattered by the atomic nuclei. A property known as neutron cross-section of an element determines how well it will scatter neutrons. Hydrogen atoms have the largest neutron cross-section of all elements. Single crystal neutron diffraction is therefore the method of choice for determining the position of hydrogen atoms.

^{1}H-NMR studies - HD coupling

The magnitude of the NMR coupling constant between atoms A and B, J_{AB}, is related to the spatial orientation of those atoms. Non-interacting atoms will have J_{AB}

values at or near zero hertz. The largest values of J_{AB} will occur when atoms A and B are connected by a direct chemical bond.

The J_{HD} coupling constant provides a measure of the H-D interaction in η^2-HD complexes. The observed J_{HD} coupling constant for HD gas is 43.2 Hz.[64] The coordination of HD to a transition metal center leads to weakening of the H-D bond, an increase in the H-D distance, and a decrease in the J_{HD} coupling constant. Morris, Heinekey, and their respective coworkers have shown that the value of J_{HD} for a given η^2-HD complex are linearly related to the H-H distance of the corresponding η^2-H_2 complex as determined by neutron diffraction.[65,66] The J_{HD} coupling constant is expected to range from maximum value of 43.2 Hz for free HD to 0-5 Hz for cis hydride-deuteride complexes.[44]

^{1}H-NMR studies – proton relaxation time - T_1 measurements

It has been observed that the proton spin lattice relaxation time, T_1, measured for the hydrogen atoms of the η^2-H_2 ligand is extraordinarily short (tens of milliseconds) when compared to dihydride complexes (hundreds of milliseconds). Crabtree and coworkers have shown that in general the value of T_1 is related to the inverse of the sixth power of the H-H distance.[67-70] Unfortunately the interpretation of T_1 can be complicated by other factors, such as the magnetogyric ratio of the metal nucleus and the proximity of other ligands to the η^2-H_2 ligand.[71,72]

Infrared and Raman spectral studies – ν(HH) measurements

The analysis of the infrared or Raman spectra of the H-H stretching band of η^2-H_2 complexes can give qualitative and semi-quantitative information about the strength of the H-H interaction, but suffers from several drawbacks. For infrared spectroscopy, the ν(HH) band is often weak and/or obscured by the infrared bands of co-ligands. Since both $H_2 \rightarrow M$ donation and $M \rightarrow H_2$ back-donation weaken the H-H bond, the ν(HH) stretch does not correlate exactly with the electron density provided by the metal center. The H-H stretch becomes a H-M-H bend as the H-H distance increases.[56,73] In other words, the ν(HH) band observed in the spectra of an η^2-H_2 complex is not a pure H-H stretch; it contains a mixture of H-H, M-H stretching and H-M-H bending motions. The nature of the metal center and the co-ligands exert a large influence on the H-M-H bend, and the value of the "ν(HH)" band in the spectra of these complexes.

The coordination of H_2 to a metal center leads to weakening of the H-H bond as evidenced by the ν(HH) stretching frequency. The ν(HH) stretching frequency of free H_2 as measured by gas phase Raman spectroscopy is 4161 cm^{-1}.[74] As shown in Table I-3, the ν(HH) stretching frequencies of η^2-H_2 complexes are significantly lower than

Table I-3. Infrared Date for Several η^2-H_2 Complexes

complex	ν(HH)	ref
Tp*RuH(η^2-H_2)(THT)	2250	75
Tp*RuH(η^2-H_2)$_2$	2361	75
CpNb(CO)$_3$(η^2-H_2)	2600	76
CpV(CO)$_3$(η^2-H_2)	2642	76
W(CO)$_3$(PCy$_3$)$_2$(η^2-H_2)	2690	77
W(CO)$_3$(P-iPr$_3$)$_2$(η^2-H_2)	2695	77
W(CO)$_5$(η^2-H_2)	2711	78
Cr(CO)$_5$(η^2-H_2)	3030	78,79
Mo(CO)$_5$(η^2-H_2)	3080	78
H_2 gas	4161	80

the ν(HH) stretch of free H_2. The comparison of Tp*RuH(η^2-H_2)$_2$ and Tp*RuH(η^2-H_2)(THT) (THT=tetrahydrothiofuran) or W(CO)$_5$(η^2-H_2) and W(CO)$_3$(PR$_3$)$_2$(η^2-H_2) shows that the presence of better donor ligands in the complex lowers the ν(HH) stretching frequency. The comparison of CpM(CO)$_3$(η^2-H_2) (M = Nb or V) or M(CO)$_5$(η^2-H_2) (M = Cr, Mo, or W) shows that the heaviest congener has the lowest ν(HH) stretching frequency.

Intramolecular Hydrogen Atom Exchange

Metal bound hydrogen atoms undergo a number of unique intermolecular and intramolecular exchange processes. In the words of Greg Kubas: "Transition metal complexes containing η^2-H_2 ligands and hydride ligands are unquestionably the most dynamic ligand systems known."[4]

In general, the rapid exchange of metal-bound hydrogen atoms benefits from the nature of the 1s valence orbital of hydrogen. The spherical shape of the 1s orbital allows hydrogen atom exchange to occur by associative mechanisms (with low barriers) in which H-H bond formation coincides with metal-hydrogen bond breaking.

Theoretical studies of the reductive elimination reactions of Pd(II) and Pt(II) bis-hydride, bis-alkyl, and cis hydride alkyl complexes illustrate the important role of the shape of 1s valence orbital of hydrogen on the rates of these reactions. It had been observed experimentally that CH_4 loss from $Pt(H)(CH_3)(PPh_3)_2$ is quite facile even at – 25 °C,[81] while the $Pt(CH_3)_2(PPh_3)_2$ complex is stable against CH_3CH_3 loss up to 237 °C.[82] Low and Goddard, utilizing electronic structure calculations, demonstrated that the observed reactivity (or lack thereof) was a result of the barrier to reductive elimination and not the thermodynamics of the reaction.[83-86] They argue that while the sp^3 hybridized orbital of CH_3 requires nearly completely scission of the M-C bond prior to C-C bond formation for $Pt(CH_3)_2(PPh_3)_2$ the spherical nature of the 1s orbital of H allows for the formation of the C-H bond to begin without conplete cleavage of M-C and M-H bonds of $Pt(H)(CH_3)_2(PPh_3)_2$.

Rotation of η^2-H_2 ligands

In many true η^2-H_2 complexes (H-H distance < 1.0 Å), the hydrogen atoms of the η^2-H_2 ligand rapidly interconvert on the NMR timescale, even at very low temperatures. The putative exchange process involves rotation of the η^2-H_2 ligand about the M-H_2 axis (*viz* the rotation of an airplane propellor) (Scheme I-5).

Scheme I-5

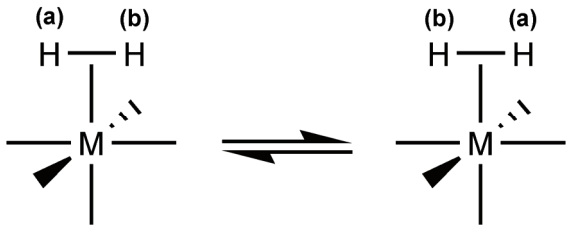

The electronic portion of the barrier to H_2 rotation is directly related to the change in M→H_2 back-donation between the minimum and transition state structures.[17] The H_2 ligand's orientation is largely dictated by M→H_2 back-donation. The H_2→M portion of η^2-H_2 bonding is relatively unaffected by the orientation of the H_2 ligand with respect to the M-H_2 axis.

Complexes of low-spin d^6 metals have the d_{xy}, d_{xz}, and d_{yz} orbitals fully occupied. In η^2-H_2 complexes of low-spin d^6 metals, the d_{xz}, d_{yz}, or a linear combination of the d_{xz}, and d_{yz} orbitals can effectively overlap with the σ* orbital of H_2. Therefore, the orientation of the η^2-H_2 ligand is largely dictated by the π-donating or π-accepting abilities of the ligands bound cis to the η^2-H_2 ligand. For complexes in which the cis ligands are similar to one another, the change in M→H_2 back-donation and the barrier to H_2 rotation is expected to be relatively small. For complexes in which the cis ligands are very different from one another, the change in M→H_2 back-donation and the barrier to H_2 rotation is expected to be relatively large.

Complexes such as $(\eta^2\text{-}H_2)W(CO)_3(PCy_3)_2$, in which the d orbitals responsible for $M\rightarrow H_2$ back-donation are all filled and have reasonably similar energies, generally have low barriers to $\eta^2\text{-}H_2$ rotation ($\Delta G^{\ddagger}$ = 2.2 kcal mol^{-1}).[40] For complexes that have only one filled orbital that is capable of $M\rightarrow H_2$ back-donation or in which the filled d-orbitals have drastically different energies, the barrier to $\eta^2\text{-}H_2$ rotation can be quite large. The d^2 complexes, $[CpTa(CO)(\eta^2\text{-}H_2)]^{1+}$ and $[Cp'Nb(CNR)(\eta^2\text{-}H_2)]^{1+}$ (Cp' = $C_5H_4Si(CH_3)_3$) have been shown experimentally to have particularly large barriers to $\eta^2\text{-}H_2$ rotation (~10 kcal mol^{-1}).[87-89] In these complexes, the low-energy orientation of the $\eta^2\text{-}H_2$ ligand generally corresponds to that which optimizes $M\rightarrow H_2$ back-donation between the sole filled d orbital on the metal center and the $\eta^2\text{-}H_2$ ligand. In the transition state for $\eta^2\text{-}H_2$ rotation there is complete loss of $M\rightarrow H_2$ back-donation.

Electrostatic interactions between the bound $\eta^2\text{-}H_2$ ligand and the co-ligands can also affect the barrier to H_2 rotation. Upon binding to a transition metal center, the hydrogen atoms of the $\eta^2\text{-}H_2$ ligand attain a partial positive charge. The orientation of the $\eta^2\text{-}H_2$ ligand can be dramatically affected by the presence of anionic co-ligands such as hydride or chloride located cis to the $\eta^2\text{-}H_2$ ligand.[90] This effect is illustrated by the computed barriers to $\eta^2\text{-}H_2$ rotation for the closely related complexes $Ir(Cl)_2(H)(\eta^2\text{-}H_2)(PH_3)_2$ ($\Delta G^{\ddagger}$ = 6.5 kcal mol^{-1}) and $Ir(Cl)(H)_2(\eta^2\text{-}H_2)(PH_3)_2$ ($\Delta G^{\ddagger}$ = 2.2 kcal mol^{-1}).[91,92]. The difference in the computed barriers is ascribed to the presence of a chloride ligand cis to $\eta^2\text{-}H_2$ in $Ir(Cl)_2(H)(\eta^2\text{-}H_2)(PH_3)_2$.

Eckert and coworkers have used inelastic neutron scattering (INS) experiments to measure transitions between the rotational energy levels of the bound H_2 ligand, which allows the determination of the barrier to rotation of the η^2-H_2 ligand[93-95] and the H-H distance.[96] One difficulty in INS experiments is that the large number of hydrogen atoms present in the co-ligands can obscure the transitions due to the η^2-H_2 ligands. This problem is often remedied by measuring the difference spectrum between the η^2-H_2 complex and the corresponding η^2-D_2 complex or by synthesizing a complex which contains per-deuterated co-ligands.

H_2/H^- exchange

There is often rapid exchange between η^2-H_2 ligands and neighboring hydrides as evidenced by NMR experiments. Even at very low temperatures, a single "hydride" resonance is observed in the ^{1}H-NMR spectra of most of these complexes. In addition, reaction of the protio form of many of these complexes with D_2 gas leads to the incorporation of deuterium into the complex, and the formation of HD.

In one mechanism, the H_2/H^- exchange process can be considered an example of internal heterolytic cleavage of the η^2-H_2 ligand (Figure I-3). The protonation of hydride ligands by an external acid, and deprotonation of η^2-H_2 by an external base are common processes. In the H_2/H^- exchange process η^2-H_2 acts as an internal acid, and the hydride ligand acts as an internal base. In this process, the η^2-H_2 ligand transfers H^+ to the neighboring hydride ligand to afford a new hydride and a new η^2-H_2 ligand. The transition state structures for this type of rearrangement often feature a linear or nearly

linear orientation of the three hydrogen atoms, such that it appears that a H_3^- ligand appears bound to the metal center in the transition state. For example, low-temperature protonation of d^0 pentahydride complexes of the form $[Cp^*M(H)_5(PR_3)]^{1+}$ (M = Mo, W) leads to thermally unstable "hexahydride" species.[97] These complexes display a single resonance in the hydride region of their ^{1}H-NMR spectra. Bayse *et al.*, utilizing electronic structure calculations, demonstrated that the lowest energy structure for these complexes corresponds to a dihydrogen/tetrahydride complex of the form $[Cp^*M(H)_4(\eta^2\text{-}H_2)(PR_3)]^{1+}$. Both η^2-H_2 rotation and H_2/H^- exchange pathways were computed to have low activation energies. The structure of the transition state for hydrogen atom exchange between the η^2-H_2 ligand and its neighboring hydride ligands resembles a linear H_3^- molecule bound to the Mo center.

An alternative mechanism for H_2/H^- exchange requires oxidative addition of the η^2-H_2 ligand (also shown in Figure I-3). The $IrX(H)_2(\eta^2\text{-}H_2)(P(i\text{-}Pr)_3)_2$ (X = Cl, Br, I) complexes undergo rapid hydrogen atom exchange.[98-100] Hall and coworkers conclude on the basis of density functional theory calculations that the most likely mechanism involves oxidative addition of the η^2-H_2 ligand to form a transient tetra-hydride complex, followed by pairwise reductive elimination of hydride ligands.

Hydride-Hydride exchange

There is often rapid exchange between neighboring hydride ligands as evidenced by NMR experiments. Even at very low temperatures, a single hydride resonance is observed in the ^{1}H-NMR spectra of most of these complexes. The most common

mechanism proposed for hydrogen atom exchange in polyhydride complexes involves the formation of transient η^2-H_2 ligands (Scheme I-6).In this mechanism, a pair of neighboring hydride ligands interact to form an η^2-H_2 ligand. The η^2-H_2 ligand can undergo rotation about the M-H_2 axis before converting back to two hydride ligands. When three or more hydride ligands are found to be exchanging, it is generally assumed that rapid pair-wise exchange between each neighboring set is involved.

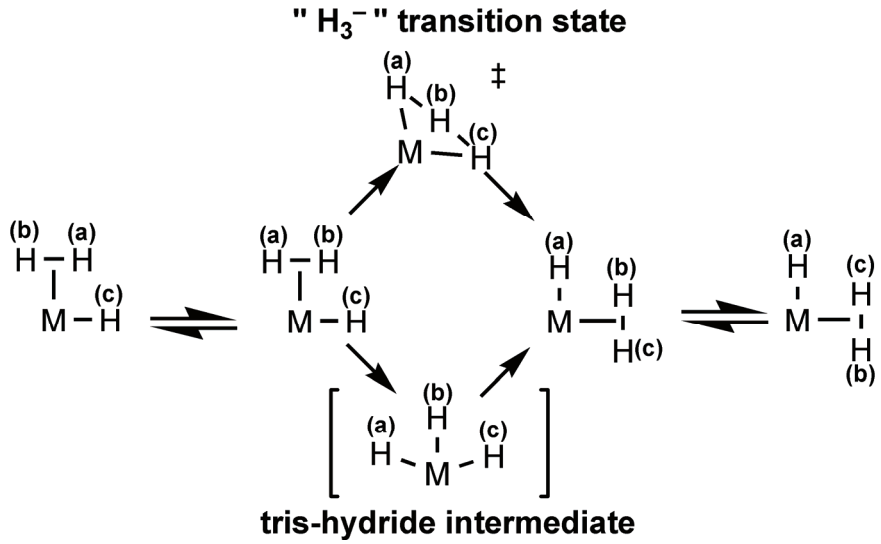

Figure I-3. Possible mechanisms of hydrogen atom exchange for a complex containing both an η^2-H_2 ligand and a single hydride ligand. In the top mechanism, there is direct exchange of "H^+" between the η^2-H_2 and H^- ligands. In the bottom mechanism, the η^2-H_2 ligand oxidatively adds to the metal center to yield a tris-hydride species. Reductive elimination of hydrides (b) and (c) yields a "new" hydride/η^2-H_2 complex. Either mechanism requires η^2-H_2 rotation for complete hydrogen atom exchange.

Scheme I-6

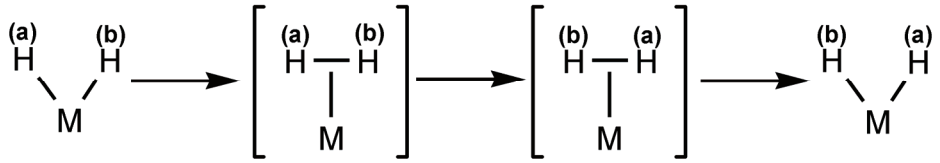

Although pairwise exchange of hydride ligands via formation of transient η^2-H_2 is the most commonly invoked mechanism to explain hydride-hydride exchange in polyhydride complexes, other low energy pathways may exist. In examining possible hydride exchange processes for pentahydride complex $CpOs(H)_5$, Bayse, Couty, and Hall concluded the hydride ligands of this complex exchange three at a time via a trigonal twist mechanism.[101]

Non-Classical Hydrogen Bonds

Scheme I-7

H^- as a hydrogen bond acceptor

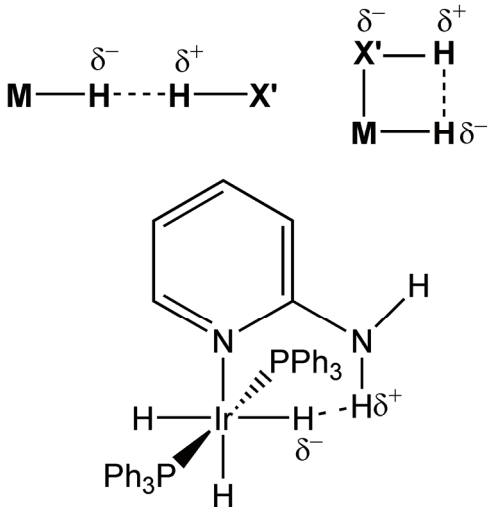

Hydride ligands as non-classical hydrogen bond acceptors

The hydride ligand can act as a non-classical hydrogen bond acceptor (Scheme I- 7). The non-covalent interaction between hydrogen bond donors and hydride ligands are often referred to as protonic-hydridic bonding interactions. Morris, Crabtree and their respective coworkers reported examples of intramolecular protonic-hydridic interactions, which produce hydrogen-hydrogen distances of 1.7–1.8 Å.[102,103] It remained difficult for some time to prove definitively that the protonic-hydridic interaction is a stabilizing interaction, and not simply a consequence of the steric constraints imposed by the ligand set. Crabtree and coworkers[104-107] co-crystallized indole and $Re(H)_5(PPh_3)_3$. The solid state structure demonstrated the presence of an intermolecular non-classical hydrogen bond between the N-H hydrogen of indole and a hydride ligand of $Re(H)_5(PPh_3)_3$.

η^2-H_2 as a non-classical hydrogen bond donor

The donation of electron density from dihydrogen to the metal center depletes the electron density of the η_2-H_2 ligand. The η^2-H_2 ligand, therefore, can act as a non-classical hydrogen bond donor (Scheme I-8). The η^2-H_2 ligand may act as an

Scheme I-8

η^2-H_2 as a hydrogen bond donor

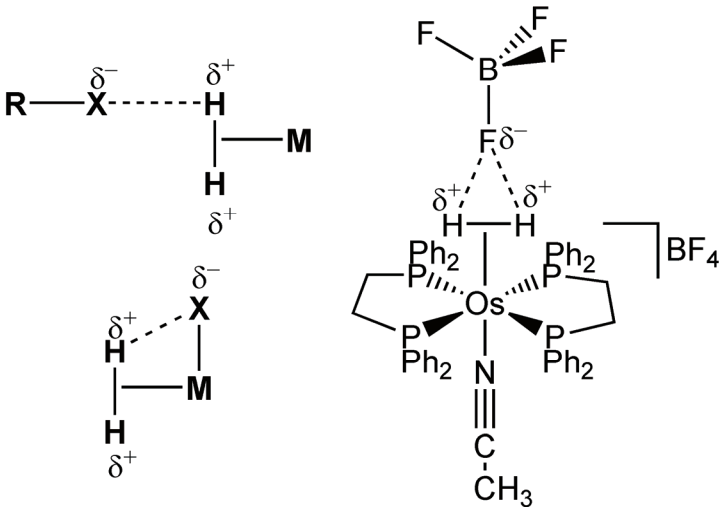

intramolecular hydrogen bond donor to hydrides, halides, and other negatively charged ligands. Neutron diffraction studies often find that the η^2-H_2 ligand is oriented to place its hydrogen atoms as close as possible to cis hydride ligands. In fact, the preference for the hydrogen atoms of the η^2-H_2 ligand to be coplanar with a cis hydride ligand is so common that it has been termed the "cis effect of hydrides".[90] The η^2-H_2 ligand is also capable of forming intermolecular hydrogen bonds. Morris and coworkers have noted that one of the fluorine atoms of the BF_4^- or PF_6^- counterions is consistently oriented toward the η^2-H_2 ligand in the solid-state structures of a series of cationic η^2-H_2 complexes.[66,108]

Reactivity of Metal-Bound Hydrogen Atoms

How does the reactivity of metal-bound hydrogen atoms compare to that of free H_2?

The binding of dihydrogen to a transition metal center can greatly change its reactivity (Scheme I-9). The H-H bond of an η^2-H_2 complex is weaker that the H-H

Scheme I-9

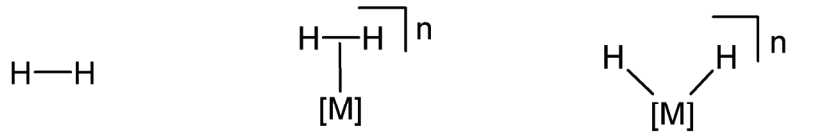

strong H–H bond	weakened H–H bond	no H–H bond
non-polar	δ^+ charge on H_2	δ^- charge on H
poor acid	stronger acid	
poor base		stronger base
poor nucleophile		better nucleophile
poor electrophile	better electrophile	

bond in free dihydrogen, making cleavage of the H-H more thermodynamically feasible. An η^2-H_2 complex is therefore generally more thermodynamically acidic than free H_2. When coordinated to an electrophilic transition metal center, in which $H_2 \rightarrow M$ donation dominates, the hydrogens atoms of the η^2-H_2 ligand become positively charged, and therefore more kinetically acidic than free H_2. When coordinated to an electron-rich transition metal center, in which $M \rightarrow H_2$ donation dominates, dihydrogen may oxidatively add to the metal center to generate bis-hydride complex. The resulting hydride ligands may be either hydridic or protonic in nature.

Metal-monohydride species - " hydride ligands can be acidic! "

Before venturing into the more complicated case of polyhydrides, there is one point that should be made about transition metal hydrides in general. The term hydride is sometimes misleading. To many chemists, this term implies an H^- ionically bound to metal. This term may be used with relative impunity for main group hydrides such as NaH, (Na^+H^-). When applied to transition metal complexes, however, this term is sometimes a misnomer. In terms of their reactivity, transition metal hydrides can function as hydride (H^-) donors, proton (H^+) donors, or be quite covalent in their bonding.

Morris and coworkers have measured the proton dissociation constants for a series of mono-protic species in THF solution (pK_a^{THF}) and/or estimated these values from pK_a measurements in other solvents. The selected pK_a^{THF} values given in Table I-4 span 24 pKa units. The most acidic of these complexes, $[(\eta^5\text{-}C_5Me_5)_2Os\mathbf{H}]^{1+}[OTf]^{1-}$ is significantly more acidic than $[HNEt_3]^{1+}[BPh_4]^{1-}$

Norton and coworkers examined the thermodynamic and kinetic acidity of a series of transition metal complexes.[109-114] They found that the rates of H^+ transfer from transition metal hydrides can be quite slow when compared to organic and mineral acids of similar pK_a's.[115]

Walker, Pearson, and Ford attribute the slow rates of H^+ transfer from hydride ligands to the following factors (illustrated in Scheme I-10) : (1) Bases generally have a partial negative charge on the atom that is to accept H^+. This partial negative charge is repelled by the anionic nature of the hydride ligand. (2) The acid and conjugate base

Table I-4. Proton Dissociation Constants for a Series of Compounds in THF Solvent

compound	pK_α (THF)
HH	49[a]
$(\eta^5\text{-}C_5H_5)W\mathbf{H}(PMe_3)(CO)_2$	32[a]
$(\eta^5\text{-}C_5Me_5)Fe\mathbf{H}(CO)_2$	31 ± 4
$[Pt\mathbf{H}(dmpe)_2]^{1+}[PF_6]^{1-}$	21[a]
$[Ni\mathbf{H}(dmpe)_2]^{1+}[PF_6]^{1-}$	18[a]
$(\eta^5\text{-}C_5H_5)Mo\mathbf{H}(CO)_3$	17 ± 1
$[Pt\mathbf{H}(dppe)_2]^{1+}[PF_6]^{1-}$	16[a]
$[\mathbf{H}NEt_3]^{1+}[BPh_4]^{1-}$	12.5
$[(\eta^5\text{-}C_5Me_5)_2Os\mathbf{H}]^{1+}[OTf]^{1-}$	6[a]

(a) estimated from pK_α in another solvent.

may have very different orientation of the ligand set. (3) The steric bulk of the co-ligands may not allow the base to approach to the hydride ligand closely.

Seminal work: increased acidity of η^2-H_2

Dihydrogen gas is a very poor acid (pK_a of H_2 dissolved in tetrahydrofuran = 49). The binding of dihydrogen to a transition metal complex to form a η^2-H_2 complex can greatly increase both its thermodynamic and kinetic acidity.[8,16] The *thermodynamic acidity* of an given acid in a given solvent is related to the change in free energy (ΔG) upon proton loss in that solvent. The pK_a of an acid, which is measured when the acid and its conjugate base have reached equilibrium, is a measure of that acid's

thermodynamic acidity. *Kinetic acidity* deals with the rate of proton transfer. Acids with a high kinetic acidity lose H^+ at a fast rate.

Scheme I-10

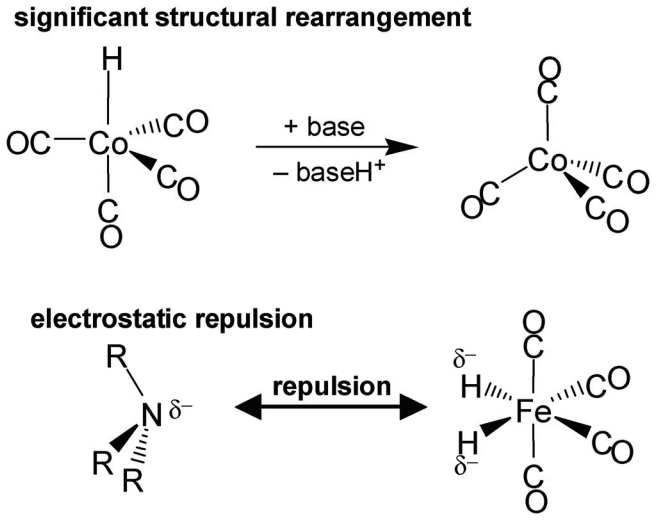

The binding of dihydrogen to a metal to form an $(\eta^2\text{-}H_2)[M]$ can increase the thermodynamic acidity of the H_2 molecule relative to free H_2 in at least two ways: (1) The binding of H_2 to a metal to form an $\eta^2\text{-}H_2$ complex weakens the H-H bond. (2) The metal fragment acts as a built-in hydride acceptor following deprotonation:

$$(\eta^2\text{-}H_2)M + B \rightarrow BH^+ + MH^-$$

The binding of dihydrogen to a metal to form an $(\eta^2\text{-}H_2)M$ can increase the kinetic acidity of the H_2 molecule relative to free H_2. Molecular hydrogen is completely non-polar. Dihydrogen to metal ($H_2(\sigma) \rightarrow M$) donation induces a partial positive charge on the H atoms, making these atoms more kinetically accessible to nucleophiles (bases).

The binding of dihydrogen to a metal center can lead to highly acidic η^2-H_2 complexes. Although the most acidic of these complexes are generated by protonation of a hydride complex by strong acid, a few η^2-H_2 complexes have been prepared using dihydrogen gas. Morris and Jagirdar and their respective coworkers have demonstrated that the coordination of dihydrogen to a Ru^{II} center produces an η^2-H_2 complex that is as acidic as triflic acid (CF_3SO_3H) (Scheme I-11).[116,117]

Scheme I-11

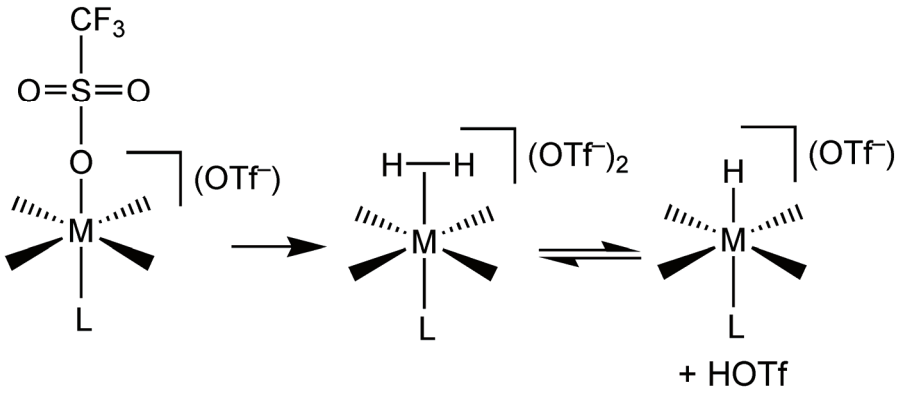

Many η^2-H_2 complexes are in dynamic equilibrium with the corresponding bis-hydride complexes. The η^2-H_2 complex and corresponding bis-hydride complex generally differ in terms of thermodynamic and kinetic acidity. The minor tautomer is the stronger thermodynamic acid (lowest pK_a).[118,119] Deprotonation of either the η^2-H_2 complex or bis-hydride complex generally leads to the same mono-hydride complex. As shown in Scheme I-12, the minor tautomer is necessarily less stable in terms of its free

energy (ΔG). Therefore, the difference in free energy between the protonated and deprotonated forms is smaller for the minor tautomer, and hence the pK_a of the minor tautomer is lower than that of the major tautomer. The hydrogen atoms of an η^2-H_2 complex generally have a partial positive charge, while those of a bis-hydride complex

Scheme I-12

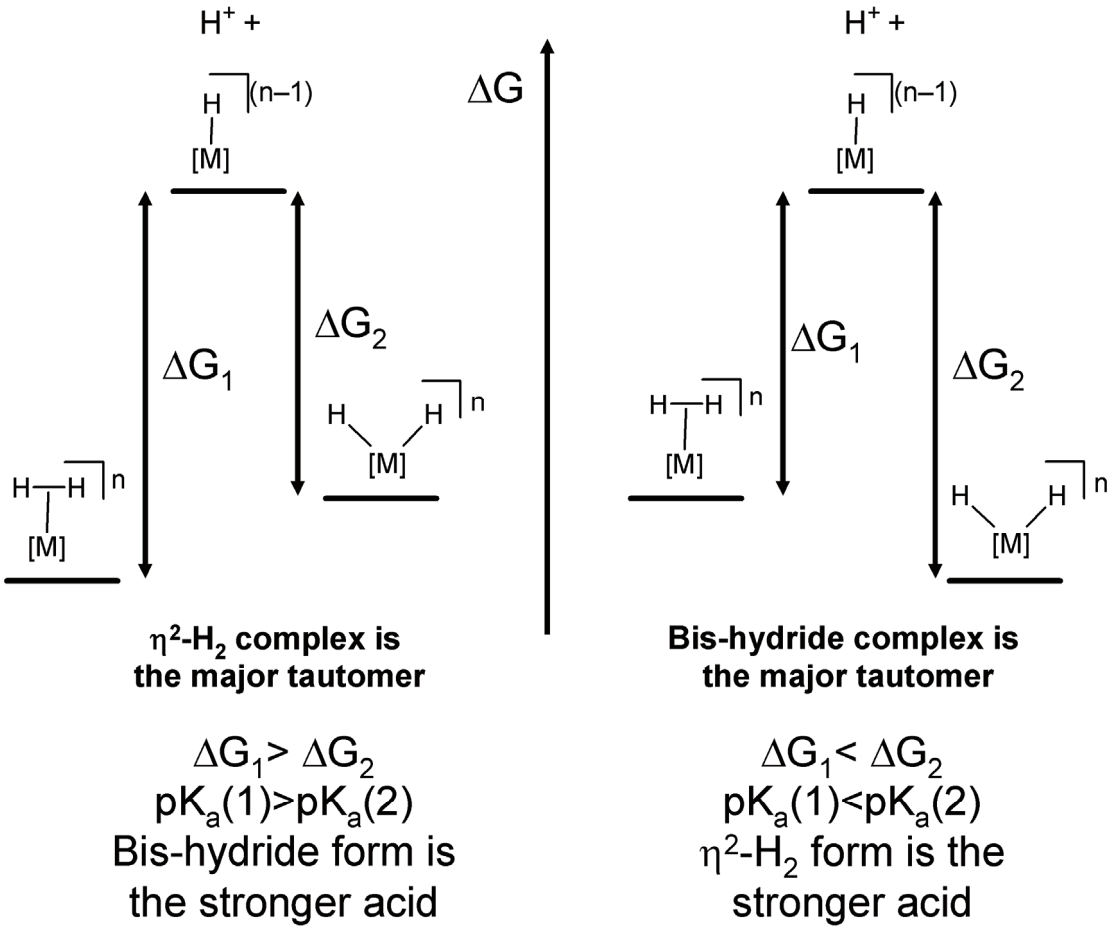

generally have a partial negative charge. Thus, the η^2-H_2 complex generally has a higher kinetic acidity than the corresponding bis-hydride complex.

Seminal work: intramolecular heterolytic cleavage of H_2

Morris,[120] Crabtree,[121] and their respective coworkers have investigated the binding of dihydrogen to transition metal centers which contain "built-in" basic functionalities near the H_2 binding site (as shown in Scheme I-13). Using these complexes, they observed the intramolecular heterolytic splitting of dihydrogen.

Scheme I-13

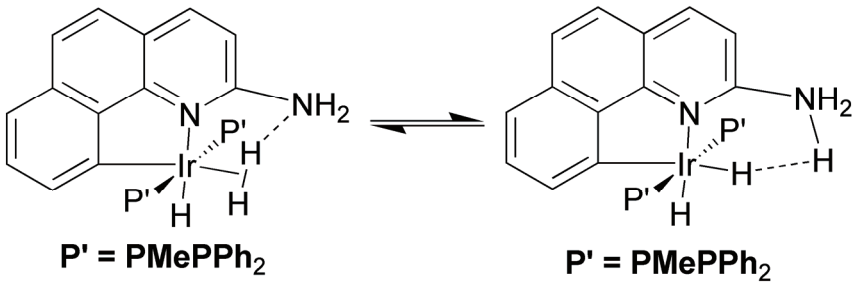

Scheme I-14

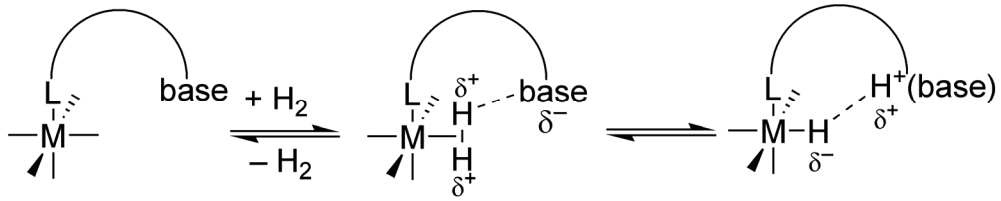

Non-classical hydrogen bonding has an important role in the intramolecular heterolytic cleavage of H_2 in these complexes (as illustrated in Scheme I-14).

Hydrogen-bonding between the internal base and the η^2-H_2 ligand stabilizes the η^2-H_2 complex with respect to H_2 loss, and orients the reactant atoms for efficient H^+ transfer. The stabilization of the η^2-H_2 form with respect to H_2 loss is quite important since the most acidic η^2-H_2 complexes often contain the most labile H_2 ligands. Once H^+ transfer has occurred, a non-classical hydrogen bond between the resulting hydride ligand and protonated base adds to the stability of the deprotonated form.

Enzymatically Catalyzed Dihydrogen Oxidation and Proton Reduction

Two major classes of H_2 activating and/or producing enzymes are the hydrogenases (H_2ases)[122-124] and nitrogenases (N_2ases)[125,126]. The H_2ase enzymes are known to catalyze dihydrogen oxidation, proton reduction, dihydrogen detection, and dihydrogen utilization in cells. The N_2ase enzymes catalyze the reduction of molecular nitrogen to ammonia (nitrogen fixation). For reasons that are not completely clear, the N_2ase enzymes couple H^+ reduction to the N_2 reduction process: ie $N_2 + 8H^+ + 8e^- \rightarrow 2NH_3 + H_2$.

General information about hydrogenase enzymes

The H_2ase enzymes may be broadly classified by specifying the transition metal content of their active sites. The three main classes of hydrogenase enzymes are the nickel-iron ([NiFe])[127-129], iron-iron ([FeFe])[130,131] and the so called iron-sulfur cluster free hydrogenases, which until recently were thought to be "metal-free"[132-135]. The [NiFe] enzymes are primarily utilized for hydrogen oxidation, while the [FeFe] enzymes are primarily utilized for proton reduction. The iron-sulfur cluster free hydrogenases are

H_2 utilizing enzymes, which activate dihydrogen for use in catabolic processes within the cell, but do not catalyze H^+ reduction or H_2 oxidation. Certain organisms also contain H_2-sensing hydrogenases, which regulate H_2 oxidation and/or H^+ reduction in these organisms.[136,137]

Nickel-Iron hydrogenase enzymes

Single-crystal x-ray diffraction studies have defined the basic framework of the active site of the nickel-iron hydrogenase enzymes ([NiFe]H_2ases) as consisting of an iron center and a nickel center bridged by cysteinate sulfur atoms (Scheme I-15).[138-142]

Scheme I-15

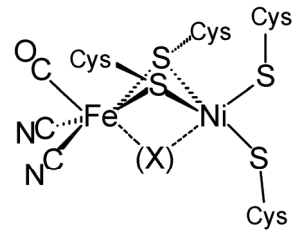

(X) = O^{2-},OH^-, HO_2^-, H^-, H_2, CO, or nothing

The nickel center is further coordinated by terminal cysteinate sulfur ligands, and the iron center is further coordinated by two CN^- ligands and one CO ligand. The nature of a third ligand, which bridges the two metal centers in certain redox states of the enzyme, is currently a matter of some contention[143,144]. A gas access channel[145] and a series of

ferrodoxin-like iron-sulfur clusters extend from the enzyme active site to the protein surface.

The use of infrared and electron paramagnetic resonance spectroscopies have demonstrated the existence of at least seven different forms of the Ni-Fe center. EPR studies on the enzyme active site have identified three S = 1/2, EPR-active states designated as Ni-A, Ni-B, and Ni-C.[146-152] Infrared studies on the enzyme identified four EPR-silent states with have been designated as Ni-SU, Ni-SI_I, Ni-SI_{II}, and Ni-SR (alternatively known as Ni-R).

The structures of the various species, their roles in the catalytic cycle, and the details of their interconversions remains unclear. The Ni-A and Ni-B forms correspond to over-oxidized species, which are not active in the catalytic cycle for H_2 oxidation. Both Ni-A and Ni-B may be re-activated by reduction, although the rate of re-activation is markedly slower for Ni-A. Species designated as Ni-C* and Ni-R are believed to be intermediates in the oxidation of H_2. Other species designated as Ni-SU, Ni-SI_I, and Ni-SI_{II} are presumed to be intermediates in the re-activation of the over-oxidized forms of the enzyme, although one of the Ni-SI species may play a role in the catalytic cycle.[139,153-159]

The nickel center is the putative site of H_2 activation. It appears that the iron center remains low-spin Fe^{II}, while the nickel center takes the electrons and passes protons to nearby bases. In the active cycle, nickel changes from Ni^{III} to Ni^{II}, and finally to Ni^{I}, which has not been observed because of its rapid electron transfer. All of the observed EPR-active species appear to be Ni^{III}, while the remaining, observed species

appear to be Ni^{II}. Interestingly, the Ni^{II} forms were assumed to be low-spin, but calculations suggest that the enzyme structure (ie the twisted ligand arrangement about the nickel center) would result in high-spin Ni^{II} in all the EPR-silent forms.[160]

Scheme I-16

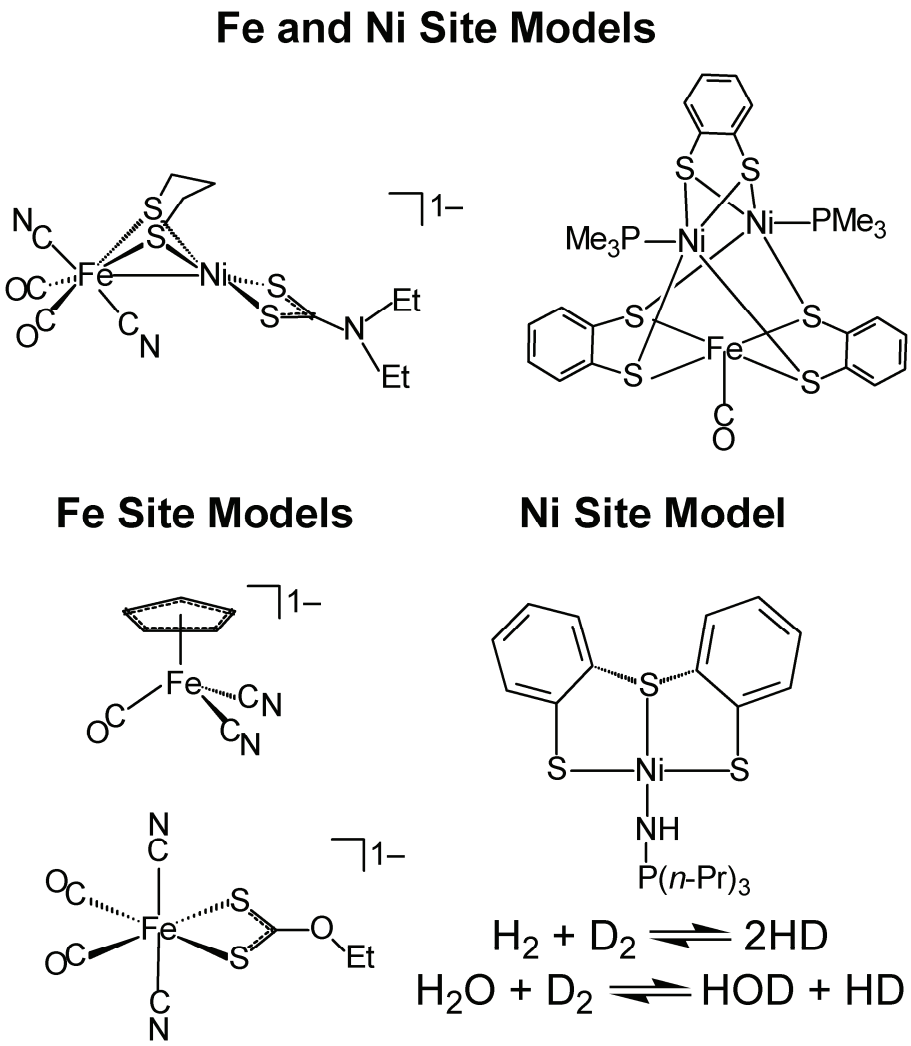

The addition of CO gas to preparations of the active enzyme leads to essentially no change in the ν(CO) band (~2 cm^{-1}) of the $Fe(CO)(CN)_2$ unit, and the appearance of a new ν(CO) band at 2055 cm^{-1} in the infrared spectrum.[158] The CO-inhibited form of the enzyme is incapable of catalyzing H^+ reduction or H_2 oxidation. The molecular structure derived from single-crystal x-ray diffraction studies of the CO-inhibited form of the Ni-Fe hydrogenase enzyme from *Desulvibrio vulgaris* (Miyazaki) clearly shows that the exogenous CO ligand is bound to the Ni center, but predicts Ni-C-O angles that range from 136.2 to 160.9°.[161]

The synthesis of small-molecule models of the active site of [NiFe]H_2ase has proven quite difficult.[162] A variety of synthetic active site models complexes are presented in Scheme I-16. The majority of [NiFe]H_2ase model complexes, synthesized to date, are mononuclear models that attempt to model either the Fe site or the Ni site. Liaw and coworkers synthesized the mononuclear iron complex $[Fe(CO)_2(CN)_2(\eta^2\text{-}S_2COCH_2CH_3)]^{1-}$ and found it to be an excellent model of the coordination environment of the Fe center of [NiFe]H_2ase.[163] M. Y. Darensbourg, D. J. Darensbourg and coworkers showed that the infrared spectrum of the $[CpFe(CO)(CN)_2]^{1-}$ complex is similar to the infrared spectra of the oxidized forms of [NiFe]H_2ase.[164] Sellmann and coworkers designed a mononuclear nickel complex capable of catalyzing D_2/H_2O exchange.[165] Very recently, Tatsumi and coworkers developed the $[(\mu\text{-}S(CH_2)_3S)[Fe(CO)_2(CN)_2][Ni(\eta^2\text{-}S_2CNR_2)]^{1-}$complex as models of the composition of the [NiFe]H_2ase active site.[166] The laboratory of Dieter Sellmann has also published a series

of trinuclear ($FeNi_2$) complexes which (ignoring the extra Ni center) serve as excellent models of the structural and compositional models of the [NiFe]H_2ase active site.[167,168]

Iron-Iron hydrogenase enzymes

Single-crystal x-ray diffraction studies have defined the basic framework of the active site of the iron-iron hydrogenase enzymes ([FeFe]H_2ases) as consisting of two iron centers bridged by a novel dithiolate ($^-SCH_2XCH_2S^-$; X = CH_2, NH, or O) linker (Scheme I-17).[130,169-172] Each of the iron centers is further coordinated by one terminal CO ligand and one terminal CN^- ligand. The proximal iron center is further coordinated by a sulfur atom from a protein-bound cysteinate ligand, which bridges the FeFe active site and a nearby ferrodoxin-like [Fe_4S_4] cluster. (The two iron centers are commonly designated as proximal and distal by noting their spatial relation to the nearby [Fe_4S_4] cluster.) An additional CO ligand either bridges the two iron centers or is terminally coordinated to the distal iron center, depending on the redox state of the di-iron center.

Scheme I-17

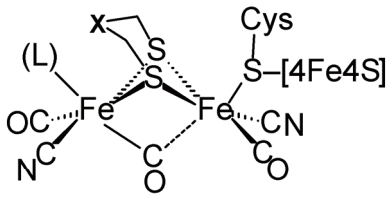

(L) = H_2O, OH^-, HO_2^-, H^-, H_2, CO, or nothing

A gas access channel[173] and a series of ferrodoxin-like iron-sulfur clusters extend from the enzyme active site to the protein surface.

The use of infrared[172,174-176] and electron paramagnetic resonance (EPR)[177-180] spectroscopies have demonstrated the existence of at least four different forms of the [FeFe]-[Fe_4S_4] active site. EPR studies on the enzyme active site have identified two S=1/2, EPR-active states designated as $H_{ox(-2.06)}$ and $H_{ox(-2.10)}$. Infrared studies on the enzyme identified two EPR-silent states with have been designated as H_{ox}^{air} and H_{red}. The H_{ox}^{air} form corresponds to over-oxidized species, which is not an active catalyst for H^+ reduction or H_2 oxidation. The H_{ox}^{air} form may be re-activated either electrochemically or via the introduction of chemical reductants. In the presence of low potential reductants, the H-cluster undergoes a one-electron reduction. The added electron is found to initially localize on the [Fe_4S_4] portion of the 6-Fe active site, generating a species designated as $H_{ox(-2.06)}$. A conformational change of the protein superstructure is believed to initiate the transfer of the electron from the [Fe_4S_4] cluster to the [FeFe] cluster, yielding a species designated as $H_{ox(-2.10)}$. The addition of high potential reductants leads to a second one-electron reduction to yield a species designated as H_{red}.

The distal iron center is the putative site of H_2 activation. The addition of CO gas to preparations of the $H_{ox(-2.10)}$ form of the enzyme derived from *Desulfovibrio desulfuricans* Hildenborough (DdH) or *Clostridium pasteurianum* I (CpI) leads to an inhibited form of the enzyme that is incapable of catalyzing H^+ reduction or H_2 oxidation and the appearance of an additional ν(CO) band. The molecular structure derived from

single-crystal x-ray diffraction studies of the CO-inhibited form of the [FeFe]H_2ase enzyme shows that the distal iron center is coordinated by an additional CO ligand.

The synthesis of small-molecule models of the active site of [FeFe]H_2ase have contributed to a better understanding of its basic structure and the catalytic mechanism of H_2 oxidation and H^+ reduction.[162] A variety of synthetic active site models complexes are presented in Scheme I-18. Simple dithiolate bridged di-iron clusters have been found to act as structural and functional models of the active site of [FeFe]H_2ase. Complexes of the form, $[(\mu\text{-}SCH_2XCH_2S)[Fe(CO)_2(CN)]_2]^{2-}$ (X = CH_2, NH, or O) are excellent models of the composition of the [FeFe]H_2ase active site.[181-185] Darensbourg argued for a formal Fe^IFe^I redox state assignment for the H_{red} form of [FeFe]H_2ase on based on the similarity of the ν(CO) bands of $[(\mu\text{-}SCH_2CH_2CH_2S)[Fe(CO)_2(CN)]_2]^{2-}$ and those of the enzyme active site.[186] Pickett and coworkers thoroughly explored the chemistry of first generation Fe_2S_3 models, which feature coordination of a pendant thioether sulfur (RSR) to one of the iron centers.[187-192] Complexes synthesized by Pickett, Song and their respective coworkers feature coordination of an external iron-bound thiolate ligand to one of the iron centers of the $Fe_2S_2(CO)_5$ core.[185,193] A range of simple dithiolate bridged di-iron complexes have been shown to act as solution electrocatalysts for H_2 production.[194-201] Darensbourg and coworkers have demonstrated that the $[(\mu\text{-}S(CH_2)_3S)\ [Fe(CO)_2(PMe_3)]_2]^{1+}$ complex catalyzes isotopic exchange in H_2/D_2 and D_2/H_2O mixtures, under photolytic, CO loss conditions.[202-204]

Scheme I-18

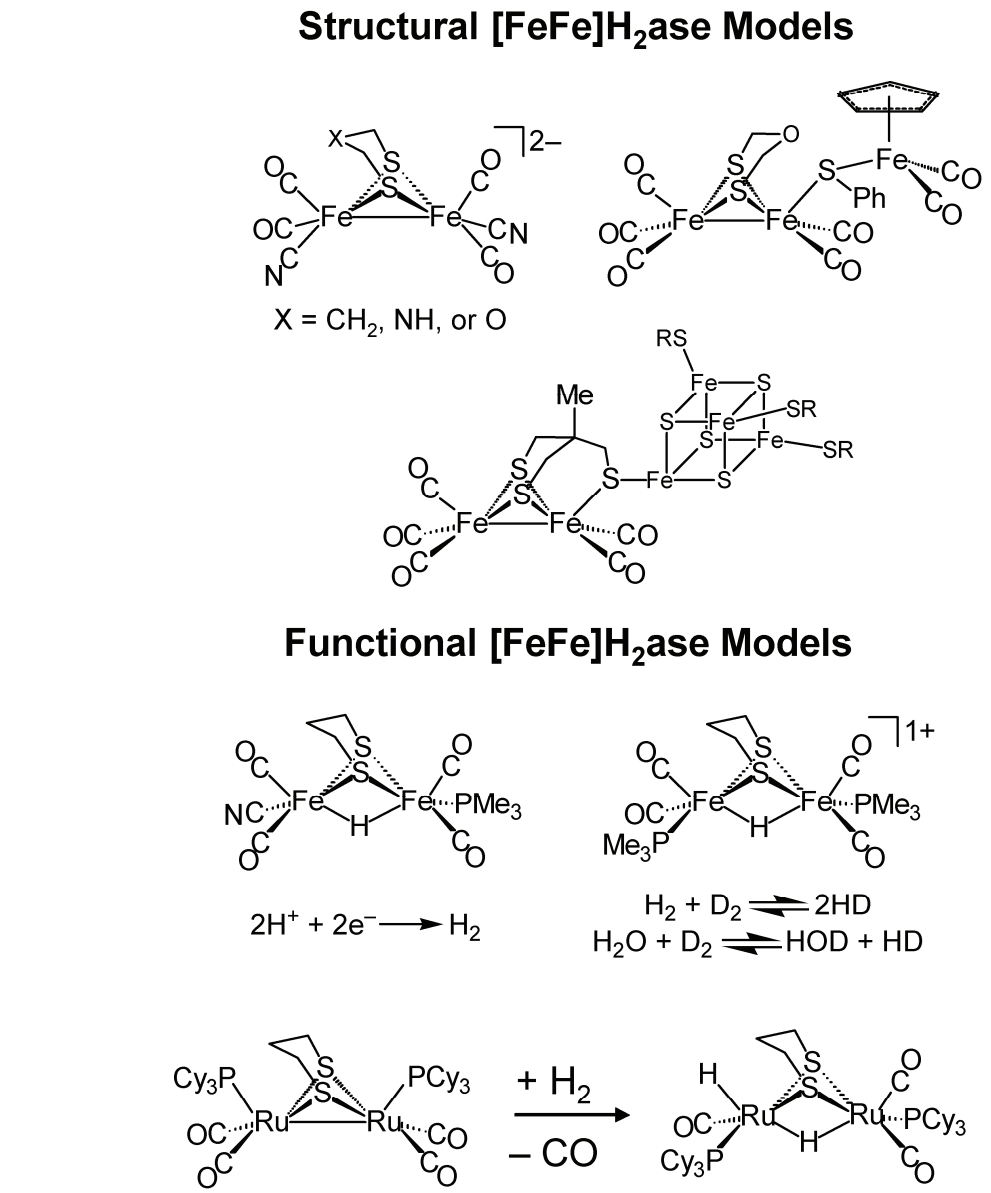
Structural [FeFe]H2ase Models
X = CH2, NH, or O
Functional [FeFe]H2ase Models
2H+ + 2e− → H2
H2 + D2 ⇌ 2HD
H2O + D2 ⇌ HOD + HD
+ H2
– CO

Cao and Hall utilized the experimentally determined ν(CO) and ν(CN) stretching frequencies for the $(\mu\text{-}S(CH_2)_3S)[Fe(CO)_3]_2$ and $[(\mu\text{-}S(CH_2)_3S)[Fe(CO)_2(CN)]_2]^{2-}$ complexes in order to calibrate their computationally derived ν(CO) and ν(CN) stretching frequencies. Using this method, they were able to show that the $H_{as\text{-}isolated}$, H_{ox}, and H_{red} forms of the [FeFe]H_2ase enzymes must correspond to the $Fe^{II}Fe^{II}$, $Fe^{I}Fe^{II}$, and $Fe^{I}Fe^{I}$ formal oxidation states of the FeFe cluster, rather than the higher formal oxidation states initially suggested.[205]

Density functional theory calculations have been applied by several research groups to give a better understanding of the molecular details of H_2 oxidation and H^+ reduction at the [FeFe] active site. The various proposed mechanisms differ mainly in the prospective location of H_2 binding to the [FeFe] cluster (as shown in Figure I-4). Hall[205,206] and coworkers have established that a bridgehead N atom provides a kinetically and thermodynamically favorable route for the heterolytic cleavage of H_2 bound at the distal iron. Hu[207,208] later reported similar results. De Gioia[209,210] and Zhou[211,212] and their respective coworkers found an alternative kinetically and thermodynamically favorable route for the heterolytic cleavage of bound H_2. In mechanisms of De Gioia and Zhou, the active site rearranges from the structure observed in the x-ray structures of the enzyme. Dihydrogen then binds to the proximal iron in the area "between" the two iron atoms. A proton is transferred from the bound η^2-H_2 to a μ-S atom of the dithiolate cofactor to afford heterolytic cleavage.

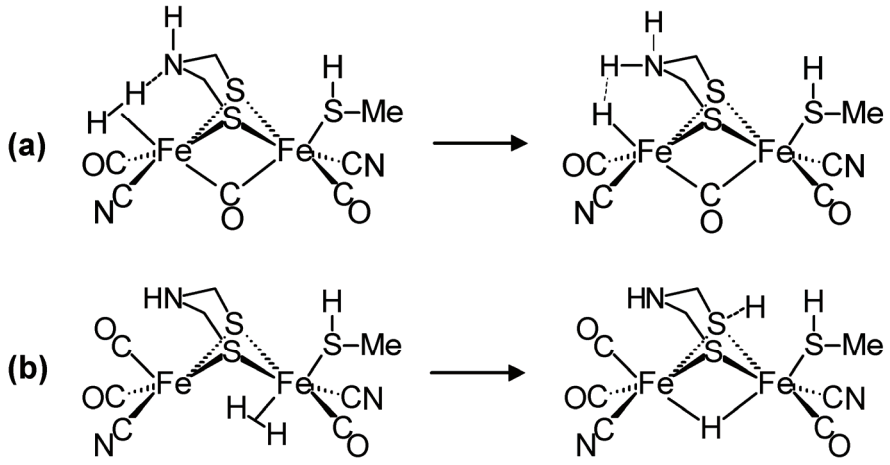

Figure I-4. Heterolytic cleavage of H_2 using small molecule computational models of the [FeFe]H_2ase active site. Hall, and Hu and Liu (a) favor heterolytic cleavage of H_2 bound to the distal iron center and utilizing the central nitrogen of the S-to-S linker as an internal base. De Gioia and Zhou (b) favor heterolytic cleavage of H_2 bound to the proximal iron and utilizing a bridging thiolate sulfur atom as an internal base.

Conclusions

The looming shortage of fossil fuels is a global problem. We are in immediate need of alternative energy sources. In theory, the generation of dihydrogen and its use as a source of thermal and electrochemical energy is a potential contribution to the solution of this problem. In practice, the implication of this so-called hydrogen economy has many immediate problems. The processes of H^+ reduction and H_2 oxidation are most readily accomplished by the noble metals, Pt and Pd, but these metals are expensive and

in short supply. The storage of dihydrogen is a major problem for other applications, such as hydrogen-powered automobiles.

The new model complexes and other synthetic material inspired by the hydrogenase and nitrogenase enzymes hold out the hope of replacing Pt- and Pd-based H^+ reduction/H_2 oxidation catalysts with those constructed from the base metals Fe and Ni. The design of these new catalysts will require the cooperation of scientists from the fields of biology/biochemistry, synthetic organometallic chemistry, and theoretical chemistry.

CHAPTER II

THEORETICAL METHODS

Introduction

Quantum chemistry is the use of quantum mechanics to solve problems in chemistry. It can be used to explain an experimentally-observed chemical phenomenon or to design a new molecule with specific chemical properties. The current widespread use of quantum chemistry is based largely on the development of "user-friendly" software packages that perform quantum mechanical computations.

The Schrödinger Equation

The total energy and all other observable properties of an atom or molecule are determined by the coordinates of the protons and electrons in that atom or molecule. A wavefunction is a function that relates all of the observable properties of an atom or molecule to the coordinates of the protons and electrons in that atom or molecule. If the exact wavefunction is known, then all of the observable properties may be computed using the appropriate operator. Schrödinger postulated that the total energy, E, of an atom or molecule can be determined from a wavefunction, Ψ, using the energy operator known as the Hamiltonian, $\hat{H}$.[213] The Schrödinger equation is shown in eq II-1.

$$\hat{H}\Psi = E\Psi \qquad \text{(II-1)}$$

Schrödinger's equation shows that the total energy of a system may be determined from that system's wavefunction, but does not show how this wavefunction may be determined. The exact form of the wavefunction for a given system is generally

not known. In practice, an approximate wavefunction is used to compute the energy and other properties of an atom or molecule.

The Variational Principle

The variational principle states that the energy calculated using an approximate wavefunction is necessarily higher than or equal to the true energy. In other words, the energy that one computes using an approximate wavefunction can never be lower than the true energy. In this way, the variational principle provides a criterion for evaluating approximate wavefunctions: the energy. When comparing two trial wavefunctions, the wavefunction that produces the lower energy is a better approximation to the true wavefunction. Generally, an initial trial wavefunction is constructed by the linear combination of two or more functions and the 'best' approximate wavefunction is found by systematic minimization of the coefficients of these functions.

The Born-Oppenheimer Approximation

The general form of the Hamiltonian for a molecule consisting of M nuclei and N electrons is given in eq II-2. The first two terms refer to the kinetic energy of the

$$\hat{H} = -\frac{1}{2}\sum_{i=1}^{N}\nabla^2{}_i - \frac{1}{2M_A}\sum_{i=1}^{M}\nabla^2{}_A - \sum_{i=1}^{N}\sum_{A=1}^{M}\frac{Z_A}{|R_A - R_i|} + \sum_{i=1}^{N}\sum_{j>i}^{N}\frac{1}{|R_i - R_j|} + \sum_{A=1}^{M}\sum_{B>A}^{M}\frac{Z_A Z_B}{|R_A - R_B|} \quad \text{(II-2)}$$

electrons and nuclei in the molecule, respectively. (In this equation, the capital letters (A, B, etc.) refer to nuclei and the lower case letters (i, j, etc.) refer to electrons.) The third, fourth, and fifth terms refer to nucleus-electron attractions, electron-electron repulsions, and nucleus-nucleus repulsions, respectively. Since the nucleus-electron attraction term depends on the positions of both the nuclei and the electrons, it impossible to separate

this Hamiltonian into terms that depend solely on the electronic positions and terms that depend solely on the nuclear positions. In other words, the position of a given electron depend on the positions of all of the other electrons and the positions of all of the nuclei and the position of a given nucleus depends on positions of all the other nuclei and the positions of all of the electrons. The Born-Oppenheimer approximation seeks a practical method to resolve this impasse. It states that since the nuclei are significantly heavier and therefore much slower moving than the electrons the kinetic energy of the nuclei can be ignored and the repulsion between the nuclei is effectively constant.[214] The resulting electronic Hamiltonian is given in eq II-3. Using eq II-3 the electronic energy of the molecule is computed for fixed positions of the nuclei.

$$\hat{H}_{elec} = -\frac{1}{2}\sum_{i=1}^{N}\nabla^2{}_i - \sum_{i=1}^{N}\sum_{A=1}^{M}\frac{Z_A}{|R_A - R_i|} + \sum_{i=1}^{N}\sum_{j>i}^{N}\frac{1}{|R_i - R_j|} \qquad \text{(II-3)}$$

The Hartree-Fock Approximation

An approximate wavefunction for an atom or molecule can be constructed as a product of functions that are referred to as either atomic or molecular orbitals, depending on the context. Pauli showed that an electronic wavefunction must be totally antisymmetric with respect to the interchange of any two electrons.[215] In general, an n-electron wavefunction that is totally antisymmetric with respect to the interchange of electrons may be constructed by forming a Slater determinant (eq II-4) of one-electron

$$\Psi(r_1, r_2 ... r_n) = \frac{1}{\sqrt{n!}} \begin{vmatrix} \chi_1(1) & \chi_2(1) & \cdots & \chi_n(1) \\ \chi_1(2) & \chi_2(2) & \cdots & \vdots \\ \vdots & \vdots & \ddots & \vdots \\ \chi_1(n) & \chi_2(n) & & \chi_n(n) \end{vmatrix} = \frac{1}{\sqrt{n!}} \left| \chi_1(1) \quad \chi_2(2) \quad \cdots \quad \chi_n(n) \right| \quad \text{(II-4)}$$

spin orbitals where the χ_x (χ_1, χ_2, etc.) are the molecular orbitals and the numbers given in parentheses are the labels of the electrons in those orbitals.[216-221] The rightmost form is a shorthand form of the full matrix given in the center of eq II-4.

The electronic Hamiltonian, given in eq II-3, cannot be solved exactly. The difficulty lies in the computation of the electron-electron repulsion term (the third term in eq II-3). The energy and position of every electron in an atom or molecule depends on the energy and position of every other electron in that atom or molecule. The main idea of the Hartree-Fock approximation is that each electron in atom or molecule resides in an orbital, χ, and experiences an average field produced by the other electrons. The Fock operator for energy of the ith electron is given in eq II-5. The application of the

$$\hat{f} = -\frac{1}{2}\nabla^2{}_i - \sum_{A=1}^{M} \frac{Z_A}{\left|R_A - R_i\right|} + \sum_{j \neq i}^{N} \frac{1}{\left|R_i - R_j\right|} \quad \text{(II-5)}$$

Fock operator to an orbital yields the energy of that orbital as shown in eq II-6. The use of a Slater determinant construction of the wave function and application of the

$$\hat{f}\chi_i = \chi_i \varepsilon_i \quad \text{(II-6)}$$

Slater-Condon rules yields the total electronic energy, E_{elec}, shownin eq II-7. The J and K terms are referred to as Coulomb and exchange terms, respectively.

$$E_{elec} = 2\sum_{a}\langle a|h|a\rangle + \sum_{n>m}^{N}\left(2\langle aa|bb\rangle - \langle ab|ba\rangle\right) = 2\sum_{a} h_{aa} + \sum_{ab}^{N}\left(2J_{ab} - K_{ab}\right) \qquad \text{(II-7)}$$

Basis Sets

The wavefunction of an atom is composed of the product of atomic orbitals. The functions that the calculation uses to build these optimized atomic orbitals are called basis functions. There are two main types of basis functions that are used. The Slater-type basis functions are exact solutions for the orbitals of a hydrogen-like atom (atoms with one electron such as H, He^{+}, Li^{2+}, etc).[222] These functions are of the mathematical form $\exp(-\zeta r)$, where ζ is referred to as the orbital coefficient. Slater-type basis functions are generally considered the best available in terms of accuracy. The gaussian basis function is the more commonly used, however because gaussian basis functions reduce the computational cost of evaluating the two-electron Coulomb and exchange integrals. Gaussian functions have the mathematical form $\exp(-\zeta r^2)$.[223-226] Although a single gaussian function is much poorer representation of an atomic orbital that a single Slater-type function, the linear combination of several gaussian functions can approximate the form of a Slater-type function, while retaining a significant savings in computational cost.

One measure of the quality of a given basis set is the number of basis functions used to represent each atomic orbital. In general, a basis set that uses N basis functions to represent each atomic orbital is referred to as an N zeta or NZ basis set. For example, a basis set that uses five basis functions to represent each atomic orbital is referred to as

a five zeta or 5Z basis set. As the number of basis functions increases, the computed energy decreases.

Two specific types of basis functions are diffuse functions and polarization functions. Diffuse functions are functions that have a small orbital coefficient value, ζ, and thus extend a significant distance from the atomic center. Diffuse functions are particularly important for the treatment of anions, since these species have significant electron density at distances far from the atomic or molecular center. Polarization functions are important for molecules. The formation of a molecule can lead to polarization of the atomic orbitals of the constituent atoms, relative to their forms in the isolated atoms. Polarization functions allow the atomic orbitals to polarize in the formation of a chemical bond. The polarization functions are empty atomic functions of a higher angular momentum than are normally used in the atom. For example, a set of polarization functions for the hydrogen atom are the 2p orbitals.

Correlation Energy

As the number and type of basis functions are increased, the Hartree-Fock energy will asymptotically approach a minimum value, known as the Hartree-Fock limit. The Hartree-Fock energy at the infinite basis set limit is larger than the true energy. The difference between the energy calculated at the Hartree-Fock limit and the true energy is referred to as the correlation energy (as shown in eq II-8). This energy arises due to

$$E_{corr} = E_{true} - E_{HF\ limit} \qquad \text{(II-8)}$$

fact that the Hartree-Fock single determinant wavefunction does not properly describe the correlated motion of electrons with different spins. In a real atom or molecule

motions of all of the electrons are correlated, meaning that the negatively charged electrons avoid the areas around one another. The use of a Slater determinant wave function in Hartree-Fock theory includes only exchange correlation meaning that only the electrons with the same spin are correlated in this method.

There are several methods for dealing with the electron correlation problem. Configuration interaction (CI) is one method of obtaining the correlation energy. It defines the true, fully correlated wavefunction of a system as a linear combination of the ground-state Hartree-Fock determinant and some number of excited state determinants.[227,228] In accord with the variational principle, the coefficients used in the linear combination of these determinants are those that minimize the computed energy. Perturbation theory is another method for obtaining the correlation energy. The central idea of this perturbation theory is that the true wavefunction is largely similar to the Hartree-Fock single determinant wavefunction. Perturbation theory treats electron correlation as a perturbation of the Hartree-Fock single determinant wavefunction. Mathematically, this entails expanding the true wavefunction as a power series. The most commonly used implementation of perturbation theory is Møller-Plesset perturbation theory.[229-231] Configuration interaction and Møller-Plesset perturbation theory are both computationally intense, and generally intractable for all but the smallest molecules.

Density Functional Theory

Hartree-Fock, configuration interaction, and perturbation theory computations all seek to determine the physical properties of an atom or molecule by determining its

many-body wavefunction. This task is quite complicated since the wavefunction is determined by the 3N spatial coordinates and N spin coordinates of the N electrons. Density functional theory (DFT) seeks to determine the total energy (including the correlation energy) and other physical properties of an atom or molecule using only the 3 spatial coordinates of the electron density. The major advantage of DFT calculation is that it provides an accurate estimate of the total electronic energy at a computational cost similar to that of a Hartree-Fock calculation.

The work of Kohn, Hohenberg, and Sham provided the foundation for density functional theory. The Hohenberg-Kohn Theorem states that the ground-state electron density uniquely specifies the ground-state wavefunction and all other properties, and that the ground-state electron density is the one that minimizes the computed energy.[232] Kohn and Sham developed a method for computing the ground-state electron density and using it to compute ground-state energy.[233] This method relates the system of interest to a fictitious system of non-interacting electrons that experience the same external potential, υ_{ext}, as the real system. The Kohn-Sham Hamiltonian can be written as shown in eq II-9. The first and second terms in eq II-9 are the kinetic energy and

$$\hat{H}_{KS} = -\frac{1}{2}\nabla^2 + \upsilon_H + \upsilon_{XC} + \upsilon_{ext} \qquad \text{(II-9)}$$

electron-electron repulsions terms. The third term, υ_{xc}, is the exchange-correlation term. The exact functional dependence of the υ_{xc} term on the electron density is not known. The first, second, and fourth terms are computed in much the same way as their counterparts in Hartree-Fock Theory. In theory, DFT obviates the need to compute a

wavefunction, however, Kohn and Sham found it convenient to define a wavefunction in order to compute the electron density.

The Hohenberg-Kohn Theorem proves that a relationship exists between the physical properties of an atom or molecule and electron density, but does not define this relationship. A major, unsolved problem of density functional theory is to determine the precise functional dependence of the energy on the electron density. In theory, the exact exchange energy is given by Hartree-Fock theory and only the functional dependence of the correlation energy is not known. In practice, more accurate energies result from the optimization of both exchange and correlation functionals. Modern correlation-exchange functionals attempt to approximate the true correlation-exchange functional. Most modern DFT functional contain empirical corrections that allow them to more accurately reproduce the experimentally-observed thermodynamics of small-molecule reactions.

There are several different types of approximate correlation-exchange functionals that are currently used. Hybrid density functional methods add some fraction of exact (Hartree-Fock) exchange to the energy calculated using the exchange functional. Pure density functional methods do not use any exact exchange. Local functionals directly relate the energy and electron density. Gradient-corrected functionals explicitly consider both the density and its first derivative (the gradient).

The performance of approximate density functionals are typically evaluated by their ability to accurately reproduce experimentally determined reaction thermodynamics. In terms of this ability, currently, the best density functionals are

hybrid, gradient-corrected exchange-correlation functionals such as B3LYP, which was shown to reproduce experimental enthalpies of formation to within 5 kcal mol^{-1} for a set of 376 molecules.[234] The B3LYP functional gets its name from the 3-parameter exchange functional of Becke (B3)[235] and the correlation functional of Lee, Yang, and Parr (LYP)[236].

CHAPTER III

SYNERGY BETWEEN THEORY AND EXPERIMENT AS APPLIED TO H/D EXCHANGE ACTIVITY ASSAYS IN [FeFe]H_2ase ACTIVE SITE MODELS*

Introduction

In view of its application to fuel cell development, research into hydrogen activation remains a forefront area for chemists, physicists, and biologists[237]. A rekindling of opportunity and excitement in this field of chemistry has come from the delineation of simple catalytic sites of hydrogenase enzymes as displayed by protein crystal structures published within the last decade.[128,138-141,169-171] These active sites hold out promise of using complexes comprised of base metals such as iron or a combination of Fe/Ni instead of platinum metal as catalysts for such important technical processes.

The starting point for the chemist is the preparation of synthetic analogues of composition and structure as similar as possible to the natural active site, with the expectation that the electronic properties of the latter might be reproduced in the model complex, ultimately engendering similar function.[238] In the case of [FeFe] and [NiFe] hydrogenases, the fortunate presence of diatomic ligands, well known to serve as reporters of electron density, has facilitated a comparison between the natural and the synthetic active sites by providing credible reference points for the use of spectroscopy in assigning redox levels for the enzyme at various stages of catalytic activity or

* Reprinted with permission from "Synergy Between Theory and Experiment as Applied to H/D Exchange Activity Assays in [Fe]H_2ase Active Site Models" by Tye, J. W.; Hall, M. B; Georgakaki, I. P.; Darensbourg, M. Y. *Adv. Inorg. Chem.* **2004**, *56*, 1-24. Copyright 2004 by Elsevier Inc.

deactivation.[172] These comparisons have encouraged a unique synergism between computations, spectroscopy and synthetic model development.[172,205] The work described herein is an attempt to move such interactions even closer to the goal of predicting properties needed for synthetic catalysts designed for hydrogen activation.

Hydrogenases are biological catalysts responsible for H_2 uptake or production, in which the required H_2 cleavage has been established to occur in a reversible and heterolytic manner (H^+/H^-).[239] This activity is typically assayed by H/D exchange reactivity in H_2/D_2O or $H_2/D_2/H_2O$ mixtures.[239-242] The active site of iron-iron hydrogenase, [FeFe]H_2ase,[169-172] consists of a 2Fe2S butterfly core in which the sulfur atoms are linked by three light atoms of undetermined identity, but typically modeled by either propane dithiolate (pdt), or $^-SCH_2N(R)\ CH_2S^-$. The active site is connected to the first 4Fe4S cluster of the electron-transport chain via a bridging cysteine. Although unusual in nature, the diatomic ligands (CO, CN^-) that fill the remaining coordination sites of each metal center harken to the genesis of the ancient organisms and the harsh terrestrial conditions under which these enzymes evolved.[243]

The [FeFe]H_2ase enzyme exists in at least three different redox levels. The oxidized-active form, assigned as $Fe^{II}Fe^{I}$, is the state that takes up and activates H_2.[172] In this state both metals are in octahedral coordination geometry by virtue of a μ-CO group, and the distal Fe (the one further removed from the 4Fe4S cluster), is tentatively assigned as Fe^{II}. This iron is coordinated by a labile H_2O molecule in the oxidized form[169], and a CO in the CO-inhibited oxidized form[170] as shown in Figure III-1.

Photolytic (CO-loss) conditions allow the CO inhibited form of enzyme to regain activity as assayed by H/D exchange in H_2/D_2O mixtures.[244]

The rapid development of [FeFe]H_2ase active site model chemistry benefited greatly from early organometallic studies of (μ-S_2)[$Fe(CO)_3$]$_2$, (μ-SRS)[$Fe(CO)_3$]$_2$, and (μ- SRS) [$Fe(CO)_2(L)$]$_2$. Reihlen reported the synthesis of (μ-$SEt)_2$[$Fe(CO)_3$]$_2$ in

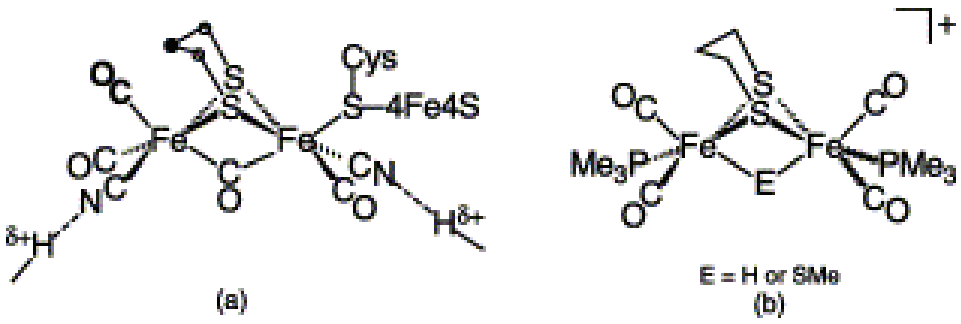

Figure III-1. Stick drawing structures of (a) CO-inhibited oxidized form of [FeFe]H_2ase active site; and (b) $Fe^{II}Fe^{II}$ functional models. The specific orientation of the PMe_3 ligands is E dependent: E = H, transoid; E = SMe, cisoid.

1929.[245] In the 1960s Poilblanc[246] examined the ligand exchange process for a series of complexes of the form (μ-$SR)_2$[$Fe(CO)_3$]$_2$. Poilblanc[246] and Treichel[247] investigated the attack of electrophiles on the metal–metal bond of (μ-$SR)_2$[$Fe(CO)_2(L)$]$_2$ complexes to generate $\{(\mu\text{-E})(\mu\text{-SR})_2[Fe(CO)_2(L)]_2\}^+$. In the 1980s, Seyferth[248] developed the chemistry of the bridged dithiolate complexes of the form (μ-$S(CH_2)_xS$)[$Fe(CO)_3$]$_2$.

Diiron(II) complexes of the type $\{(\mu\text{-E})(\mu\text{-pdt})[Fe(CO)_2(PMe_3)]_2\}^+$ (E=H or SMe) as seen in Figure III-1 were examined as potential structural/spectroscopic models of the

[FeFe]H_2ase active site, using PMe_3 as a substitute for the reactive cyanide ligands.[202,203,249]

With the encouragement of Prof. Dieter Sellmann in 2001, and using his experimental protocol[165] we explored the reactivity of $Fe^{II}Fe^{II}$ complexes toward D_2 and D_2/H_2O mixtures. In order to establish the factors affecting such reactions, solutions of these complexes under various conditions were pressurized with D_2 in a medium pressure NMR sample tube. The ^2H NMR spectroscopic monitor of the reactions indicated the build-up of D-incorporated species.[202,203,249] Control experiments established that the activation of D_2 in these reactions was facilitated by light and was inhibited by coordinating solvents or the addition of CO.[202,203] This last feature is in agreement with the CO-inhibition of [FeFe]H_2ase activity and strongly suggests the need for creation of an open site prior to D_2 binding to Fe^{II}.

The relatively simple active site of [FeFe]H_2ase and the limited involvement of the protein as ligands in the first coordination sphere has appealed to computational chemists as an appropriate system to explore by Density Functional Theory.[205-209,250] The calculations published to date have focused on correlating ν(CO)/ν(CN) vibrational frequencies of the different redox levels of the diiron active site with model complexes, on defining plausible possibilities for the unique three light-atom S to S linker, and on delineating mechanistic possibilities for H_2 activation.[205,207,209,211,212,250] Until now, none of the published computational models have attempted to explore how the [FeFe]H_2ase active site performs the activity assay, i.e., the H/D exchange reactivity in H_2/D_2O or D_2/H_2O mixtures. Herein, DFT calculations are described that suggest reasonable

mechanistic explanations for the experimentally observed H/D exchange reactivity, not of the enzyme active site, but of $Fe^{II}Fe^{II}$ functional model complexes. New experiments have also been carried out in order to test the hypotheses implied by some of the individual steps of the proposed mechanism, which were calculated to be energetically feasible.

Experimental Section

Reagents used in the preparation of starting materials, procedures, and instrumentation have been described earlier.[202,203]

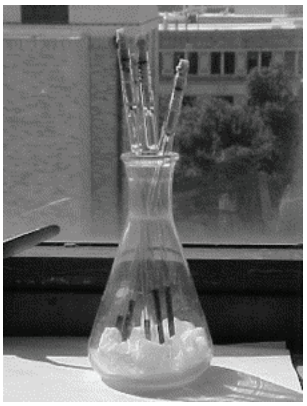

Figure III-2. Medium pressure NMR sample tubes containing solutions of the diiron complexes, pressurized with 10 bar D_2 and were exposed to sunlight on the windowsill.

H/D exchange in D_2/H_2O mixtures with Fe^IFe^I complexes as catalyst

In a typical experiment 0.8 mL portions of solutions made from 0.029 g (μ-pdt)$[Fe(CO)_2(PMe_3)]_2$ in 1 mL CH_2Cl_2 were placed in medium-pressure NMR sample tubes (Wilmad, 528-PV-7) together with 2 μL H_2O. The tubes were degassed,

pressurized with 10 bar D_2 and exposed to sunlight as shown in Figure III-2. ^{2}H NMR spectra were taken at time intervals to follow the formation of HOD.

Reactions of {(μ-H)(μ-pdt)[Fe(CO)$_2$(PMe$_3$)]$_2$}$^+$[PF$_6$]$^-$ with acetone

A solution made from 0.095 g {(μ-H)(μ-pdt)[Fe(CO)$_2$(PMe$_3$)]$_2$}$^+$[PF$_6$]$^-$ in 10 mL acetone was exposed to sunlight for 50 min. The acetone was removed under vacuum and the resulting solid was redissolved in 7–10 mL CH_2Cl_2. The IR spectrum (ν(CO) region only) of this solution showed a mixture of the starting complex (bands at 2031(s) and 1978(s) cm^{-1}) and the presumed acetone complex (bands at 2031(s), 1989(m), 1978(s), and 1945(s) cm^{-1}). After bubbling CO through the solution for 5 min, the IR spectrum showed the disappearance of the ν(CO) bands at 2031, 1989, 1978, and 1945 cm^{-1}, while the ν(CO) bands at 2031 and 1978 cm^{-1} regained intensity. A similar reaction was carried out in an NMR sample tube using 10 mg of {(μ-H)(μ-pdt)[Fe(CO)$_2$(PMe$_3$)]$_2$}$^+$ [PF$_6$]$^-$ in 0.8 mL acetone-d_6. After exposure to sunlight for 1 h the ^{1}H NMR spectrum showed two sets of resonances in the upfield region. A quartet centered at −7.7 ppm with J_{H-P} coupling constants of 29.7 and 21.3 Hz was assumed to be the acetone complex, {(μ-H)(μ-pdt)[Fe(CO)$_2$(PMe$_3$)][Fe(CO)(PMe$_3$)(acetone)]}$^+$; and a triplet centered at −15.0 ppm with J_{H-P} 22.8 Hz, derived from the parent compound, {(μ-H)(μ-pdt)[Fe(CO)$_2$(PMe$_3$)]$_2$}$^+$. The ^{31}P{^{1}H} NMR spectrum displayed a doublet centered at 24.3 ppm and another doublet centered at 22.4 ppm, both with J_{P-P} coupling of 7.4 Hz. Three microliters of CH_3CN were added and the sample was maintained in the dark for 30 min. The ^{1}H NMR spectrum of this sample showed the disappearance of the hydride resonance at −7.7 ppm and the appearance of a new hydride resonance as a

doublet of doublets centered at −10.9 ppm. This hydride signal was identical to that of a bona fide sample of $\{(\mu\text{-H})(\mu\text{-pdt})[Fe(CO)_2(PMe_3)][Fe(CO)(PMe_3)(CH_3CN)]\}^+$, whose preparation and full characterization was reported earlier.[251]

Computational Details

All DFT calculations were performed using a hybrid functional [the three-parameter exchange functional of Becke (B3)[235] and the correlation functional of Lee, Yang, and Parr (LYP)[236]] (B3LYP) as implemented in Gaussian 98[252]. The iron, sulfur, and phosphorus atoms used the effective core potential and associated basis set of Hay and Wadt (LANL2DZ)[253,254]). For iron, the two outermost *p* functions were replaced by the re-optimized 4*p* functions as suggested by Couty and Hall.[255] For phosphorus and sulfur, the basis set was augmented by the *d* polarization function of Höllwarth *et al.*[256] Dunning's correlation-consistent polarized valence double zeta basis set (cc-pVDZ)[257] was employed for the CO ligands, H_2O, CH_2Cl_2, the carbonyl group of $CH_3C(O)CH_3$, the nitrile group of CH_3CN, hydridic hydrogens, and dihydrogen. The carbon and hydrogen atoms of the ethane dithiolate bridge, the hydrogen atoms of PH_3, and the methyl groups of CH_3CN, $CH_3C(O)CH_3$, and $P(CH_3)_3$ use Dunning's double zeta basis (D95).[258,259] Unless otherwise noted, all geometries are fully optimized and confirmed as minima or *n*-order saddle points by analytical frequency calculations at the same level. Transition states were fully optimized beginning from either a scan of the metal–ligand distance or the Quadratic Synchronous Transit (QST3) method as implemented in Gaussian 98.

NMR shielding tensors were calculated using the Gauge-Independent Atomic Orbital (GIAO) method as implemented in Gaussian 98.[260-262] The basis sets and level of theory are the same as used in the geometry optimizations and frequency calculations mentioned above.

Results and Discussion

Homovalent $Fe^{II}Fe^{II}$ complexes may be derived from $Fe^{I}Fe^{I}$ precursors via binuclear oxidative addition of electrophiles such as H^+ or SMe^+ yielding $\{(\mu\text{-H})(\mu\text{-pdt})[Fe(CO)_2(PMe_3)]_2\}^+$ and $\{(\mu\text{-SMe})(\mu\text{-pdt})\ [Fe(CO)_2(PMe_3)]_2\}^+$, respectively, from $(\mu\text{-pdt})[Fe(CO)_2(PMe_3)]_2$.[202,203,249] The role of the PMe_3 ligands in the precursor complex (analogues to cyanide in the enzyme active site) is to increase both the basicity of the $Fe^{I}Fe^{I}$ bond and to stabilize the $Fe^{II}Fe^{II}$ oxidation level of the resulting compound. The protonation of $\{(\mu\text{-pdt})[Fe(CO)_2(CN)]_2\}^{2-}$ to yield $\{(\mu\text{-H})(\mu\text{-pdt})[Fe(CO)_2(CN)]_2\}^-$ is complicated by the basicity of the cyanide nitrogen, which leads to decomposition presumably via the loss of HNC (or HCN).[183,202,263] The $\{(\mu\text{-SMe})(\mu\text{-pdt})[Fe(CO)_2(CN)]_2\}^-$ analogue was prepared by a different route to obviate the electrophilic attack on the cyanide nitrogen.[264]

Using ^2H NMR spectroscopy as an *in situ* reaction monitor, the $Fe^{II}Fe^{II}$ complexes were assayed for hydrogenase-like activity. In the presence of D_2, the observation of incorporation of deuterium into the bridging hydride position of the diiron complex, indicated activation of D_2. Consistent with this result, even in the absence of added water, H_2 and D_2 mixtures underwent H/D scrambling with $\{(\mu\text{-H})(\mu\text{-pdt})[Fe(CO)_2(PMe_3)]_2\}^+$ as a catalyst, concomitantly with H/D exchange into the μ-H

position. Experiments under various conditions showed that in all cases the H/D scrambling process was facilitated by light and inhibited by the coordinating solvents, CH_3CN and acetone, or by the addition of CO. These conclusions suggested that an open site is required for H_2 activation and that the required open site is created under photolytic CO-loss conditions (as in the CO inhibited form of the enzyme). As confirmation of this view, ^{13}CO was incorporated into the model complexes under similar photolytic conditions.[251] From such test reactions, $\{(\mu\text{-H})(\mu\text{-pdt})[Fe(CO)_2(PMe_3)]_2\}^+$ was found to serve as a functional model of [FeFe]H_2ase in the catalytic isotopic scrambling of D_2/H_2O mixtures. As in the CO-inhibited oxidized enzyme, our model catalysts require photolytic conditions to affect CO-loss and to achieve activity.

Analogous studies found that $\{(\mu\text{-SMe})(\mu\text{-pdt})[Fe(CO)_2(PMe_3)]_2\}^+$ can also catalyze the H/D exchange reaction in D_2/H_2O mixtures under similar conditions as the μ-H analogue. The μ-SMe derivative, however, does not catalyze the H_2/D_2 scrambling process under standard anhydrous conditions. Neither was there any evidence for formation of MeSD or $\{(\mu\text{-D})(\mu\text{-pdt})[Fe(CO)_2(PMe_3)]_2\}^+$ when solutions of the μ-SMe complex were pressurized with D_2. In other words, H/D exchange reactions employing $\{(\mu\text{-SMe})(\mu\text{-pdt})[Fe(CO)_2(PMe_3)]_2\}^+$ do not proceed via a $\{(\mu\text{-D})(\mu\text{-pdt})[Fe(CO)_2(PMe_3)]_2\}^+$ intermediate. These results taken together suggest that D_2/H_2O scrambling can occur independently of μ-H/D_2 scrambling and that the former may proceed via reversible deprotonation of $\{(\mu\text{-E})(\mu\text{-S}(CH_2)_xS)[Fe(CO)_2(PMe_3)][Fe(L)(L')(\eta^2\text{-}H_2)]\}^+$.

Based on the above experimental results, and given the lability of the CO ligands under photolytic conditions, the mechanism presented in Scheme III-1 was proposed as a

Scheme III-1

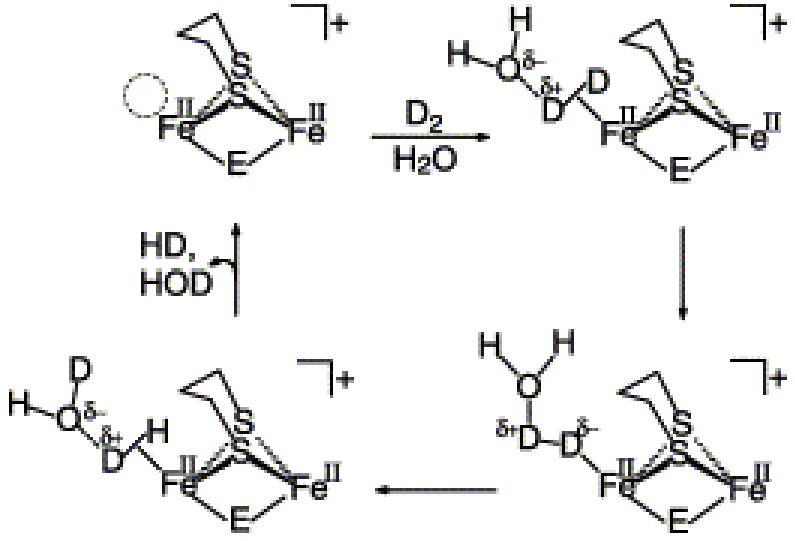

reasonable first attempt to accommodate the observations.[265] Scheme III-1 is not intended to suggest the location of the open site, but is drawn in this way to accent the similarities between our model and the active site of [FeFe] hydrogenase, given in Figure III-1. In fact, products isolated from solvent inhibition studies, *vide infra*, suggested that in the case of $\{(\mu\text{-H})(\mu\text{-pdt})[Fe(CO)_2(PMe_3)]_2\}^+$ the open site should be *cis* to the μ-H.[251]

The computations presented herein use Scheme III-1 as a starting point to support and thoroughly explore such mechanistic possibilities in terms of the energetically favorable possibilities for the open site and the detailed steps of the H_2 activation.

Choice and validation of the computational model

Only minor experimental differences were observed for H/D exchange catalysis using different μ-S$(CH_2)_x$S bridges in {(μ-H)(μ-S$(CH_2)_x$S)[Fe$(CO)_2(PMe_3)]_2$}$^+$, where x = 2 (ethanedithiolate ≡ edt) or x = 3 (propanedithiolate ≡ pdt). It seems therefore likely that the reaction proceeds via a similar mechanism for these two dithiolate bridges. The molecular structures, derived from X-ray crystallography for the two- and three-carbon bridged compounds, overlay very well.[203] If only the Fe, S, and P atoms and CO ligands are considered, the RMS deviation for the two molecules is 0.098 Å; inclusion of the carbon atoms involved in S-C bonding increases the RMS deviation to 0.227 Å. Because of the structural and experimental similarities we have used the smaller edt bridge in the computations as it is computationally less expensive and the higher symmetry of this molecule limits the number of isomers to be considered at each step in the reaction.

Most of the calculations presented use what we designate as the small model, {(μ-H)(μ-edt)[Fe$(CO)_2$(**PH_3**)$]_2$}$^+$, where the PMe_3 ligand has been replaced by the simple phosphine, PH_3. In order to test the validity of this model, we have computed the bond dissociation energies as defined in eqs III-1 and III-2.

$$[Fe_2L]^+ \rightarrow [Fe_2]^+ + L \qquad \text{(III-1)}$$

$$\Delta E_0 = [E_0([Fe_2]^+) + E_0(L)] - E_0([Fe_2L]^+) \qquad \text{(III-2)}$$

For this process, the ΔE_0, is the total energy, including only the zero-point correction, of each independently optimized fragment. Values determined for Fe–P, Fe–CO_{ap}, and Fe–CO_{ba} are listed in Table III-1. Calculations comparing the full model,

Table III-1. Comparison of the Small and Full Models: Computed Bond Energies

M-L	ΔE_0 small model[a]	ΔE_0 full model[b]
Fe-P	+34.2	+50.0
Fe-COap[c]	+39.6	+39.2
Fe-CObas[c]	+37.3	+36.6

[a] $\{(\mu\text{-H})(\mu\text{-edt})[Fe(CO)_2(PH_3)]_2\}^+$. [b] $\{(\mu\text{-H})(\mu\text{-edt})[Fe(CO)_2(PMe_3)]_2\}^+$. [c] Designation of apical and basal derived from such positions in the edge-bridged square pyramids present in $(\mu\text{-edt})[Fe(CO)_2(PR_3)]_2$.

given in Table III-1, $\{(\mu\text{-H})(\mu\text{-edt})[Fe(CO)_2(\mathbf{PMe_3})]_2\}^+$, and the small model $\{(\mu\text{-H})(\mu\text{-edt})[Fe(CO)_2(\mathbf{PH_3})]_2\}^+$, show that the Fe-P bond of Fe-PH_3 is significantly weaker than that of Fe-PMe_3. However, the energy of a given Fe-CO bond is very similar for the two models. Thus reaction steps that involve PMe_3 ligand-loss directly are poorly modeled by PH_3, while the reactivity of the Fe-CO bond (or other Fe-L bonds) in the small model should generally parallel that of the larger model.

A major supposition of this computational mechanistic study is the separation of the photochemical and thermal reaction events. It has been assumed, Scheme III-1, that a photochemical reaction takes place to generate a coordinatively unsaturated intermediate that subsequently reacts thermally with dihydrogen. In other words, we are assuming that the reaction is photochemically initiated but that light plays no role in later steps of the reaction (for at least one cycle).

The iron atoms of the reactant $\{(\mu\text{-H})(\mu\text{-S}(CH_2)_x\text{S})[Fe(CO)_2(PMe_3)]_2\}^+$ are both electronically and coordinatively saturated. Therefore, even a minimal mechanism must call for the first step to be the creation of an open site on one of the iron centers via

either an internal rearrangement or ligand loss. Unfortunately, the need for continuous photolysis makes it difficult to delineate further mechanistic details by experiment alone. As the reaction progress of dark-quenched samples was monitored by ^{1}H or ^{2}H-NMR spectroscopy, only the products and reactants were observed. There was no indication of intermediates. The displaced ligands, PMe_3 and CO, were trapped in the closed system of the medium pressure NMR sample tube and, in the absence of photolysis, returned to displace weak ligands such as η^2-H_2. In this context, density functional theory was used to examine energetically reasonable intermediates for possible reaction paths.

Creation of the open site

Figure III-3 shows five possible paths, designated a–e, generating η^2-H_2 complexes from **1** via open site intermediates. Note that paths a–d, leading from **1** to species **7**–**10**, are all overall endothermic processes. Paths a–c can be resolved into the endothermic creation of the open site, followed by the exothermic coordination of dihydrogen. Species **2**, **3**, and **4** are generated by photo-ejection of either CO or a phosphine ligand via paths a, b, and c. In path d, irradiation initiates the shift of the hydride from fully bridging between the two irons to terminal on one of the iron atoms. The final path calls for photolysis to heterolytically cleave the Fe-S bond in order to convert the face-bridged bioctahedral structure of the reactant into the edge-bridged complex indicated in Figure III-3.

The first three paths in Figure III-3 all involve terminal-ligand dissociation. With either the small or the full model, the calculated Fe-CO bond dissociation energies are in the order: $Fe\text{-}CO_{apical}$>$Fe\text{-}CO_{basal}$. (See Table III-1 for apical/basal definitions. These

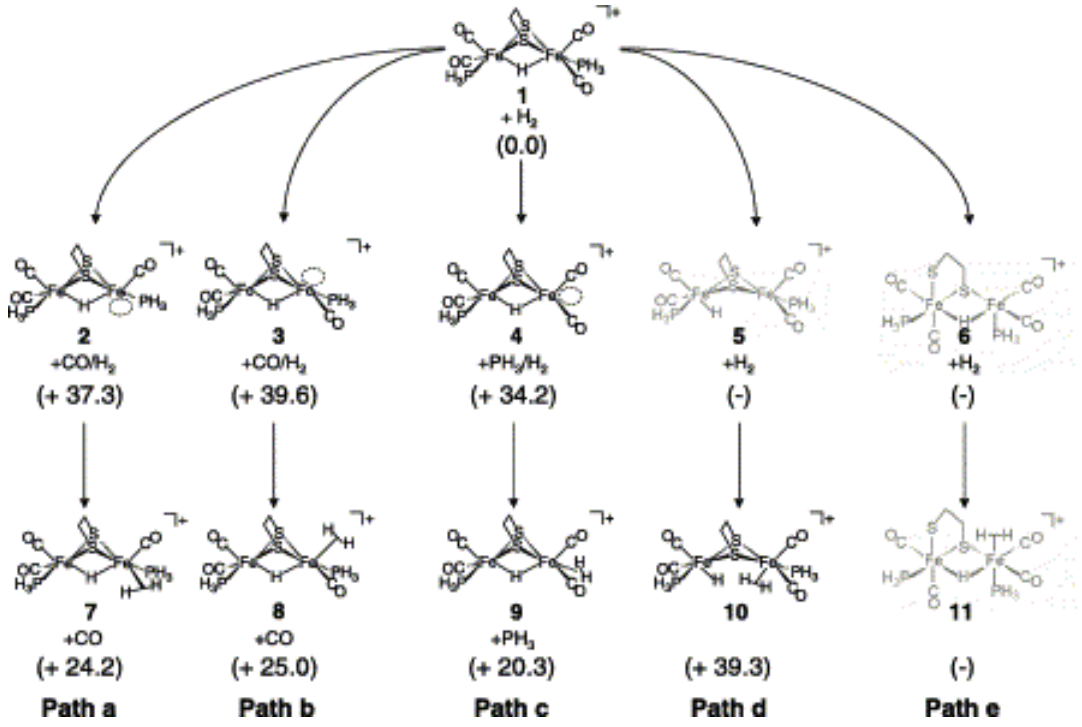

Figure III-3. Creation of the open site and dihydrogen coordination. The energies indicated are relative to $E_0(1) + E_0(H_2) = 0$ and are given in kcal mol^{-1}. (Species corresponding to **5**, **6**, and **11** were not located.)

energies are calculated as the difference in the total energies, ΔE_0, of the separately optimized products and reactants, *vide supra*.) Noted in Table III-1 is the Fe-P bond energies for Fe-PH_3 and Fe-PMe_3 showing that Fe-PMe_3 is 10 kcal mol^{-1} stronger than Fe-CO. Due to the large amount of energy available from the sunlight (estimated from the cutoff of Pyrex glass at λ = 280 nm to be about 100 kcal mol^{-1}), the bond energies alone do little to differentiate the three ligand-loss mechanisms. Three experimental facts, however, suggest that CO loss is more likely than phosphine loss.[203] First, photolysis of $\{(\mu\text{-H})(\mu\text{-pdt})[Fe(CO)_2(PMe_3)]_2\}^+$ under a ^{13}CO atmosphere leads to

$^{12}CO/^{13}CO$ exchange with no displacement of PMe_3. Second, the photolysis of the reactant, in the presence of 1 equivalent of CH_3CN, forms $\{(\mu\text{-H})(\mu\text{-pdt})[Fe(CO)_2(PMe_3)][Fe(CO)\ (CH_3CN)(PMe_3)]\}^+$. (This complex is shown by X-ray crystallography to contain a basal CH_3CN.[251] These processes most likely occur via dissociative mechanisms. Finally, the addition of PMe_3 to a solution of the starting materials results in deprotonation of the bridging hydride. It is likely, therefore, that a mechanism that calls for phosphine loss would lead to decomposition via this route. While the formation of $DPMe_3^+$ is observed after prolonged photolysis, it does not occur on the same time scale as that for H/D exchange. Thus, the basal CO loss mechanisms seem the most likely.

The fourth and fifth paths share several similarities. Both call for a ligand which bridges the iron centers in the starting material to shift away from one of the metal centers and bind to a single iron. Minima corresponding to complexes **5** and **6** could not be located. Unrestrained geometry optimization with a variety of ligand starting geometries (both semi-bridging and non-bridging) led back to the fully-bridging $\{(\mu\text{-H})(\mu\text{-edt})[Fe(CO)_2(PH_3)]_2\}^+$ complex **1**, Figure III-3.

The difficulty in optimizing a structure analogous to **5** did not extend to the η^2-H_2 adduct, **10**. In fact, a transition state has been found that directly connects species **1** and **10** of Figure III-3. As shown in Figure III-4, species **10**, should it be formed, has a very low barrier, +0.7 kcal mol^{-1}, to proton exchange via a trihydride transition state. In addition, the hydride shift mechanism, forming **10** directly from **1** and H_2, can also explain the inhibition of H/D exchange by added CO and coordinating solvents, as well

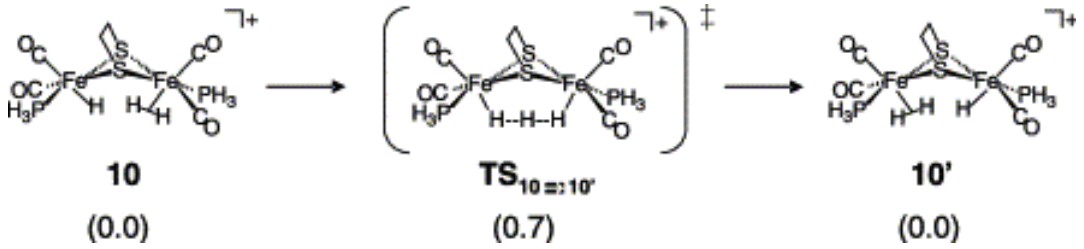

Figure III-4. Hydrogen exchange without ligand loss. Complex **10** over a low energy C_2 symmetric transition state to the structural isomer **10'**. Relative energies are given in kcal mol^{-1}.

as D_2/H_2O scrambling if complex **10** is formed. In fact, the process of forming CO or acetone analogues of species **10** from complex **1**, is less endothermic than formation of the η^2-H_2 species, a result that reflects the better binding ability of CO and acetone to the Fe^{II} center. Furthermore, the calculated gas phase proton affinity shows that the acidity of the bound dihydrogen in species **10** is comparable to that of species **7**, **8**, and **9**.

For the reasons described above, species **10**, if accessible, should be competent for H/D exchange of H_2/D_2 and D_2/H_2O mixtures. Species **10**, however, lies 39.3 kcal mol^{-1} above its separated components, complex **1** and dihydrogen, and the transition state from complex **1** to **10** lies an additional 5 kcal mol^{-1} higher. For a normal thermal reaction, such a barrier is higher than the energy required to break the M-L bonds and decompose the compound. Thus, for this process to occur, the high-energy excited state molecule would have to bind dihydrogen more rapidly than it decays by ligand loss. In fact, during the short lifetime of an excited state molecule the unimolecular process of ligand loss

seems far more likely than the bimolecular process of dihydrogen capture. Furthermore, it should be noted that the computed barrier for dihydrogen loss to reform complex **1** is only 5 kcal mol^{-1}.

No minima resembling species **6** or **11** in Figure III-3 were located. All attempts at optimization of these potential intermediates resulted in previously optimized species **1** and **12**, respectively. Interestingly, the thermodynamics of **1** + H_2 → **12** (+27.8 kcal mol^{-1}) represents the lowest energy cleavage of η^2-H_2, not involving water (Figure III-5).

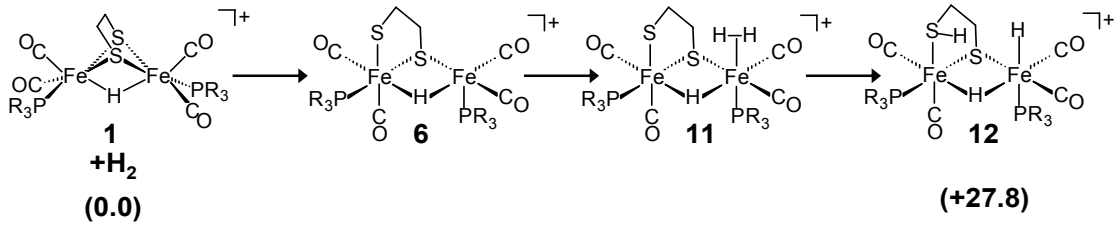

Figure III-5. Insertion of dihydrogen. Complex **12** is formed the formal insertion of H_2 into the Fe-S bond. The energy of complex **12** is relative to the energy of **1** + H_2 and given in kcal mol^{-1}.

Our conclusion is that paths d and e of Figure III-3 are the least likely and thus these paths will not be considered further.

Dihydrogen complexes

For the first three paths in Figure III-3 the coordination of dihydrogen to the open site forming η^2-H_2 species **7**, **8**, and **9**, are comparably, exothermic processes (−13.1,

−14.6, and −13.9 kcal mol^{-1}, respectively). The similarity of these values does not permit discrimination between the terminal ligand-loss mechanisms. The binding of dihydrogen to complex **1**, without ligand loss, to give species **10** is a very endothermic process (+39.3 kcal mol^{-1}), *vide supra*.

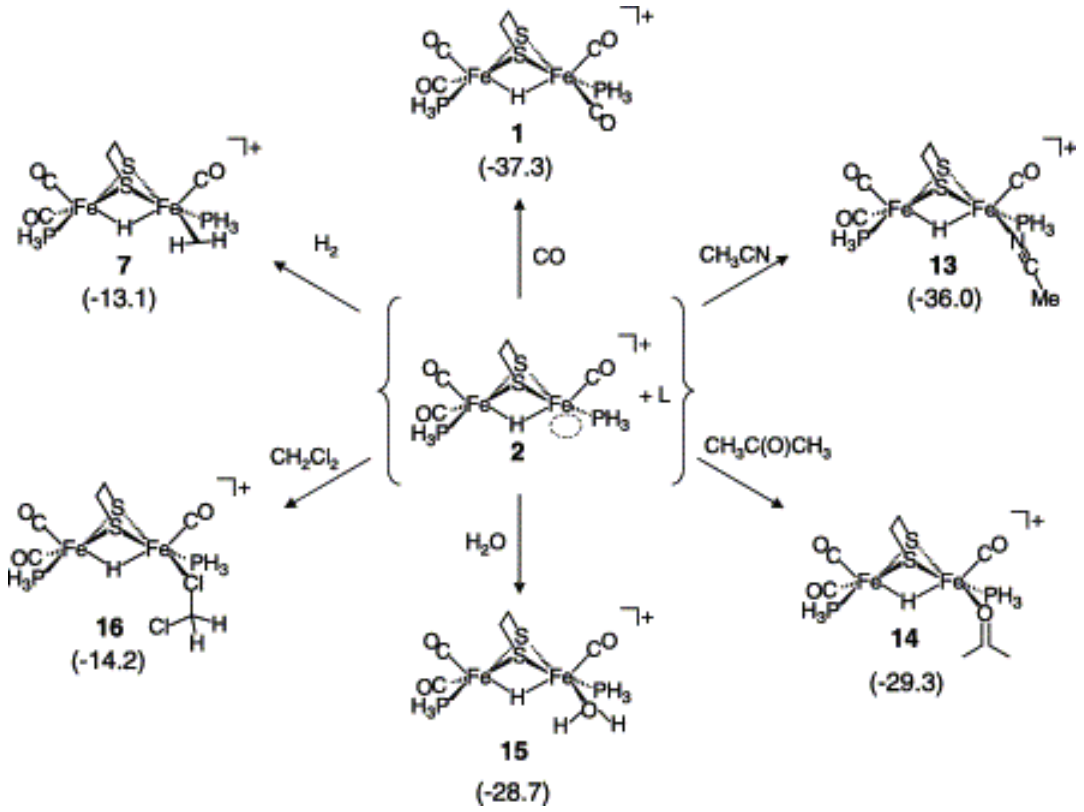

Figure III-6. Trapping the open site. The energy released by coordination of a series of relevant ligands to the open site of **2**. Bond energies are calculated according to **eq III-4** and are given in kcal mol^{-1}.

H/D exchange inhibition

Figure III-6 presents results of binding a variety of potential ligands or solvent molecules to the basal open site of **2**. The energies, determined according to **eqs III-3 and III-4**, include zero-point corrections only.

$$[Fe_2]^+ + L \rightarrow [Fe_2L]^+ \quad \text{(III-3)}$$

$$\Delta E_0 = E_0([Fe_2L]^+) - [E_0([Fe_2]^+) + E_0(L)] \quad \text{(III-4)}$$

In all these cases, formation of the iron–ligand bond is calculated to be an exothermic process. Consistent with their roles as inhibitors of H/D exchange catalysis, the coordinating solvents, acetonitrile and acetone, bind some 15–20 kcal mol^{-1} more strongly to the iron center than does dihydrogen. Dichloromethane, on the other hand, is similar to dihydrogen. Furthermore, the isolation of a stable acetonitrile complex, vide supra, is explained by the fact that the strengths of the Fe-NCMe and Fe-CO bonds are similar (ΔE_0 = −36.0 vs. −37.3 kcal mol^{-1}). Paradoxically, water, which is known to accelerate the rate of H/D exchange into the μ-H position, coordinates to the iron with the same affinity as acetone and much more strongly than H_2.

We have not systematically examined the open site capture process for species **3** and **4**. However, it seems reasonable that the same trend as observed for **2**, and presented in Figure III-6 will be followed for **3** and **4**: (i.e. Fe-CO> Fe-NCMe>Fe-O=$C(CH_3)_2$≈Fe-OH_2> Fe-H_2≈Fe($ClCH_2Cl$)). In other words, CO, acetonitrile, and acetone (and H_2O) should be inhibitors of H/D exchange regardless of the location of the open site.

Cleavage of the H-H bond

We have explored both water-free and water-assisted routes to the cleavage of the H-H bond in certain η^2-H_2 species of Figure III-3. For the former route, the bridging thiolate sulfur donor and the bridging hydride were considered as possible internal bases for the heterolytic cleavage of H_2 from each of the dihydrogen species, Figure III-7. In the water-assisted routes, H_2O is used as an external base to deprotonate H_2, Figure III-8.

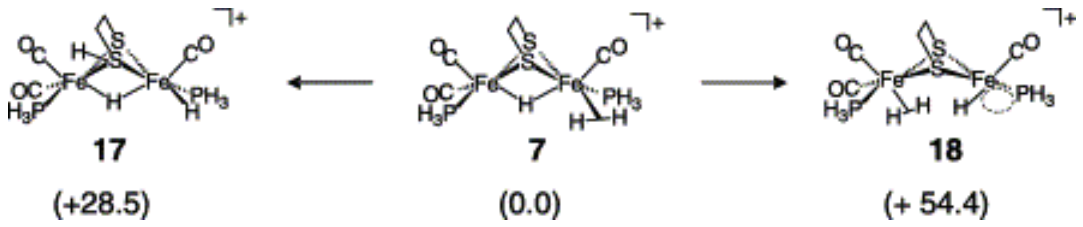

Figure III-7. Water-free activation of dihydrogen via Path a. The anhydrous activation of dihydrogen using the thiolate sulfur (left) or hydride (right). Relative energies in kcal mol^{-1}.

The water-assisted mechanism of H-H cleavage is a challenge for our gas-phase DFT calculations. An attempt was made to gain a qualitative understanding for the energetics of this step by calculating the species with explicit water molecules and the resulting "deprotonated species" as given by eqs III-5 and III-6.

Complexes of the form $(\mu\text{-H})(\mu\text{-edt})[Fe(CO)_2(PH_3)][Fe(CO)(PH_3)(H\cdots H(H_2O)_x)]\}^+$, where x = 1 or 2 returned to the form $(\mu\text{-H})(\mu\text{-edt})[Fe(CO)_2(PH_3)][Fe(CO)(PH_3)(\eta^2\text{-}H_2) \cdot x(H_2O))]\}^+$ upon relaxed geometry

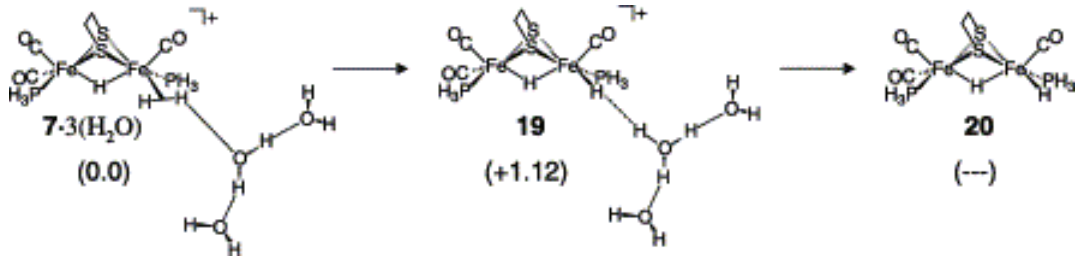

Figure III-8. Water assisted activation of dihydrogen via path a. The water-assisted cleavage of the H-H bond. Differences in charge does not allow the direct comparison of the energies of **19** and **20**. Relative energies given in kcal mol^{-1}.

$$\{Fe_2(H_2)\}^+ \cdot x(H_2O) \rightarrow \{Fe_2H\bullet\bullet\bullet H(H_2O)_x\}^+ \qquad \text{(III-5)}$$

$$\Delta E_0 = E_0(\{Fe_2H \cdots H(H_2O)_x\}^+) - E_0(\{Fe_2(H_2)\}^+ \cdot x(H_2O)) \qquad \text{(III-6)}$$

optimization. In other words, either one or two water molecules were insufficient as a gas-phase base for deprotonation of species **7**. Addition of three water molecules led to the optimization of $\{(\mu\text{-H})(\mu\text{-edt})[Fe(CO)_2(PH_3)][Fe(CO)(PH_3)(H^{\cdots}H(H_2O)_3)]\}^+$; the latter is shown as its optimized structure in Figure III-7. Using this method we calculated the deprotonation of these η^2-H_2 complexes to be essentially thermoneutral. (Our test calculations show that the extremely acidic dihydrogen complex of Morris, $\{(\eta^2\text{-}H_2)Fe[PEt_2(CH_2)_2PEt_2]_2CO\}^{2+}$,[266] modeled by us as $\{(\eta^2\text{-}H_2)Fe[PH_2(CH_2)_2PH_2]_2CO\}^{2+}$, also requires two water molecules for deprotonation.) While we have not been able to address the exact energetics or the activation energy for this process, the results *suggest* that these complexes are sufficiently acidic to be deprotonated by small water clusters or perhaps by small clusters of water with other polar molecules.

Figure III-7 gives two modes of cleavage of the H-H bond starting from the η^2-H_2 species, **2** that do not involve water. The first route is the heterolytic cleavage of dihydrogen using the lone pair on the bridging thiolate sulfur to yield **17**. The thermodynamic difference for this path is 28.5 kcal mol^{-1}. The other route, which uses the hydride to effect cleavage of the H-H bond, giving **18**, is even higher in energy, 54.4 kcal mol^{-1}. Although the hydride route is clearly energetically non-viable, the route through S is not impossible. However, the water-assisted route is clearly the more energetically favorable than either of the water-free routes.

In all cases heterolytic cleavage of the bound dihydrogen of the apical η^2-H_2 species, **8**, was high in energy relative to those derived from the basal η^2-H_2 species, **7**. The deprotonation of **8** by either an external base or the thiolate sulfur leads to a high energy intermediate due to the presence of a *trans* hydride ligand in the resulting intermediate. In addition, experimental data, vide supra, suggest that H/D exchange most likely occurs from the basal position.

H/D exchange into the μ-H position

Theory and experiment, taken together, suggest that the dihydrogen species **7–10**, Figure III-1 are sufficiently acidic to be deprotonated by small water-containing clusters and re-deuterated to affect D_2/H_2O (or H_2/D_2O) exchange. This process alone, however, does not explain how deuterium gets exchanged into the μ-H position. Experimentally, the incorporation of deuterium into the μ-H from the reaction of $\{(\mu\text{-H})(\mu\text{-pdt})[Fe(CO)_2(PMe_3)]_2\}^+$ with D_2O, with or without light, is exceedingly slow. In other

words, while the bridging hydride exchanges readily with deuterium from D_2 or D_2/H_2O, there is a high barrier to exchange with with D_2O alone.

The computations have suggested a somewhat unexpected, but energetically reasonable route for H/D exchange into the μ-H position, Figure III-9. As mentioned

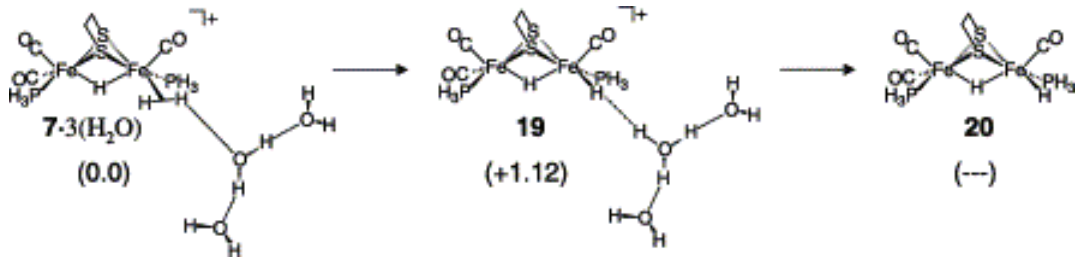

Figure III-9. Binuclear reductive elimination. The dihydride complex, **20**, passes over a low energy transition state to form a dihydrogen complex, **21**. Relative energies given in kcal mol^{-1}.

earlier, the cationic η^2-H_2^* species, **7**, can readily be deprotonated to afford the *neutral* species, **20** that contains both a bridging and a terminal hydride. This dihydride can pass over a low-energy transition state ($\Delta E_{20\rightarrow TS}$ = +6.6 kcal mol^{-1}) to form the *neutral* Fe^IFe^I η^2-HH* species, **21**. The formation of μ-H* can then be accomplished in one of two ways. The Fe-Fe bond may be reprotonated by $\{(H_2O)_xH^*\}^+$ to form μ-H*. Another possibility is a rotation of the η^2-HH* ($\Delta E_{21\rightarrow TS}$ = +4.4 kcal mol^{-1}), followed by reformation of the dihydride can also afford μ-H*.

The overall mechanism

When taken together, the theoretical and experimental data suggest a integrated mechanism for H/D exchange in D_2/H_2O mixtures as catalyzed by $\{(\mu\text{-E})(\mu\text{-S(CH}_2)_x\text{S})[\text{Fe(CO)}_2\text{PMe}_3]_2\}^+$. Figure III-10 presents this mechanism in a way that is equally valid for the μ-H and for the μ-SMe complex. The most important feature in the main cycle (right side of Figure III-10) is η^2-H_2 binding at a single Fe^{II} site that is deprotonated by the external base, D_2O. The left side of Figure III-10 shows a binuclear reductive elimination process that produces a η^2-HD bound to the Fe^IFe^I binuclear complex and holds only for the μ-H parent catalyst.

This mechanism thus invokes a species, **2**, whose trapping by exogenous bases or ligands might account for inhibition of H/D exchange. It also suggests the possibility of H/D exchange facilitated by a η^2-H_2 complex of Fe^IFe^I. Experiments designed to test such implications are described below.

D_2/H_2O scrambling catalyzed by (μ-pdt)[Fe(CO)$_2$(PMe$_3$)]$_2$

While most η^2-H_2 complexes of iron are in Fe^{II} complexes, the results presented above suggest that the creation of an open site on the Fe^IFe^I species, (μ-pdt)$[\text{Fe(CO)}_2(\text{PMe}_3)]_2$, might also bind and activate dihydrogen. Gas-phase calculations show that binding of H_2 to (μ-edt)$[\text{Fe(CO)}_2(\text{PH}_3)][\text{Fe(CO)}(\text{PH}_3)]$ to form (μ-edt)$[\text{Fe(CO)}_2(\text{PH}_3)][\text{Fe(CO)}(\eta^2\text{-H}_2)(\text{PH}_3)]$, **21**, is an exothermic process. This complex may rearrange, proceeding over a very small barrier (see Figure III-9; $\Delta E_{21\rightarrow TS}$ = +0.6 kcal mol^{-1}) to form species **20**. The reversible conversion between **20** and **21** would lead

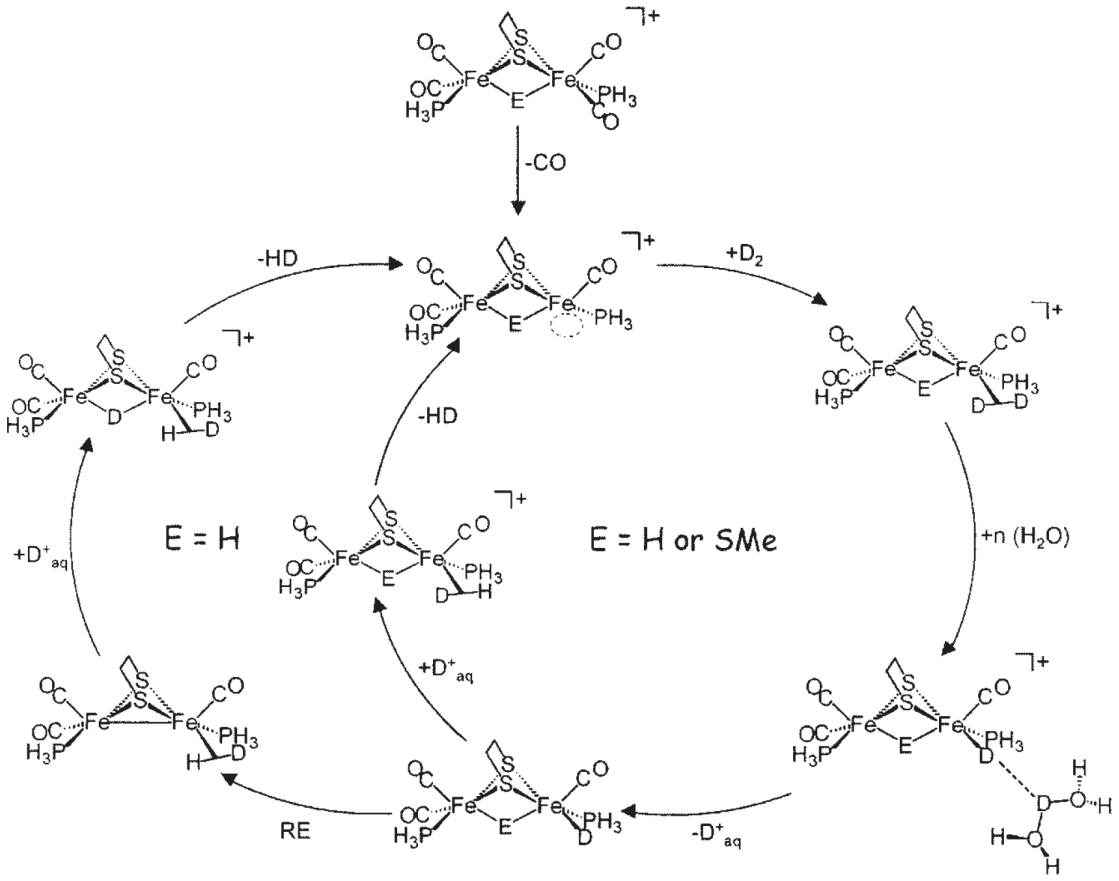

Figure III-10. The general mechanism of H/D exchange.The right cycle for E = H or SMe. The left cycle holds only for E = H. $D^{+}_{aq} = (H_2O)_nD^{+}$ and RE = reductive elimination.

to scission of the H-H or D-D bond but no isotope exchange in the absence of water. The deprotonation of a η^2-H_2 intermediate, like **21**, however, could lead to the H/D exchange of D_2/H_2O mixtures.

In order to establish the viability of the $Fe^{I}Fe^{I}$ species for activation of dihydrogen for H/D exchange in D_2/H_2O mixtures, an experiment similar to the one performed for

$\{(\mu\text{-E})(\mu\text{-pdt})[Fe(CO)_2PMe]_2\}^+$ (E = H and SMe) was carried out using the $(\mu\text{-pdt})[Fe(CO)_2PMe_3]_2$ complex as a potential H/D exchange catalyst.[202,203,249] The formation of HOD was monitored by ^2H NMR spectroscopy. The ^2H-NMR spectra, presented in Figure III-11, were recorded before exposure of the solutions to light and at intervals during several hours of exposure. For $(\mu\text{-pdt})[Fe(CO)_2PMe_3]_2$, the intensity of the resonance at 1.65 ppm corresponding to D-enriched H_2O in the solvent increased from 1.03 (4 h) to 3.76 (13 h). While this isotopic exchange activity is poorer than that emanating from the $Fe^{II}Fe^{II}$ catalysts, the fact that the $Fe^{I}Fe^{I}$ catalyst is competent at all is consistent with the computational prediction of an $(\eta^2\text{-H}_2)Fe^{I}Fe^{I}$ intermediate.

Reaction of $\{(\mu\text{-H})(\mu\text{-pdt})[Fe(CO)_2(PMe_3)]_2\}^+$ with acetone

One of our basic assumptions was that the only role of light in the reaction was the creation of an open site on one of the metal centers. Our computations showed that an $\eta^2\text{-H}_2$ intermediate, if formed, could facilitate D_2/μ-H exchange thermally in the presence of water. In other words, if a basal open site could be generated in the absence of light then D_2/μ-H exchange should proceed via a dark, thermal reaction.

The acetonitrile complex, $\{(\mu\text{-H})(\mu\text{-pdt})[Fe(CO)_2(PMe_3)][Fe(CO)(CH_3CN)(PMe_3)]\}^+$, was not active for thermal H/D exchange. Computations suggested that acetone should bind to the iron center somewhat more weakly than acetonitrile. A similar experimental approach to the preparation and isolation of $\{(\mu\text{-H})(\mu\text{-pdt})[Fe(CO)_2(PMe_3)][Fe(CO)(CH_3CN)(PMe_3)]\}^+$ was attempted with acetone, albeit with poor results. The prolonged photolysis of mixtures of $\{(\mu\text{-H})(\mu\text{-pdt})[Fe(CO)_2(PMe_3)]_2\}^+$ and 1–5 equivalents of acetone in CH_2Cl_2 lead to extensive

decomposition. Although attempts to isolate and fully characterize the complex formed in this case were unsuccessful, infrared and NMR spectral data support the formation of an acetone complex *in situ* as described below.

When a solution of $\{(\mu\text{-H})(\mu\text{-pdt})[Fe(CO)_2(PMe_3)]_2\}^+$ in acetone was exposed to sunlight for one hour the color gradually changed from orange-red to dark brown-red. The IR spectrum showed the presence of the starting (ν(CO) = 2031, 1991 cm^{-1}) complex together with a species with ν(CO) stretching frequencies displaced by ca. 50 cm^{-1} (Figure III-12). (While few acetone complexes of metal carbonyls have been isolated, available data suggest the electron donating ability of $(CH_3)_2C{=}O$ is better than that of CO,[267] consistent with the lower values of ν(CO) observed here.) Bubbling CO through this solution led to the disappearance of the new ν(CO) bands and the reappearance of the ν(CO) bands of $\{(\mu\text{-H})(\mu\text{-pdt})[Fe(CO)_2(PMe_3)]_2\}^+$, indicating the replacement of acetone by CO had reformed the starting complex.

Further support for the formation of the acetone complex was provided by an experiment carried out in an NMR sample tube. When an acetone solution of $\{(\mu\text{-H})(\mu\text{-pdt})[Fe(CO)_2(PMe_3)]_2\}^+$ was exposed to sunlight for one hour, two hydride resonances were observed as shown in Figure III-12. The doublet of doublets centered at −7.7 ppm with J_{H-P} coupling of 21 and 30 Hz corresponded to the coupling of the bridging hydride to two non-equivalent phosphines of the presumed acetone complex, $\{(\mu\text{-H})(\mu\text{-pdt})[Fe(CO)_2(PMe_3)][Fe(CO)(PMe_3)(acetone)]\}^+$; a triplet at −15.0 ppm with J_{H-P} of 22 Hz was characteristic of the starting hydride species $\{(\mu\text{-H})(\mu\text{-pdt})[Fe(CO)_2(PMe_3)]_2\}^+$.

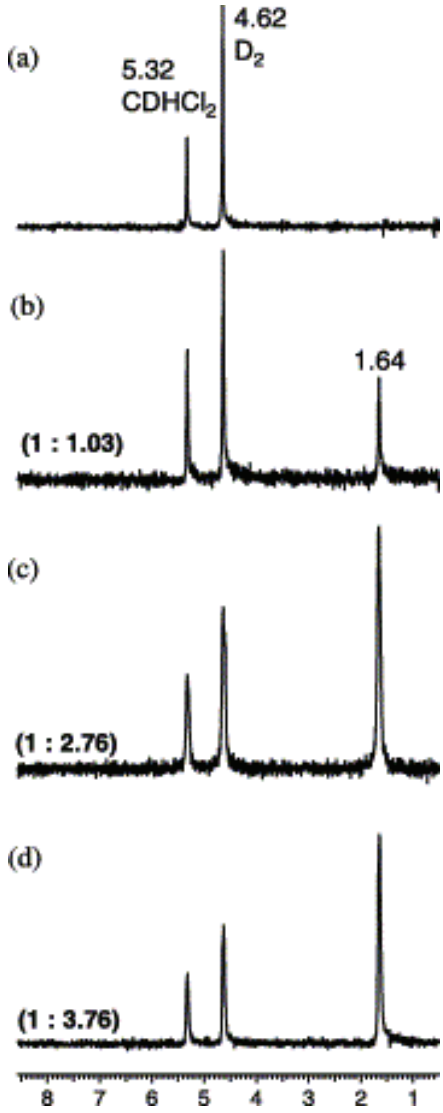

Figure III-11. ^2H NMR spectra showing the formation of HOD (δ = 1.64 ppm) in CH_2Cl_2 solution containing (μ-pdt)$[Fe(CO)_2PMe_3]_2$, 10 bar D_2 and 2 mL H_2O: (a) before exposure to sunlight, (b) after 4 h of photolysis, (c) after 10 h of photolysis and (d) after 13 h of photolysis. Relative ratios of the intensity of the resonance of $CHDCl_2$ (natural abundance) to HOD are given in parentheses.

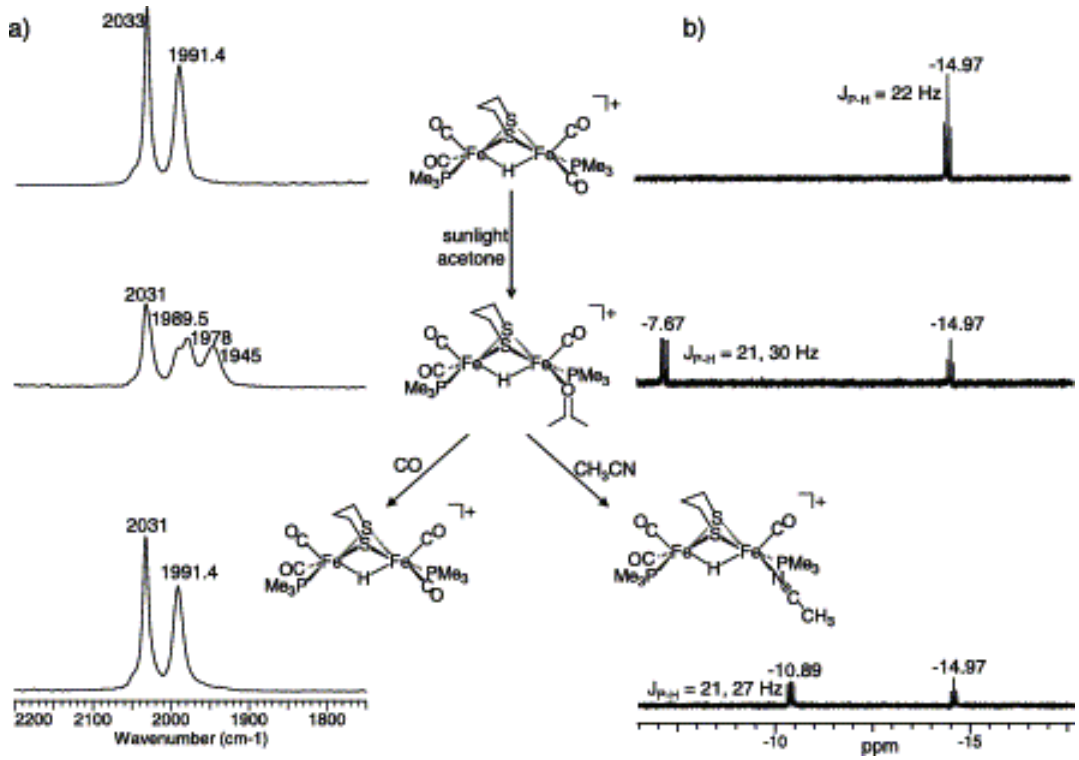

Figure III-12. (a) Infrared spectra (CO region) and (b) ^{1}H NMR spectra (hydride region) of $\{(\mu\text{-H})(\mu\text{-pdt})[Fe(CO)_2PMe_3]_2\}^+$ as it reacts with $Me_2C{=}O$ to form $\{(\mu\text{-H})(\mu\text{-pdt})[Fe(CO)PMe_3(O{=}CMe_2)][Fe(CO)_2PMe_3]\}^+$ and acetone displacement upon reaction with CO to reform $\{(\mu\text{-H})(\mu\text{-pdt})[Fe(CO)_2PMe_3]_2\}^+$ and CH_3CN to form $\{(\mu\text{-H})(\mu\text{-pdt})[Fe(CO)PMe_3(CH_3CN)][Fe(CO)_2PMe_3]\}^+$, respectively.

Addition of CH_3CN to this sample in the dark caused the resonance at −7.7 ppm to disappear with the appearance of a new signal centered at −10.9 ppm (doublet of doublets with $J_{H\text{-}P}$ of 21 and 27 Hz) corresponding to the acetonitrile complex, $\{(\mu\text{-H})(\mu\text{-pdt})[Fe(CO)_2(PMe_3)][Fe(CO)(PMe_3)(CH_3CN)]\}^+$. An identical sample of $\{(\mu\text{-H})(\mu\text{-pdt})[Fe(CO)_2(PMe_3)]_2\}^+$ in d_6-acetone, maintained in the dark, gave no indication of the *thermal* displacement of CO by acetone; neither did subsequent addition of CH_3CN result in CO/CH_3CN exchange in the dark. We conclude that the acetone complex, generated by photolytic CO loss followed by solvent molecule capture, can be converted to the acetonitrile complex in a thermal (non-photolytic) ligand exchange process. The acetonitrile complex, here generated in situ from the acetone complex, is known to contain a basally coordinated CH_3CN ligand.[251] Since the most likely mechanism for this exchange is a dissociative replacement of an acetone molecule by a CH_3CN molecule, we conclude that the photolysis of $\{(\mu\text{-H})(\mu\text{-pdt})[Fe(CO)_2(PMe_3)]_2\}^+$ in acetone results in the formation of $\{(\mu\text{-H})(\mu\text{-pdt})[Fe(CO)_2(PMe_3)][Fe(CO)(acetone)\ (PMe_3)]\}^+$.

Unfortunately, the acetone complex did not give clear answers about the validity of a dark, thermal H/D exchange process. Acetone solutions of the complex did not catalyze H_2/D_2 or D_2/μ-H exchange. The complex decomposes in the presence of water and in solutions other than acetone.

Calculation of NMR shielding tensors

The experimentally observed ^{1}H-NMR spectrum of the "acetone complex" shows a doublet of doublets centered at −7.7 ppm. To help assign this resonance, a series of structural candidates for the acetone complex, as well as the known parent hydride, **1**,

and the CH_3CN complex, **12**, were geometry optimized and their NMR spectra were calculated. (NOTE: The edt/PH_3 model was used for these calculations while experiments were carried out with the pdt/PMe_3 complex.) The NMR chemical shift calculation gives absolute shielding values. These values were scaled by setting the value for μ-H hydrogen of $\{(\mu\text{-H})(\mu\text{-edt})[Fe(CO)_2PH_3]_2\}^+$ equal to the observed chemical shift for the hydride of $\{(\mu\text{-H})(\mu\text{-pdt})[Fe(CO)_2(PMe_3)]_2\}^+$ in acetone (−15.0 ppm). Accordingly, the chemical shift of the μ-H of the acetonitrile complex, **12**, was computed to be at −10.5 ppm (experimental value = −10.8 ppm). Examples of structural isomers computed for the acetone complex are shown in Figure III-13.

The experimental value of −7.7 ppm is in good agreement with the basal-substituted species, **13** that is computed to have a μ-H hydride shift of −7.4 ppm. The next closest match is the μ-acetone-terminal hydride species, **22**, with a calculated hydride chemical shift of −7.2 ppm. This structure is less likely than **13**, both for its

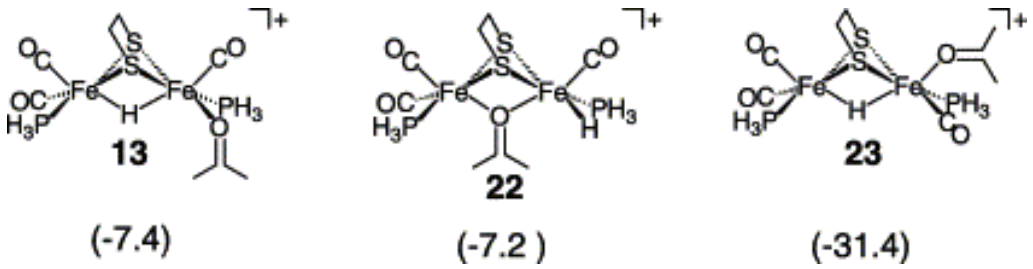

Figure III-13. Possible isomers for the monosubstituted acetone complex. Calculated chemical shifts, given in parentheses, are in ppm and scaled to that of species **2** = –15.0 ppm.

higher energy (+28.7 kcal mol $^{-1}$ relative to **13**), as well as the expected coupling pattern for this structure (a doublet is expected for **22**, as opposed to the doublet of doublets observed experimentally.) The apically substituted acetone species, **23**, calculated to have a chemical shift of −31.4 ppm, is much too far upfield to be considered a viable candidate for the structure of the experimentally observed acetone complex.

Conclusions

The growing importance of computational chemistry in mechanistic inorganic chemistry may be ascribed to the broad accessibility and application of Density Functional Theory and related techniques to large molecules, in this case a diiron complex with 10 to 12 coordination sites filled with diatomic or larger ligands. For simple substrates, as in the H/D isotopic scrambling process described here, conclusions from experimental techniques are typically limited to issues involving the rate-determining step of the reaction path. While chemical intuition arising from knowledge of stable ground state structures assists in formulating experimental tests of reasonable scenarios for events prior to and following the highest barrier, experimental proofs of these steps are often difficult; here calculation may be critical to formulating a complete mechanism.

The case in point in our studies of simple isotopic exchange in H_2/D_2O or D_2/H_2O mixtures as facilitated by Fe(II) in dinuclear complexes is a particular mechanistic challenge as the catalysis is light-driven and the experiments thus far have been non-wavelength specific. The critical step of ligand loss preceding a most reasonable step of H_2 binding draws on the experimental verification and chemical precedence of (η^2-

H_2)Fe^{II} complexes in organometallic-like coordination environments.[266] Experimental data suggested CO labilization was the most likely effect of sunlight.

The observation of inhibition of the H/D exchange reaction by CO and CH_3CN implicates coordinatively unsaturated intermediates in the H_2 capture process. As a part of this chapter, we report evidence for the existence of an acetone derivative of the (μ-H)$(Fe^{II})_2$ complex, as suggested by theory. As it has obvious ramifications for technical development of such H_2-uptake catalysts, the possibility that water might similarly compete for the open site and serve both as a required reagent and a catalyst inhibitor deserves a future detailed study.

The reaction paths explored by theory were closely tied to published experimental results, and provided support for previously suggested mechanisms. The predictive power of theory beyond what the experimentalist can readily do was displayed in steps likely to follow the highest barrier process. Most notably, theory accounted for the enhanced H/D exchange into the bridging hydride position of $\{(\mu\text{-H})(\mu\text{-pdt})[Fe(CO)_2]PMe_3]_2\}^+$ from D_2/H_2O mixtures over either of the individual components, D_2 or D_2O as D-sources independent of each other. An unexpected path (reductive elimination) from a terminal hydride/bridging hydride intermediate suggested the possibility that the Fe^IFe^I parent complex might facilitate H/D exchange in H_2/D_2O mixtures. This possibility was substantiated by experiment.

Many issues are involved in decisions as to the detail required to "complete" a mechanistic study, i.e., to further test assumptions used to formulate the proposed reaction path that have gained credibility from theory. Prominent in decisions to go

further are the effective use of time and resources, and the technical feasibility of more sophisticated experiments. As development of H_2 uptake and activation by base metal catalysts, hopefully linked to electrode surfaces, appear to be exceedingly important for technological progress, further study of this system seems to be mandated.

CHAPTER IV

THE REACTION OF ELECTROPHILES WITH MODELS OF IRON-IRON HYDROGENASE: A SWITCH IN REGIOSELECTIVITY*

Introduction

The iron-iron hydrogenase enzymes ([FeFe]H_2ases) facilitate the reversible oxidation of dihydrogen to protons and electrons, $H_2 \rightarrow 2H^+ + 2e^-$.[130,131,173] The active site of these enzymes consists of a dithiolate bridged dinuclear iron assembly,[169-172] which is similar in structure and composition to simple dithiolate-bridged dinuclear iron complexes of the form, (μ-SRS)[$Fe(CO)_2L]_2$ as shown in Figure IV-1.[248,268]

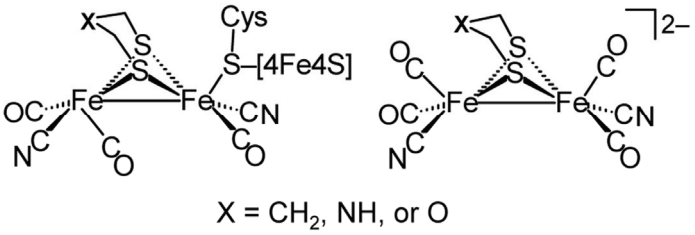

Figure IV-1. A comparison between the active site of the [FeFe]H_2ase enzymes (left) and closely related dithiolate bridged dinuclear iron clusters (right).

* Reprinted with permission from "The Reaction of Electrophiles with Models of Iron-Iron Hydrogenase: A Switch in Regioselectivity" by Tye, J. W.; Darensbourg, M. Y.: Hall, M. B. *THEOCHEM* in press. Copyright 2006 by Elsevier, Inc.

The reactions of models of [FeFe]H_2ase with electrophilic species are important for a number of reasons. First, the reaction of these complexes with H^+ is a critical step in the electrocatalysis of H_2. Second, the iron-based reaction of the formally Fe^IFe^I complexes with certain electrophiles, generates the corresponding formally $Fe^{II}Fe^{II}$ complexes, which are capable of binding and activating H_2.[202] Third, the reaction of these complexes with various alkylating agents tunes the reactivity of the resulting di-iron complexes by modulating the donor ability of the bridging sulfur atoms. Finally, the reaction of these complexes with electrophiles provide another point of attachment (in addition to the S-to-S linker and donor ligands) for pendant functionalities, which may be used to attach potential electrocatalysts to the surface of an electrode.

Dithiolate-bridged dinuclear iron complexes have been shown to react with a range of electrophilic species. The two main targets for electrophilic attack are the sulfur lone pairs of the bridging dithiolate ligand and the Fe-Fe bond, Scheme IV-1.

Scheme IV-I

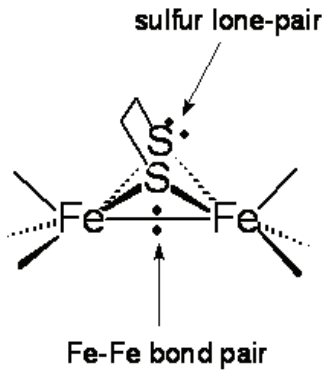

Most common is the reaction of an electrophile, E^+, with the Fe-Fe bond density to generate the corresponding $[(\mu\text{-}\mathbf{E})(\mu\text{-SRS})[Fe(CO)_2L]_2]^{1+}$.[196] In a few cases, however, the electrophile adds to a sulfur atom of the dithiolate bridge to form the corresponding $[(\mu\text{-SRS}\mathbf{E})[Fe(CO)_2L]_2]^{1+}$ complex.

Specifically, the $(\mu\text{-}SCH_2CH_2S)[Fe(CO)_2(PMe_3)]_2$ complex has been shown to react differently with the electrophiles H^+ and Et^+, as determined by single-crystal x-ray diffraction and ^{1}H-NMR and IR spectral studies on the resulting products.[203,251] The reaction of $(\mu\text{-}SCH_2CH_2S)[Fe(CO)_2(PMe_3)]_2$ with H^+ leads to the protonation of the Fe-Fe bond density (Scheme IV-1) generating the corresponding bridging hydride species, $[(\mu\text{-}\mathbf{H}))(\mu\text{-}SCH_2CH_2S)[Fe(CO)_2(PMe_3)]_2]^{1+}$, while its reaction with Et^+ leads to alkylation of a sulfur atom of the S-to-S linker (Scheme IV-1) generating the corresponding bridging thioether/bridging thiolate complex, $[(\mu\text{-}SCH_2CH_2S\mathbf{Et})[Fe(CO)_2(PMe_3)]_2]^{1+}$.

Since experimental studies of reactions between di-iron dithiolate complexes and electrophiles are of current interest, qualitative rules for predicting whether the reaction will lead to the sulfur-bound or di-iron bound form would be quite useful. In the present study, we utilize density functional theory calculations to determine the factors which contribute to the relative stabilities of sulfur-bound and iron-iron bridging forms for the electrophiles H^+ and Et^+.

Computational Method

All DFT calculations were performed using a hybrid functional [the three-parameter exchange functional of Becke (B3)[235] and the correlation functional of Lee, Yang, and Parr (LYP)[236]] (B3LYP) as implemented in Gaussian 98[252]. The iron, phosphorus, and sulfur atoms use the effective core potential and associated basis set of Hay and Wadt (LANL2DZ).[253,254] For iron, the two outermost p functions were replaced by re-optimized 4p functions as suggested by Couty and Hall.[254] For sulfur and phosphorus, the basis set was augmented by the d polarization function of Höllwarth *et al*.[256] The carbon and hydrogen atoms of the S-to-S linker, and the hydrogen atoms of the PH_3 ligand use Dunning's double zeta basis (D95). [258,269] The CO ligands, use Dunning's correlation-consistent polarized valence double zeta basis set (cc-pVDZ).[257] Unless otherwise noted, all geometries are fully optimized and confirmed as minima or n-order saddle points by analytical frequency calculations at the same level. All energies given in this text are relative electronic energies (zero-point corrected) in kcal mol^{-1}.

Results and Discussion

Fundamental properties of (μ-$S(CH_2)_2S)[Fe(CO)_2(PR_3)]_2$

The coordination geometry about the iron centers of complexes of the form, (μ-$SCH_2CH_2S)[Fe(CO)_2(PR_3)]_2$ may be described as square pyramidal (see Figure IV-2). The structure adopted by these complexes forces the bridging thiolate sulfur atoms to occupy two of the four positions in the basal plane. In this context, the CO and PR_3 ligands may be conveniently designated as either apical (trans to the Fe-Fe bond) or basal (cis to the Fe-Fe bond). These complexes, react with certain electrophiles, E, to

generate the corresponding face bridged octahedral, μ-E species, [(μ-**E**)(μ-SCH_2CH_2S) $[Fe(CO)_2(PR_3)]_2]^{1+}$. For clarity, the apical and basal designations of the parent complex will be retained for the octahedral complexes of the form, [(μ-**E**)(μ-$SCH_2CH_2S)[Fe(CO)_2(PR_3)]_2]^{1+}$. For these complexes, apical and basal refer to ligands which are *trans* and *cis*, respectively, to the bridging E group.

The geometries of the bis-phosphine complexes, presented herein, will be designated by indicating the position of the PH_3 ligands about each iron center in that complex. For bis-phosphine complexes of the form, (μ-$SCH_2CH_2S)[Fe(CO)_2(PR_3)]_2$, two basal/basal isomers exist. These isomers may be conveniently described in relation

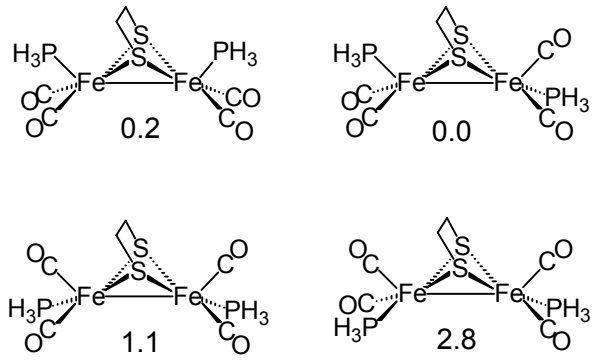

Figure IV-2. Relative zero-point corrected electronic energies for four phosphine positional isomers of (μ-$SCH_2CH_2S)[Fe(CO)_2(PH_3)]_2$. Energies are reported in kcal mol^{-1}.

to a plane which includes the two iron centers and a point half-way between the two sulfur atoms. Complexes in which both PH_3 ligands are on the same side of this plane will be described as basal/basal cisoid, and complexes in which the PH_3 ligands are on opposite sides of this plane will be described as basal/basal transoid.

There are four unique phosphine positional isomers possible for bis-phosphine complexes of the form, $(\mu\text{-}SCH_2CH_2S)[Fe(CO)_2(PR_3)]_2$. Variable-temperature nuclear magnetic resonance (VT-NMR) spectral studies performed on the $(\mu\text{-}SCH_2CH_2S)[Fe(CO)_2(PMe_3)]_2$ complex indicate that it undergoes intramolecular site exchange of the CO and PMe_3 ligands about the individual iron centers at and below room temperature.[203]

The four PH_3 positional isomers for the complex $(\mu\text{-}SCH_2CH_2S)[Fe(CO)_2(PH_3)]_2$ were geometry-optimized and their relative energies are given in Figure IV-2. These four isomers are computed to have very similar energies. The apical/basal PH_3 isomer is the most stable. The apical/apical PH_3 isomer is nearly isoenergetic with the apical/basal isomer with a relative energy of 0.2 kcal mol^{-1}. The C_2 symmetric basal/basal transoid geometry and C_s symmetric, basal/basal cisoid geometry are, respectively, 2.8 and 1.1 kcal mol^{-1} less stable than the apical/basal PH_3 isomer.

The reaction of (μ-SCH_2CH_2S)$[Fe(CO)_2(PH_3)]_2$ with H^+:bridging hydride complexes of the form $[(\mu\text{-}H)(\mu\text{-}SCH_2CH_2S)\ [Fe(CO)_2(PH_3)]_2]^{1+}$

The frontier molecular orbitals of complexes of the form (μ-SCH_2CH_2S)$[Fe(CO)_2(PR_3)]_2$ (R = Me, H) are the HOMO, which is predominately Fe-Fe bonding in character and the LUMO, which is predominately Fe-Fe antibonding in character.[203] The Fe-Fe bond electron density of the (μ-SCH_2CH_2S)$[Fe(CO)_2(PH_3)]_2$ complex may react with H^+ to generate a bridging hydride complex of the form, [(μ-**H**)(μ-SCH_2CH_2S)$[Fe(CO)_2(PH_3)]_2]^+$. The relative energies of the four phosphine positional isomers of the bridging hydride complex are very similar to one another (as shown in Figure IV-3). The lowest energy structure corresponds to the basal/basal transoid PH_3 isomer. The basal/basal cisoid and apical/basal PH_3 isomers are 1.1 and 1.7 kcal mol^{-1}, respectively, less stable than the basal/basal transoid PH_3 isomer. The least stable PH_3 isomer is the apical/apical PH_3 isomer, which is 3.4 kcal mol^{-1} less stable than the basal/basal transoid PH_3 isomer.

The reaction of (μ-SCH_2CH_2S)$[Fe(CO)_2(PH_3)]_2$ with H^+: bridging thiolate/thiol complexes of the form $[(\mu\text{-}SCH_2CH_2SH)\ [Fe(CO)_2(PH_3)]_2]^{1+}$

Alternatively, one could envision protonation of one of the sulfur atoms of the dithiolate linker of (μ-SCH_2CH_2S)$[Fe(CO)_2(PH_3)]_2$ to yield a bridging thiolate/thiol complex of the form (μ-SCH_2CH_2S**H**)$[Fe(CO)_2(PH_3)]_2$. The relative energies of the six phosphine positional isomers of the bridging thiolate/thiol complex are very similar to

one another. (The energy of each complex, relative to the most stable isomer of the bridging hydride complex, is given in

Figure **IV-4**). All six PH_3 positional isomers of $[(\mu\text{-}SCH_2CH_2S\mathbf{H})[Fe(CO)_2(PH_3)]_2]^+$ are significantly less stable than the bridging hydride complexes (29.0 kcal mol^{-1} or more). Thus, the most stable isomer of the bridging thiolate/thiol complex is significantly less stable than the least stable isomer of the bridging hydride complex.

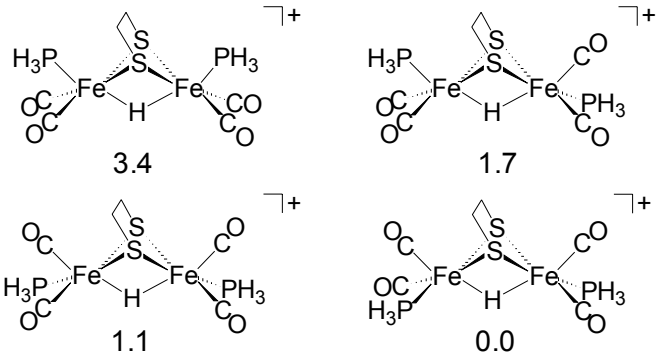

Figure IV-3. Relative zero-point corrected electronic energies for four phosphine positional isomers of $[(\mu\text{-}H)(\mu\text{-}SCH_2CH_2S)[Fe(CO)_2(PH_3)]_2]^{1+}$. Energies are reported in kcal mol^{-1}.

The reaction of $(\mu\text{-}SCH_2CH_2S)[Fe(CO)_2(PH_3)]_2$ with Et^+: generation of $[(\mu\text{-}SCH_2CH_2SEt)[Fe(CO)_2(PH_3)]_2]^{1+}$ species

One of the sulfur atoms of the dithiolate linker of the $(\mu\text{-}SCH_2CH_2S)[Fe(CO)_2(PH_3)]_2$ complex may react with Et^+ to generate the corresponding bridging thiolate/thioether complex of the form $(\mu\text{-}SCH_2CH_2S\mathbf{Et})[Fe(CO)_2(PH_3)]_2$. The

relative energies of the six phosphine positional isomers of the bridging thiolate/thioether complex are very similar to one another (as shown in Figure IV-5). The most stable isomer corresponds to an apical/basal configuration of the phosphine ligands, in which the ethyl group is furthest from the basal PH_3 ligand. The least stable structure corresponds to a basal/basal cisoid orientation of the PH_3 ligands, in which, both of the PH_3 ligands are trans to the bridging thiolate sulfur.

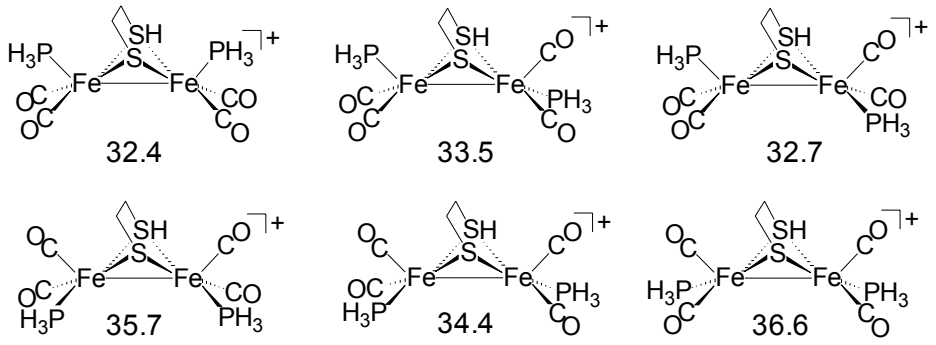

Figure IV-4. Relative zero-point corrected electronic energies for six phosphine positional isomers of $[(\mu\text{-}SCH_2CH_2SH)[Fe(CO)_2(PH_3)]_2]^{1+}$. Energies are relative to the most stable isomer of $[(\mu\text{-}H)(\mu\text{-}SCH_2CH_2S)[Fe(CO)_2(PH_3)]_2]^{1+}$ from Figure IV-3 and reported in kcal mol^{-1}.

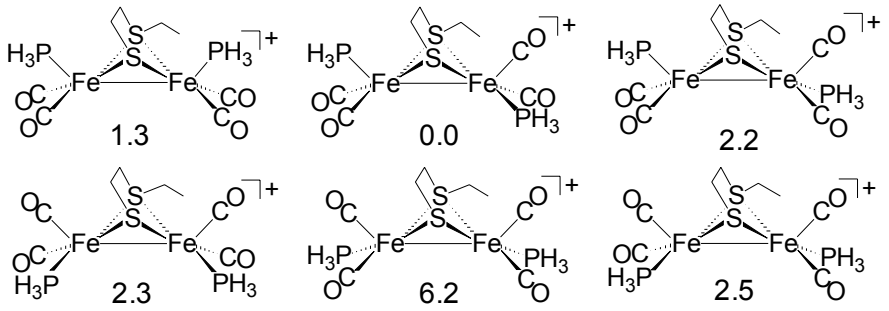

Figure IV-5. Relative zero-point corrected electronic energies for six phosphine positional isomers of $[(\mu\text{-}SCH_2CH_2SEt)[Fe(CO)_2(PH_3)]_2]^{1+}$. Energies are reported in kcal mol^{-1}.

The reaction of $(\mu\text{-}SCH_2CH_2S)[Fe(CO)_2(PH_3)]_2$ with Et^+: generation of $[(\mu\text{-}Et)(\mu\text{-}SCH_2CH_2S)[Fe(CO)_2(PH_3)]_2]^{1+}$ species

Alternatively, one could envision the reaction of Et^+ with the Fe-Fe bond density of $(\mu\text{-}SCH_2CH_2S)[Fe(CO)_2(PH_3)]_2$ to generate a "bridging" ethyl complex, $[(\mu\text{-}\mathbf{Et})(\mu\text{-}SCH_2CH_2S)[Fe(CO)_2(PH_3)]_2]^{1+}$. A complex with a fully bridging ethyl group (i.e., a complex with approximately equal distances between the methylene carbon of the ethyl group and the two iron centers) is not a stable minimum on the potential energy surface of complexes of the general formulation $[(\mu\text{-}\mathbf{Et})(\mu\text{-}SCH_2CH_2S)[Fe(CO)_2(PH_3)]_2]^{1+}$. Repeated attempts at the optimization of a species with a fully bridging ethyl group yielded structures with unequal distances (≈ 2.1 Å and ≈ 2.5 Å) between the methylene carbon of the ethyl group and the two iron centers, and a short distance (≈ 1.8 Å) between one of the methylene hydrogen atoms and the adjacent iron center. The

complex may be forced to optimize with a symmetrically bridging ethyl group by requiring C_s symmetry throughout the geometry-optimization. This symmetrically bridged structure corresponds to a transition state for shifting the Fe-C bond of ethyl group from one iron center to the adjacent iron center. Thus, in the stable structures the ethyl group forms one 2c-2e$^-$ Fe-C bond with one iron center and an agostic interaction with the adjacent iron center rather and one 3c-2e$^-$ Fe-C-Fe bond.

The relative energies of the nine phosphine positional isomers of the iron-ethyl complexes are similar to one another. The lowest energy structure corresponds to a basal/basal cisoid PH_3 isomer which orients the CH_3 of the ethyl group away from the PH_3 ligands. This structure is 13.9 kcal mol^{-1} less stable than the most stable structure of $[(\mu\text{-}SCH_2CH_2S\mathbf{Et})[Fe(CO)_2(PH_3)]_2]^{1+}$. (The energy of each isomer of $[(\mu\text{-}SCH_2CH_2S\mathbf{Et})[Fe(CO)_2(PH_3)]_2]^{1+}$, relative to the most stable isomer of the bridging thiolate/thioether complex, is given in Figure IV-6). All nine PH_3 positional isomers of $[(\mu\text{-}\mathbf{Et})(\mu\text{-}SCH_2CH_2S)[Fe(CO)_2(PH_3)]_2]^{1+}$ are less stable than (8.0 kcal mol^{-1} or more) the bridging thiolate/bridging thioether complexes, of the form $[(\mu\text{-}SCH_2CH_2S\mathbf{Et})[Fe(CO)_2(PH_3)]_2]^{1+}$. In other words, the most stable isomer of the iron-ethyl complex is significantly less stable than the least stable isomer of the bridging thioether complex.

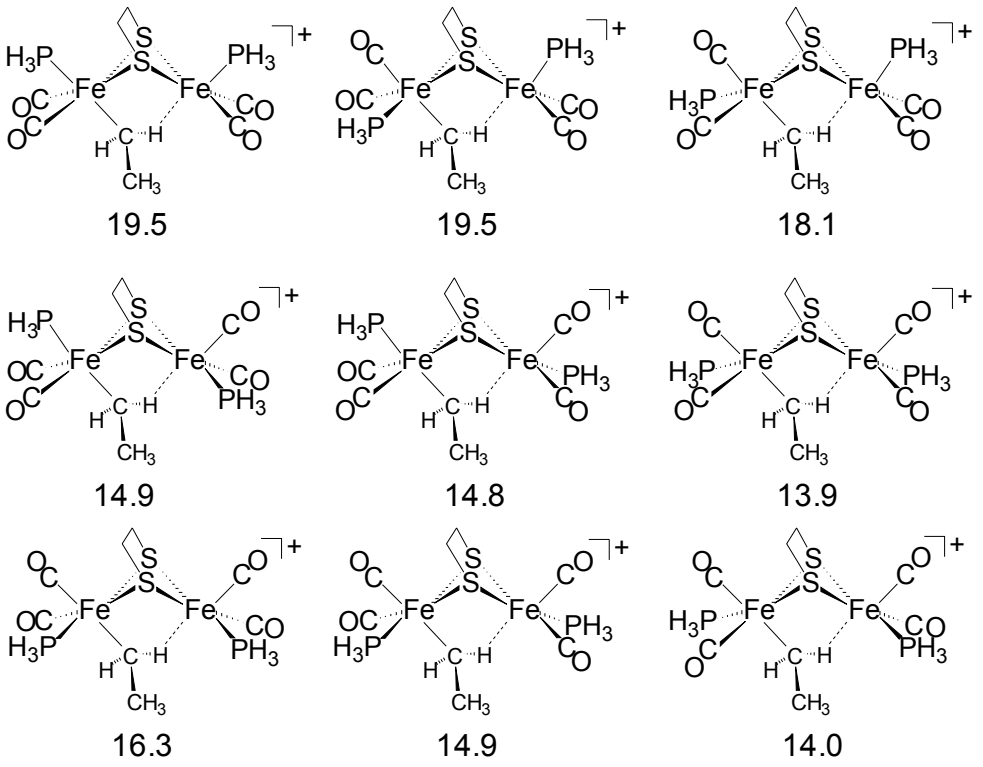

Figure IV-6. Relative zero-point corrected electronic energies for nine phosphine positional isomers of $[(\mu\text{-Et})(\mu\text{-SCH}_2\text{CH}_2\text{S})[\text{Fe(CO)}_2(\text{PH}_3)]_2]^{1+}$. Energies are relative to the most stable isomer of $[(\mu\text{-SCH}_2\text{CH}_2\text{SEt})[\text{Fe(CO)}_2(\text{PH}_3)]_2]^{1+}$ from Figure IV-5 and reported in kcal mol^{-1}.

Decomposition of energy contribution leading to difference between H^+ and Et^+

In agreement with the experimental results, the computations show that the bridging hydride complexes are far more stable than the corresponding bridging thiolate/thiol complexes, and that the bridging thiolate/thioether complexes are much

more stable than the corresponding "bridging" ethyl complexes. The origin of the differences, however, is not clear. For example, are the relative energies of these

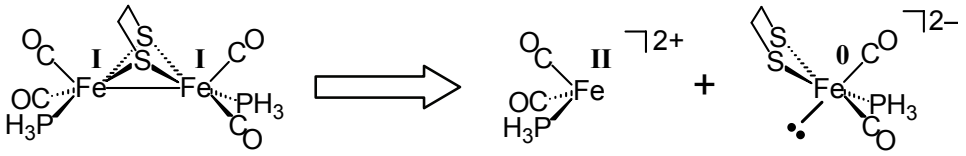

Figure IV-7. Fragment analysis is accomplished by breaking the formally $Fe^{I}Fe^{I}$ dithiolate complex into an dicationic Fe^{II} fragment and a dianionic Fe^{0} fragment.

complexes due to inherent differences in the Fe-E and S-E for E = H and E = Et) bond energies or other factors? The presence of two iron centers in close proximity to one another makes a simple analysis of the Fe-E and S-E bonding interactions difficult. In order to estimate the importance of the Fe-E and S-E interactions in the absence of the complicating bridging interaction, the $[Fe(CO)_2(PH_3)]^{2+}$ fragment was removed from $(\mu\text{-}SCH_2CH_2S)[Fe(CO_2(PH_3)]_2$ to yield a simple, mononuclear iron complex of the form $[(\mu\text{-}SCH_2CH_2S)Fe(CO_2(PH_3)]^{2-}$, as shown in Figure IV-7. After examining formation of these Fe-E and S-E bonds with this mononuclear fragment, the $[Fe(CO)_2(PH_3)]^{2+}$ will be returned to the fragments to form the final products.

Reaction of H^+ and Et^+ with the mononuclear iron fragment, $[(\mu\text{-}SCH_2CH_2S)Fe(CO)_2(PH_3)]^{2-}$

Mononuclear iron complexes of the forms, $[(\eta^2\text{-}SCH_2CH_2S\mathbf{E})Fe(CO)_2(PH_3)]^{1-}$ and $[(\eta^2\text{-}SCH_2CH_2S)Fe(CO)_2(PH_3)(\mathbf{E})]^{1-}$ were geometry-optimized for E = H and E = Et. The $[(\eta^2\text{-}SCH_2CH_2S\mathbf{E})Fe(CO)_2(PH_3)]^{1-}$ complex optimizes to five-coordinate, trigonal bi-pyramidal structures, while the $[(\eta^2\text{-}SCH_2CH_2S)Fe(CO)_2(PH_3)(\mathbf{E})]^{1-}$ complexes optimize to six-coordinate octahedral structures. These optimized mononuclear iron complexes are shown Figure IV-8 and Figure IV-9. These computations show that the $[(\eta^2\text{-}SCH_2CH_2S)Fe(CO)_2(PH_3)(\mathbf{E})]^{1-}$ forms are significantly more stable than the corresponding $[(\eta^2\text{-}SCH_2CH_2S\mathbf{E})Fe(CO)_2(PH_3)]^{1-}$ forms for both E = H and E = Et. Thus, the origin of the instability of the $[(\mu\text{-Et})(\mu\text{-}SCH_2CH_2S)[Fe(CO)_2(PH_3)]_2]^{1+}$ must arise from the di-iron character.

Reforming the full di-iron complexes from the fragments

Figure IV-10 and Figure IV-11 illustrate a computational experiment in which one isomer oeach of the di-iron complexes given in Figure IV-3, Figure IV-4, Figure IV-5, and Figure IV-6 are built-up from the mononuclear fragments given in Figure IV-8 and Figure IV-9 via the formal addition of a $[Fe(CO)_2(PH_3)]^{2+}$ fragment. For both the mononuclear and dinuclear species, given in Figure IV-10, the metal hydride species is more stable than the corresponding protonated sulfur species. For the species arising from the addition of Et^+, given in Figure IV-11, the situation is quite different. While the mononuclear iron-alkyl complex is more stable than the corresponding alkylated

sulfur complex, the dinuclear iron-alkyl complex is much less stable that the corresponding species with an alkylated sulfur.

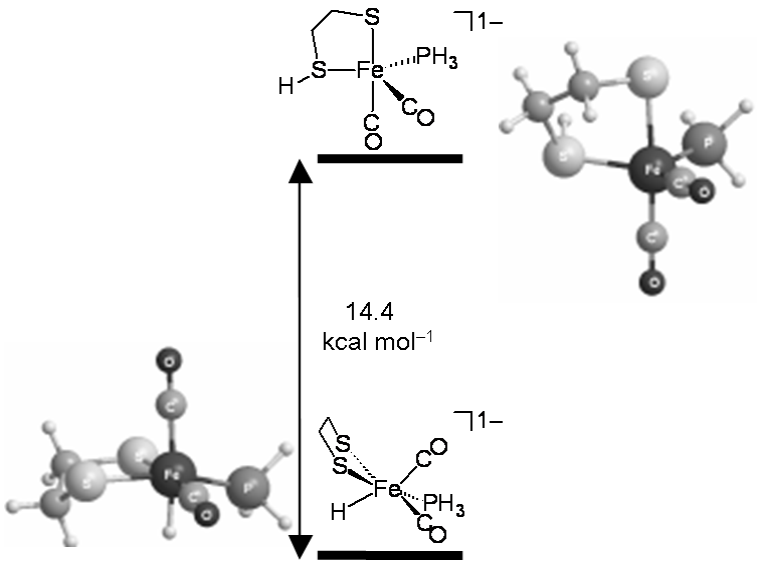

Figure IV-8. Relative zero-point corrected electronic energies for DFT geometry-optimized mononuclear iron complexes, derived by addition of H^+ to $[(SCH_2CH_2S)Fe(CO)_2(PH_3)]^{2-}$.

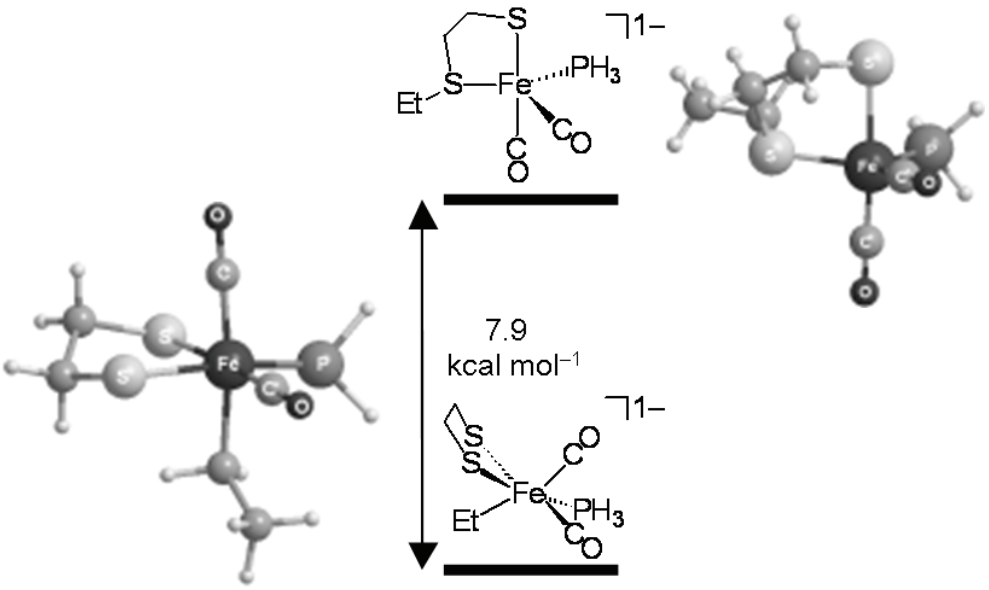

Figure IV-9. Relative zero-point corrected electronic energies for DFT geometry-optimized mononuclear iron complexes, derived by addition of Et^{+} to $[(SCH_2CH_2S)Fe(CO)_2(PH_3)]^{2-}$.

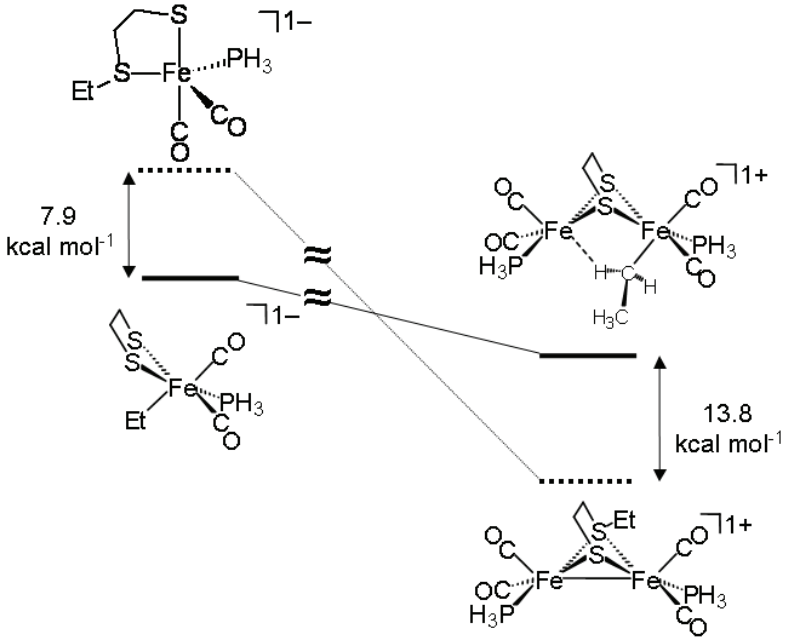

Figure IV-10. Building up the H^+ containing di-iron complexes from mononuclear iron fragments. The energy change to reform the dimer was not calculated as only the relative energies of the species are important.

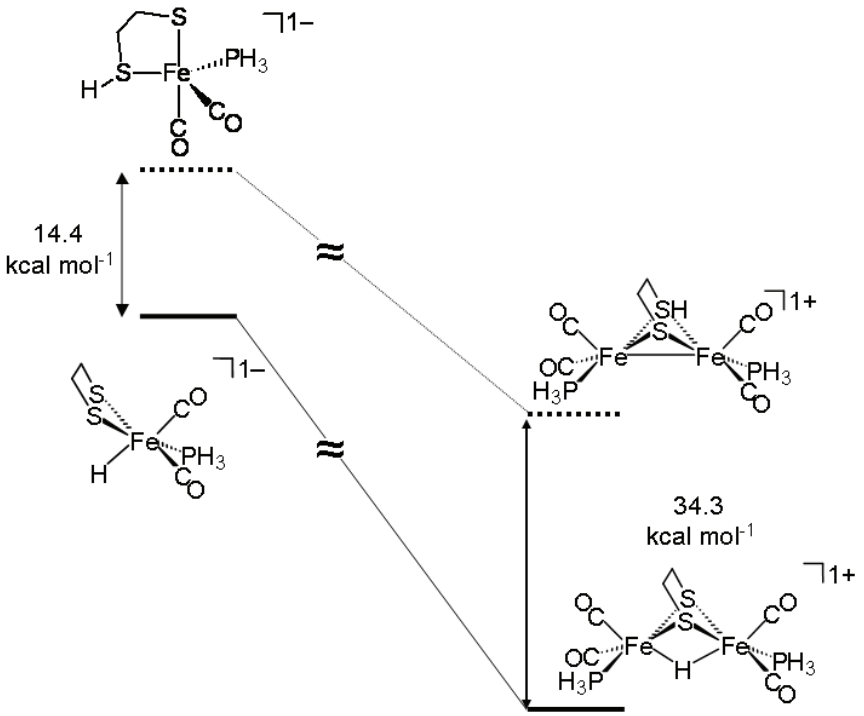

Figure IV-11. Building up the Et^+ containing di-iron complexes from mononuclear iron fragments. The energy change to reform the dimer was not calculated as only the relative energies of the species are important.

If we assume that protonation and alkylation of a sulfur atom have a similar effect on the Fe-S bond energies, then the difference observed for H and Et must lie in their differing abilities to bridge the two iron centers. The spherical nature of the 1s orbital of hydrogen allows for it to form a strong 3c-2e$^-$ bond with the two iron centers. The 18-electron count of the two iron centers are satisfied by virtue of this 3c-2e$^-$ bond. The empty sp^2 hybridized orbital on the Et^+, however does not allow for the formation of a strong 3c-2e$^-$ bond between the carbon of Et^+ and the two iron centers. As a result, it is more energetically favorable to form one strong 2c-2e$^-$ bond between carbon and one of the iron centers, and to satisfy the valence of the adjacent iron center by forming a weak agostic interaction. This weak agostic interaction cannot compensate for the loss of the bonding between the iron centers.

Conclusion

One may ask why it is more energetically favorable for the di-iron dithiolate complexes presented in this chapter to form a single Fe-C bond and an agostic interaction to the adjacent Fe center, while main group alkyls such as organo-aluminum compounds generally contain symmetrically bridging alkyl ligands. The nature of the bonding in the $[(\mu\text{-Et})(\mu\text{-SCH}_2\text{CH}_2\text{S})[\text{Fe(CO)}_2(\text{PH}_3)]_2]^{1+}$ complex is very covalent, while the nature of the bonding in a complex such as $(\mu\text{-CH}_3)_2[\text{Al(CH}_3)_2]$ is quite ionic. Strong covalent bonding requires large overlap between the orbitals of the ethyl group and the iron centers, and the very directional nature of the sp^3 hybrid orbital of the ethyl group does not allow for large overlap with both iron centers simultaneously. Since the

bonding in $(\mu\text{-}CH_3)_2[Al(CH_3)_2]$ is very ionic, it much less directional. Therefore, the largely ionic $\mu\text{-}CH_3$ group of $(\mu\text{-}CH_3)_2[Al(CH_3)_2]$ can effectively bond to the two aluminum centers simultaneously.

In general, we believe that the nature of the thermodynamic product resulting from attack of an electrophile, E, on complexes of the form, $(\mu\text{-}SCH_2CH_2S)[Fe(CO)_2(PR_3)]_2$ is determined by the ability of the resulting E^- to bridge the two iron centers. This contention is supported by computations on a mononuclear iron dithiolate complex, which show that for E = H or Et, Fe-E bond formation leads to more stable complexes that S-E bond formation. Therefore, the thermodynamic preference for S alkylation and Fe-Fe protonation is not due to some inherent difference in the Fe-E bond, but rather the differing ability of Et^- and H^- to effectively bridge the two iron centers.

CHAPTER V

CORRELATION BETWEEN COMPUTED GAS-PHASE AND EXPERIMENTALLY DETERMINED SOLUTION-PHASE INFRARED SPECTRA: MODELS OF THE IRON-IRON HYDROGENASE ENZYME ACTIVE SITE*

Introduction

Infrared (IR) spectroscopy is a powerful tool for studying metalloproteins that contain metal-bound diatomic ligands. When a diatomic ligand, such as CO, CN^-, or NO is bound to a transition metal center, it becomes a sensitive indicator of its environment and its characteristic frequency is modulated by changes in the metal oxidation state, in the nature of nearby residues such as their protonation state, and in its hydrogen bond network.[270] These diatomic ligands may be extrinsic (such as the NO and CO ligands present in the NO and CO inhibited forms of hemoglobin[271,272]) or intrinsic (such as the CO and CN^- ligands present in the hydrogenase enzymes[173,273]) to the protein or enzyme being studied.

Infrared spectroscopy has proven particularly useful in the study of the hydrogenase (H_2ases) enzymes. All H_2ases, studied to date, have been shown to contain iron-bound CO ligands. The nickel-iron ([NiFe]) and iron-iron ([FeFe]) enzymes contain both CO and CN^- as intrinsic ligands to their iron

* Reprinted with Permission from "Correlation Between Computed Gas-Phase and Experimentally-Determined Solution Phase Infrared Specrea: Models of the Iron-Iron Hydrogenase Enzyme Active Site" by Tye, J. W.; Darensbourg, M. Y.; Hall, M. B. J. Comput. Chem. submitted. Copyright 2006 by Wiley Periodicals, Inc.

centers.[130,138,139,142,169-171] When exposed to CO gas, both the [NiFe] and [FeFe] H_2ases bind an additional CO ligand that inhibits catalysis. This extrinsic CO appears as a new ν(CO) band in their infrared spectra, and as an additional CO ligand in their solid-state structures (as determined by EXAFS or single-crystal x-ray diffraction).[158,161,172]

Protein crystallography has defined the basic framework of the [FeFe]H_2ase active site (shown in Figure V-1), as consisting of a typical [4Fe-4S] cluster bridged

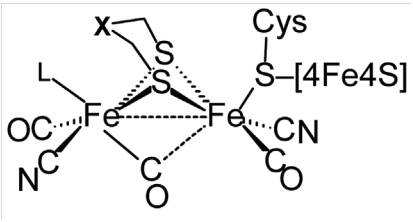

Figure V-1. Consensus structure for the active site of [FeFe]H_2ases. The two iron centers are commonly designated by their spatial relation to the [4Fe4S] cluster, and thus are referred to as the distal iron (left) and proximal iron (right). The nature of the L ligand and the "bridging" CO ligand (fully bridging vs. semi-bridging vs. terminal to the distal iron) apparently depends on the redox state of the FeFe cluster.

via a cysteinyl sulfur to a unique [FeFe] center.[169,171,172] The two iron centers are bridged by the two sulfur atoms of a five-atom dithiolate linker. Each iron of the di-iron cluster is further coordinated by one terminal CO ligand and one terminal CN^- ligand. A third CO ligand is found to either bridge the two iron centers or is terminally bound to the distal iron center. (The two iron centers are generally designated as either

proximal or distal to the [4Fe-4S] cluster.) The nature of the L ligand bound to the distal iron center and the orientation of the bridging CO ligand apparently depends on the crystallization conditions and the redox state of the enzyme active site.[172]

At least four distinct forms of the di-iron active site of [FeFe]H_2ase enzyme have been identified by the application of IR spectroscopy. Aerobic purification of the enzyme results in an over-oxidized, catalytically inactive form of the enzyme, known alternatively as $H_{as\text{-}isolated}$ or H_{ox}^{air}.[172,186,274] Reduction of the enzyme (electrochemically or chemically using H_2 gas or chemical reductants such as dithionite), leads to a reduced, catalytically active form of the enzyme, known as H_{red}.[172,186,274] Oxidation of the H_{red} form (electrochemically or chemically by auto-oxidation via H_2 loss or reaction with mild chemical oxidants) produces a species of intermediate oxidation state, known as H_{ox} (i. e. H_{ox} is more reduced than H_{ox}^{air}, but more oxidized than H_{red}).[172,186,274] The addition of CO gas to preparations of the catalytically active, H_{ox} form, yields a catalytically inactive, CO-inhibited form, known as H_{ox}-CO.[170,172]

Although the single-crystal x-ray diffraction studies of Peters, Fontecilla-Camps and their respective coworkers have defined the basic structure of the [FeFe]H_2ase active site, important questions remain. Which, if any, spectroscopically observed form of the [FeFe] cluster (H_{ox}^{air}, H_{ox}, H_{red}) do each of the solid-state structures represent? Electron density centered at a distance of ~2.6 Å from the distal iron in the native enzyme from *Clostridium pasteurianum* I (CpI) was modeled by the crystallographers as a terminally bound water molecule.[169] A recent re-evaluation of the x-ray structure of the Ni-A form of [NiFe] hydrogenase enzyme derived from *Desulfovibrio fructosovorans* showed that

the metal center is most likely bridged by a OOH^- ligand rather than the OH^- ligand that was originally proposed.[144] Could a similar species form at the [FeFe] active site? Single-crystal x-ray diffraction studies are generally unable to accurately locate hydrogen atoms. Therefore, what are the protonation states of the iron centers and iron-bound ligands in the various forms of the [FeFe]H_2ase active site?

The goal of this study is develop and test a computational methodology for predicting the infrared spectra of di-iron complexes that are similar in composition and structure to the active site of the [FeFe]H_2ase enzyme. In the present study, predicted IR spectra are used determine the best molecular structure for a spectroscopically observed intermediate in the electrochemical production of H_2 by a synthetic model of the active site of [FeFe]H_2ase and to predict the structure of one spectroscopically observed form of the [FeFe]H_2ase active site. This methodology will used in a subsequent study to discriminate between a series of structural candidates for various spectroscopically observed forms of the [FeFe]H_2ase enzyme.

Computational Details

All DFT calculations were performed using a hybrid functional [the three-parameter exchange functional of Becke (B3)[235] and the correlation functional of Lee, Yang, and Parr (LYP)[236]] (B3LYP) as implemented in Gaussian 03[275]. The iron, phosphorus, and sulfur atoms use the effective core potential and associated basis set of Hay and Wadt (LANL2DZ)[253,254]. For iron, the two outermost p functions were replaced by reoptimized 4p functions as suggested by Couty and Hall[254] and an f polarization function[276] was added. For sulfur and phosphorus, the basis set was augmented by the d

polarization function of Höllwarth *et al*.[256] The CO, CN^- ligands, the nitrile CN unit of the CNMe ligands, amine nitrogens, and hydrogen atoms attached to amine nitrogens use the 6-31G(d',p') basis set.[277-279] All other atoms use the 6-31G basis set.[280] Solvation calculations use the Onsager model as implemented in Gaussian 03.[281-286] Unless otherwise noted, all geometries are fully optimized and confirmed as minima or n-order saddle points by analytical frequency calculations at the same level.

Generation of simulated infrared spectra

The DFT calculations yield values for the energy (in cm^{-1}) and relative IR intensity of each ν(CX) stretching mode. The absolute intensity and width of the IR bands is not determined by the DFT calculation, and differs from experiment to experiment based on a number of experimental factors, such as concentration of the species, the solvent, and the nature of counterions for charged species. We simulate these computed IR bands by centering a gaussian function of the form $y = I*\exp[-S*(C-x)^2]$ (I and C, respectively, are the computed relative intensity and energy of the IR band; S is a scaling factor that adjusts the width of the gaussian function) about the value of the computed IR band, C. The width of an IR band at one-half of its maximum intensity, known as the half-width, is a commonly used measure of the width of experimentally-determined IR bands. Using the relation $S = (4/h^2)*\ln(1/2)$, $y = I*\exp[-S*(C-x)^2]$ can be written in terms of the half-width, h to yield $y = I*\exp[-(4/h^2)*\ln(1/2)*(C-x)^2]$. In order to plot n IR bands, n gaussian functions are summed to yield $y = \sum_{i=1}^{n}\{I_i * \exp[-(4/h^2) * \ln(1/2) * (C_i - x)^2]\}$. In general, we find it convenient to

define the same half-width for all of the IR bands in a given simulated IR spectrum. Infrared spectra are plotted using Microsoft Excel.

Results and Discussion

Selection of the training set

In order to be able to predict experimentally-determined solution-phase IR spectra from DFT-derived gas-phase values, we must determine a scaling factor between the experimental and theoretical values. This scaling factor is determined using a training set of complexes in which both the structure of the complex and its infrared spectrum is known. The selection of an appropriate training set is critical to the prediction of accurate ν(CO) and ν(CN) stretching frequencies. Three factors were considered in the selection of each member of this training set: (1) The total charge and chemical composition of the molecule is similar to the molecule of interest. Since the scaling factor adjusts the theoretically-determined values for the effects of solvation and systematic error in the experimental and theoretical values, the use of a scaling factor determined for molecules that are drastically different from the molecule of interest is ill-advised. For example, the use of a series of ruthenium carbonyl complexes to determine the scaling factor for ν(CO) bands for an iron carbonyl complex may yield poor results since the systematic error arising from the Ru basis set is different than that arising from the Fe basis set. (2) The solvent used for the experimentally-determined IR spectra are non-protic. (3) For charged species, only complexes with large, weakly-coordinating counterions were considered. Small, strongly coordinating counterions and highly polar, protic solvents may form strong interactions with the CO and CN^- ligands,

shifting their values, relative to the same complex with large, weakly coordinating and/or non-protic, weakly-polar solvent. Obviously, the latter conditions are more appropriate for predicting solution-phase spectra based on gas-phase calculations of the "naked" complex ion. The training set used in this chapter is presented in Table V-1 and Figure V-2.

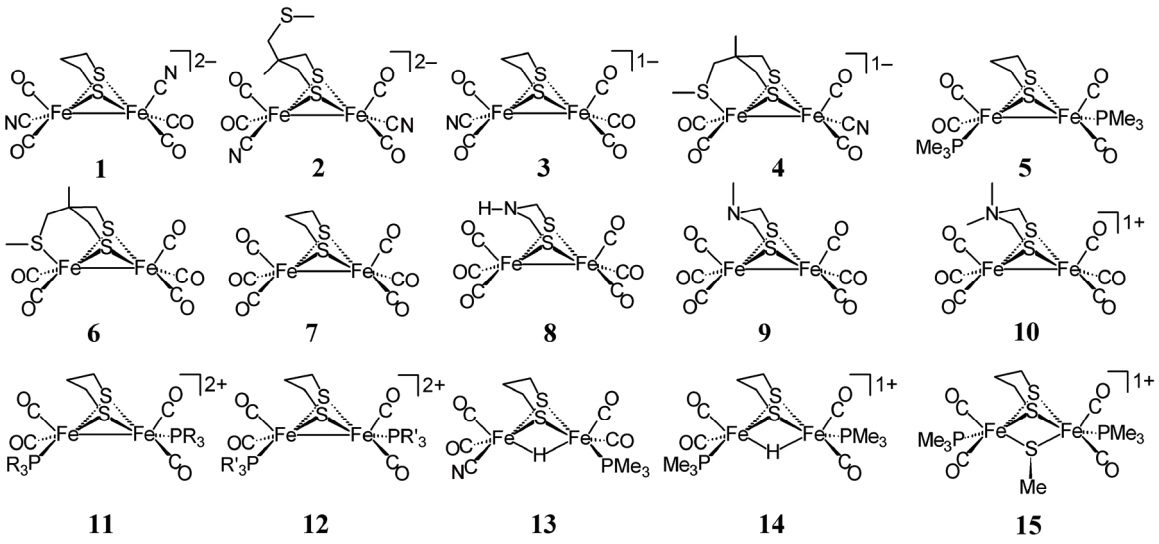

Figure V-2. Structures for a series of synthetic models for the active site of [FeFe]H_2ase. PR_3 and PR'_3 refer, respectively, to singly N-protonated and N-methlylated 1,3,5-triaza-7-phosphaadamantane. References to the experimental data are given in Table V-1.

Assignment of the computed spectra

Three cases are observed in examination of experimentally-determined IR spectra: (1) The number of ν(CX) bands is the same as the number of CX ligands in the

complex. (2) The number of ν(CX) bands is less than the number of CX ligands in the complex. For highly symmetric molecules, two or more of the C-X stretching modes may be degenerate (same ν(CX) value) or have no IR intensity by symmetry. (A stretching mode does not result in a change in the molecular dipole moment is not observed by IR spectroscopy.) Alternatively, one or more of the experimentally observed ν(CX) "bands" may in fact correspond to the accidental degeneracy (degeneracy that is not required by the symmetry of the molecule) of two or more fundamental stretching modes, or the concentration of the sample may be such one or more low-intensity ν(CX) bands are indistinguishable from the spectral baseline. (3) The number of ν(CO) or ν(CN) bands is more than the number of CO and CN ligands in the complex. This situation occurs when there is a mixture of two or more CX-containing species present in the sample solution.

For case 1 situations, each of the computed ν(CX) stretching frequencies should correlate in a one-to-one manner with the experimentally observed ν(CX) bands, and the spectra should be simple to assign. The $[(\mu\text{-}S(CH_2)_3S)[Fe(CO)_3][Fe(CO)_2(CN)]]^{1-}$ complex (**3**) provides an example of case 1. The experimentally determined IR spectrum of $[(\mu\text{-}S(CH_2)_3S)[Fe(CO)_3][Fe(CO)_2(CN)]]^{1-}$ features five ν(CO) bands and one ν(CN)

Table V-1. Counterions and Solvent Used for the Experimentally-Determined IR Spectra

complex[1]	counterion(s)	solvent	reference
1	$[18\text{-crown-6-K}]^{1+}$	CH_3CN	182
2	$[18\text{-crown-6-K}]^{1+}$	CH_3CN	190
3	$[NEt_4]^{1+}$	THF	181,287
4	$[NEt_4]^{1+}$	CH_3CN	190
5	n/a	CH_3CN	203
6	n/a	CH_3CN	190
7	n/a	hexanes	181,288
8	n/a	hexanes	184
9	n/a	CH_3CN	263
10	n/a	CH_3CN	263
11	$[F_3CSO_3]^{1-}$	CH_3CN	195
12	$[PF_6]^{1-}$	CH_3CN	195
13	n/a	THF	196
14	$[PF_6]^{1-}$	CH_3CN	203
15	$[BF_4]^{1-}$	CH_2Cl_2	249

1. Chemical structures of these complexes given in Figure V-2.

band.[287] Each of the six C-X stretching frequencies of the computed spectrum of **3** is assigned to one of the bands of the experimentally-determined IR spectrum (as shown in Figure V-3). These six vibrations correspond to the group vibrations of the six CX ligands in the following manner: (see legend in Figure V-3(c) for labels) 2022 cm^{-1} [r2−r6]; 2037 cm^{-1} [$r_1-r_5-r_6$]; 2044 cm^{-1} [$r_2-r_4-r_5+r_6$]; 2067 cm^{-1} [$r_1-r_4+r_5$]; 2105 cm^{-1} [$r_1+r_2+r_4+r_5+r_6$]; 2223 cm^{-1} [r_3].

For case 2a situations, the assignment of the spectra should be simple if the "missing" bands correspond to degenerate stretching modes, or stretching modes that are

not IR active by symmetry. In other words, for case 2a, the number of ν(CX) bands is the same as that one would predicted by analyzing the molecule by group theory. In the case of degenerate vibrations, the computation should predict that two or more of the fundamental stretching modes will occur at approximately the same energy. In the case of vibrations that are not IR active, the computation should predict that these vibrations have little or no IR intensity. The $(\mu\text{-}S(CH_2)_3S)[Fe(CO)_3]_2$ complex (**7**) provides one example of case 2. Simple group theoretical analysis of this pseudo-C_{2v} molecule predicts five IR-active bands, and five ν(CO) bands are observed in the experimentally determined IR spectrum of **7** in hexanes.[288] Consistent with these results, five of the sixν(CO) bands are computed to have non-negligible IR intensities (The six computed intensities, given in order of increasing intensity, are 0.02, 35.81, 571.60, 828.89, 1180.05, and 2217.82). The band with a computed intensity of 0.02 is the C-O stretch mode predicted by group theory to have no intensity in the IR spectrum. The assignment of the computed ν(CO) bands of **7** is given in Figure V-4. These six vibrations correspond to the group vibrations of the six CO ligands in the following manner: (see legend in Figure V-4(c) for labels) 2083 cm^{-1} $[r_1-r_2+r_3-r_4-r_5+r_6]$; 2089 cm^{-1} (no IR intensity) $[r_1-r_2-r_3+r_4]$; 2093 cm^{-1} $[r_1+r_2+r_3+r_4-r_5-r_6]$; 2105 cm^{-1} $[r_1+r_2-r_3-r_4]$; 2111 cm^{-1} $[r_1-r_2+r_3-r_4+r_5-r_6]$; 2157 cm^{-1} $[r_1+r_2+r_3+r_4+r_5+r_6]$

For other case 2 examples, the situation is more complex when one or more of the experimentally observed ν(CX) "bands" corresponds to the overlap of two or more accidentally degenerate, fundamental C-X vibrational modes (case 2b), or when one or

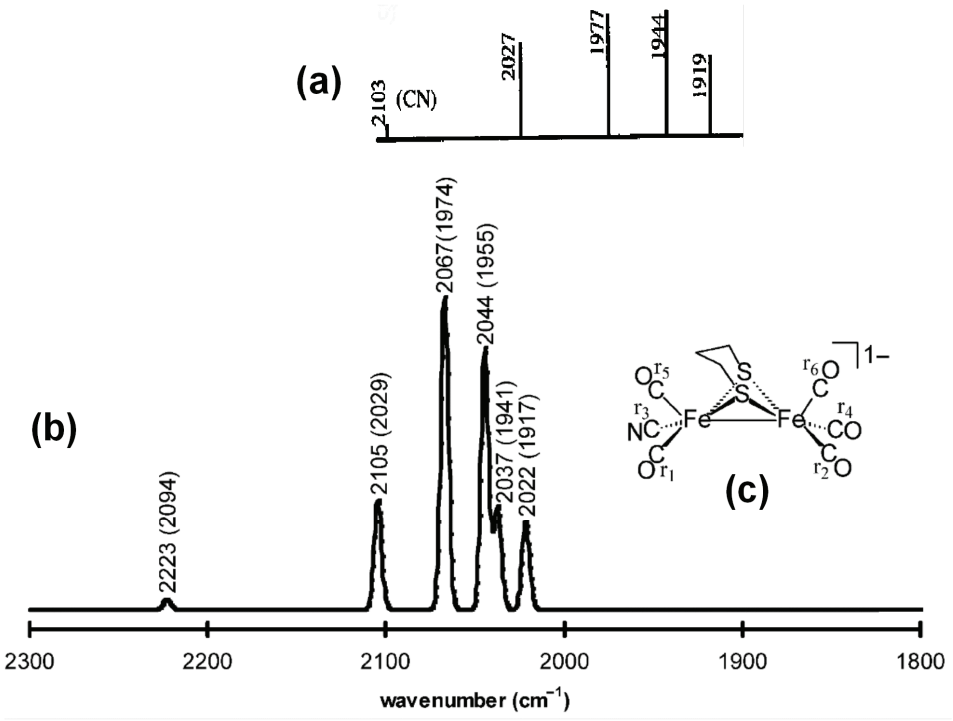

Figure V-3. Simulation of the IR spectrum of $[(\mu\text{-}S(CH_2)_3S)[Fe(CO)_3][Fe(CO)_2(CN)]]^{1-}$ (3). In (a), a line diagram of the experimental spectrum of **3** is reproduced from reference 41. In (b), the simulated IR spectrum of **3** is presented. A half-width of 5 cm^{-1} was used in the simulation of each ν(CX) band. The unscaled computed energy of each C-X stretching mode is given above the simulated ν(CX) band. The value of the corresponding experimentally-determined ν(CX) band from ref 40 is given in parentheses. In (c), the labeling scheme for CO and CN ligands complex **3** is given.

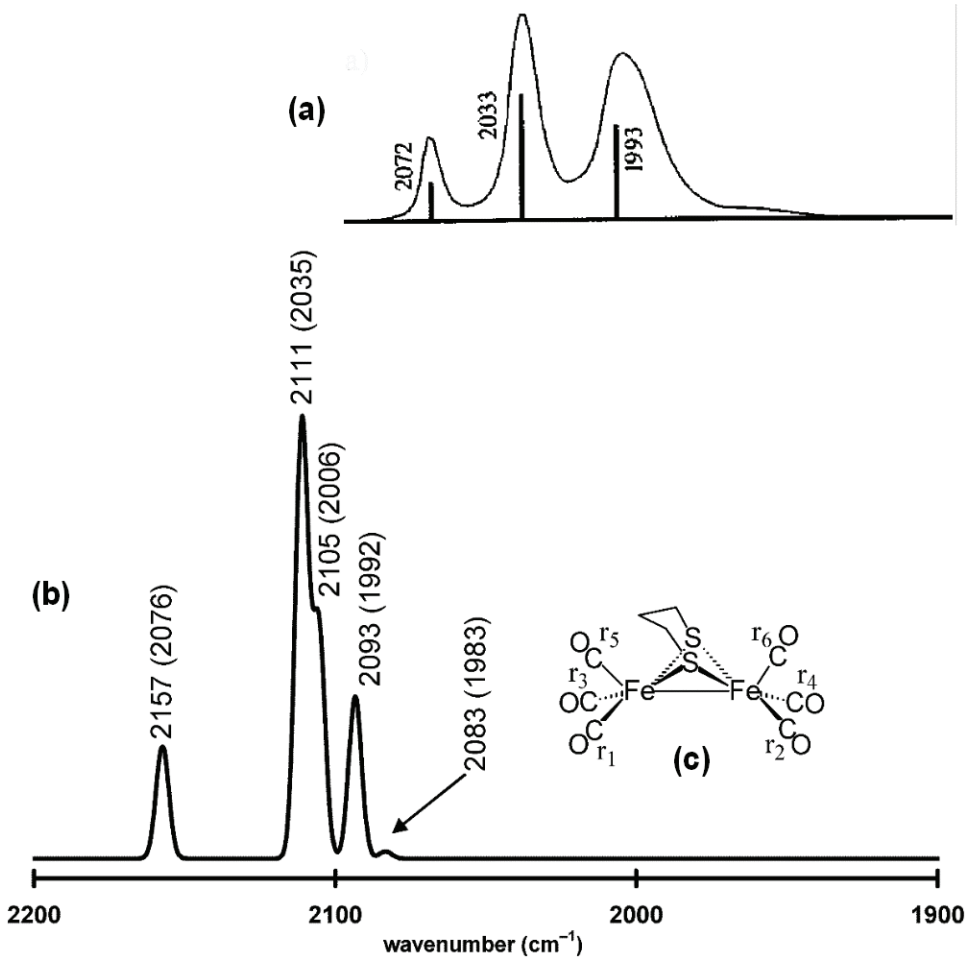

Figure V-4. Simulation of the IR spectrum of $(\mu\text{-}S(CH_2)_3S)[Fe(CO)_3]_2$ (**7**). In (a), the experimental spectrum of **7** is reproduced from reference 41. In (b), the simulated IR spectrum of **7** is presented. A half-width of 5 cm^{-1} was used in the simulation of each ν(CO) band. The unscaled computed energy of each C-X stretching mode is given above the simulated ν(CO) band. The value of the corresponding experimentally-determined ν(CO) band from reference 43 is given in parentheses. In (c), the labeling scheme for CO ligands complex **7** is given.

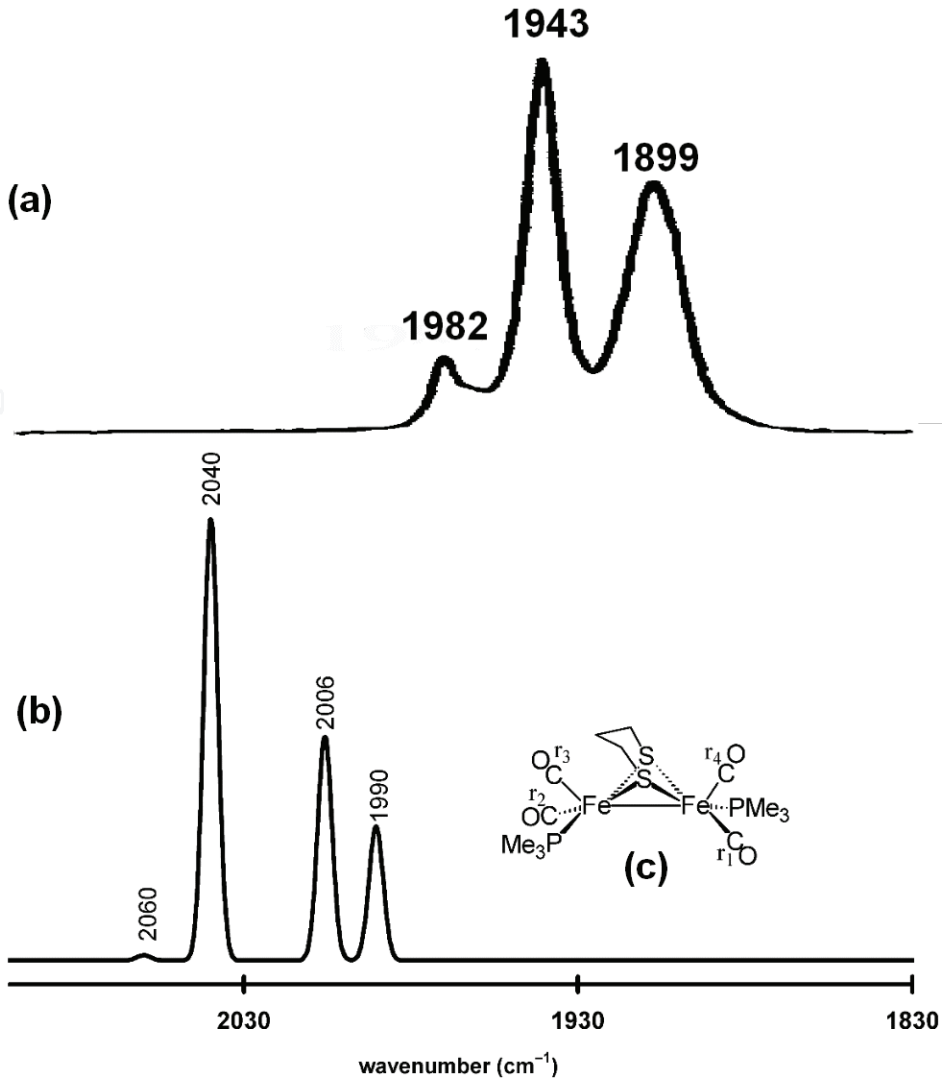

Figure V-5. Simulation of the IR spectrum of (μ-S(CH$_2$)$_3$S)[Fe(CO)(PMe$_3$)$_2$]$_2$ (**5**). In (a), the experimental spectrum of **5** is reproduced from reference 42. In (b), the simulated IR spectrum of **5** is presented. A half-width of 5 cm^{-1} was used in the simulation of each ν(CO) band. The unscaled computed energy of each C-X stretching mode is given above the simulated ν(CO) band. In (c), the labeling scheme for CO ligands complex **7** is given.

more bands with low relative intensities are present (case 2c). The (μ-$S(CH_2)_3S)[Fe(CO)_2(PMe_3)]_2$ complex (**5**) provides such an example. The experimentally-determined IR spectrum of **5** features ν(CO) bands at 1979, 1942, and 1898 cm^{-1}.[203] The computed ν(CO) stretching frequencies (and corresponding computed IR intensities) are 2060 cm^{-1} (22.47), 2040 cm^{-1} (1877.01), 2006 cm^{-1} (950.11), and 1990 cm^{-1} (568.45). In the absence of a graphic of the experimental IR spectrum, one might be tempted to assign the three experimentally-observed ν(CO) bands to the three computed C-O stretching frequencies with large relative intensities. The direct comparison of experimentally-determined spectrum and the computed spectrum of **5** clearly shows that 1979, 1942, and 1898 cm^{-1} bands in the experimental spectrum correspond to the 2060, 2040, and 2006 cm^{-1} C-O stretching frequencies of the computed spectrum (shown in Figure V-5). These four vibrations correspond to the group vibrations of the six CO ligands in the following manner: (see legend in (c) for labels) 1990 cm^{-1} $[r_1-r_2+r_3-r_4]$; 2006 cm^{-1} $[r_1+r_2-r_3-r_4]$; 2040 cm^{-1} $[r_1-r_2-r_3+r_4]$; 2060 cm^{-1} $[r_1+r_2+r_3+r_4]$.

In general, we find that the best method to accurately assign these spectra is to simulate the computed spectrum and visually compare it to the experimentally-determined spectrum. Even when only ν(CX) values are reported and no graphic of the experimentally-determined spectrum is available, simulation of the computed spectrum is beneficial for estimating which fundamental C-X stretching modes contribute to each ν(CX) band observed in the experimentally-determined spectrum.

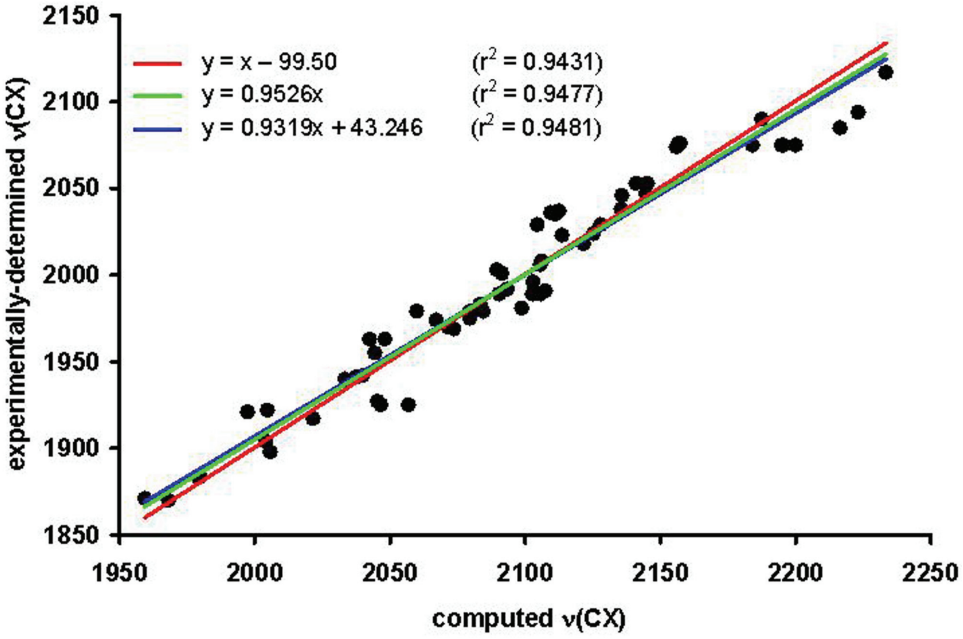

Figure V-6. A plot of experimentally-determined ν(CX) frequencies versus computed ν(CX) frequencies.

Evaluation of the training set

The experimentally-determined ν(CO) and ν(CN) values are plotted versus the corresponding computed C-X stretching frequencies as shown in Figure V-6. We use a standard method of scaling computed frequencies in which a multiplicative scaling factor (i.e. a linear regression in which the y-intercept is set to 0; y = mx) in order to scale the computed ν(CX) frequencies.[289-291] This method gave the equation y =

0.9526x with an r^2 value of 0.9477 (The r^2 value is a measure of how well a regression line represents a series of data. Mathematically, it is the ratio of regression varience to total variance.)

Two other linear regressions have been performed on this data set and they will be discussed for illustrative purposes (see Figure V-6). If the slope is set to 1.0 and the y-intercept is optimized, this gives the equation $y = x - 99.50$ with an r^2 value of 0.9431. If both the slope of the line and the y-intercept are allowed to optimize, this gives the equation $y = 0.9319x + 43.246$ with an r^2 value of 0.9481. It is interesting that optimizing the y-intercept and slope, optimizing only the y-intercept, and optimizing only the slope give comparable descriptions of this data set in terms of the r^2 value of the linear regression. In terms of basic statistics, these results show that the x and y values highly correlated, and there is no unique values of the y-intercept and slope of the line that define the data set. This phenomenon occurs when one is plotting a narrow set of values especially for deterministic data. Deterministic data is data that contains only systematic errors (i. e. no random errors). The standard procedure for scaling frequency data (y-intercept = 0) will be used throughout the text.

The value of the scaling factor, 0.9526 (σ = standard deviation = 0.0067), calculated using the experimentally-determined and computed values for the entire training set (complexes **1**–**15** in Figure V-2), is similar to the value that one may compute for the various subsets of molecules from the training set. The values vary from 0.9491 ($\sigma = 0.0048$) for the monocationic $Fe^{II}Fe^{II}$ complexes **14** and **15** to 0.9556 ($\sigma = 0.0033$) for monocationic $Fe^{I}Fe^{I}$ complex, **10**. The experimentally-determined

infrared spectra used in this correlation were measured using solvents with a wide range of polarity: hexane (dielectric constant at 20° C = ε_{20} = 1.9), THF (ε_{20} = 7.5), CH_2Cl_2 (ε_{20} = 8.9), CH_3CN (ε_{20} = 36.6).[292] The value of the scaling factor determined for the subsets based on solvent vary from 0.9502 (σ = 0.0055) for complex **15** in CH_2Cl_2 solvent to 0.9566 (σ = 0.0059) for complexes **7** and **8** in hexanes solvent. These results indicate that there are no large systematic errors introduced by correlating computed gas-phase IR spectra with experimentally-determined IR spectra in solvents with a wide range of polarity (ε_{20} values range from 1.9 to 36.6) or by using the same scaling factor for species of different charge.

The prediction of ν(CO) frequencies for bridging CO ligands

For terminal CO and CN^- ligands, the experimentally-determined ν(CO) and ν(CN) stretching frequencies are reproduced remarkably well by simple scaling of the computed ν(CO) and ν(CN) stretching frequencies. For bridging CO ligands, however, the predictions become more difficult. For example, the $[(\mu\text{-CO})(\mu\text{-S(CH}_2)_2\text{S})[\text{Fe(CNMe)}_3]_2]^{2+}$ and $[(\mu\text{-CO})(\mu\text{-S(CH}_2)_3\text{S})[\text{Fe(CNMe)}_3]_2]^{2+}$ complexes have been shown, experimentally to have a ν(CO) stretching frequencies of 1914 cm^{-1} and an Fe-Fe distances of ~ 2.5 Å.[293] Full geometry optimization of these complexes leads to predicted ν(CO) stretching frequencies of 1960 and 1985 cm^{-1} and Fe-Fe distances of 2.57 and 2.65 Å, respectively, for the $[(\mu\text{-CO})(\mu\text{-S(CH}_2)_2\text{S})[\text{Fe(CNMe)}_3]_2]^{2+}$ and $[(\mu\text{-CO})(\mu\text{-S(CH}_2)_3\text{S})[\text{Fe(CNMe)}_3]_2]^{2+}$ complexes. Partial geometry optimization of these complexes with the Fe-Fe distance frozen at its experimentally determined distance of

~2.5 Å led to predicted ν(CO) stretching frequencies of 1949 and 1951 cm^{-1}, respectively, for the $[(\mu\text{-CO})(\mu\text{-S(CH}_2)_2\text{S})[\text{Fe(CNMe)}_3]_2]^{2+}$ and $[(\mu\text{-CO})(\mu\text{-S(CH}_2)_3\text{S})[\text{Fe(CNMe)}_3]_2]^{2+}$ complexes. The predicted ν(CN) stretching frequencies of the terminal CNMe ligands are very similar to the experimental determined ν(CN) stretching frequencies in both cases, and are essentially unaffected by this small change in the Fe-Fe distance. The improved Fe-Fe distance improved agreement and brought the frequencies to the same value, but the calculated ν(CO) values for the bridging CO bands are still a little too high in part because the test set does not have any bridging CO ligands. Other functionals need to be tested to determine if another functional will yield a better Fe-Fe distance and improved ν(CO) frequencies for bridging CO ligands. For example, it is likely that a functional could be found that gives a slope of 1.0 for the ν(CO) training set and therefore does not need scaling.

Application 1: structural assignment of a transient, electrochemically-generated species

The close structural analogy between simple di-iron dithiolate complexes and the active site of [FeFe]H_2ase has led several research groups to examine the ability of di-iron dithiolate assemblies to act as functional models of [FeFe]H_2ase.[194-199,294] The $(\mu\text{-S(CH}_2)_3\text{S})[\text{Fe(CO)}_3]_2$ complex, **7**, has been shown to function as a simple and robust electrocatalyst for proton reduction.[194,294] In this context, the molecular details of the electrochemical reduction process of complexes such as complex **7** are of current interest.

Darensbourg, Best and Pickett, and their respective coworkers have undertaken in-depth studies of the species generated upon reduction of **7** and related complexes at a graphite electrode.[194,294] These workers present evidence that complex **7** undergoes a one-electron reduction at ~ –1.1 V vs. SCE (SCE = standard calomel electrode) to form a one-electron reduced, odd-electron species. The early results of Darchen and coworkers on the electrochemistry of **7** at a mercury drop electrode suggests that this complex undergoes a simultaneous two-electron reduction at –1.17 V vs SCE.[295]

Best, Pickett, and coworkers utilized thin-layer spectroelectrochemical techniques to obtain infrared spectroscopic data for a short-lived species resulting from the reduction of complex **7.**[294] Four possible structural candidates for this spectroscopically-observed species are presented in Figure V-7. Species **[7-I]**$^{1-}$ and **[7-III]**$^{2-}$, respectively, are one- and two-electron reduced species in which both

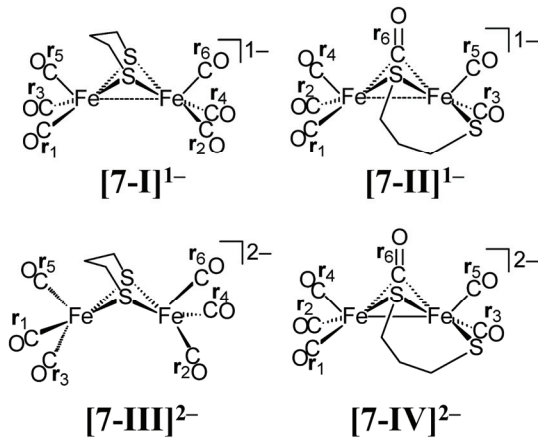

Figure V-7. Structural candidates for a spectroscopically-observed species resulting from the electrochemical reduction of complex **7** .

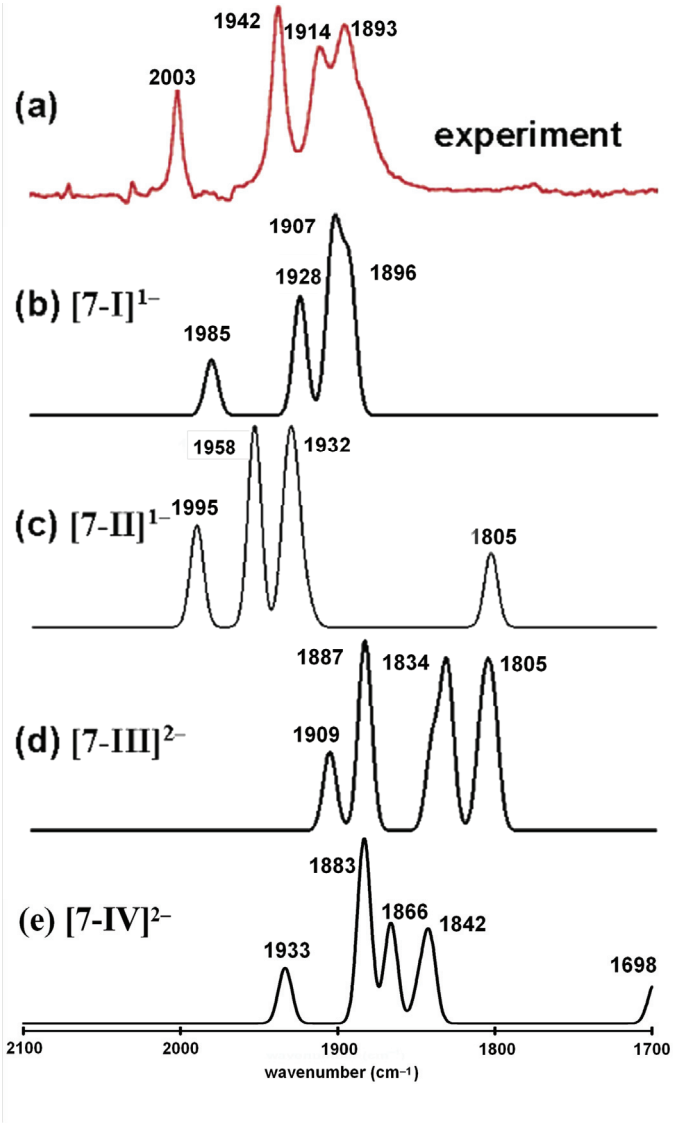

Figure V-8. A comparison of an experimentally-determined IR spectrum (reproduced from reference 59) for a species resulting from the reduction of complex **7**, (a), and DFT-derived simulated spectra for various structural candidates for this species (b)-(e). Simulated spectra use a half-width of 10 cm^{-1} and the computed ν(CX) values are scaled using a factor of 0.9526.

bridging thiolate sulfur atoms are fully bridging (i.e. a structure that is largely similar to **7**). Species **[7-II]**$^{1-}$ and **[7-IV]**$^{2-}$, respectively, are one- and two-electron reduced species in which a thiolate sulfur atom and one CO ligand bridges the two iron centers and the other thiolate sulfur is terminally coordinated to one of the iron centers. The experimentally-determined IR spectrum of this species is given in Figure V-8**(a)**, and the DFT-derived simulated spectra of four structural candidates for this species are given in Figure V-8**(b)-(e)**. A comparison of the experimentally determined IR spectrum (Figure V-8**(a)**) and the DFT-derived simulated IR spectra clearly shows that the **[7-I]**$^{1-}$ species (given in Figure V-8**(b)**) is the best match to experimentally-determined spectrum in terms of both the range and relative intensities of the ν(CO) bands. Comparison of the sum of the squares of the differences between the computed and experimentally-determined ν(CO) bands of the electrochemically-generated product and the candidate species shows that **[7-I]**$^{1-}$(sum of the squares of the difference for the CO ligands = b = 587) is a mcuh better structural candidate for this product form than the **[7-II]**$^{1-}$ (b = 8178), **[7-III]**$^{2-}$ (b = 26065), or **[7-IV]**$^{2-}$ (b = 13227) structural candidates.

The six vibrations of each model correspond to the group vibrations of the six CO ligands in the following manner: (see legend in Figure V-7 for labels) **[7−I]1−** 1896 cm^{-1} [r_5−r_6]; 1904 cm^{-1} [r_4−r_5−r_6]; 1907 cm^{-1} [r_1−r_2−r_4]; 1911 cm^{-1} [r_1−r_2−r_3+r_4]; 1928 cm^{-1} [r_1+r_2−r_3−r_4]; 1985 cm^{-1} [r_1+r_2+r_3+r_4+r_5+r_6], **[7−II]1−** 1805 cm^{-1} [r_6]; 1924 cm^{-1} [r_1+r_2−r_3−r_4+r_5]; 1932 cm^{-1} [r_1−r_2+r_3−r_4−r_5]; 1937 cm^{-1} [r_2−r_4]; 1958 cm^{-1} [r_3+r_5]; 1995 cm^{-1} [r_1+r_2+r_3+r_4], **[7−III]2−**1805 cm^{-1} [r_2−r_3+r_5−r_6]; 1811 cm^{-1} [r_1−r_5−r_6]; 1834 cm^{-1}

$[r_1+r_2-r_3-r_4]$; 1843 cm^{-1} $[r_1-r_2-r_3+r_4]$; 1887 cm^{-1} $[r_1+r_2-r_3+r_4-r_5+r_6]$; 1909 cm^{-1} $[r_1+r_2+r_3+r_4+r_5+r_6]$, **[7−IV]2−** 1698 cm^{-1} $[r_6]$; 1842 cm^{-1} $[r_1+r_2-r_4]$; 1848 cm^{-1} $[r_1-r_2+r_4]$; 1866 cm^{-1} $[r_3-r_5]$; 1883 cm^{-1} $[r_1+r_2-r_3+r_4]$; 1933 $[r_2+r_3+r_4]$ cm^{-1}

Application 2: structural assignment of a IR spectroscopically-observed form of the active site of the [FeFe]H_2ase enzyme

The solid-state structure of the [FeFe]H_2ase enzyme derived from CpI indicates the presence of a water molecule "coordinated" to the distal iron center with a rather long Fe-O distance of 2.6 Å.[169] Although there is no definitive proof, it has been suggested on the basis of the crystallization conditions that this structure corresponds to the mixed valent, S = 1/2, H_{ox} form of this enzyme.[172] Four potential structural models for the H_{ox} form were geometry-optimized and their predicted ν(CO) and ν(CN) stretching frequencies were computed. (The CH_3SH ligand is used to model the Cys-S-$[Fe_4S_4]$ portion of the enzyme active site.) The geometry-optimized H_2O-containing models do not show coordination of the water molecule to the iron center (Fe-O distance > 3 Å). Representation of these four structural candidates for the H_{ox} form are given in Figure V-9. The experimentally-determined IR spectrum of the EPR-active, S = 1/2, H_{ox} form of the [FeFe]H_2ase enzyme derived from CpI is compared to the predicted spectra for four structural candidates of the H_{ox} form in Figure V-10. In terms of their predicted stretching frequencies and relative intensities of the ν(CO) bands, all four of the structural candidates are qualitatively similar to one another and a fairly good match to the experimentally-determined IR spectrum. The computed C-X bands correspond to the vibrations in the same manner for all four models (see legend in Figure V-9 for

labels). The highest energy bands correspond to uncoupled vibrations of the cyanide ligands r_4 and r_1, respectively. The highest and intermediate energy CO bands correspond to r_2 and r_3, respectively. The lowest energy CO band corresponds to the bridging CO ligand, r_5. Comparison of the sum of the squares of the differences between the computed and experimentally-determined terminal ν(CO) band shows that **H_{ox}(I)** (sum of the squares of the difference for the terminal CO ligands = a = 29.7) is a slightly better structural candidate for the H_{ox} form than the **H_{ox}(II)** (a = 36.1), **H_{ox}(III)** (a = 38.3), or **H_{ox}(IV)** (a = 35.5) structural candidates. In addition, Mulliken spin analysis shows that the unpaired electron density is localized on the distal iron center in all of these models, which agree with the EPR studies performed on the H_{ox} form of the enzyme.

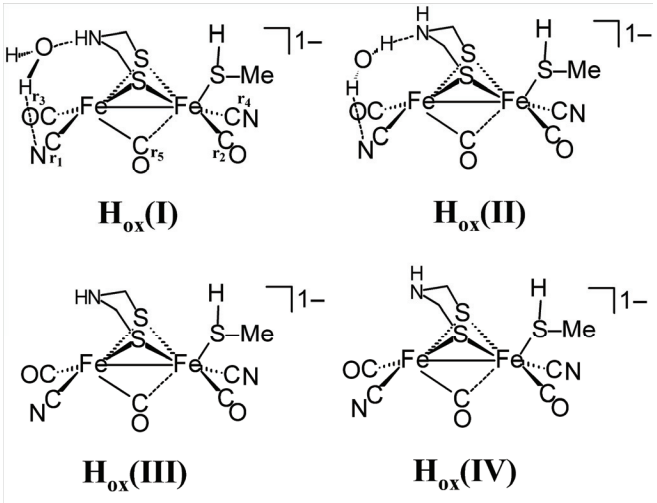

Figure V-9. Structural candidates for the spectroscopically-observed H_{ox} form of the [FeFe]H_2ase enzyme derived from CpI .

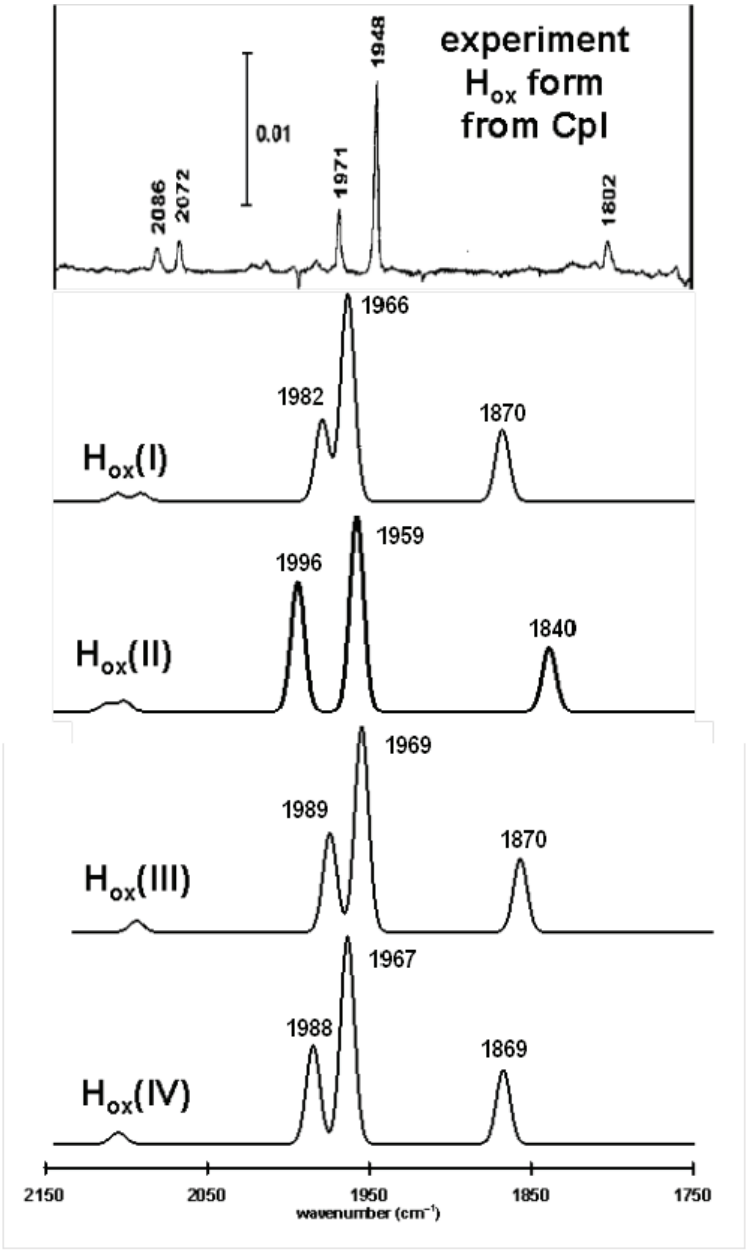

Figure V-10. A comparison of the experimentally-determined H_{ox} form of the [FeFe]H_2ase enzyme from CpI (reproduced from reference 11) and predicted infrared spectra for various structural candidates. Simulated spectra use a half-width of 10 cm^{-1} and the computed ν(CX) values are scaled using a factor of 0.9526.

These computations show that the $Fe^{I}Fe^{II}$ formal oxidation state, in which the unpaired electron is localized on the distal iron center is a good model for the H_{ox} form of the active site of the [FeFe]H_2ase enzyme derived from CpI in terms of the predicted IR spectra.[186,274] In this context it is interesting to not that recent computations of Brunold and coworkers recently found that a model similar to ours fails to reproduce the experimentally-observed magnetic properties of the H_{ox} and H_{ox}-CO forms of the [FeFe]H_2ase active site and that inclusion of the proximal [4Fe4S] is necessary to accurately reproduce the magnetic properties.[296] Geometry-optimization of the H_2O-containing forms do not show as short Fe-O distance as that determined in the x-ray diffraction study. However, the absence or presence of a water molecule near the distal iron center does not have a profound effect on the predicted IR spectra. Therefore, it is not clear if this water molecule is an important and intrinsic part of the active site of this [FeFe]H_2ase.

Conclusions

We have been demonstrated that gas-phase DFT calculations can yield accurate estimates of experimentally-determined solution-phase ν(CO) and ν(CN) stretching frequecies for a series of di-iron dithiolate complexes when multiplied by a scaling factor. The scaling factor that we determine for this series of complexes appears to be quite robust, but depends on the basis set and DFT functional. The value of the scaling factor predicted by each sub-set of complexes is very similar and demonstrates no obvious effect of the total charge or the formal oxidation states of the irons centers.

Studies of these model complexes can improve the value of IR calculation on a larger, more complex model of the [FeFe]H_2ase enzyme.

CHAPTER VI

DUAL ELECTRON UPTAKE BY SIMULTANEOUS IRON AND LIGAND REDUCTION IN AN N-HETEROCYCLIC CARBENE SUBSTITUTED [FeFe] HYDROGENASE MODEL COMPOUND*

Introduction

The hydrogenase enzymes catalyze the reversible reduction of protons to dihydrogen: $2H^+ + 2e^- \leftrightarrow H_2$,[237] utilizing dinuclear active sites comprised of sulfur-bridged [NiFe] or [FeFe] assemblies. In a non-biological setting, proton reduction and H_2 oxidation are normally most readily accomplished at a platinum electrode. Almost immediately after their discovery, the prospect of replacing such expensive catalysts by these base metal-containing enzymes was recognized. In fact, when absorbed onto a graphite electrode the [NiFe] hydrogenase enzyme from *Allochromatium vinosum* has been shown to function as a heterogeneous catalyst for H_2 oxidation.[297] Although the [NiFe] enzymes are generally more thermally and O_2 stable,[237] the [FeFe] enzyme active site has proven more amenable to small molecule model studies due to its resemblance to well-known organometallic complexes of the type $(\mu\text{-SR})_2[Fe^I(CO)_2L]_2$.[181-183] We and others have found that these complexes function as solution electrocatalysts for H_2 production.[194-196,294]

---

*Reprinted with permission from "Dual Electron Uptake by Simultaneous Iron and Ligand Reduction in an N-Heterocyclic Carbene Substituted [FeFe] Hydrogenase Model Compound" by Tye, J. W.; Lee, J.; Wang, H.-W.; Mejia-Rodriguez, R.; Reibenspies, J. H.; Hall, M. B.; Darensbourg, M. Y. *Inorg. Chem.* **2005**, *44*, 5550-5552. Copyright 2005 by American Chemical Society.

The model complexes, synthesized to date, require strong acids and/or much more negative reduction potentials to produce H_2. The difference could lie in the substitution pattern and donor strength of the non-CO ligands, as shown in Figure VI-1.

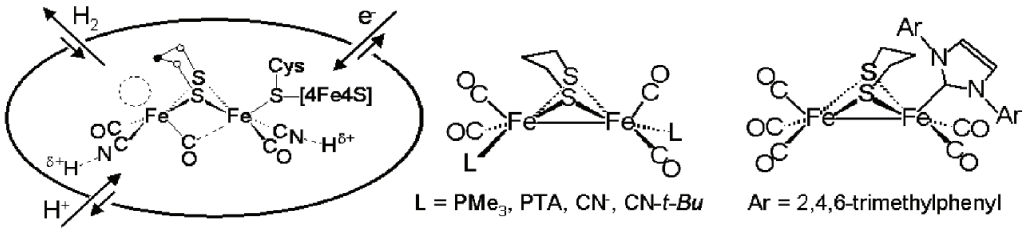

Figure VI-1. Comparison of the enzyme active site (a), symmetrically substituted model complexes (b), and an asymmetrically substituted model complex (c).

DFT calculations suggest that an asymmetrically substituted complex which has one end locked in position by a sterically encumbered ligand with excellent donating ability might have special features conducive to H_2 electrocatalysis.[298] We have thus prepared the N-heterocyclic carbene-containing model compound, (μ-$S(CH_2)_3S$)[$Fe(CO)_3$] [$Fe(CO)_2$IMes], **1-IMes**, Figure VI-1(C). (IMes = 1,3-bis(2,4,6-trimethylphenyl)imidazol-2-ylidene). The x-ray derived molecular structure of **1-IMes** is given in Figure VI-2.

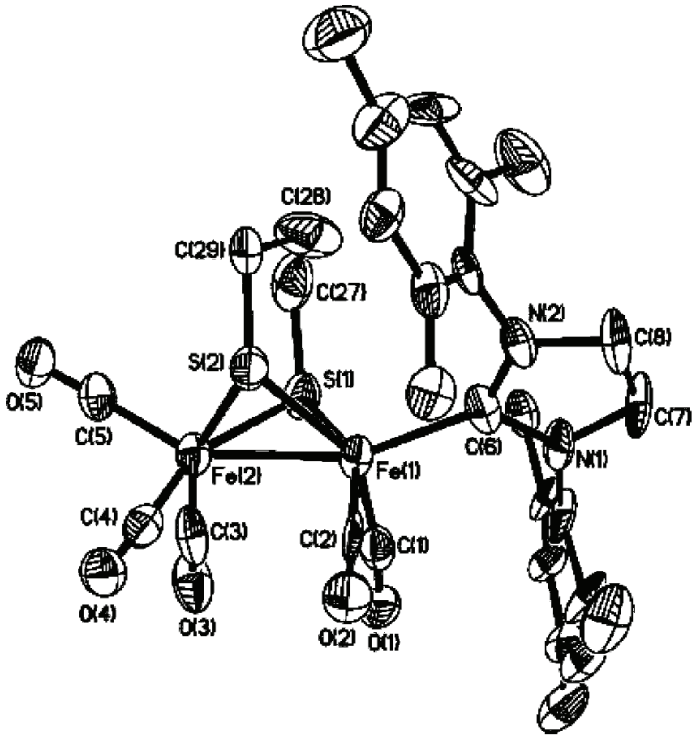

Figure VI-2. Molecular structure of **1-IMes** (TEP at 50% probability). Hydrogen atoms are omitted for clarity.

Herein we report that the asymmetric **1-IMes** complex in the presence of weak acid (HOAc) shows electrocatalytic activity. This complex is particularly exciting as an electrocatalyst because it appears that the conjunction of Fe and IMes ligand valence orbitals permits the uptake of 2 electrons at the same potential.

Experimental

Synthesis of 1-IMes

The procedure of Arduengo *et al.* was followed for deprotonation of 1,3-bis(2,4,6-trimethylphenyl)imidazolium chloride and isolation of the neutral IMes

ligand.[299] The IMes ligand was dissolved in THF (15 mL) and a solution of (μ-$S(CH_2)_3S)[FeCO)_3]_2$, (0.779 g, 2.02 mmol in 4 mL THF) was added via cannula. This solution was heated in a water bath (50 ºC for 1.5 hr). The reaction mixture was filtered through celite and the solvent was removed under vacuum. After prolonged drying under vacuum (ca. 12 hr), **1-IMes** was obtained as a red solid in 75% isolated yield. IR (ν(CO) region in THF, cm-1) 2035(s), 2027(sh), 1969(vs), 1947(m), 1916(w); in toluene, 2039(m), 2029(m), 1973(vs), 1949(m), 1914(w); 1H NMR (ppm, acetone-d6) 4.51 (s, 6 H), 4.13(s, 6H), 1.99 (t, 4 H, SC*H*2, J = 5.9 Hz), 1.77 (q, 2 H, CC*H*2C, J = 5.9 Hz). Elemental analysis found (calculated) %: C 52.1 (52.6), H 4.17 (4.56), N 4.65 (4.23).

X-ray structure determination

The X-ray diffraction data were collected on a Bruker Smart 1000 CCD diffractometer and covered a hemisphere of reciprocal space by a combination of three sets of exposures. The space groups were determined based on systematic absences and intensity statistics. The structures were solved by direct methods. Anisotropic displacement parameters were determined for all non-hydrogen atoms. Hydrogen atoms were placed at idealized positions and refined with fixed isotropic displacement parameters. The following is a list of programs used: for data collection and cell refinement, SMART,[300] data reduction, SHELXTL,[301] structure solution, SHELXS-97 (Sheldrick),[302] structure refinement, SHELXL-97 (Sheldrick),[303] and molecular graphics and preparation of material for publication, SHELXTL-Plus, version 5.1 or later (Bruker).[304]

Crystal data for **1-IMes·0.5 THF**: Crystals suitable for X-ray analysis were grown from a layered THF-hexanes solution maintained at –5 °C. A single crystal was mounted on a glass fiber with epoxy cement at 110 K in a N_2 cold stream. $Fe_2C_{29}H_{30}N_2O_5S_2$, M = 644.2, monoclinic, space group I2/a, with a = 19.158(17) Å, b = 11.432(10) Å, c = 30.15(3) Å, α = 90°, β = 107.148(17)°, γ = 90°, and Z = 4, R1 = 0.0720 and wR2 = 0.1426 for 13741 reflections.

Electrochemistry

Cyclic voltammograms were recorded on a BAS-100A electrochemical analyzer using three electrodes. The working electrode was a glassy carbon disk (0.071 cm^2), the reference electrode was Ag/Ag^+ prepared by anodizing a silver wire in an CH_3CN solution of 0.01 M $AgNO_3$/0.1 M *n*-Bu_4NBF_4, and the counter electrode was a coiled platinum wire. The glassy carbon working electrode was polished with 15, 3, and 1 μm diamond pastes, successively, and then sonicated in ultrapure (Millipore) water for 10 min. Deaeration of all solutions was accomplished by bubbling argon through the solution for 5-10 min (or CO bubbling for ~15 min) and then maintaining a blanket of argon (or CO) over the solution during the electrochemical measurements. All experiments were performed on CH_3CN solutions containing 0.1 M *n*-Bu_4NBF_4 at room temperature. Cp_2Fe or Cp^*_2Fe for the samples whose oxidation peaks were overlapped with Cp_2Fe/Cp_2Fe^+ redox wave served as internal reference. The measured potential difference between Cp_2Fe/Cp_2Fe^+ and $Cp^*_2Fe/Cp^*_2Fe^+$ was 505 mV. Thus, all potentials are able to be reported relative to the normal hydrogen electrode (NHE) using

Cp_2Fe/Cp_2Fe^+ as standard ($E_{1/2}$ = 400 mV vs NHE in CH_3CN). During the electrocatalytic experiments under Ar, increments of glacial acetic acid were added by microsyringe. Controlled potential coulometry for the determination of the number of electrons transferred per molecule was carried out using BAS 100A potentiostat and BAS bulk electrolysis cell containing ca. 40 mL of CH_3CN which was 1.0 mM in **1-IMes** and 0.1 M in *n*-Bu_4NBF_4 under an argon atmosphere. The working electrode of BAS bulk electrolysis cell was a reticulated vitreous carbon working electrode.

Control experiment

In order to further confirm the two-electron assignment for the first reduction wave of **1-IMes,** a control experiment was performed: when the total charge (Q) passed during bulk electrolysis at an applied potential of –1.80 V approached calculated values for the passage of 1.25, 1.50, 1.75, and 2.10 electrons, respectively, per molecule of **1-IMes**, the bulk electrolysis was stopped and CV's were obtained on this solution. The CV obtained at the theoretical value of 1.25 electrons per molecule of **1-IMes** still showed a noticeable reduction wave at -1.70 V, indicative of the incomplete reduction of the molecules of **1-IMes** present in the bulk solution. The CV's obtained at the theoretical values of 1.50 and 1.75 electrons per molecule of **1-IMes** also showed a reduction wave at –1.70 V, although the size of this wave continued to decrease. A CV obtained at the theoretical value of 2.10 electrons per molecule of **1-IMes** did not show any reduction wave at –1.70 V, indicating the complete reduction of the bulk solution.

Computational Details

All DFT calculations were performed using a hybrid functional [the three-parameter exchange functional of Becke (B3)[235] and the correlation functional of Lee, Yang, and Parr (LYP)[236]] (B3LYP) as implemented in Gaussian 03[305]. The iron, and sulfur atoms use the effective core potential and associated basis set of Hay and Wadt (LANL2DZ)[253,254]. For iron, the two outermost p functions were replaced by reoptimized 4p functions as suggested by Couty and Hall[254]. For sulfur, the basis set was augmented by the d polarization function of Höllwarth et al.[256]. For the model (μ-$S(CH_2)_3S$)[$Fe(CO)_3$][$Fe(CO)_2$(IMes)] all carbon, nitrogen, oxygen, and hydrogen atoms are represented using Dunning's double zeta valence basis (D95V)[269]. The smaller model complex, (μ-$S(CH_2)_3S$)[$Fe(CO)_3$][$Fe(CO)_2$(IH)], employed Dunning's correlation-consistent polarized valence double zeta basis set (cc-pVDZ)[257] on the CO ligands and the carbene ligand. The carbon and hydrogen atoms of the propane dithiolate bridge, used Dunning's double zeta basis (D95)[258,269]. Unless otherwise noted, all geometries are fully optimized and confirmed as minima or n-order saddle points by analytical frequency calculations at the same level.

Results and Discussion

In the absence of a proton source, **1-IMes** in CH_3CN undergoes one irreversible reduction at –1.70 V (vs NHE) and two irreversible oxidations at 0.51 V and 1.12 V. The observed irreversibility of the reduction peak at –1.70 V is most likely not due to CO loss. Even at low temperature (–15°C) and fast scan rates (20 V s^{-1}), CO-saturated solutions of **1-IMes** show no sign of reversibility. The **1-IMes** complex was

investigated as an electrocatalyst for dihydrogen production from a weak acid. The addition of 1 to 5 equivalents of HOAc to a 2.0 mM CH3CN solution of **1-IMes** (Figure VI-3) shows an enhancement of the peak current for the reduction wave at –1.70 V, while having very little effect on the remainder of the cyclic voltammogram (CV). This result is consistent with electrocatalytic H_2 production.[158,195]

Controlled-potential coulometry for 1-IMes demon-strated the event at –1.70 V to be a two-electron reduction process in the absence of added acid. The two-electron assignment for **1-IMes** was confirmed by the following control experiment: when the

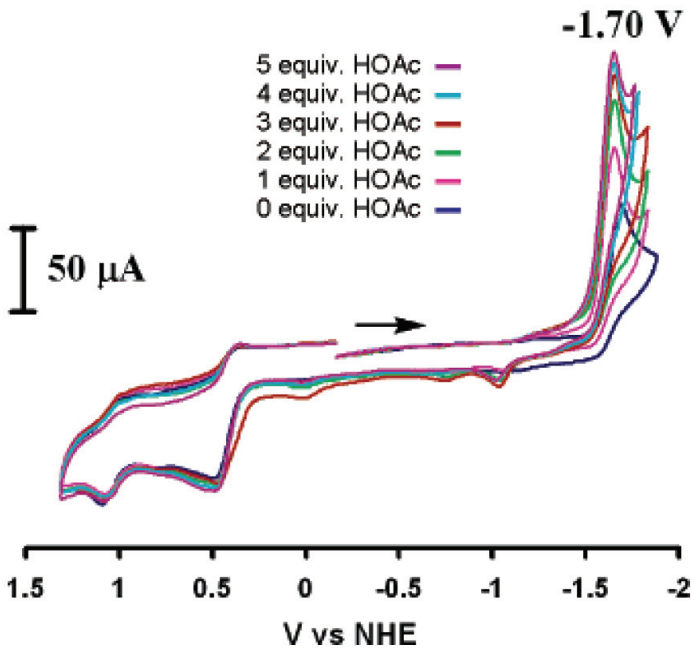

Figure VI-3. CV's of **1-IMes** (2.0 mM) with HOAc (0-10 mM) in a CH_3CN solution (0.1 M *n*-Bu_4NBF_4) with a glassy carbon electrode at a scan rate of 200 mV s^{-1}.

total charge (Q) passed during the bulk electrolysis at an applied potential of –1.80 V approached a calculated value of ~1.25 electrons per **1-IMes** molecule, the bulk electrolysis was stopped and a CV was obtained on this solution. The CV still showed a noticeable reduction wave at –1.70 V indicating incomplete reduction of the bulk solution (Figure VI-4). Interestingly, this is in contrast to one-electron reduction previously observed for a series of $Fe^{I}Fe^{I}$ dithiolate complexes.[194,196] For direct comparison, the controlled-potential experiment was performed for the analogous mono-phosphine complex, **1-PTA** (PTA = 1,3,5-triaza-7-phosphaadamantane), under identical conditions, and clearly showed a one-electron reduction process, as previously reported.[196]

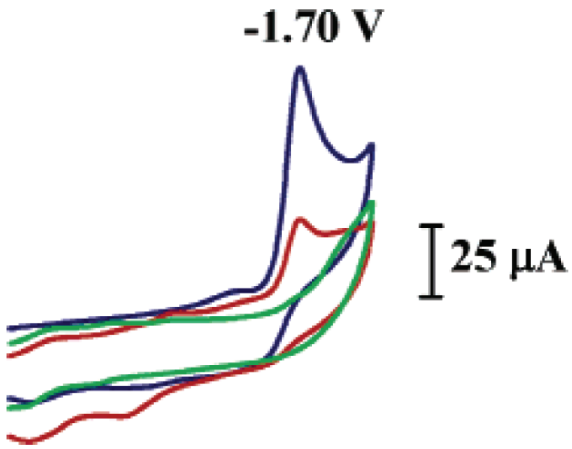

Figure VI-4. CVs of **1-IMes** (1.0 mM) in a CH_3CN solution (0.1 M *n*-Bu_4NBF_4) before bulk electrolysis (blue), after the passage of a total charge equivalent to 1.25 electrons (red), and after the passage of a total charge equivalent to 2.10 electrons (green).

DFT has proven itself a valuable tool for addressing the molecular details of electrochemical problems.[306,307] In order to better understand the nature of **1-IMes** and the reduced species **[1-IMes]$^{1-}$** and **[1-IMes]$^{2-}$**, DFT calculations were undertaken on these species. The optimized structure of **1-IMes** overlays well with the molecular structure derived from x-ray crystallography. The HOMO and LUMO of **1-IMes** are predominantly Fe-Fe bonding and Fe-Fe antibonding, respectively. Since the first added electron occupies an Fe-Fe antibonding orbital, the main structural change upon geometry optimization of **[1-IMes]$^{1-}$** is elongation of the Fe-Fe bond from 2.52 Å to 2.80 Å. From the unpaired Fe spin densities of 0.22 and 0.99 of the $Fe(CO)_3$ and $Fe(CO)_2$(IMes) units, respectively, the **[1-IMes]$^{1-}$** species is assigned as an $Fe^0Fe^I(IMes^0)$ species. That is, the added electron is localized on the $Fe(CO)_3$ moiety, benefiting from the delocalization of three CO ligands.

The addition of a second electron to **1-IMes** can conceivably lead to either an second iron-iron based reduction or an IMes ligand-based reduction. If the second reduction is iron based, then a singlet state should result from the two thiolate bridged low-spin pseudo trigonal pyramidal Fe^0 centers. If the second reduction is IMes ligand based, then a triplet state should result from the unpaired electrons in the IMes ligand and the Fe-Fe manifold. Single-point energy calculations on species formed on addition of a second electron, **[1-IMes]$^{2-}$**, constrained at the **[1-IMes]$^{1-}$** geometry, show that the lowest energy triplet state is 5.3 kcal mol^{-1} more stable than the lowest energy singlet

state, column II of Figure VI-5. Geometry-optimization of the singlet and triplet structures of **[1-IMes]$^{2-}$** reverses this energy difference and finds the triplet structure 7.0 kcal mol^{-1} higher in energy than the singlet structure, column III of. Geometry optimization of the singlet state of **[1-IMes]$^{2-}$**, which has formal Fe-Fe bond order of 0, leads to a non-bonding Fe-Fe distance of 3.39 Å. The singlet structure of [1-IMes]$^{2-}$ is therefore assigned as an $Fe^0Fe^0(IMes^0)$ species. Geometry optimization of the triplet state of **[1-IMes]$^{2-}$**, which has a formal Fe-Fe bond order of ½, leads to an Fe-Fe distance of 2.95 Å. It is noteworthy that the Fe-Fe distance in the triplet structure of **[1-IMes]$^{2-}$** lies much closer to that of **[1-IMes]$^{1-}$** than that of singlet **[1-IMes]$^{2-}$**. Mulliken spin analysis of the optimized triplet structure computes unpaired spin densities of 0.07 and 1.23 on the irons of the $Fe(CO)_3$ and $Fe(CO)_2$(IMes) units, respectively. A total spin density of is 0.91 on the IMes ligand; 8.0 % on the carbenoid carbon and 79.7 % on the carbon atoms of the aryl rings. A total spin density of –0.20 is spread over the five CO ligands. The triplet state of **[1-IMes]$^{2-}$** is therefore assigned as an $Fe^0Fe^I(IMes^{-1})$ species.

In other words, the **[1-IMes]$^{1-}$** immediately produced at the electrode surface on reduction of **1-IMes**, represented as I in Figure VI-5, may then accept a second electron into the redox active NHC ligand.[308] Alternatively, **[1-IMes]$^{1-}$** may accept a second electron into the Fe-Fe bond antibonding orbital, yielding a singlet state. The former possibility is more likely, since electron transfer is a fast process and the lower energy triplet state of **[1-IMes]$^{2-}$** results in only a small overall structural change from **[1-IMes]$^{1-}$**; whereas production of the singlet state results in a major structural change. In

support of this hypothesis, the $Fe^{I}Fe^{0} + e^{-} \rightarrow Fe^{0}Fe^{0}$ reduction is not observed for the mono-phosphine complex.[195]

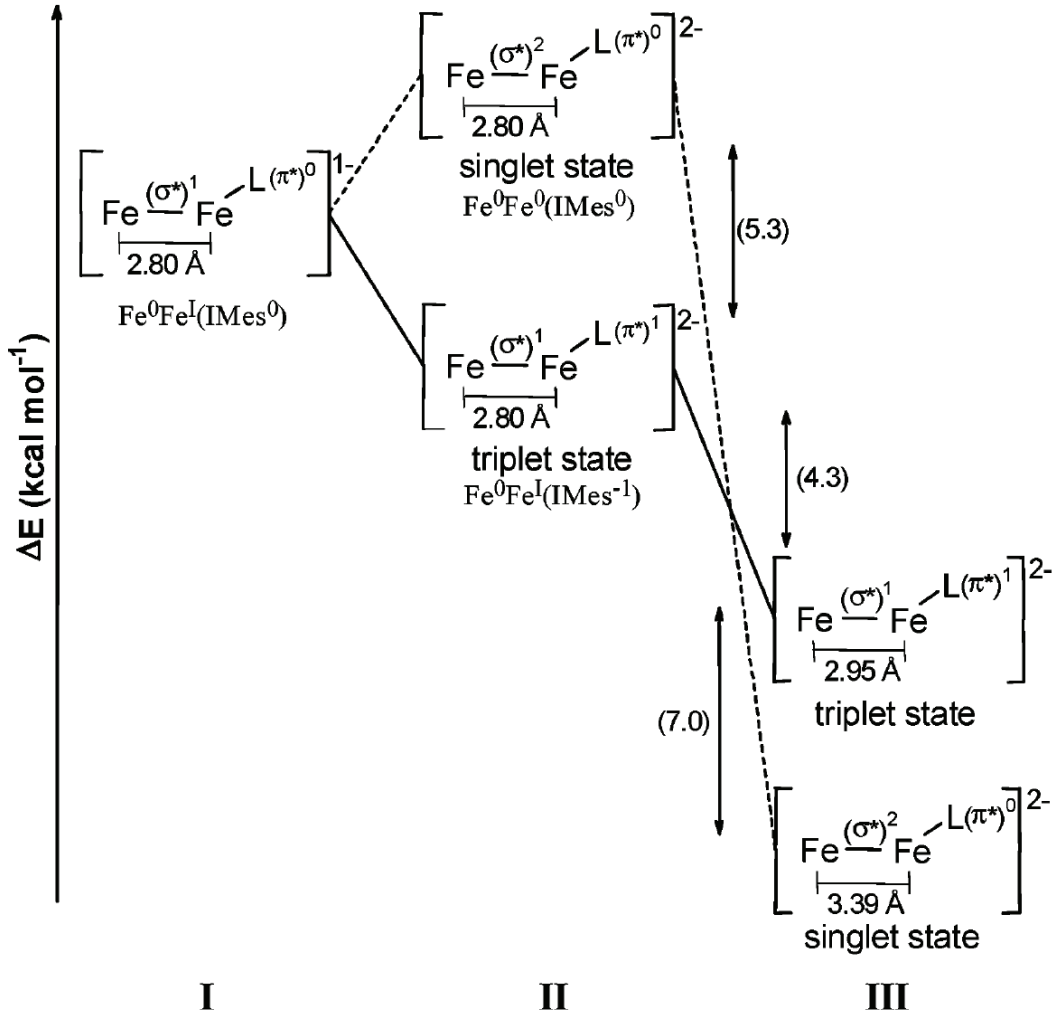

Figure VI-5. Energies and Fe-Fe distances for the geometry-optimized [**1-IMes**]$^{1-}$ (I), singlet and triplet states for [**1-IMes**]$^{2-}$ at the [**1-IMes**]$^{1-}$ geometry (II), and fully optimized structures of [**1-IMes**]$^{2-}$ (III).

The extended π system present in the IMes ligand is apparently a requirement for this type of carbene-based reduction to occur. Computations on a simplified model of **[1-IMes]$^{2-}$**, in which the 2,4,6-trimethylphenyl rings have been replaced by hydrogen atoms, predict the lowest energy triplet state to arise from a high-spin Fe^0 center, and not from one-electron reductions of the Fe-Fe manifold and the IMes ligand.

Capon *et al.* published a synthetic and electrochemical study of an apically substituted N-heterocyclic carbene complex of the form, (μ-$S(CH_2)_3S)[Fe(CO)_3][Fe(CO)_2(L_{Me})]$, ($L_{Me}$ = 1,3-bis(methyl)imidazol-2-ylidene).[309] Their complex undergoes one-electron reduction at −1.66 V vs NHE in CH_3CN. Their finding of a single one-electron reduction for the bis-methyl carbene is consistent with our computation on the small model of the IMes ligand.

From previous electrochemical results on the mono-phosphine complex, **1-PTA**, we proposed an ECCE mechanism for H_2 production by **1-PTA** in the presence of the weak acid, HOAc.[196] For **1-IMes**, however, it is more likely that a two-electron reduction (one electron at the Fe-Fe center and one electron on the IMes ligand) precede protonation at iron to yield an $[HFeFe]^{1-}$ moiety. A second protonation and internal electron transfer from the reduced IMes ligand to the iron center results in the release of dihydrogen and regeneration of the Fe^IFe^I starting material. Overall the electrochemical process is described as an EECC mechanism. A similar mechanism was proposed for H_2 production by cofacial bisorganometallic diruthenium and diosmium porphyrins.[310]

Conclusion

In summary, the use of the IMes ligand permits the uptake of two electrons at the same reduction potential, resulting in a change in mechanism from that observed for the closely related mono-phosphine and mono-carbene complexes. DFT calculations suggest that this difference in mechanism arises from the involvement of the IMes ligand as an electroactive participant. By analogy to the [FeFe]H_2ase site, the electroactive IMes ligand may serve as a model for the electroactive 4Fe4S cluster.

CHAPTER VII

DE NOVO DESIGN OF SYNTHETIC DI-IRON(I) COMPLEXES AS STRUCTURAL MODELS OF THE REDUCED FORM OF IRON-IRON HYDROGENASE*

Introduction

Hydrogenase enzymes are used by many microorganisms in nature to facilitate the reversible oxidation of dihydrogen to protons and electrons, $H_2 \leftrightarrow 2H^+ + 2e^-$.[124,173,273] The structurally-characterized hydrogenase enzymes can be broadly divided into [NiFe][127,128,311,312] and [FeFe][130,131] hydrogenases based on the metal content of their active sites. In nature, the [NiFe] enzymes generally function as hydrogen oxidation catalysts, while the [FeFe] enzymes generally catalyze the production of dihydrogen.

These enzymes are of considerable interest because of their potential uses in biotechnological applications.[313] A major drawback is the fact the organisms that produce hydrogenase enzymes are generally anaerobic extremophiles that require high temperatures, high pressures, and the exclusion of oxygen to live. The [NiFe] enzymes are generally considered more thermally and O_2 stable than the [FeFe] enzymes, and therefore potentially more suitable to act large-scale bio-catalysts for H_2 oxidation and H^+ reduction. On the other hand, the synthesis of small molecule analogues of the [FeFe] enzyme active site, has proven to be more straightforward due to limited direct

involvement of the protein in the enzyme active site and its resemblance to the previously known organometallic complex (μ-$S(CH_2)_3S)[Fe(CO)_3]_2$.[248]

Darensbourg, Pickett, Rauchfuss, and their respective coworkers have synthesized simple dinuclear iron complexes that have structural, spectroscopic, and functional properties similar to the active site of [FeFe]H_2ase. Darensbourg and coworkers have examined the ability of formally Fe^IFe^I complexes (synthetic analogues of the reduced form, known as H_{red}) to function as solution electrocatalysts for H_2 production in the presence of acid.[194,195] Pickett and coworkers presented infrared spectral data for the formation of a short lived $Fe^{II}Fe^I$ species derived from the oxidation of the Fe^IFe^I complex $[Fe_2\{MeSCH_2C(Me)(CH_2S)_2\}(CN)_2(CO)_4]^{2-}$.[189] The resulting $Fe^{II}Fe^I$ complex contains a bridging CO ligand as evidenced by infrared spectroscopy, and the ν(CO) and ν(CN) values of this complex are very similar to those observed for the H_{ox} form of the active site of [FeFe]H_2ase.[170,172,173] Rauchfuss and coworkers have synthesized a series of $Fe^{II}Fe^{II}$ complexes that contain bridging CO ligands, and serve as models of the H_{ox}^{air} form of the enzyme active site.[293]

The Fe^IFe^I complexes synthesized to date require much harsher conditions than those employed in the enzymatic catalysis in order to afford proton reduction. Direct electrochemistry performed on the [FeFe]H_2ase enzyme from *Megasphaera elsdenii* shows that this enzyme catalyzes H_2 production at pH 7 and at a mild overpotential of -0.421 ± 0.010 V vs. SHE (SHE = standard hydrogen electrode).[314] In general, these complexes require reduction to the Fe^IFe^0 or Fe^0Fe^0 formal oxidation state to produce

H_2, while the enzyme apparently utilizes the Fe^IFe^I formal oxidation state. In addition, the Fe^IFe^I complexes synthesized to date require either strong acids (i. e. tolunesulfonic acid) and moderate overpotentials (≈ −1.0 to −1.2 V vs. SHE)[196-199,294] or weak acids (i.e. acetic acid) and even more negative overpotentials (≈ −1.3 to −1.9 V vs. SHE) to produce H_2. [194,195]

The Fe^IFe^I complexes, synthesized to date, also fail to mimic the precise orientation of the diatomic ligands about the Fe_2S_2 core (Figure VII-1) that is observed

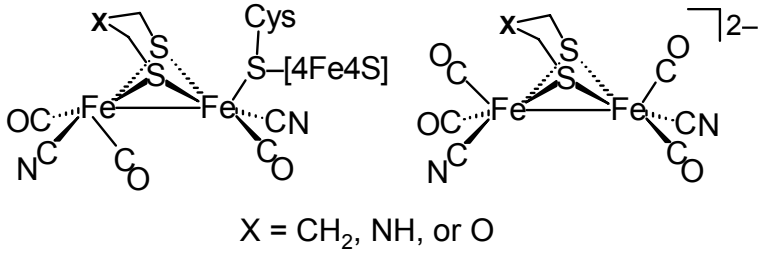

Figure VII-1. A comparison between the putative Fe^IFe^I form (H_{red}) of the active site of [FeFe]H_2ase from *Desulfovibrio desulfuricans* (left) and closely related synthetic Fe^IFe^I complexes (right). The major structural difference is the placement of a CO ligand on the left-most iron in each complex (known as the distal iron in the enzyme).

in the reduced form of the enzyme.[172] It may be that this unique orientation of the diatomic ligands about the distal iron of the active site of [FeFe]H_2ase promotes H^+ acceptance. This unique structure may be due to a combination of the electronic effect of ligands bonded directly to the iron centers and specific interactions between the first

and second coordination spheres (such as hydrogen bonds between the cyanide nitrogens and the remainder of the protein). The precise placement and orientation of hydrogen bond donors observed in the protein is difficult to reproduce with small synthetic analogues. As an alternative strategy, changes to the primary coordination sphere of the synthetic compounds may be able to compensate for the lack of specific interactions provided by the protein.

Here, we use computational chemistry to design viable $Fe^{I}Fe^{I}$ complexes that more closely resemble the structure of the active site of [FeFe]H_2ase. Specifically, we determine modifications of S-to-S linker and donor ligands that act to stabilize a structure similar to that observed in the molecular structure of the enzyme active site. In this text, we will refer to structures in which one of the CO ligands resides in the area "between" the two iron centers, structures which more closely resemble the enzyme active site, as *rotated structures* and structures where the $Fe(CO)_2L$ units roughly eclipse one another with no ligand in the area "between" the two iron centers, as in all $Fe^{I}Fe^{I}$ complexes synthesized to date, as *unrotated structures*. Thus, we are trying to predict designs for abiotic, $Fe^{I}Fe^{I}$ complexes with this observed biological structural feature. Previous computational work in this area has focused on the catalytic mechanism for H^+ reduction/H_2 oxidation, [207-211] the nature of the S-to-S linker in the enzyme active site,[206] the electronic structure and reactivity of synthetic analogues of the [FeFe]H_2ase active site,[193,196,263,293,315-317] and factors that influence the active site structure.[298]

Computational Details

All DFT calculations were performed using a hybrid functional [the three-parameter exchange functional of Becke (B3)[235] and the correlation functional of Lee, Yang, and Parr (LYP)[236]] (B3LYP) as implemented in Gaussian 03[318]. The iron, phosphorus, and sulfur atoms use the effective core potential and associated basis set of Hay and Wadt (LANL2DZ)[253,254]. For iron, the two outermost p functions were replaced by re-optimized 4p functions as suggested by Couty and Hall.[255] For sulfur and phosphorus, the basis set was augmented by the d polarization function of Höllwarth *et al*.[256]. The carbon and hydrogen atoms of the dithiolate and bis-thiolate ligands, and the hydrogen atoms of the PH_3 ligand use Dunning's double zeta basis (D95)[258,269]. The CO and CN^- ligands, and the BH_x (x = 1,2), NH_x (x = 1,2), OH_x (x = 0, 1) components of the dithiolate bridges use Dunning's correlation-consistent polarized valence double zeta basis set (cc-pVDZ)[257]. Unless otherwise noted, all geometries are fully optimized and confirmed as minima or n-order saddle points by analytical frequency calculations at the same level.

Results and Discussion

Fundamental Properties of $(\mu\text{-SR})_2[Fe(CO)_3]_2$

Knowledge of the different conformational isomers observed for the $(\mu\text{-SRS})[Fe(CO)_3]_2$ and $(\mu\text{-SR})_2[Fe(CO)_3]_2$ complexes is important to the following discussion. For the S-to-S linked complexes such as $(\mu\text{-SCH}_2\text{CH(R)CH}_2\text{S})[Fe(CO)_3]_2$ there are two conformations which differ in the orientation of the R group. These

orientations will be labeled as the *up* and *down* orientations as shown in Figure VII-2(a). For the $(\mu\text{-SR})_2[Fe(CO)_3]_2$ complexes, three conformational isomers are possible, which differ in the orientation of the carbon atom α to the thiolate sulfur. These isomeric forms will be labeled as *anti*, *syn*, and *syn′* as shown in Figure VII-2(b). For monosubstituted complexes such as $(\mu\text{-SRS})[Fe(CO)_3][Fe(CO)_2(PH_3)]$, there are two PH_3 positional isomers. These PH_3 positional isomers will be labeled as *apical* and *basal* isomers as shown in Figure 2(c). In general, all of these isomeric forms have similar energies, and readily interconvert at and below room temperature.

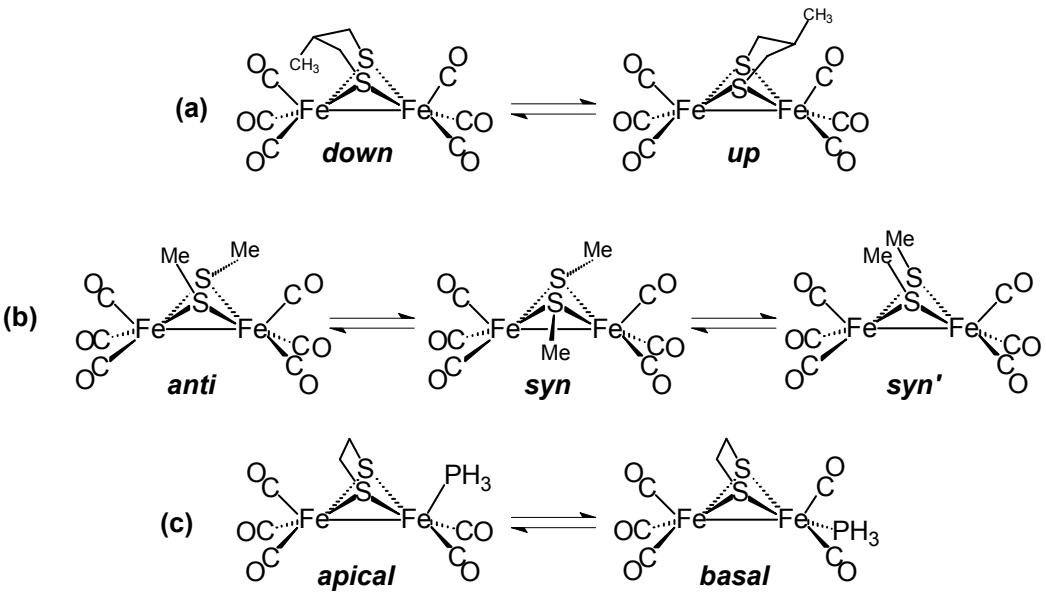

Figure VII-2. Intramolecular site-exchange processes in di-iron-dithiolate and di-iron bis-thiolate complexes. (a) dithiolate FeS_2C_3 ring inversion, (b) inversion at S, and (c) apical-basal exchange of the PH_3 ligand.

Electronic effect in (μ-SC(R)C(R)S)[Fe(CO)$_3$]$_2$

In order to determine how the electronic characteristics of the dithiolate linker might affect the energy difference between the most stable rotated form and most stable unrotated form, the rotated and unrotated forms of a series of complexes, (μ-SC(R)C(R)S)[Fe(CO)$_3$]$_2$ (R = CF_3, F, H, or CH_3) were geometry-optimized. The computed energy differences (Scheme VII-1) show no correlation to the electron donating ability of the R group as measured by its Hammett constant[319] and are very similar for the series (ΔG = 14.3-15.3 kcal mol^{-1}). The ethylenedithiolate framework was chosen for the S-to-S linker because it directs the steric bulk of the R groups away from the Fe(CO)$_3$ rotors, allowing one to determine the way in which the energy difference between the most stable rotated form and most stable unrotated form is affected by electronic character of the S-to-S linker by minimizing competing steric effects. The energy difference between the most stable rotated form and most stable unrotated form is shown to be invariant to the electron donating or accepting nature of the S-to-S linker.

Linked versus non-linked sulfurs

In order to determine how the electronic characteristics of the non S-to-S linked bis-thiolate affect the energy difference between the most stable rotated form and most stable unrotated form, complexes of the form, (μ-SR)$_2$[Fe(CO)$_3$]$_2$ (R = CH_3, H, or F), complexes were geometry optimized. Although the nature of the R group has a large effect on the relative energies of the anti, syn, and syn′ isomers, the energy difference

between the most stable rotated structure and most stable unrotated structure is similar for all of these complexes (Scheme VII-2). Therefore, the energy difference between the

Scheme VII-1

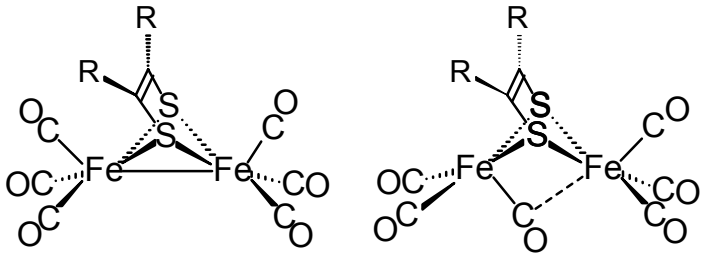

R = Me	0.0	14.5
R = H	0.0	14.3
R = F	0.0	14.8
R = CF_3	0.0	15.3

Scheme VII-2

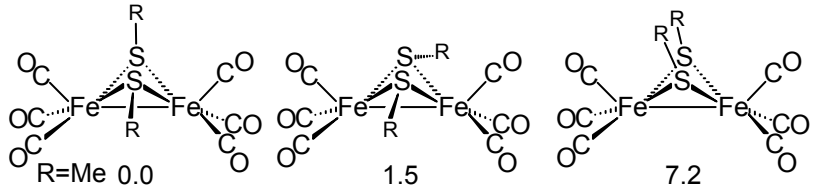

R=Me	0.0	1.5	7.2
R=H	0.0	1.4	1.7
R=F	0.0	3.9	5.4

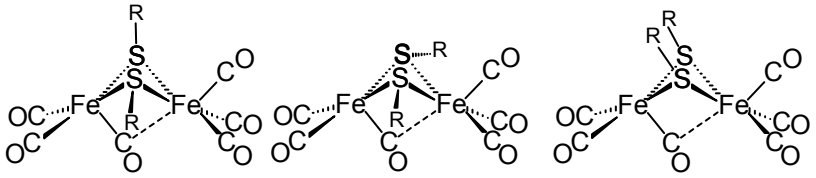

R=Me	13.1	13.4	20.7
R=H	13.5	12.4	15.1
R=F	13.3	15.3	19.5

most stable rotated form and most stable unrotated form for non-S-to-S linked complexes of the type $(\mu\text{-SR})_2[Fe(CO)_3]_2$ are also unrelated to the electron-donating or accepting ability of the R group.

It is useful to compare the isomeric forms of non-linked $(\mu\text{-SCH}_3)_2[Fe(CO)_3]_2$, with the closely related S-to-S linked $(\mu\text{-S(CH}_2)_2\text{S})[Fe(CO)_3]_2$ complex. The $(\mu\text{-S(CH}_2)_2\text{S})[Fe(CO)_3]_2$ complex has a computed energy difference between the most stable rotated form and most stable unrotated form of 14.7 kcal mol^{-1}. The difference between the most stable rotated form and most stable unrotated form is 13.1 kcal mol^{-1} for $(\mu\text{-SCH}_3)_2[Fe(CO)_3]_2$. Therefore, the non-linked complexes lead to a small relative stabilization of the rotated structures with respect to the unrotated structures.

$S(CH_2)_xS$ linkers (x = 2, 3, 4, or 5)

In order determine the role of the length of the dithiolate linker in the stabilization or destabilization of the rotated structure, the rotated and unrotated forms of a series of complexes $(\mu\text{-S(CH}_2)_x\text{S})[Fe(CO)_3]_2$ (x = 2–5; Scheme VII-3) were geometry optimized. For the x = 3 complex and certain conformations of the dithiolate linker for the x = 4 and x = 5 complexes, the two $Fe(CO)_3$ rotors are inequivalent. The energy difference between the most stable rotated form and most stable unrotated form for the less hindered end of the molecule (the $Fe(CO)_3$ unit furthest from the central methylene unit(s) of the dithiolate linker) are very similar to one another for x = 3–5 species and to that of the x = 2 species. The energy difference between the most stable rotated form and most stable unrotated form of the more hindered end of the molecule (the $Fe(CO)_3$

unit nearest to the central methylene unit(s) of the dithiolate linker) is shown to be directly related to the length of the S-to-S linker. Increasing the length of the S-to-S linker leads to an increased steric repulsion between the nearby apical CO ligand and the central methylene unit(s) of the S-to-S linker in the unrotated structure. This steric repulsion is alleviated by rotation of the $Fe(CO)_3$ unit, leading to a lower relative energy for the rotated structures. In addition, the longer S-to-S linkers may also allow the formation of a stabilizing agostic interaction between the hydrogen atoms of the bridge and the "open site" present on the iron center in the rotated structures. The longer S-to-S linker alone lowers the energy difference between the most stable rotated form and most stable unrotated form from 14.7 kcal mol^{-1} for the x = 2 complex down to 7.4 kcal mol^{-1} for x = 5 complex.

The replacement of one or more of the hydrogen atoms of S-to-S linker by larger alkyl groups should further destabilize the apical ligands of the unrotated forms. The x = 3 linker provides the best framework for the addition of steric bulk. Figure VII-3 compares the geometry optimized structures for x = 3 and x = 5 complexes. For the x = 3 complex, either orientation of the central methylene unit of the S-to-S linker places it near one of the apical CO ligands. The substitution of the central hydrogen atoms of the x = 3 by larger groups will result in destabilization of the apical CO of the unrotated form. The situation for the x = 5 complex is quite different. While certain conformations of the x = 5 complex direct the central methylene groups of the bridge toward the apical CO, low energy transition states convert these structures into other low energy structures which direct the steric bulk away from the apical CO. For the x = 5

linker, the steric interaction with the apical ligands can be easily relieved by reorienting the S-to-S linker. Therefore, the x = 4 (not shown in Figure VII-3) and x = 5 linker provide a poor framework for forcing a strong interaction with the apical CO ligand.

Scheme VII-3

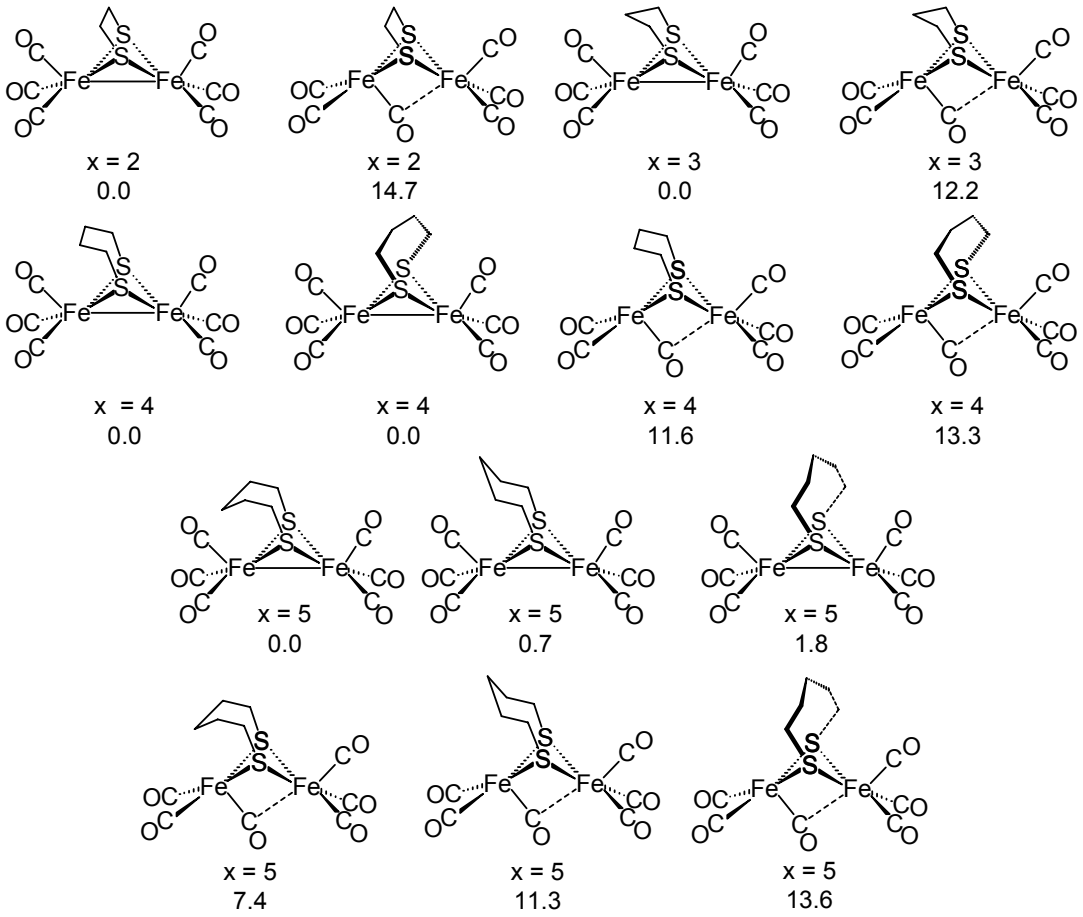

$SCH_2CH(R)CH_2S$ linkers

In order determine the role of the steric bulk of the S-to-S linker in the stabilization or destabilization of the rotated structure, the rotated and unrotated forms of a series of complexes, $(\mu\text{-}SCH_2CH(R)CH_2S)[Fe(CO)_3]_2$ were geometry-optimized. Two conformations are possible for the S-to-S linker in complexes of this form (Scheme VII-4). The "down" conformation directs the R group down and toward one of the $Fe(CO)_3$

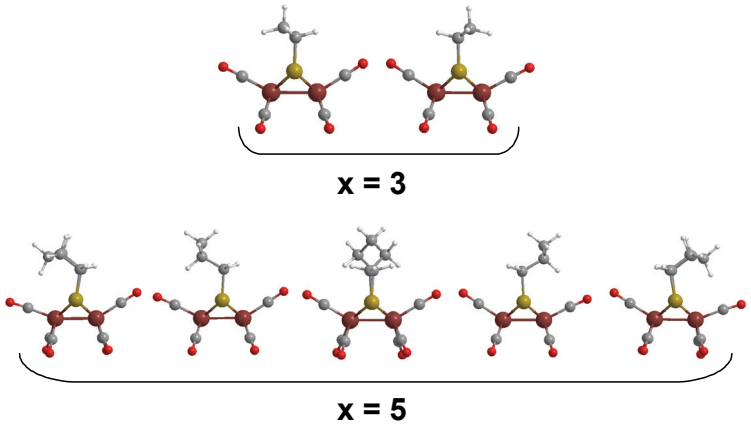

Figure VII-3. DFT-optimized structures for the $(\mu\text{-}S(CH_2)_xS)[Fe(CO)_3]_2$ series for x = 3,5. Either orientation of the x = 3 bridge places the central methylene unit near one of the apical CO ligands. While some orientations of the x = 5 bridge places the central methylene units near one of the apical CO ligands, other structures, which are computed to have comparable energies, orient the central methylene groups away from either apical CO ligand.

Scheme VII-4

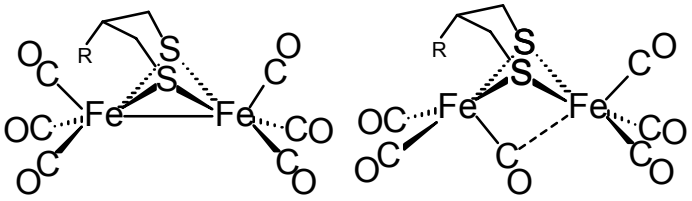

R = H	0.0	12.2
R = Me	0.0	9.4
R = *t*-Bu	0.0	7.4

units, while the "up" conformation directs the R group up and away from the $Fe(CO)_3$ units. For the down orientation of the R group, the energy difference between the most stable rotated form and most stable unrotated form decreases as the steric bulk of the R group increases. Surprisingly, even the sterically demanding *tert*-butyl group does not force the rotated structure to be lower in energy. Instead, the $Fe(CO)_3$ unit tips away from the *tert*-butyl group to ease this interaction. The energy difference between the most stable rotated form and most stable unrotated form is nearly invariant to the nature of the R group for the up orientation of the R group.

SCH_2XCH_2S linkers

The identity of the central atom(s) of 3-atom dithiolate linkers of the form, SCH_2XCH_2S (X = CH_2, NH_{down}, or O) has very little effect on the energy difference between the most stable rotated form and most stable unrotated form (as shown in Scheme VII-5). (We were unable to optimize a structure in which the NH hydrogen was oriented up. Multiple attempts at the geometry optimization an NH_{up} species resulted in

optimization of the NH_{down} species. This phenomenon has been observed and discussed previously.[263]) The 3-atom bridge directs the central atom(s) of the bridge away from the

Scheme VII-5

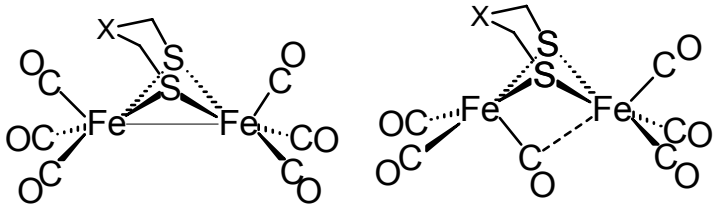

$X=CH_2$	0.0	12.2
$X=NH_{down}$	0.0	12.4
X=O	0.0	14.1

apical ligands in the unrotated structures and away from the iron center in the rotated structures. The rigid structure of these bridges limits the central atom(s) ability to destabilize the unrotated structures and/or to stabilize the rotated structures. The energy differences between the rotated and unrotated structures of the X = CH_2 and X = NH_{down} species are slightly smaller than that of the X = O species, because the hydrogen atom of the central X = CH_2 and X = NH species destabilizes the apical CO of the unrotated structures.

$S(CH_2)_2X(CH_2)_2S$ linkers

The identity of the central atom(s) of dithiolate linkers of the form, $S(CH_2)_2X(CH_2)_2S$ (X = BH, CH_2, NH, or O) has a dramatic effect on the energy difference between the most stable rotated form and most stable unrotated form (as

shown in Scheme VII-6). The 5-atom bridge allows the central atom(s) of the bridge to interact strongly with the apical CO in the unrotated structures and/or the iron center in the rotated structures. The X = CH_2 and X = O complexes give similar results. The lowest energy structures **2a-CH2** and **2a-O** place the central CH_2 or O close to one of the apical CO ligands. Related structures in which the central CH_2 or O (**2b-CH2** and **2b-O**) is oriented away from the apical CO and the C_2 symmetric structures (**2c-CH2** and **2c-O**) are slightly less stable. The most stable rotated structures (**2d-CH2** and **2d-O**) have short Fe-X distances and μ-CO, but are still 7.4-7.8 kcal mol^{-1} less stable than **2a**. The **2d-CH2** and **2d-O** complexes are shown by vibrational analysis (frequency calculations) to be minima on the B3LYP potential energy surface.

The X = BH complex has the largest energy difference between the most stable rotated structure and most stable unrotated structure for this series of 5-atom S-to-S linked complexes (10.9 kcal mol^{-1}). As with the other species the most stable rotated structure is **2d-BH**, which has a bridging CO ligand and a short Fe-B distance, but in contrast to the other species the most stable structural isomer of the unrotated form is **2b-BH**.

For X = NH the most stable structure, **2d-NH**, corresponds to the one which has a short Fe-N distance and a bridging CO ligand. This structure represents a minima on the potential energy surface as indicated by vibrational analysis. This result is markedly different from those found for the X = BH, CH_2 or O. The **2a-NH** complex is nearly

Scheme VII-6

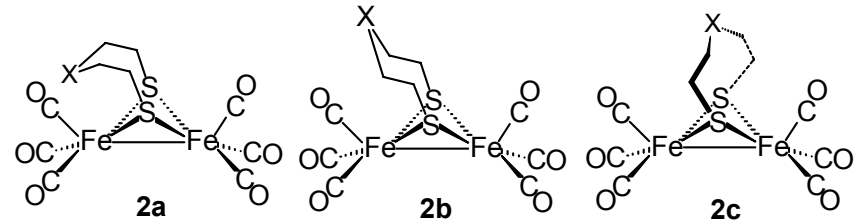

	2a	**2b**	**2c**
X = BH	7.5	0.0	5.1
X = CH_2	0.0	0.7	1.8
X = NH	0.1	3.3	4.6
X = O	0.0	3.4	5.1

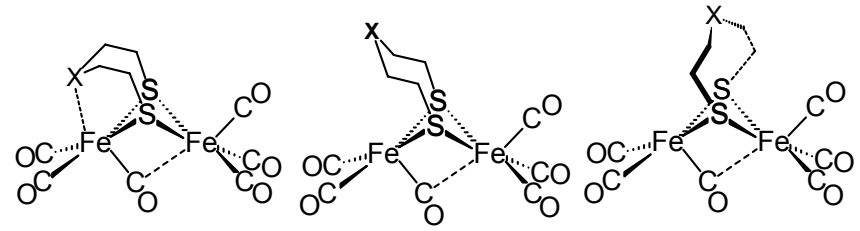

	2d	**2e**	**2f**
X = BH	10.9	18.8	n/l
X = CH_2	7.4	11.3	13.6
X = NH	0.0	14.4	17.2
X = O	7.8	14.1	17.2

isoenergetic with this species. The energies of the other relevant species are given in Scheme VII-6.

$SCH_2CH(X)CH_2S$ linkers – pendant functionalities

The nature of the pendant group attached to the central atom of the 3-carbon S-to-S linker has a dramatic effect on difference in energy between the rotated and unrotated structures (as shown in Scheme VII-7). For X = BH_2 and X = CH_3, the energy differences are 7.2 and 9.4 kcal mol^{-1}. Pendant NH_2 and OH groups give energies of 3.9 and 11.7 kcal mol^{-1} for the rotated, μ-CO structures relative to the energies of the

Scheme VII-7

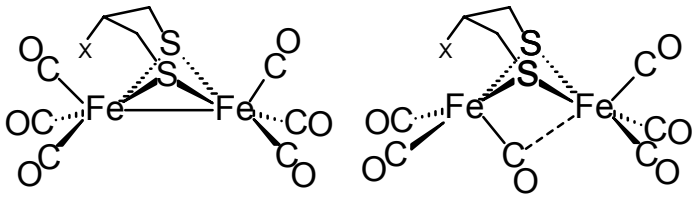

X = BH_2	0.0	7.2
X = CH_3	0.0	9.4
X = NH_2	0.0	3.9
X = OH	0.0	11.7

respective unrotated structures. Vibrational analysis shows that the rotated, μ-CO structures for X = NH_2 and X = OH correspond to minima on the B3LYP potential energy surface.

Ligand effects - monosubstituted complexes

We[316] and others[298] have discussed the role of the donor strength of non-CO ligands in stabilizing structures of small molecule analogues that resemble those of the enzyme active site. We found that $Fe(CO)_3$ rotation in $(\mu\text{-}S(CH_2)_3S)[Fe(CO)_3]_2$ induces the transfer of electron density from the unrotated $Fe(CO)_3$ unit to the rotated $Fe(CO)_3$ unit. In this context, the replacement of CO by a better donor ligand, L, facilitates the rotation of the $Fe(CO)_3$ unit and hinders the rotation of the $Fe(CO)_2L$ unit. The replacement of CO by a poorer donor ligand than CO, L', facilitates the rotation of the $Fe(CO)_2L'$ unit and hinders the rotation of the adjacent $Fe(CO)_3$ unit.

Oxidized and reduced species

The frontier molecule orbitals of the $(\mu\text{-}S(CH_2)_2S)[Fe(CO)_3]_2$ complex are the HOMO, which is primarily Fe-Fe bonding in nature, and the LUMO which is primarily Fe-Fe antibonding in nature. The addition or removal of one electron from this complex will reduce the Fe-Fe bond order from 1 to ½, and therefore weaken the Fe-Fe bond.

Since the rotation of the an $Fe(CO)_3$ unit of $(\mu\text{-}S(CH_2)_2S)[Fe(CO)_3]_2$ requires breaking the Fe-Fe bond, the energy difference between the most stable rotated form and most stable unrotated form is lowered by the addition or removal of electrons from $(\mu\text{-}S(CH_2)_2S)[Fe(CO)_3]_2$. The neutral $(\mu\text{-}S(CH_2)_2S)[Fe(CO)_3]_2$ complex has a computed energy difference between the most stable rotated form and most stable unrotated form of 14.7 kcal mol^{-1}. The rotated structures of the one-electron reduced complex, $[(\mu\text{-}S(CH_2)_2S)[Fe(CO)_3]_2]^{1-}$, and one-electron oxidized complex, $[(\mu\text{-}S(CH_2)_2S)[Fe(CO)_3]_2]^{1+}$ are, respectively, 8.0 and 1.4 kcal mol^{-1} less stable than the unrotated structures. For the two-electron oxidized complex, $[(\mu\text{-}S(CH_2)_2S)[Fe(CO)_3]_2]^{2+}$, the rotated structure is 8.8 kcal mol^{-1} *more stable* than the unrotated structure. These results are not unexpected since Pickett, Rauchfuss, and their respective coworkers have synthesized $Fe^{II}Fe^{II}$ and $Fe^{II}Fe^{I}$ complexes, which contain bridging CO ligands.[189,293]

Additivity - ligand effects - disubstituted complexes

A series of bis-PH_3 complexes of the forms $(\mu\text{-}S(CH_2)_2S)$ $[Fe(CO)_2(PH_3)]_2$ and $(\mu\text{-}S(CH_2)_2S)[Fe(CO)_3][Fe(CO)(PH_3)_2]$ and their respective $Fe(CO)_3$ $Fe(CO)_2(PH_3)$, and

$Fe(CO)(PH_3)_2$ rotated structures are given in Scheme VII-8. For the symmetrically substituted bis-PH_3 complexes of the form (μ-$S(CH_2)_2S$) $[Fe(CO)_2(PH_3)]_2$, the most stable rotated structure lies at 14.1 kcal mol^{-1} relative to the most stable unrotated structure. This value is larger than the energy difference between the most stable rotated form and most stable unrotated form for mono-PH_3 complexes, (μ-$S(CH_2)_2S)[Fe(CO)_3][Fe(CO)_2(PH_3)]$, (12.6 kcal mol^{-1}) and comparable to the value of

Scheme VII-8

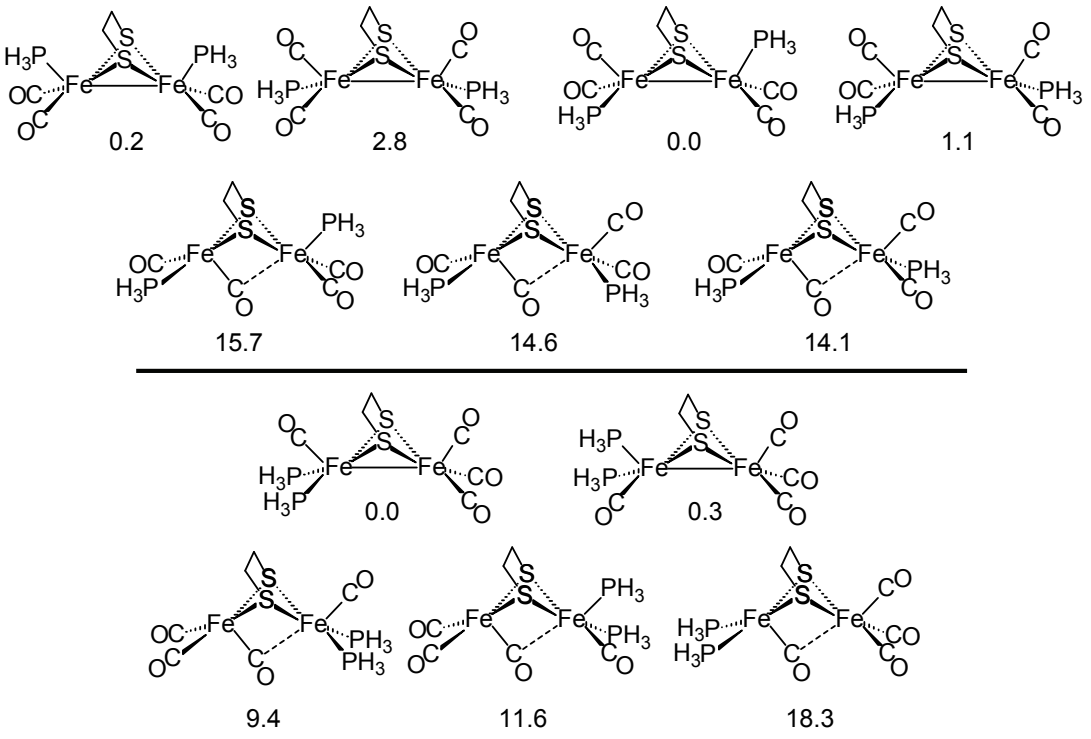

14.7 kcal mol^{-1} computed for all-CO complex (μ-$S(CH_2)_2S)[Fe(CO)_3]_2$, due to the symmetric substitution pattern of the PH_3 ligands. For the asymmetrically substituted

bis-PH_3 complexes of the form (μ-$S(CH_2)_2S$) $[Fe(CO)_3][Fe(CO)(PH_3)_2]$ complexes, the most stable rotated structure lies at 9.4 kcal mol^{-1} relative to the most stable unrotated structure. The difference is these structural isomers lies in the substitution pattern. In the mono-PH_3 complex, the transfer of electron density from the $[Fe(CO)_2(PH_3)]$ unit stabilizes rotation of the adjacent $Fe(CO)_3$ unit. The substitution of one of the CO ligands of the $Fe(CO)_2(PH_3)$ unit to yield the asymmetrically substituted (μ-$S(CH_2)_2S)[Fe(CO)_3][Fe(CO)(PH_3)_2]_2$ complexes, lowers the relative energy of the $Fe(CO)_3$ rotated structures relative to the unrotated structures by further facilitating the transfer of electron density from the $Fe(CO)(PH_3)_2$ unit into the adjacent $Fe(CO)_3$ unit. Symmetrical substitution of the PH_3 ligand stifles the transfer of electron density between the two iron centers.

Additivity – the combination of ligand and linker effects

With the exception of oxidation or reduction, the most stabilizing modifications for the Fe^IFe^I complexes were the addition of an borane or amine functionality, the addition of a tertiary butyl group to the central methylene unit of the propanedithiolate linker, and the substitution of the CO ligand by a better donor ligand, L, to yield asymmetric complexes of the forms (μ-SRS)$[Fe(CO)_3][Fe(CO)_2L]$ and (μ-SRS)$[Fe(CO)_3][Fe(CO)L_2]$.

The replacement of CO by better donor ligands and the amine functionalized bridges are incompatible for the stabilization of the rotated form. The amine-functionalized bridge lowers the relative energy of the rotated structures by donating

electron density to stabilize the "open site" created upon the Fe center by $Fe(CO)_3$ rotation. A good donor ligand, L, also lowers the relative energy of the rotated structures by making the unrotated $Fe(CO)_2L$ unit a better electron donor to the rotated $Fe(CO)_3$ unit (Figure VII-4(a)). When both the amine functionalized bridge and a good

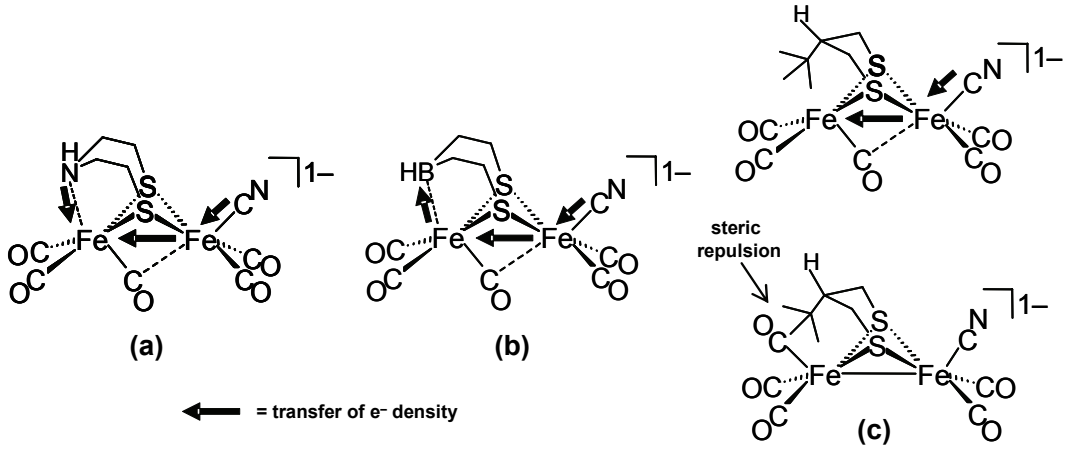

Figure VII-4. The combination of effects. In (a)–(c), the CN^- ligand stabilizes the rotated structure by the making the unrotated $Fe(CO)_2(CN)$ unit a better donor to the rotated $Fe(CO)_3$ unit. In (a) the amine nitrogen atom competes with the $Fe(CO)_2(CN)$ unit to donate into the rotated $Fe(CO)_3$ unit. In (b), the borane makes the $Fe(CO)_3$ unit a better electron density acceptor. In (c), the unrotated form is destabilized by the interaction with the tertiary butyl group.

donor ligand are present in the same complex, they compete for donation into the rotated $Fe(CO)_3$ unit. For the all-CO complex $(\mu\text{-}S(CH_2)_2NH(CH_2)_2S)[Fe(CO)_3]_2$, the most

stable rotated structure and most stable unrotated structure are isoenergetic. The most stable rotated structure and most stable unrotated structure remain isoenergetic for the mono-cyanide complex, $[(\mu\text{-}S(CH_2)_2NH(CH_2)_2S)[Fe(CO)_3][Fe(CO)_2(CN)]]^{1-}$. The replacement of one CO ligand of $(\mu\text{-}S(CH_2)_2NH(CH_2)_2S)[Fe(CO)_3]_2$ by CN^- therefore imparts no additional stabilization to the amine-stabilized rotated structures.

The replacement of CO by better donor ligands and the borane functionalized bridges are compatible for the stabilization of the rotated form. The borane-functionalized bridge lowers the relative energy of the rotated structures by making the rotated $Fe(CO)_3$ unit a better electron acceptor (Figure VII-4(b)). A good donor ligand, L, lowers the relative energy of the rotated structures by making the unrotated $Fe(CO)_2L$ unit a better electron donor to the rotated $Fe(CO)_3$ unit. When both the borane functionalized bridge and a good donor ligand are present in the same complex, they cooperate to facilitate the transfer of electron density from the unrotated $Fe(CO)_2L$ unit into the rotated $Fe(CO)_3$ unit. The energy difference between the most stable rotated form and most stable unrotated form is 10.9 kcal mol^{-1} for the all-CO complex $(\mu\text{-}S(CH_2)_2BH(CH_2)_2S)[Fe(CO)_3]_2$. The energy difference between the most stable rotated form and most stable unrotated form is 2.4 kcal mol^{-1} for the mono-cyanide complex, $[(\mu\text{-}S(CH_2)_2BH(CH_2)_2S)\ [Fe(CO)_3][Fe(CO)_2(CN)]]^{1-}$. The replacement of one CO ligand of $(\mu\text{-}S(CH_2)_2BH(CH_2)_2S)[Fe(CO)_3]_2$ by CN^- therefore imparts additional stabilization to the borane-stabilized rotated structures.

The replacement of CO by better donor ligands and addition of steric bulk to the propanedithiolate framework are compatible for the stabilization of the rotated form. The addition of steric bulk to the propanedithiolate bridge destabilizes the unrotated forms by forcing a strong steric repulsion between the bridge and the apical ligands of the unrotated structures. A good donor ligand, L, stabilizes the rotated structures by making the unrotated $Fe(CO)_2L$ unit a better electron donor to the rotated $Fe(CO)_3$ unit. These two factors work together to lower the relative energy of the rotated structures with respect to the unrotated structures (Figure VII-4(c)). The energy difference between the rotated and unrotated structures for the down orientation of the *tert*-butyl group of the all-CO complex (μ-$SCH_2C(t\text{-}Bu)HCH_2S)[Fe(CO)_3]_2$ is 7.4 kcal mol^{-1}. The replacement of one CO ligand by CN^- to yield the monocyanide complex, $[(\mu\text{-}SCH_2C(t\text{-}Bu)HCH_2S)[Fe(CO)_3][Fe(CO)_2(CN)]]^{1-}$, lowers this value to 1.9 kcal mol^{-1}.

Conclusions

In order for a synthetic complex with the rotated structure to be isolated experimentally, at least one conformation of the rotated form must be more stable than the most stable conformation of the unrotated form. For this reason, all conformations of a given dithiolate bridge, anti, syn, and syn′ orientations of bis-thiolates, and all possible orientations of the ligands must be considered. The (μ-$SCH_2CH(CH_3)CH_2S)[Fe(CO)_3]_2$ complex, 1, provides an illustrative example: The down orientation of the methyl group of the S-to-S linker of complex 1 leads to a small energy difference between the most stable rotated form and most stable unrotated form (ΔG = 9.4 kcal mol^{-1}) for the $Fe(CO)_3$ unit nearest to the methyl group. Complex 1,

however, can rearrange to the lower energy structure 1′ in which the methyl group is oriented up and away from the $Fe(CO)_3$ units via a low energy transition state which exchanges the axial and equatorial equatorial groups of the FeS_2C_3 ring (*viz.* the exchange of axial and equatorial hydrogens in cyclohexane). The up orientation of the methyl group leads to energy difference between the most stable rotated form and most stable unrotated form of 12.1 kcal mol^{-1} for rotation of the $Fe(CO)_3$ unit nearest to the central methylene hydrogen of complex 1′. The 2,2-dimethyl-propane-1,3-dithiolate bridge would be more appropriate for generating a stable rotated structure experimentally, since either conformation of this bridge leads to steric repulsion with an apical ligand.

The combination of a sterically demanding dithiolate bridge and asymmetric substitution of strong donor ligands is the most viable method of making better synthetic di-iron complexes that will serve as both structural and functional models of active site of [FeFe]H_2ase. The amine and borane functionalized complexes stabilize the rotated form, but potentially block the site of H^+ acceptance on the selfsame iron center.

There are sufficient synthetic precedents for the ready synthesis of the preceding complexes or derivatives thereof. Rauchfuss[184,263] , Sun and Äkermark[199,320] , and their respective coworkers have reported the synthesis of a whole range of sterically demanding tertiary amine functionalized dithiolate bridges based on the (μ-$SCH_2N(R)CH_2S$) framework and their conversion into the corresponding ammonium salts of the form (μ-$SCH_2N^+(R)_2CH_2S$). Darensbourg,[181,195] Pickett,[193,187]

Rauchfuss[181,321] and their respective coworkers have reported the synthesis of asymmetrically substituted complexes. Our study suggests that the combination of these features into one synthetic complex will generate a better structural and functional model of the active site of [FeFe]H_2ase.

CHAPTER VIII

CONCLUSIONS

The frontier in iron-iron hydrogenase model chemistry is the development of functional synthetic models of the enzyme active site into working catalysts for dihydrogen uptake and production. Computational chemistry provides a necessary link between the enzyme active site and inorganic/organometallic synthetic analogs. This dissertation describes research projects that have focused on the computation of viable reaction pathways for isotopic scrambling of D_2/H_2O and D_2/H_2 mixtures using dinuclear $Fe^{II}Fe^{II}$ complexes as catalysts, the reaction of $Fe^{I}Fe^{I}$ complexes with electrophiles, the calculation of infrared spectra for CO- and CN- containing di-iron complexes and the role of asymmetry in creating a flexible coordination sphere about iron in $Fe^{I}Fe^{I}$ complexes which serve as solution electrocatalysts for H_2 production.

Bis-phosphine substituted di-iron dithiolate hydride complexes of the form $[(\mu\text{-}H)(\mu\text{-}SRS)[Fe(CO)_2(PMe_3)]_2]^{1+}$ (R = CH_2CH_2, $CH_2CH_2CH_2$, $CH_2(C_6H_4)CH_2$) have been shown experimentally to catalyze isotopic exchange in H_2/D_2 and D_2/H_2O mixtures under continuous exposure to sunlight. Density Functional Theory (DFT) calculations are described in Chapter III that suggest reasonable mechanistic explanations for the experimentally observed H/D exchange reactivity of these $Fe^{II}Fe^{II}$ functional model complexes. A combination of experimental and computational data suggests that the singular role of sunlight is CO ligand labilization to create an open site on the di-iron catalyst for D_2 binding. The calculations suggest that a reasonable path for D_2/H_2O

scrambling involves deprotonation of iron-bound η^2-D_2 by a water cluster, $(H_2O)_n$, to generate a bridging hydride, terminal deuteride species. This complex may then reductively eliminate HD to generate a η^2-HD bound Fe^IFe^I complex. The Fe-Fe bond may then be protonated by D^+ from $[D(H_2O)_n]^{1+}$ to afford D_2/μ-H exchange.

These results have an important implication for the development of H_2 uptake catalysts. While the cleavage of H_2 is generally believed to occur from the Fe^IFe^{II} or more oxidized form of the [FeFe]H_2ase active site, these computational results suggest that the formally Fe^IFe^I bis-phosphine complexes may be able to catalyze H-H bond cleavage subsequent to CO loss (as shown in Scheme VIII-1). ^{1}H- or ^{2}H-NMR spectra should be useful to examine the ability of these complexes to catalyze isotopic exchange of D_2/H_2O mixtures. These results show that simple dithiolate-bridged di-iron complexes in low oxidation states are capable of binding and activating dihydrogen. As these FeIFeI complexes are also starting points for electrocatalysis of H_2 production, the intermediates suggested by the H_2 activation analysis are expected to be appropriate to H2 production mechanisms. This raises the point of whether the electrocatalysis might benefit from coordinative unsaturation, i. e., photolysis coupled with electrolysis.

Scheme VIII-1

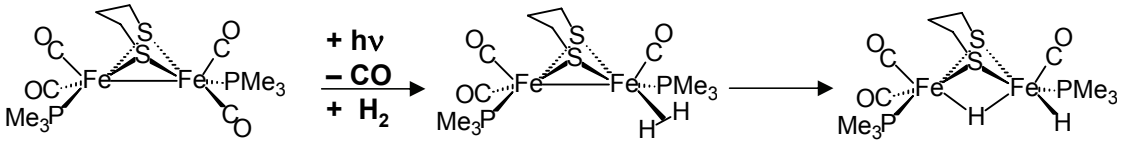

The dithiolate-bridged dinuclear iron complex, (μ-SCH_2CH_2S)[$Fe(CO)_2(PMe_3)$]$_2$, has been shown experimentally to react with the electrophilic species, H^+ and Et^+ (Et^+ = $CH_3CH_2^+$) with differing regioselectivity; H^+ reacts to form a 3c-2e$^-$ Fe^{II}-H-Fe^{II} bond, while Et^+ reacts to form a new C-S bond, creating a bridging thioether and leaving the iron oxidation states as Fe^IFe^I. In Chapter IV, DFT calculations are described that examine the reaction of these two electrophilic species using the computational model (μ-SCH_2CH_2S)[$Fe(CO)_2(PH_3)$]$_2$. In agreement with the experimental results, protonation of the Fe-Fe bond density is found to yield a much more stable complex than protonation of a bridging sulfur atom, while alkylation of a sulfur atom of the bridging thiolate is found to yield a much more stable complex than alkylation of an iron center. Additional computations show that a mononuclear iron(II) complex with an Fe-E bond (E = H or Et) is significantly more stable than its constitutional isomer with iron(0) and an S-E bond. The instability of a bridging ethyl complex is attributed to the inability of the ethyl group, in contrast to a hydride, to form a stable 3c-2e$^-$ bond with the two iron centers. Nevertheless these dinuclear iron(II) complexes can form a third bridge with an additional μ-SR, accounted for by the excellent bridging ability of the electron-rich thiolate.

One of the forefront areas in the study of synthetic models of iron-iron hydrogenase active site is the study of the electrochemistry and electrocatalytic mechanisms for proton reduction catalyzed by these complexes. Since these complexes contain CO ligands, they often can be conveniently monitored by *in situ* infrared

spectroscopic monitoring (IR spectroelectrochemistry). Gas-phase density functional theory calculations are described in Chapter V that are used to predict the solution-phase infrared spectra for a series of well-characterized CO and CN-containing di-iron complexes. These results show that simple linear scaling of the computed C-O and C-N stretching frequencies yields accurate predictions of the experimentally determined ν(CO) and ν(CN) values for a set of related complexes. The 0.9526 scaling factor (i. e. $\nu_{observed} = 0.9526\nu_{computed}$) correlation is used to assign structures to spectroscopically-observed species. This methodology may be used to discriminate between a series of structural candidates for species that have been observed by IR spectroscopy, but not structurally characterized. One should exercise caution in the use of this scaling factor for systems that are very different that those in the training set. The basis set used to describe the CX ligands is the most important determinant since different basis sets can lead to significant changes in the computed C-X distance and ν(CX) stretching frequencies.

Simple synthetic di-iron dithiolate complexes provide good models of the composition of the active site of the iron-iron hydrogenase enzymes. However, the formally $Fe^{I}Fe^{I}$ complexes synthesized to date fail to reproduce the precise orientation of the diatomic ligands about the iron centers that is observed in the molecular structure of the reduced form of the enzyme active site. This structural difference is often used to explain the fact that the synthetic di-iron complexes are generally poor catalysts when compared to the enzyme. Our assumption is that rotation of one of the $Fe(CO)_2L$ units

computations to generate a structure more like the enzyme active site creates an electron-rich "open site" on that iron center, making it a better acceptor for protons in the proton/electron coupling process (as shown for rotation of one $Fe(CO)_3$ unit of (μ-$SCH_2CH_2CH_2S$)$[Fe(CO)_3]_2$ in Scheme VIII-2).

Scheme VIII-2

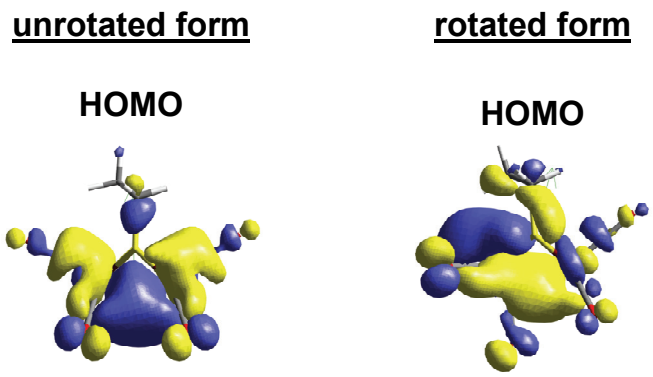

The differing ability of the (μ-pdt)$[Fe(CO)_3][Fe(CO)_2L]$ and (μ-pdt)$[Fe(CO)_3][Fe(CO)_2L']$ complexes (where L' is a better electron donor than L) to stabilize the μ-CO transition states is best understood beginning with an analysis of the electronic structure and properties of (μ-pdt)$[Fe(CO)_3]_2$, and {(μ-pdt)(μ-CO)$[Fe(CO)_2][Fe(CO)_3]$}‡. The effects of substitution of CO on the $Fe(CO)_3$ units by a better donor can then be gauged.

Population analysis by the Natural Bonding Orbital (NBO) method shows that rotation of one $Fe(CO)_3$ unit leads to the transfer of charge from the unrotated $Fe(CO)_3$ to the rotated $Fe(CO)_3$ unit. The NBO method yields charges of –0.340 and –0.354 for

the iron atoms of (μ-pdt)[$Fe(CO)_3$]$_2$ and total charges of +0.034 and +0.018 when the Fe, C, and O charges are summed for each of the $Fe(CO)_3$ units. A similar analysis of the NBO results for rotated structure gives charges of –0.313 and –0.346 for the iron atoms and –0.054 and +0.149 for the rotated and unrotated $Fe(CO)_3$ units, respectively. In other words, the rotated $Fe(CO)_3$ gains 0.088 electrons and the unrotated unit loses 0.131 electrons.

The metric data from the geometry-optimized structures of unrotated and rotated are in agreement with the NBO assigned charges. The NBO charge analysis predicts that M (d^{π}) → CO (π^*) should increase for the rotated $Fe(CO)_3$ unit and decrease for the unrotated $Fe(CO)_3$ unit as electrons are transferred from the unrotated to the rotated $Fe(CO)_3$ unit. The expected shortening of the Fe-C bonds and lengthening of C-O bonds of the rotated $Fe(CO)_3$ unit and the concomitant lengthening Fe-C bonds and shortening of the C-O bonds of the unrotated $Fe(CO)_3$ unit are observed in the optimized structures.

The assignment of the NBO charges of {(μ-CO)(μ-pdt)[$Fe(CO)_2$][$Fe(CO)_3$]}‡ shows the (μ-CO)$Fe(CO)_2$ unit to be an electron acceptor and the unrotated $Fe(CO)_3$ unit to be an electron donor. The substitution of one CO of the unrotated $Fe(CO)_3$ unit by a better donor ligand would make the resulting $Fe(CO)_2$(L) unit a better donor to the (μ-CO)$Fe(CO)_2$ unit, and this would stabilize the transition state species. Conversely, the substitution of one CO of the (μ-CO)$Fe(CO)_2$ unit by better donor ligand would raise the relative energy of the this species by making it a poorer electron acceptor.

The analysis of the molecular orbitals and computed charges demonstrated the chameleon-like nature of the electronic structure of these di-iron complexes. Scheme VIII-3 highlights four possible ways of describing of the electronic structure of the

Scheme VIII-3

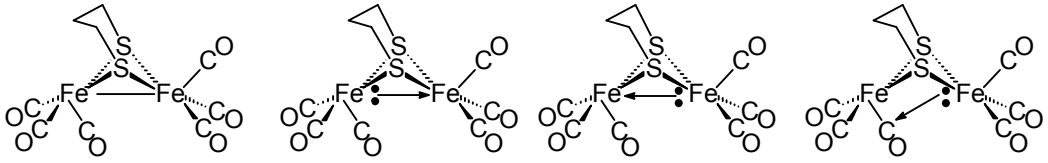

rotated form of (μ-pdt)[Fe(CO)$_3$]$_2$. In the first structure, a normal covalent bond is drawn between the two iron centers. In the second structure, the Fe-Fe bond is polarized toward the leftmost iron so that the complex is simplistically, in terms of oxidation states, described as Fe^0Fe^{II} rather than Fe^IFe^I. This type of electronic structure should be stabilized by the attaching an electron-acceptor to the leftmost iron center. In the third structure, the Fe-Fe bond is polarized toward rightmost iron so that the complex is simplistically described as $Fe^{II}Fe^0$ rather than Fe^IFe^I. This type of electronic structure should be stabilized by the attaching an electron-donor to the leftmost iron center. In the last structure, the Fe-Fe bond is polarized toward rightmost iron but the rightmost iron is donating into the "bridging CO" ligand. As shown in Chapter VII, the attachment of either an electron donor or electron acceptor to rotated Fe(CO)$_3$ unit lowers its energy relative to the unrotated form.

DFT computations were used to examine how the nature of L in a series of mono-substituted complexes of the form $\{(\mu\text{-SRS})[Fe(CO)_3][Fe(CO)_2L]\}^{n-}$ affects the energy difference between the rotated and unrotated forms of a series of di-iron complexes. The computed energy differences for rotation of the $Fe(CO)_3$ and $Fe(CO)_2L$ units are shown to be directly related to the donor strength of L. As the donor strength of L is increased, the energy difference for $Fe(CO)_3$ rotation decreases and the energy difference for $Fe(CO)_2L$ rotation increases. Analysis of the calculated atomic charges and molecular orbitals shows that rotation of the $Fe(CO)_3$ unit leads to transfer of electron density from the unrotated $Fe(CO)_2L$ unit to the rotated $Fe(CO)_3$ unit (similar to that shown in Scheme VIII-2).

Since the N-heterocyclic carbenes are among the strongest neutral donor ligands, one of them was chosen for the synthesis of an asymmetrically substituted model complex. The sterically-encumbered and commercially-available 1,3-bis(2,4,6-trimethylphenyl)-imidazol-2-ylidene (IMes) ligand was reacted with $(\mu\text{-}SCH_2CH_2CH_2S)[Fe(CO)_3]_2$ in order to generate a monosubstituted complex, $(\mu\text{-}SCH_2CH_2CH_2S)[Fe(CO)_3][Fe(CO)_2(IMes)]$ (as described in Chapter VI). This complex, whose X-ray structure displays an apical carbene, shows an unexpected two-electron reduction to be involved in its electrocatalytic dihydrogen production. Density functional calculations showed, in addition to a one-electron Fe-Fe reduction, that the arylsubstituted N-heterocyclic carbene can accept a second electron more readily than the Fe-Fe manifold. (N. B., the methyl-substituted NHC does <u>not</u> follow this pathway).

The juxtaposition of these two one-electron reductions resembles the [FeFe]H_2ase active site with an FeFe di-iron unit joined to the electroactive 4Fe4S cluster. It suggests that the attachment of electroactive ligands should facilitate electrocatalysts.

In Chapter VII, density functional theory computations are used for the rational design of synthetic complexes as structural models of the reduced form of the enzyme active site. These computations suggest several possible synthetic targets. The synthesis of complexes containing five-atom S-to-S linkers of the form $S(CH_2)_2X(CH_2)_2S$ (X = CH_2, NH, or O) or pendant functionalities attached to the three-carbon framework is one

Scheme VIII-4

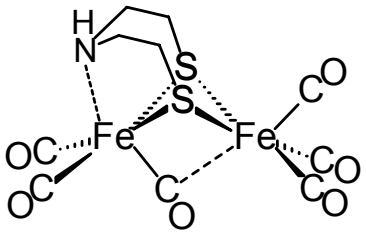

method. The complex given in Scheme VIII-4 is computed to be one of the best candidates. Another approach is the synthesis of asymmetrically substituted complexes, in which one iron center has strongly electron donating ligands and the adjacent iron center has strongly electron accepting ligands. The combination of a sterically demanding S-to-S linker and asymmetric substitution of the CO ligands is predicted to be a particularly effective synthetic target. Two potential synthetic targets that

incorporate strong donor ligands and a sterically-demanding S-to-S linker are given in Scheme VIII-5.

Scheme VIII-5

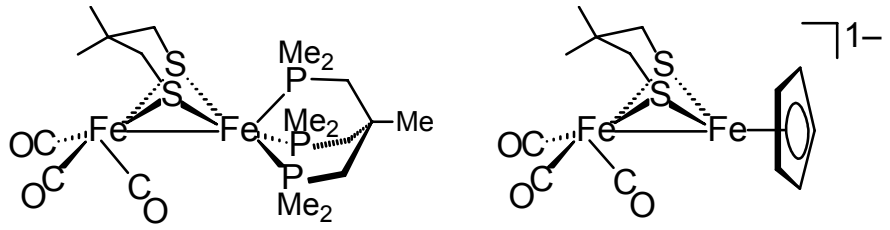

The complexes proposed in Scheme VIII-6 are expected to be better catalysts for H_2 production that the unrotated di-iron dithiolate complexes. The protonation of the unrotated Fe^IFe^I complex requires strong acids, and the resulting bridging hydride resists protonation even by the strongest acids. In other words, protonation of the unrotated Fe^IFe^I complex results in a bridging hydride ligand that is thermodynamically and kinetically a very poor base. Protonation of one of the $Fe(CO)_3$ centers of the complexes given in Scheme VIII-5, however, should result in the production of a terminal hydride ligand. In general, terminal hydride ligands are much more basic (thermodynamically and kinetically) than the analogous bridging hydrides.

A mechanism for H_2 production using one of these proposed di-iron catalysts is given in Scheme VIII-6. In the first step, the Fe^IFe^I complex is protonated by an acid to

Scheme VIII-6

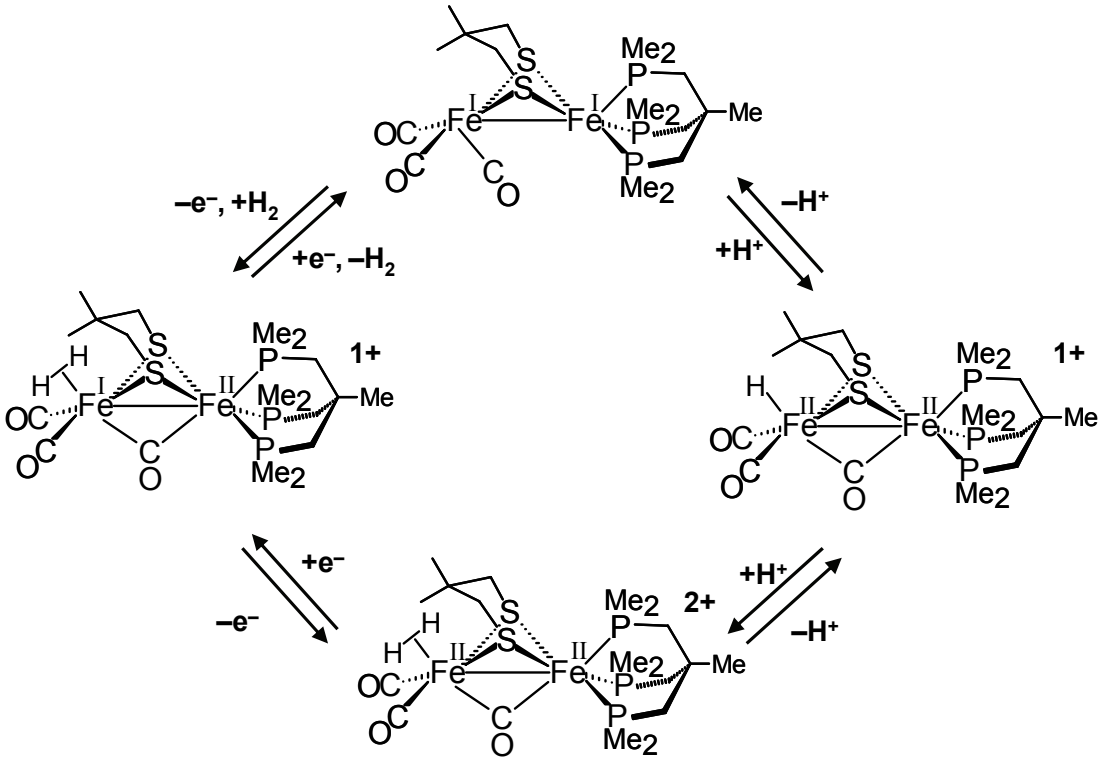

yield an $Fe^{II}Fe^{II}$ terminal hydride ligand. In the second step, the hydride ligand is protonated to yield an η^2-H_2 ligand bound to the $Fe^{II}Fe^{II}$ complex. This complex will then undergo two one-electron reductions to release H_2 and regenerate the $Fe^{I}Fe^{I}$ starting complex. One might expect the reverse of this process to proceed with possibly greater facility.

In the simplest sense, the electrocatalytic production of dihydrogen requires getting two protons and two electrons onto the catalyst. The total energy that is required to yield this doubly-protonated, doubly reduced species is a constant given by eq VIII-1,

$$\Delta G_{H_2 prod} = -nFE_1^0 - nFE_2^0 + 2.312RT(\Delta pKa_1) + 2.312RT(\Delta pKa_2) \quad \text{(VIII-1)}$$

where ΔpKa_1 and ΔpKa_2 are the differences in the pKa of the single and doubly protonated catalyst and that of the acid that is used as the proton source. This relation shows the interdependence of the reduction potential and the pKa of the acid used as a proton source. In laymen's terms, this can be stated as follows: As the catalyst is protonated, its increasing positive charge will make it easier to reduce, and as the catalyst is reduced the increasing negative charge will make it more basic. In other words, in the limit of a very strong acid, the catalyst should be protonated and relatively easy to reduce, and highly reduced species should be basic and relatively easy to protonate.

The solvent will have a major influence on the reduction potential and the strength of acid required to protonate the catalyst. Polar, protic solvents such as water will lower the reduction potential of a neutral molecule by stabilizing the anionic product. Likewise, these solvents will promote protonation of the catalyst by stabilizing the cationic, protonated form.

The Darensbourg group has investigated the effects of added water on the electrochemistry of complexes of the forms, (μ-pdt)[$Fe(CO)_3$][$Fe(CO)_2$(PTA)] and (μ-pdt)[$Fe(CO)_2$(PTA)]$_2$.[195] In these investigations, they have found that the addition of water to acetonitrile solutions of these complexes leads to a positive shift in the reduction potential. These complexes were found to serve as solution electrocatalysts for H_2 production from the weak acid, HOAc.

The (μ-pdt)[$Fe(CO)_3$][$Fe(CO)_2$(PTA)] and (μ-pdt)[$Fe(CO)_2$(PTA)]$_2$ complexes are soluble in acetonitrile:water mixtures up to 1:3 by volume, but are insoluble in pure water. To my knowledge, the only totally water-soluble iron-iron hydrogenase model complex sythesized to date is the [NEt_4]$_2$[(μ-pdt)[$Fe(CO)_2(CN)]_2$].[182] The [NEt_4]$_2$[(μ-pdt)[$Fe(CO)_2(CN)]_2$] complex, however, does not function as a solution electrocatalyst for H_2 production in water over the pH range 8.4-4.0.

Recently, I have synthesized a series of hydroxy-functionalized di-iron complexes that when converted to the PTA derivatives are totally soluble in water. The (μ-$SCH_2CH_2OH)_2[Fe(CO)_3]_2$ starting complex is not totally soluble in water, but is soluble and stable in alcohols and alcohol/water mixtures. Reaction of the (μ-$SCH_2CH_2OH)_2[Fe(CO)_3]_2$ complex with the PTA ligand yield the bis-substituted complex of the form (μ-$SCH_2CH_2OH)_2[Fe(CO)_2(PTA)]_2$. This complex is more soluble in water than in organic solvent such as acetonitrile.

Cyclic voltammetry of (μ-$SCH_2CH_2OH)_2[Fe(CO)_3]_2$ and (μ-$SCH_2CH_2OH)_2$ $[Fe(CO)_2(PTA)]_2$ in CH_3CN is also very similar to (μ-$SCH_2CH_3)_2[Fe(CO)_3]_2$ and (μ-$SCH_2CH_3)_2[Fe(CO)_2(PMe_3)]_2$ analogues. In water, the reduction (μ-$SCH_2CH_2OH)_2$ $[Fe(CO)_2(PTA)]_2$ is not observed within the solvent window. In other words, the reduction of (μ-$SCH_2CH_2OH)_2[Fe(CO)_2(PTA)]_2$ occurs at a potential more negative than the reduction of water. However, the addition of acetic acid leads to an increase in the peak potential near –1.14 V vs methyl viologen. This increase is much less dramatic in the absence of the di-iron catalyst. These results are consistent with the (μ-

$SCH_2CH_2OH)_2[Fe(CO)_2(PTA)]_2$ acting as an electrocatalyst for H_2 production. The value of the reduction potential shows that this particular complex only offers a small improvement on the uncatalyzed reduction of water.

Simple dithiolate bridged di-iron complexes can act as functional models of the [FeFe]H_2ase enzyme albeit under harsher conditions. Hydride-bridged $Fe^{II}Fe^{II}$ complexes are shown to bind and activate dihydrogen, but require continuous photolysis in order to remain catalytically active. The $Fe^{I}Fe^{I}$ complexes are shown to catalyze the reduction of protons to produce dihydrogen, but require either strong acids or high reduction potentials to do so. Therefore, an important goal of future work is the design of new di-iron catalysts that function under less harsh conditions. For the dihydrogen-binding $Fe^{II}Fe^{II}$ complexes, this process entails stabilization of an "open site" on one of the iron centers to obviate the need for continuous photolysis. This stabilization may entail site isolation or the synthesis of a complex with a very labile ligand coordinated to one of the iron centers. A prerequisite for the design of $Fe^{I}Fe^{I}$ complexes as better catalysts for proton reduction is a better understanding of the catalytic mechanism. The use of computed infrared spectra for possible catalytic intermediates in this process, as described in Chapter VI, may aid in the elucidation of this mechanism.

While we and others have been diligently working on the development of small-molecule analogues of the hydrogenase enzyme active sites as functional catalysts for H_2 uptake and H_2 production, other workers have been searching for more robust enzymes to use directly as catalysts. In 2002, Armstrong, Albracht and coworkers reported that graphite electrodes that had been coated with a [NiFe] hydrogenase enzyme derived

from *Allochromatium vinosum* performed as well as platinum for the oxidation of dihydrogen.[322] An attractive feature of this hydrogenase enzyme-modified electrode as compared with a platinum electrode is that, when exposed to CO, the former quickly regain catalytic activity once the CO gas is removed. Unfortunately, this [NiFe] hydrogenase enzyme, derived from *Allochromatium vinosum*, reacts with dioxygen to generate an "overoxidized", catalytically inactive form of the enzyme, which does not immediately regain catalytic activity once the O_2 gas is removed. The reactivation of this enzyme is possible, but requires an extended period. More recently, Armstrong, Friedrich, and coworkers examined the reaction of a [NiFe] hydrogenase enzyme derived from the aerobic bacterium *Ralstonia eutropha*.[323] They found that enzyme-modified electrodes derived from this enzyme are capable of oxidizing H_2 in the presence of large concentrations of CO. This enzyme is inhibited by the addition of O_2, but immediately regains function when the O_2 gas is removed. Such impressive discoveries suggest the synergy between biology, experimental chemistry, and computational chemistry should continue to provide a fertile research area, with results of potential use to mankind.

REFERENCES

(1) Penner, S. S. *Energy* **2006**, *31*, 33–43.

(2) Sherif, S. A.; Barbir, F.; Veziroglu, T. N. *Solar Energy* **2005**, 78, 647–660.

(3) Dedieu, A., Ed. *Transition Metal Hydrides*; VCH: New York, 1992.

(4) Kubas, Gregory J., Ed. *Metal Dihydrogen and σ-Bond Complexes: Structure, Theory and Reactivity*; Kluwer Academic/Plenum Publishers: Dordrecht, Netherlands, 2001.

(5) Peruzzini, M., Poli, R., Eds. *Recent Advances in Hydride Chemistry*; Elsevier: Amsterdam, 2001.

(6) Kubas G. J. *J. Less-Common Metals* **1991**, *173*, 475–484.

(7) Espinet, P.; Esteruelas, M. A.; Oro, L. A.; Serrano, J. L.; Sola E. *Coord. Chem. Rev.* **1992**, *117*, 215–274.

(8) Jessop, P. G.; Morris, R. H. *Coord. Chem. Rev.* **1992**, *121*, 155–284.

(9) Heinekey, D. M.; Oldham, W. J. Jr. *Chem. Rev.* **1993**, *93*, 913–926.

(10) Kuhlman, R. *Coord. Chem. Rev.* **1997**, *167*, 205–232.

(11) Crabtree, R. H. *J. Organomet. Chem.* **1998**, *557*, 111–115.

(12) Crabtree, R. H.; Eisenstein, O.; Sini, G.; Peris E. *J. Organomet. Chem.* **1998**, *567*, 7–11.

(13) Esteruelas, M. A.; Oro, L. A. *Chem. Rev.* **1998**, *98*, 577–588.

(14) Sabo-Etienne, S.; Chaudret B. *Coord. Chem. Rev.* **1998**, *178–180*, 381–407.

(15) Sabo-Etienne, S.; Chaudret B. *Chem. Rev.* **1998**, *98*, 2077–2091.

(16) Jia, G.; Lau, C.-P. *Coord. Chem. Rev.* **1999**, *190–192*, 83–108.

(17) Maseras, F.; Lledos, A.; Clot, E.; Eisenstein, O. *Chem. Rev.* **2000**, *100*, 601–636.

(18) Darensbourg, M. Y.; Lyon, E. J.; Smee, J. J. *Coord. Chem. Rev.* **2000**, *206–207*, 533–561.

(19) McGrady, G. S.; Guilera, G. *Chem. Soc. Rev.* **2003**, *32*, 383–392.

(20) Heinekey, D. M.; Lledos, A.; Lluch, J. M. *Chem. Soc. Rev.* **2004**, *33*, 175–182.

(21) Bakhmutov, V. I. *Eur. J. Inorg. Chem.* **2005**, 245–255.

(22) Heller, A. *Acc. Chem. Res.* **1981**, *14*, 154–162.

(23) Kreuter, W.; Hofmann H. *Int. J. Hydrogen Energy* **1998**, *23*, 661–666.

(24) Losiewicz, B.; Budniok, A.; Rowinski, E.; Lagiewka, E.; Lasia, A. *Int. J. Hydrogen Energy* **2003**, *29*, 145–157.

(25) Schaefer, H. F. III *Acc. Chem. Res.* **1977**, *10*, 287–293.

(26) Lee, T. R.; Whitesides, G. M. *Acc. Chem. Res.* **1992**, *25*, 266–272.

(27) Uchida H. *Int. J. Hydrogen Energy* **1999**, *24*, 861–869.

(28) Kroes, G.-J.; Gross, A.; Baerends, E.-J.; Scheffler, M.; McCormack, D. A. *Acc. Chem. Res.* **2002**, *35*, 193–200.

(29) Jacobsen, H. *Angew. Chem., Int. Ed.* **2004**, *43*, 1912–1914.

(30) Zhang, X.-M.; Bruno, J. W.; Enyinnaya, E.*J. Org. Chem.* **1998**, *63*, 4671–4678.

(31) Darwent B. Nat. Stand. Ref. Data Ser., Nat. Bur. Stand. 1970, (NSRDS–NBS 31).

(32) Kistiakowsky, G. B.; Romeyn, H. Jr.; Ruhoff, J. R.; Smith, H. A.; Vaughan W. E. *J. Am. Chem. Soc.* **1935**, *57,* 65–75.

(33) Gordon, M. S.; Truong, T. N.; Pople, J. A. *Chem. Phys. Lett.* **1986**, *130*, 245–248.

(34) Abdur-Rashid, K.; Fong, T. P.; Greaves, B.; Gusev, D. G.; Hinman, J. G.; Landau, S. E.; Lough, A. J.; Morris, R. H. *J. Am. Chem. Soc.* **2000**, *122*, 9155–9171.

(35) Izutsu, K. *Acid–Base Dissociation Constants in Dipolar Aprotic Solvents*; Blackwell Scientific Publications, Oxford, 1990.

(36) Kolthoff, I. M.; Chantooni, M. K., Jr. *J. Chem. Eng. Data* **1999**, *44*, 124–129.

(37) Kubas, G. J. *J. Organomet. Chem.* **2001**, *635*, 37–68.

(38) Noell, J. O.; Hay, P. J. *J. Am. Chem. Soc.* **1982**, *104*, 4578–4584.

(39) Hay P. J.; *J. Am. Chem. Soc.* **1987**, *109*, 705–710.

(40) Eckart, J.; Kubas, G. J.; Hall, J. H.; Hay, P. J.; Boyle, C. M. *J. Am. Chem. Soc.* **1990**, *112*, 2324–2332.

(41) Haynes, G. R.; Martin, R. L.; Hay P. J. *J. Am. Chem. Soc.* **1992**, *114*, 28–36.

(42) Lin, Z.; Hall, M. B. *J. Am. Chem. Soc.* **1992**, *114*, 2928–2932.

(43) Kubas, G. J.; Ryan, R. R.; Swanson, B. I.; Vergamini, P. J.; Wasserman, H. J. *J. Am. Chem. Soc.* **1984**, *106*, 451–452.

(44) Morris, R. H. *Can. J. Chem.* **1996**, *74*, 1907–1915.

(45) Gonzalez, A. A.; Zhang, K.; Mukerjee, S. L.; Hoff, C. D.; Khalsa, G. R. K.; Kubas, G. J. In *Bonding Energetics in Organometallic Compounds*, Marks, T. J. Ed. American Chemical Society, Washington, DC, 1990, pp. 133–147.

(46) Lin, Z.; Hall, M. B. *J. Am. Chem. Soc.* **1992**, *114*, 6102–6108.

(47) Lin, Z. Hall, M. B. *Inorg. Chem.* **1992**, *31*, 4262–4265.

(48) Lin, Z.; Hall, M. B. *Coord. Chem. Rev.* **1994**, *135/136*, 845–879.

(49) Bayse, C. A.; Hall, M. B. *J. Am. Chem. Soc.* **1999**, *121,* 1348–1358.

(50) Morris, R. H.; Earl, K. A.; Luck, R. I; Lazarowych, N. J.; Sella, A. *Inorg. Chem.* **1987**, *26*, 2674–2683.

(51) Morris, R. H. *Inorg. Chem.* **1992**, *31*, 1471–1478.

(52) Kubas, G. J.; Unkefer, C. J.; Swanson, B. I.; Fukushima, E. *J. Am.Chem. Soc.* **1986**, *108*, 7000–7009.

(53) Heinekey, D. M.; Law, J. K.; Schultz, S. M. *J. Am. Chem. Soc.* **2001,** *123,* 12728–12729.

(54) Gelabert, R.; Moreno, M.; Lluch, J. M.; Lledos, A. *J. Am. Chem. Soc.* **1997**, *119*, 9840–9847.

(55) Gelabert, R.; Moreno, M.; Lluch, J. M.; Lledos, A. *J. Am. Chem. Soc.* **1998**, *120*, 8168–8176.

(56) Torres, L.; Gelabert, R.; Moreno, M.; Lluch, J. M. *J. Phys. Chem. A* **2000**, *104*, 7898–7905.

(57) Barea, G.; Esteruelas, M. A.; Lledos, A.; Lopez, A. M.; Onate, E.; Tolosa, J. I.; *Organometallics* **1998**, *17*, 4065–4076.

(58) Barea, G.; Esteruelas, M. A.; Lledos, A.; Lopez, A. M.; Onate, E.; Tolosa, J. I. *Inorg. Chem.* **1998**, *37*, 5033–5035.

(59) Klooster, W. T.; Koetzle, T. F.; Jia, G.; Fong, T. P.; Morris, R. H.; Albinati, A. *J. Am. Chem. Soc.* **1994**, *116*, 7677–7681.

(60) Law, J. K. Mellows, H. Heinekey, D. M. *J. Am. Chem. Soc.*, **2002**, *124*, 1024–1030.

(61) V. Pons, D. M. Heinekey *J. Am. Chem. Soc.*, **2003**, *125*, 8428–8429.

(62) Eckert, J.; Webster, C. E.; Hall, M. B.; Albinati, A.; Venanzi, L.M. *Inorg. Chim. Acta* **2002**, *330*, 240–249.

(63) Finney, J. L. *Acta Crystallogr., Sect. B: Struct. Sci.* **1995**, *B51*, 447–467.

(64) Rao, B. D. N.; Anders, L. R. *Phys. Rev.* **1965**, *140*, 112–117.

(65) Luther, T. A.; Heinekey, D. M. *Inorg. Chem.* **1998**, *37*, 127–132.

(66) Schlaf, M.; Lough, A. J.; Maltby, P. A.; Morris, R. H. *Organometallics.* **1996**, 15, 2270–2278.

(67) Crabtree, R. H.; Lavin, M. *J. Chem. Soc. Chem. Commun.* **1985**, 1661–1662.

(68) Hamilton, D. G.; Crabtree, R. H. *J. Am. Chem. Soc.* **1988**, *110*, 4126–4133.

(69) Crabtree, R. H. *Acc. Chem. Res.* **1990**, *23*, 95–101.

(70) Yao, W.; Faller, J. W.; Crabtree, R. H. *Inorg. Chim. Acta* **1997**, *259*, 71–76.

(71) Desrosiers, P. J.; Cai, L.; Lin, Z.; Richards, R.; Halpern, J. *J. Am. Chem. Soc.* **1991**, *113*, 4173–4184.

(72) Bautista, M. T.; Earl, K. A.; Maltby, P. A.; Morris, R. H.; Schweitzer, C. T.; Sella, A. *J. Am. Chem. Soc.* **1988**, *110*, 7031–7036.

(73) Gelabert, R.; Moreno, M.; Lluch, J. M.; Lledos, A. *Chem. Phys.* **1999**, *241*, 155–166.

(74) Tejeda, G.; Fernandez, J. M.; Montero, S.; Blume, D.; Toennies, J. P. *Phys. Rev. Lett.* **2004**, *92*, 223401/1–223401/4.

(75) Moreno, B.; Sabo-Etienne, S.; Chaudret, B.; Rodriguez, A.; Jalon, F.; Trofimenko, S. *J. Am. Chem. Soc.* **1995**, *117*, 7441–7451.

(76) George, M. W.; Haward, M. T.; Hamley, P. A.; Hughes, C.; Johnson, F. P. A.; Popov, V. K.; Poliakoff, M. *J. Am. Chem. Soc.* **1993**, *115*, 2286–2299.

(77) Kubas, G. J.; Unkefer, C. J.; Swanson, B. I.; Fukushima, E. *J. Am. Chem. Soc.* **1986**, *108*, 7000–7009.

(78) Upmacis, R. K.; Poliakoff, M.; Turner, J. J. *J. Am. Chem. Soc.* **1986**, *108*, 3645–3651.

(79) Sweany, R. L.; Moroz, A. *J. Am. Chem. Soc.* **1989**, *111*, 3577–3583.

(80) Tejeda, G.; Fernandez, J. M.; Montero, S.; Blume, D.; Toennies, J. P. *Phys. Rev. Lett.* **2004**, *92*, 223401/1–223401/4.

(81) Abis, L.; Sen, A.; Halpern, J. *J. Am. Chem. Soc.* **1978**, *100*, 2915–2916.

(82) Chatt, J.; Shaw, B. L. *J. Chem. Soc.* **1959**, 705–716.

(83) Low, J. J.; Goddard, W. A. III *J. Am. Chem. Soc.* **1984**, *106*, 8321–8322.

(84) Low, J. J.; Goddard, W. A. III *J. Am. Chem. Soc.* **1984**, *106*, 6928–6937.

(85) Low, J. J.; Goddard, W. A. III *Organometallics* **1986**, *5*, 609–622.

(86) Low, J. J.; Goddard, W. A. III *J. Am. Chem. Soc.* **1986**, *108*, 6115–6128.

(87) Sabo-Etienne, S.; Chaudret, B.; el Makarim, H. B.; Barthelat, J.-C.; Daudey, J.-P.; Ulrich, S.; Limbach, H. H.; Moïse, C. *J. Am.Chem. Soc.* **1995**, *117*, 11602–11603.

(88) Jalon, F. A.; Otero, A.; Manzano, B. R.; Villaseñor, E.; Chaudret, B. *J. Am. Chem. Soc.* **1995**, *117*, 10123–10124.

(89) Antiñolo, A.; Carillo-Hermosilla, F.; Fajardo, M.; Garcia-Yuste, S.; Otero, A.; Camanyes, S.; Maseras, F.; Moreno, M.; Lledós, A.; Lluch, J. M. *J. Am. Chem. Soc.* **1997**, *119*, 6107–6114.

(90) Van der Sluys, L. S.; Eckert, J.; Eisenstein, O.; Hall, J. H.; Huffman, J. C.; Jackson, S. A.; Koetzle, T. F.; Kubas, G. J.; Vergamini, P. J.; Caulton, K. G. *J. Am. Chem. Soc.* **1990**, *112*, 4831–4841.

(91) Albinati, A.; Bakhmutov, V. I.; Caulton, K. G.; Clot, E.; Eckert, J.; Eisenstein, O.; Gusev, D. G.; Grushin, V. V.; Hauger, B. E.; Klooster, W. T.; Koetzle, T. F.; McMullan, R. K.; O'Loughlin, T. J.; Pelissier, M. ; Ricci, J. S.; Sigalas, M. P.; Vymenits, A. B. *J. Am. Chem. Soc.* **1993**, *115*, 7300–7312.

(92) Eckert, J.; Jensen, C. M.; Jones, G.; Clot, E.; Eisenstein, O. *J. Am. Chem. Soc.* **1993**, *115*, 11056–11057.

(93) Eckert, J. *Spectrochim. Acta, Part A* **1992**, *48A*, 271–283.

(94) Eckert, J. *Spectrochim. Acta, Part A* **1992**, *48A*, 363–378.

(95) Eckert, J.; Kubas, G. J.; Dianoux, A. J. *J. Chem. Phys.* **1988**, *88*, 466–468.

(96) Clot, E.; Eckert, J. *J. Am. Chem. Soc.* **1999,** *121,* 8855–8863.

(97) Bayse, C. A.; Hall, M. B.; Pleune, B.; Poli, R. *Organometallics* **1998**, *17*, 4309–4315.

(98) Mediati, M.; Tachibana, G. N.; Jensen, C. M. *Inorg. Chem.* **1990**, *29*, 3–5.

(99) Mediati, M.; Tachibana, G. N.; Jensen, C. M. *Inorg. Chem.* **1992**, *31*, 1827–1832.

(100) Eckert, J.; Jensen, C. M.; Koetzle, T. F.; Husebo, T. L.; Nicol, J.; Wu, P. *J. Am. Chem. Soc.* **1995**, *117*, 7271–7272.

(101) Bayse, C. A.; Couty, M.; Hall, M. B. *J. Am. Chem. Soc.* **1996**, *118*, 8916–8919.

(102) Lough, A. J.; Park, S.; Ramachandran, R.; Morris, R. H. *J. Am. Chem. Soc.* **1994**, *116*, 8356–8357.

(103) Lee, J. C. Jr.; Peris, E.; Rheingold, A. L.; Crabtree, R. H. *J. Am. Chem. Soc.* **1994**, *116*, 11014–11019.

(104) Wessel, J.; Lee, J. C. Jr.; Peris, E.; Yap, G. P. A.; Fortin, J. B.; Ricci, J. S.; Sini, G.; Albinati, A.; Koetzle, T. F.; Eisenstein, O.; Rheingold, A. L.; Crabtree, R. H. *Angew. Chem*., *Int. Ed. Engl*. **1995**, *34*, 2507–2509.

(105) Patel, B. P.; Yao, W.; Yap, G. P. A.; Rheingold, A. L.; Crabtree, R. H. *Chem. Comm.* **1996**, 991–992.

(106) Patel, B. P.; Wessel, J.; Yao, W. B.; Lee, J. C.; Peris, E.; Koetzle, T. F.; Yap, G. P. A.; Fortin, J. B.; Ricci, J. S.; Sini, G.; Albinati, A.; Eisenstein, O.; Rheingold, A. L.; Crabtree, R. H. *New J. Chem.* **1997**, *21*, 413–421.

(107) Sini, G.; Eisenstein, O.; Yao, W.; Crabtree, R. H. *Inorg. Chim. Acta* **1998**, *280*, 26–29.

(108) Maltby, P. A.; Schlaf, M.; Steinbeck, M.; Lough, A. J.; Morris, R. H.; Klooster, W. T.; Koetzle, T. F.; Srivastava, R. C. *J. Am. Chem. Soc.* **1996**, *118*, 5396–5407.

(109) Jordan, R. F.; Norton, J. R. *J. Am. Chem. Soc.* **1982**, *104*, 1255–1263.

(110) Moore, E. J.; Sullivan, J. M.; Norton, J. R. *J. Am. Chem. Soc.* **1986**, *108*, 2257–2263.

(111) Edidin, R. T.; Sullivan, J. M.; Norton, J. R. *J. Am. Chem. Soc.* **1987**, *109*, 3945–3953.

(112) Kristjansdottir, S. S.; Moody, A. E.; Weberg, R. T.; Norton, J. R. *Organometallics* **1988**, *7*, 1983–1987.

(113) Weberg, R. T.; Norton, J. R. *J. Am. Chem. Soc.* **1990**, *112*, 1105–1108.

(114) Kristjansdottir, S. S.; Loendorf, A. J.; Norton, J. R. *Inorg. Chem.* **1991**, *30*, 4470–4471.

(115) Walker, H. W.; Pearson, R. G.*;* Ford, P. C. *J. Am. Chem. Soc.* **1983,** *105,* 1179–1186.

(116) Fong, T. P.; Lough, A. J.; Morris, R. H.; Mezzetti, A.; Rocchini, E.; Rigo, P. *J. Chem. Soc. Dalton Trans.* **1998**, 2111–2114.

(117) Nagaraja, C. M.; Nethaji, M.; Jagirdar, B. R. *Inorg. Chem.* **2005**, *44*, 4145–4147.

(118) Jia, G.; Lough, A. J.; Morris, R. H. *Organometallics* **1992**, *11*, 161–171.

(119) Chinn, M. S.; Heinekey, D. M. *J. Am. Chem. Soc.* **1987**, *109*, 5865–5867.

(120) Schlaf, M.; Lough, A. J.; Morris, R. H. *Organometallics* **1996**, *15*, 4423–4436.

(121) Lee, D.-H.; Patel, B. P.; Clot, E.; Eisenstein, O.; Crabtree, R. H. *Chem. Commun.* **1999**, 297–298.

(122) Adams, M. W. W. *Biochim. Biophys. Acta* **1990**, *1020*, 115–145.

(123) Albracht, S. P. J. *Biochim. Biophys. Acta* **1994**, *1188*, 167–204.

(124) Frey, M. *Structure and Bonding*, Springer-Verlag: Berlin, **1998**, *90*, 97–107.

(125) Kim, J.; Rees, D. C. *Biochemistry* **1994**, *33*, 389–397.

(126) MacKay, B. A.; Fryzuk, M. D. *Chem. Rev.* **2004**, *104*, 385–401.

(127) Przbyla, A. E.; Robbins, J.; Menon, N.; Peck, H. D. Jr. *FEMS Microbiol. Rev.* **1992**, *8*, 10913–10915.

(128) Garcin, E.; Vernede, X.; Hatchikian, E. C.; Volbeda, A.; Frey, M.; Fontecilla-Camps, J. C. *Structure* **1999**, *7*, 557–566.

(129) Teixeira, M.; Moura, I.; Xavier, A. V.; Huynh, B. H.; DerVartanian, D. V.; Peck, H. D. Jr.; LeGall, J.; Moura, J. J. G. *J. Biol. Chem.* **1985**, *260*, 8942–8950.

(130) Nicolet, Y.; Lemon, B. J.; Fontecilla-Camps, J. C.; Peters, J. W. *Trends Biochem. Sci.* **2000**, *25*, 138–143.

(131) Peters, J. W. *Curr. Opin. Struct. Biol.* **1999**, *9*, 670–676.

(132) Lyon, E. J.; Shima, S.; Buurman, G.; Chowdhuri, S.; Batschauer, A.; Steinbach, K.; Thauer, R. K. *Eur. J. Biochem.* **2004**, *271*, 195–204.

(133) Berkessel, A.; Thauer, R. K. *Angew. Chem. Int. Ed. Engl.* **1995**, *34*, 2247–2250.

(134) Thauer, R. K.; Klein, A. R.; Hartmann, G. C. *Chem. Rev.* **1996**, *96*, 3031–3042.

(135) Lyon, E. J.; Shima, S.; Boecher, R.; Thauer, R. K.; Grevels, F.-W.; Bill, E.; Roseboom, W.; Albracht, S. P. J. *J. Am. Chem. Soc.* **2004**, *126*, 14239–14248.

(136) Vignais, P. M.; Dimon, B.; Zorin, N. A.; Tomiyama, M.; Colbeau, A. *J. Bacteriol.* **2000**, *182*, 5997–6004.

(137) Bernhard, M.; Buhrke, T.; Bleijlevens, B.; De Lacey, A. L.; Fernandez, V. M.; Albracht, S. P. J.; Friedrich, B. *J. Biol. Chem.* **2001**, *276*, 15592–15597.

(138) Volbeda, A.; Charon, M.-H.; Piras, C.; Hatchikian, E. C.; Frey, M.; Fontecilla-Camps, J. C. *Nature* **1995**, *373*, 580–587.

(139) Volbeda, A.; Garcia, E.; Piras, C.; De Lacey, A. L.; Fernández, V. M.; Hatchikian, E. C.; Frey, M.; Fontecilla-Camps, J. C. *J. Am. Chem. Soc.* **1996**, *118*, 12989–12996.

(140) Higuchi, Y.; Yagi, T.; Yasuoka, N. *Structure* **1997**, *5*, 1671–1680.

(141) Higuchi, Y.; Ogata, H.; Miki, K.; Yasuoka, N.; Yagi, T. *Structure* **1999**, *7*, 549–556.

(142) Volbeda, A.; Montet, Y.; Vernede, X.; Hatchikian, E. C.; Fontecilla-Camps, J. C. *Int. J. Hydrogen Res.* **2002**, *27*, 1449–1461.

(143) Lamle, S. E.; Albracht, S. P. J.; Armstrong, F. A. *J.Am. Chem. Soc.* **2005**, *127*, 6595–6604.

(144) Volbeda, A.; Martin, L.; Cavazza, C.; Matho, M.; Faber, B. W.; Roseboom, W.; Albracht, S. P. J.; Garcin, E.; Rousset, M.; Fontecilla-Camps, J. C. *JBIC, J. Biol. Inorg. Chem.* **2005**, *10*, 239–249.

(145) Montet, Y.; Amara, P.; Volbeda, A.; Vernede, X.; Hatchikian, E. C.; Field, M. J.; Frey, M.; Fontecilla-Camps, J. C. *Nature Struct. Biol.* **1997**, *4*, 523–526.

(146) Albracht, S. P. *J. Biochem. Soc. Trans.* **1985**, *13*, 582–585.

(147) Fernandez, V. M.; Hatchikian, E. C.; Cammack, R. *Biochim. Biophys. Acta* **1985**, *832*, 69–79.

(148) Cammack, R.; Fernandez, V. M.; Schneider, K. *Biochimie* **1986**, *68*, 85–91.

(149) Fernandez, V. M.; Hatchikian, E. C.; Patil, D. S.; Cammack, R. *Biochim. Biophys. Acta* **1986**, *883*, 145–154.

(150) Maroney, M. J.; Pressler, M. A.; Mirza, S. A.; Whitehead, J. P.; Gurbiel, R. J.; Hoffman, B. M. In *Mechanistic Bioinorganic Chemistry*, Thorp, H. H.; Pecoraro, V. L. Eds. American Chemical Society, Washington, DC, 1995, 246, pp. 21–60.

(151) Dole, F.; Fournel, A.; Magro, V.; Hatchikian, E. C.; Bertrand, P.; Guigliarelli, B. *Biochemistry* **1997**, *36*, 7847–7854.

(152) Bleijlevens, B.; Faber, B. W.; Albracht, S. P. J. *J. Biol. Inorg. Chem.* **2001**, *6*, 763–769.

(153) Berlier, Y.; Fauque, G. D.; LeGall, J.; Choi, E. S.; Peck, H. D. Jr.; Lespinat, P. A. *Biochem. Biophys. Res. Commun.* **1987**, *146*, 147–153.

(154) Bagley, K. A.; Van Garderen, C. J.; Chen, M.; Duin, E. C.; Albracht, S. P. J.; Woodruff, W. H. *Biochemistry* **1994**, *33*, 9229–9236.

(155) Bagley, K. A.; Duin, E. C.; Roseboom, W.; Albracht, S. P. J.; Woodruff, W. H. *Biochemistry* **1995**, *34*, 5527–5535.

(156) van der Spek, T. M.; Aredsen, A. F.; Happe, R. P.; Yun, S.; Bagley, K. A.; Stufkens, D. J.; Hagen, W. R.; Albracht, S. P. J. *Eur. J. Biochem.* **1996**, *237*, 629–634.

(157) de Lacey, A. L.; Hatchikian, E. C.; Volbeda, A.; Frey, M.; Fontecilla-Camps, J. C.; Fernandez, V. M. *J. Am. Chem. Soc.* **1997**, *119*, 7181–7189.

(158) de Lacey, A. L.; Stadler, C.; Fernandez, V. M.; Hatchikian, E. C.; Fan, H.-J.; Li, S.; Hall, M. B. *J. Biol. Inorg. Chem.* **2002**, *7*, 318–326.

(159) Bleijlevens, B.; van Broekhuizen, F. A.; de Lacey, A. L.; Roseboom, W.; Fernandez, V. M.; Albracht, S. P. J. *J. Biol. Inorg. Chem.* **2004**, *9*, 743–752.

(160) Fan, H.-J.; Hall, M. B. *J. Am. Chem. Soc.* **2002**, *124*, 394–395.

(161) Ogata, H.; Mizoguchi, Y.; Mizuno, N.; Miki, K.; Adachi, S.-i.; Yasuoka, N.; Yagi, T.; Yamauchi, O.; Hirota, S.; Higuchi, Y. *J. Am. Chem. Soc.* **2002**, *124*, 11628–11635.

(162) Georgakaki, I. P.; Darensbourg, M. Y. In *Comprehensive Coordination Chemistry II*; McCleverty, J. A., Meyer, T. J., Eds.; Elsevier: New York, 2004; Vol. 8, pp 549–568.

(163) Liaw, W.-F.; Lee, J.-H.; Gau, H.-B.; Chen, C.-H.; Jung, S.-J.; Hung, C.-H.; Chen, W.-Y.; Hu, C.-H.; Lee, G.-H. *J. Am. Chem. Soc.* **2002**, *124*, 1680–1688.

(164) Lai, C.-H.; Lee, W.-Z.; Miller, M. L.; Reibenspies, J. H.; Darensbourg, D. J.; Darensbourg, M. Y. *J. Am. Chem. Soc.* **1998**, *120*, 10103–10114.

(165) Sellmann, D.; Geipel, F.; Moll, M. *Angew. Chem., Int. Ed.* **2000**, *39*, 561–563.

(166) Li, Z.; Ohki, Y.; Tatsumi, K. *J. Am. Chem. Soc.* **2005**, *127*, 8950–8951.

(167) Sellmann, D.; Lauderbach, F.; Geipel, F.; Heinemann, F. W.; Moll, M. *Angew. Chem. Int. Ed.* **2004**, *43*, 3141–3144.

(168) Sellmann, D.; Lauderbach, F.; Heinemann, F. W. *Eur. J. Inorg. Chem.* **2005**, 371–377.

(169) Peters, J. W.; Lanzilotta, W. N.; Lemon, B. J.; Seefedt, L. C. *Science* **1998**, *282*, 1853–1858.

(170) Lemon, B. J.; Peters, J. W. *Biochemistry* **1999**, *39*, 12969–12973.

(171) Nicolet, Y.; Piras, C.; Legrand, P.; Hatchikian, E. C.; Fontecilla–Camps, J. C. *Structure*, **1999**, *7*, 13–23.

(172) Nicolet, Y.; de Lacey, A. L.; Vernede, X.; Fernandez, V. M.; Hatchikian, E. C.; Fontecilla-Camps, J. C. *J. Am. Chem. Soc.* **2001**, *123*, 1596–1601.

(173) Nicolet, Y.; Cavazza, C.; Fontecilla-Camps, J. C. *J. Inorg. Biochem.* **2002**, *91*, 1–8.

(174) Pierik, A. T.; Hulstein, M.; Hagen, W. R.; Albracht, S. P. J. *Eur. J Biochem.* **1998**, *258*, 572–578.

(175) de Lacey, A. L.; Stadler, C.; Cavazza, C.; Hatchikian, E. C.; Fernandez, V. M. *J. Am. Chem. Soc.* **2000,** *122,* 11232–11233.

(176) Chen, Z.; Lemon, B. J.; Huang, S.; Swartz, D. J.; Peters, J. W.; Bagley, K. A. *Biochemistry* **2002**, *41*, 2036–2043.

(177) Adams, M. W. W.; Mortenson, L. E. *J. Biol. Chem.* **1984**, *259*, 7045–7055.

(178) Adams, M. W. W. *J. Biol. Chem.* **1987**, *262*, 15054–15061.

(179) Zambrano, I. C.; Kowal, A. T.; Mortenson, L. E.; Adams, M. W. W.; Johnson, M. K. *J. Biol. Chem.* **1989**, *264*, 20974–20983.

(180) Bennett, B.; Lemon, B. J.; Peters, J. W. *Biochemistry* **2000**, *39*, 7455–7560.

(181) Lyon, E. J.; Georgakaki, I. P.; Reibenspies, J. H.; Darensbourg, M. Y. *Angew. Chem., Int. Ed.* **1999**, *38*, 3178–3180.

(182) Le Cloirec, A.; Davies, S. C.; Evans, D. J.; Hughes, D. L.; Pickett, C. J.; Best, S. P.; Borg S. *Chem. Commun.* **1999**, 2285–2286.

(183) Schmidt, M.; Contakes, S. M.; Rauchfuss, T. B. *J. Am. Chem. Soc.* **1999**, *121*, 9736–9737.

(184) Li, H.; Rauchfuss, T. B. *J. Am. Chem. Soc.* **2002**, *124*, 726–727.

(185) Song, L.-C.; Yang, Z.-Y.; Bian, H.-Z.; Hu, Q.-M. *Organometallics* **2004**, *23*, 3082–3084.

(186) Popescu, C. V.; Muenck, E. *J. Am. Chem. Soc.* **1999**, *121*, 7877–7884.

(187) Razavet, M.; Davies, S. C.; Hughes, D. L.; Pickett, C. J. *Chem. Commun.* **2001**, 847–848.

(188) George, S. J.; Cui, Z.; Razavet, M.; Pickett, C. J. *Chem.--Eur. J.* **2002**, *8*, 4037–4046.

(189) Razavet, M.; Borg, S. J.; George, S. J.; Best, S. P.; Fairhurst, S. A.; Pickett, C. J. *Chem. Commun.* **2002**, 700–701.

(190) Razavet, M.; Davies, S. C.; Hughes, D. L.; Barclay, J. E.; Evans, D. J.; Fairhurst, S. A.; Liu, X.; Pickett, C. J. *Dalton Trans.* **2003**, 586–595.

(191) Yang, X.; Razavet, M.; Wang, X.-B.; Pickett, C. J.; Wang, L.-S. *J. Phys. Chem. A* **2003**, *107*, 4612–4618.

(192) Zampella, G.; Bruschi, M.; Fantucci, P.; Razavet, M.; Pickett, C. J.; De Gioia, L. *Chem.--Eur. J.* **2005**, *11*, 509–520.

(193) Tard, C.; Liu, X.; Ibrahim, S. K.; Bruschi, M.; De Gioia, L.; Davies, S. C.; Yang, X.; Wang, L.-S.; Sawers, G.; Pickett, C. J. *Nature* **2005**, *433*, 610–613.

(194) Chong, D.; Georgakaki, I. P.; Mejia-Rodriguez, R.; Sanabria-Chinchilla, J.; Soriaga, M. P.; Darensbourg, M. Y. *Dalton Trans.* **2003**, *21*, 4158–4163.

(195) Mejia-Rodriguez, R.; Chong, D.; Reibenspies, J. H.; Soriaga, M. P.; Darensbourg, M. Y. *J. Am. Chem. Soc.* **2004**, *126*, 12004–12014.

(196) Gloaguen, F.; Lawrence, J. D.; Rauchfuss, T. B.; Benard, M.; Rohmer, M.-M. *Inorg. Chem.* **2002**, *41*, 6573–6582.

(197) Ott, S.; Kritikos, M.; Äkermark, B.; Sun, L.; Lomoth, R. *Angew. Chem. Int. Ed. Engl.* **2004**, *43*, 1006–1009.

(198) Capon, J.-F.; Gloaguen, F.; Schollhammer, P.; Talarmin, J. *J. Electroanal. Chem.* **2004**, *566*, 241–247.

(199) Liu, T.; Wang, M.; Shi, Z.; Cui, H.; Dong, W.; Chen, J.; Akermark, B.; Sun, L. *Chem.--Eur. J.* **2004**, *10*, 4474–4479.

(200) Borg, S. J.; Behrsing, T.; Best, S. P.; Razavet, M.; Liu, X.; Pickett, C. J. *J. Am. Chem. Soc.* **2004**, *43*, 5635–5644.

(201) Tye, J. W.; Lee, J.; Wang, H.-W.; Mejia-Rodriguez, R.; Reibenspies, J. H.; Hall, M. B.; Darensbourg, M. Y. *Inorg. Chem.* **2005**, *44*, 5550–5552.

(202) Zhao, X.; Georgakaki, I. P.; Miller, M. L.; Yarbrough, J. C.; Darensbourg, M. Y. *J. Am. Chem. Soc.* **2001**, *123*, 9710–9711.

(203) Zhao, X.; Georgakaki, I. P.; Miller, M. L.; Mejia-Rodriguez, R.; Chiang, C.-Y.; Darensbourg, M. Y. *Inorg. Chem.* **2002**, *41*, 3917–3928.

(204) Tye, J. W.; Hall, M. B.; Georgakaki, I. P.; Darensbourg, M. Y. *Adv. Inorg. Chem.* **2004**, *56*, 1–26.

(205) Cao, Z.; Hall, M. B. *J. Am. Chem. Soc.* **2001**, *123*, 3734–3742.

(206) Fan, H.-J.; Hall, M. B. *J. Am. Chem. Soc.* **2001**, *123*, 3828–3829.

(207) Liu, Z.-P.; Hu, P. *J. Am. Chem. Soc.* **2002**, *124*, 5175–5182.

(208) Liu, Z.-P.; Hu, P. *J. Chem. Phys.* **2002**, *117*, 8177–8180.

(209) Bruschi, M.; Fantucci, P.; De Gioia, L. *Inorg. Chem.* **2002**, *41*, 1421–1429.

(210) Bruschi, M.; Fantucci, P.; De Gioia, L. *Inorg. Chem.* **2003**, *42*, 4773–4781.

(211) Zhou, T.; Mo, Y.; Liu, A.; Zhou, Z.; Tsai, K. R. *Inorg. Chem.* **2004**, *43*, 923–930.

(212) Zhou, T.; Mo, Y.; Zhou, Z.; Tsai, K. *Inorg. Chem.* **2005**, *44*, 4941–4946.

(213) Schrödinger, E. *Ann. Physik.* **1926**, *79*, 361–365.

(214) Born, M.; Oppenheimer, R. *Ann. Physik.* **1927**, *84*, 457–484.

(215) Pauli, W. Jr. *Z. Physik* **1925**, *31*, 765–783.

(216) Hartree, D. R. *Proc. Cambridge Phil. Soc.* **1928**, *24*, 89–110.

(217) Hartree, D. R. Proc. *Cambridge Phil. Soc.* **1928**, *24*, 111–132.

(218) Hartree, D. R. Proc. *Cambridge Phil. Soc.* **1928**, *24*, 426–437.

(219) Fock, V. *Z. Physik* **1930**, *62*, 795–805.

(220) Slater, J. C. *Phys. Rev.* **1929**, *34*, 1293–1323.

(221) Slater, J. C. *Phys. Rev.* **1930**, *35*, 509–529.

(222) Slater, J. C. *Phys. Rev.* **1930**, *36*, 57–64.

(223) Boys, S. F. *Proc. Roy. Soc.* **1950**, *A200*, 542–554.

(224) Davidson, E. R.; Feller, D. *Chem. Rev.* **1986**, *86*, 681–696.

(225) Hehre, W. J.; Stewart, R. F.; Pople, J. A. *J. Chem. Phys.* **1969**, *51*, 2657–2664.

(226) Clementi, E. *IBM J. Res. Develop.* **1965**, *9*, 2–19.

(227) Boys, S. F. *Proc. Roy. Soc.* **1950**, *A201*, 125–37.

(228) Langhoff, S. R.; Davison, E. R. *Int. J. Quantum Chem.* **1974**, *8*, 61–72.

(229) Møller, C.; Plesset, M. S. *Phys. Rev.* **1934**, *46*, 618–622.

(230) Knowles, P. J.; Somasundram, K.; Handy, N. C.; Hirao, K. *Chem. Phys. Lett.* **1985**, *113*, 8–12.

(231) Christiansen, O.; Olsen, J.; Jorgensen, P.l; Koch, H.; Malmqvist, P.-A. Chem. *Phys. Lett.* **1996**, *261*, 369–378.

(232) Hohenberg, P.; Kohn, W. *Phys. Rev.* **1964**, *136*, B864–B871.

(233) Kohn, W.; Sham, L. J. *Phys. Rev.* **1965**, *140*, A1133–A1138.

(234) Curtiss, L. A.; Raghavachari, K.; Redfern, P. C.; Pople, J. A. *J. Chem. Phys.* **2000**, *112*, 7374–7383.

(235) Becke, A. D. *J. Chem. Phys.* **1993**, *98*, 5648–5652.

(236) Lee, C.; Yang, W.; Parr, R. G. *Phys. Rev.* **1988**, *37*, 785–789.

(237) Cammack, R.; Frey, M.; Robson, R. *Hydrogen as a Fuel*; Taylor and Francis: London, 2001.

(238) Lee, S.; Holm, R. H. *Proc. Nat. Acad. Sci. USA* **2003**, *100*, 3595–3600.

(239) Yagi, T. J. *Biochemistry* **1970**, *68*, 649–657.

(240) Krasna, A. I.; Rittenberg, D. *J. Am. Chem. Soc.* **1954**, *76*, 3015–3020.

(241) Adams, M. W. W.; Mortenson, L. E.; Chen, J.-S. *Biochim. Biophys. Acta* **1981**, *594*, 105–176.

(242) Farkas, A.; Farkas, L.; Yudkin, J. *Proc. Roy. Soc.* **1934**, *B115*, 373-379.

(243) Waschtershauser, G. *Science* **2000**, *289*, 1307–1308.

(244) Lemon, B. J.; Peters, J. W. *J. Am. Chem. Soc.* **2000**, *122*, 3793–3794.

(245) Hieber, W.; Spacu, P. Z. *Anorg. Allg. Chem.* **1937**, *233*, 852–864.

(246) Fauvel, K.; Mathieu, R.; Poilblanc, R. *Inorg. Chem.* **1976**, *15*, 976–978.

(247) Treichel, P. M.; Rublein, E. K. *J. Organomet. Chem.* **1989**, *359*, 195–203.

(248) Seyferth, D.; Womack, G. B.; Gallagher, M. K.; Cowie, M.; Hames, B. W.; Fackler, J. P. Jr.; Mazany, A. M. *Organometallics* **1987**, *6*, 283–294.

(249) Georgakaki, I. P.; Miller, M. L.; Darensbourg, M. Y. *Inorg. Chem.* **2003**, *42*, 2489–2494.

(250) Dance, I. *Chem. Comm.* **1999**, *17*, 1655–1656.

(251) Zhao, X.; Chiang, C.-Y.; Miller, M. L.; Rampersad, M. V.; Darensbourg, M. Y. *J. Am. Chem. Soc.* **2003**, *125*, 518–524.

(252) Frisch, M. J.; Trucks, G. W.; Schlegel, H. B.; Scuseria, G. E.; Robb, M. A.; Cheeseman, J. R.; Zakrzewski, V. G.; Montgomery, J. A.; Stratmann, R. E.; Burant, J. C.; Dapprich, S.; Millam, J. M.; Daniels, A. D.; Kudin, K. N.; Strain, M. C.; Farkas, O.; Tomasi, J.; Barone, V.; Cossi, M.; Cammi, R.; Mennucci, B.; Pomelli, C.; Adamo, C.; Clifford, S.; Ochterski, J.; Petersson, G. A.; Ayala, P. Y.; Cui, Q.; Morokuma, K.; Malick, D. K.; Rabuck, A. D.; Raghavachari, K.; Foresman, J. B.; Cioslowski, J.; Ortiz, J. V.; Stefanov, B. B.; Liu, G.; Liashenko, A.; Piskorz, P.; Komaromi, I.; Gomperts, R.; Martin, R. L.; Fox, D. J.; Keith, T.; Al-Laham, M. A.; Peng, C. Y.; Nanayakkara, A.; Gonzalez, C.; Challacombe, M.; Gill, P. M. W.; Johnson, B.; Chen, W.; Wong, M. W.; Andres, J. L.;

Gonzalez, A. C.; Head-Gordon, M.; Replogle, E. S.; Pople, J. A. *Gaussian 98*, revision A.11; Gaussian, Inc.: Pittsburgh, PA, 2002.

(253) Hay, P. J.; Wadt, W. R. *J. Chem. Phys.* **1985**, *82*, 284–298.

(254) Hay, P. J.; Wadt, W. R. *J. Chem. Phys.* **1985**, *82*, 270–283.

(255) Couty, M.; Hall, M. B. *J. Comp. Chem.* **1996**, *17*, 1359–1370.

(256) Hoellwarth, A.; Boehme, M.; Dapprich, S.; Ehlers, A. W.; Gobbi, A.; Jonas, V.; Koehler, K. F.; Stegmann, R.; Veldkamp, A.; Frenking, G. *Chem. Phys. Lett.* **1993**, *208*, 237–240.

(257) Dunning, T. H. Jr. *J. Chem. Phys.* **1989**, *90*, 1007–1023.

(258) Dunning, T. H. Jr. *J. Chem. Phys.* **1970**, *53*, 2823–2833.

(259) Dunning, T. H.; Hay, P. J. In *Modern Theoretical Chemistry*, Schaefer, H. F., Ed.; Plenum Press: New York, 1977; Vol. 3, pp 1–27.

(260) London, F. *J. Phys. Radium* **1937**, *8*, 397–409.

(261) Ditchfield, R. *Mol. Phys.* **1974**, *27*, 789–807.

(262) Wolinski, K.; Hinton, J. F.; Pulay, P. *J. Am. Chem. Soc.* **1990**, *112*, 8251–8260.

(263) Lawrence, J. D.; Li, H.; Rauchfuss, T. B.; Benard, M.; Rohmer, M.-M. *Angew. Chem., Int. Ed.* **2001**, *40*, 1768–1771.

(264) Liaw, W.-F.; Tsai, W.-T.; Gau, H.-B.; Lee, C.-M.; Chou, S.-Y.; Chen, W.-Y.; Lee, G.-H. *Inorg. Chem.* **2003**, *42*, 2783–2788.

(265) Darensbourg, M. Y.; Lyon, E. J.; Zhao, X.; Georgakaki, I. P. *Proc. Nat. Acad. Sci. USA* **2003**, *100*, 3683–3688.

(266) Landau, S. E.; Morris, R. H.; Lough, A. J. *Inorg. Chem.* **1999**, *38*, 6060–6068.

(267) Drew, D.; Darensbourg, D. J.; Darensbourg, M. Y. *Inorg. Chem.* **1975**, *14*, 1579–1584.

(268) Hieber, W.; Spacu, P. Z. *Anorg. Allg. Chem.* **1937**, *233*, 852–864.

(269) Dunning, T. H., Jr.; Hay P. J. in H.F. Schaefer III (Ed.) *Methods of Electronic Structure Theory*, Vol. 3, Plenum Press: New York, 1977.

(270) Nakamoto, K. *IR and Raman Spectra of Inorganic and Coordination Compounds*, 5th ed.; Wiley-Interscience: New York, **1997**; Parts A and B.

(271) Momenteau, M.; Reed, C. A. *Chem. Rev.* **1994**, *94*, 659–698.

(272) Lukin, J. A.; Ho, C. *Chem. Rev.* **2004**, *104*, 1219–1230.

(273) Tamagnini, P.; Axelsson, R.; Lindberg, P.; Oxelfelt, F.; Wunschiers, R.; Lindblad, P. *Microbio. Mol. Biol. Rev.* **2002**, *66*, 1–20.

(274) Pereira, A. S.; Tavares P.; Moura, I.; Moura J. J. G.; Huynh B. H. *J. Am. Chem. Soc.* **2001**, *123*, 2771–2782.

(275) Frisch, M. J.; Trucks, G. W.; Schlegel, H. B.; Scuseria, G. E.; Robb, M. A.; Cheeseman, J. R.; Montgomery, Jr., J. A.; Vreven, T.; Kudin, K. N.; Burant, J. C.; Millam, J. M.; Iyengar, S. S.; Tomasi, J.; Barone, V.; Mennucci, B.; Cossi, M.; Scalmani, G.; Rega, N.; Petersson, G. A.; Nakatsuji, H.; Hada, M.; Ehara, M.; Toyota, K.; Fukuda, R.; Hasegawa, J.; Ishida, M.; Nakajima, T.; Honda, Y.; Kitao, O.; Nakai, H.; Klene, M.; Li, X.; Knox, J. E.; Hratchian, H. P.; Cross, J. B.; Bakken, V.; Adamo, C.; Jaramillo, J.; Gomperts, R.; Stratmann, R. E.;

Yazyev, O.; Austin, A. J.; Cammi, R.; Pomelli, C.; Ochterski, J. W.; Ayala, P. Y.; Morokuma, K.; Voth, G. A.; Salvador, P.; Dannenberg, J. J.; Zakrzewski, V. G.; Dapprich, S.; Daniels, A. D.; Strain, M. C.; Farkas, O.; Malick, D. K.; Rabuck, A. D.; Raghavachari, K.; Foresman, J. B.; Ortiz, J. V.; Cui, Q.; Baboul, A. G.; Clifford, S.; Cioslowski, J.; Stefanov, B. B.; Liu, G.; Liashenko, A.; Piskorz, P.; Komaromi, I.; Martin, R. L.; Fox, D. J.; Keith, T.; Al-Laham, M. A.; Peng, C. Y.; Nanayakkara, A.; Challacombe, M.; Gill, P. M. W.; Johnson, B.; Chen, W.; Wong, M. W.; Gonzalez, C.; Pople, J. A. *Gaussian 03*, Revision B.05; Gaussian, Inc.: Wallingford CT, 2004.

(276) Ehlers, A. W.; Böhme, M.; Dapprich, S.; Gobbi, A.; Höllwarth, A.; Jonas, V.; Köhler, K. F.; Stegmann, R.; Veldkamp, A.; Veldkamp, A.; Frenking, G. *Chem. Phys. Lett.* **1993**, *208*, 111–114.

(277) Hariharan, P. C.; Pople, J. A. *Theor. Chim. Acta* **1973**, *28*, 213–222.

(278) Petersson, G. A.; Bennett, A.; Tensfeldt, T. G.; Al-Laham, M. A.; Shirley, W. A.; Mantzaris, J. *J. Chem. Phys.* **1988**, *89*, 2193–2218.

(279) Petersson, G. A.; Al-Laham, M. A. *J. Chem. Phys.* **1991**, *94*, 6081–6090.

(280) Hehre, W.J.; Ditchfield, R. Pople, J.A. *J. Chem. Phys.* **1972**, *56*, 2257–2261.

(281) Wong, M. W.; Wiberg, K. B.; Frisch, M. *J. Chem. Phys*. **1991**, *95*, 8991–8998.

(282) Wong, M. W.; Frisch, M. J.; Wiberg, K. *J. Am. Chem. Soc.* **1991**, *113*, 4776–4782.

(283) Wong, M. W.; Wiberg, K. B.; Frisch, M. J. *J. Am. Chem. Soc.* **1992**, *114*, 523–529.

(284) Wong, M. W.; Wiberg, K. B.; Frisch, M. J. *J. Am. Chem. Soc.* **1992**, *114*, 1645–1652.

(285) Onsager, L. *J. Am. Chem. Soc.* **1936**, *58*, 1486–1493.

(286) Kirkwood, J. G. *J. Chem. Phys.* **1934**, *2*, 351–361.

(287) Gloaguen, F.; Lawrence, J. D.; Schmidt, M.; Wilson, S. R.; Rauchfuss, T. B. *J. Am. Chem. Soc.* **2001**, *123*, 12518–12527.

(288) Hasan, M. M.; Hursthouse, M. B.; Kabir, S. E.; Malik, K. M. A. *Polyhedron* **2001**, *20*, 97–101.

(289) Pople, J. A.; Scott, A. P.; Wong, M. W.; Radom, L. *Israel J. Chem.* **1993**, *33*, 345–350.

(290) Fast, P. L.; Corchado, J.; Sánchez, M. L.; Truhlar, D. G. *J. Phys. Chem. A* **1999**, *103*, 3139–3143.

(291) Zhao, Y.; Lynch, B. J.; Truhlar D. G. *J. Phys. Chem. A* **2004**, *108*, 4786–4791.

(292) Lide, D. R., Ed. *CRC Handbook of Chemistry and Physics, Internet Version2005*, <http://www.hbcpnetbase.com>; CRC Press: Boca Raton, FL, 2005.

(293) Boyke, C. A.; Rauchfuss, T. B.; Wilson, S. R.; Rohmer, M.-M.; Benard, M. *J. Am. Chem. Soc.* **2004**, *126*, 15151–15160.

(294) Borg, S. J.; Behrsing, T.; Best, S. P.; Razavet, M.; Liu, X.; Pickett C. J. *J. Am. Chem. Soc.* **2004**, *126*, 16988–16999.

(295) Darchen, A.; Mousser, H.; Patin, H. *Chem. Commun.* **1988**, 968–970.

(296) Fiedler, A. T.; Brunold, T. C. *Inorg. Chem.* **2005**, *44*, 9322–9334.

(297) Lamle, S. E.; Vincent, K. A.; Halliwell, L. M.; Albracht, S. P. J.; Armstrong, F. A. D*alton Trans*. **2003**, 4152–4157.

(298) Bruschi, M.; Fantucci, P.; De Gioia, L. *Inorg. Chem*. **2004**, *43*, 3733–3741.

(299) Arduengo III, A. J.; Dias, H. V. R.; Harlow, R. L.; Kline, M. J. Am. Chem. Soc. 1992, 114, 5530–5534.

(300) *SMART 1000 CCD*; Bruker Analytical X-ray Systems: Madison, WI, 1999.

(301) SAINT-Plus, version 6.02; Bruker: Madison, WI, 1999.

(302) Sheldrick, G. *SHELXS-97*: *Program for Crystal Structure Solution*; Institüt für Anorganische Chemie der Universität: Gottingen, Germany, 1986.

(303) Sheldrick, G. *SHELXS-97*: *Program for Crystal Structure Solution*; Institüt für Anorganische Chemie der Universität: Gottingen, Germany, 1977.

(304) *SHELXTL*, version 5.1 or later; Bruker; Madison, WI, 1998.

(305) Frisch, M. J.; Trucks, G. W.; Schlegel, H. B.; Scuseria, G. E.; Robb, M. A.; Cheeseman, J. R.; Montgomery, Jr., J. A.; Vreven, T.; Kudin, K. N.; Burant, J. C.; Millam, J. M.; Iyengar, S. S.; Tomasi, J.; Barone, V.; Mennucci, B.; Cossi, M.; Scalmani, G.; Rega, N.; Petersson, G. A.; Nakatsuji, H.; Hada, M.; Ehara, M.; Toyota, K.; Fukuda, R.; Hasegawa, J.; Ishida, M.; Nakajima, T.; Honda, Y.; Kitao, O.; Nakai, H.; Klene, M.; Li, X.; Knox, J. E.; Hratchian, H. P.; Cross, J. B.; Bakken, V.; Adamo, C.; Jaramillo, J.; Gomperts, R.; Stratmann, R. E.;

Yazyev, O.; Austin, A. J.; Cammi, R.; Pomelli, C.; Ochterski, J. W.; Ayala, P. Y.; Morokuma, K.; Voth, G. A.; Salvador, P.; Dannenberg, J. J.; Zakrzewski, V. G.; Dapprich, S.; Daniels, A. D.; Strain, M. C.; Farkas, O.; Malick, D. K.; Rabuck, A. D.; Raghavachari, K.; Foresman, J. B.; Ortiz, J. V.; Cui, Q.; Baboul, A. G.; Clifford, S.; Cioslowski, J.; Stefanov, B. B.; Liu, G.; Liashenko, A.; Piskorz, P.; Komaromi, I.; Martin, R. L.; Fox, D. J.; Keith, T.; Al-Laham, M. A.; Peng, C. Y.; Nanayakkara, A.; Challacombe, M.; Gill, P. M. W.; Johnson, B.; Chen, W.; Wong, M. W.; Gonzalez, C.; and Pople, J. A.; *Gaussian 03*, Revision B.04; Gaussian, Inc., Wallingford CT, 2004.

(306) Patterson, E. V.; Cramer, C. J.; Truhlar, D. G. *J. Am. Chem. Soc.* **2001**, *123*, 2025–2031.

(307) Baik, M.-H.; Ziegler, T.; Schauer, C. K. *J. Am. Chem. Soc.* **2000**, *122*, 9143–9154.

(308) Gorodetsky, B.; Ramnial, T.; Branda, N. R.; Clyburne, J. A. C. *Chem. Commun.* **2004**, 1972–1973.

(309) Capon, J.-F.; El Hassnaoui, S.; Gloaguen, F.; Schollhammer, P.; Talarmin J. *Organometallics* **2005,** *24,* 2020–2022.

(310) Collman, J. P.; Ha, Y.; P. S. Wagenknecht, P. S.; M. A. Lopez, M. A.; R. Guilard, R. *J. Am. Chem. Soc*. **1993**, *115*, 9080–9088.

(311) Teixeira, M.; Moura, I.; Xavier, A. V.; Moura, J. J. G.; LeGall, J.; DerVartanian, D. V.; Peck, H. D., Jr.; Huynh B. H. *J. Biol. Chem*. **1989**, *264*, 16435–16450.

(312) Volbeda, A.; Fontecilla-Camps, J. C. *Dalton Trans.* **2003**, 4030– 4038.

(313) Mertens, R.; Liese, A. *Curr. Opin. Biotechnol.* **2004**, *15*, 343–348.

(314) Butt, J. N.; Filipiak, M.; Hagen, W. R. *Euro. J. Biochem.* **1997**, *245*, 116–122.

(315) Lyon, E. J.; Georgakaki, I. P.; Reibenspies, J. H.; Darensbourg, M. Y. *J. Am. Chem. Soc.* **2001**, *123*, 3268–3278.

(316) Georgakaki, I. P.; Thomson, L. M.; Lyon, E. J.; Hall, M. B.; Darensbourg M. Y. *Coord. Chem. Rev.* **2003**, *238–239*, 255–266.

(317) Fiedler, A. T.; Brunold, T. C. *Inorg. Chem.* **2005**, *44*, 1794–1809.

(318) Frisch, M. J.; Trucks, G. W.; Schlegel, H. B.; Scuseria, G. E.; Robb, M. A.; Cheeseman, J. R.; Montgomery, Jr., J. A.; Vreven, T.; Kudin, K. N.; Burant, J. C.; Millam, J. M.; Iyengar, S. S.; Tomasi, J.; Barone, V.; Mennucci, B.; Cossi, M.; Scalmani, G.; Rega, N.; Petersson, G. A.; Nakatsuji, H.; Hada, M.; Ehara, M.; Toyota, K.; Fukuda, R.; Hasegawa, J.; Ishida, M.; Nakajima, T.; Honda, Y.; Kitao, O.; Nakai, H.; Klene, M.; Li, X.; Knox, J. E.; Hratchian, H. P.; Cross, J. B.; Bakken, V.; Adamo, C.; Jaramillo, J.; Gomperts, R.; Stratmann, R. E.; Yazyev, O.; Austin, A. J.; Cammi, R.; Pomelli, C.; Ochterski, J. W.; Ayala, P. Y.; Morokuma, K.; Voth, G. A.; Salvador, P.; Dannenberg, J. J.; Zakrzewski, V. G.; Dapprich, S.; Daniels, A. D.; Strain, M. C.; Farkas, O.; Malick, D. K.; Rabuck, A. D.; Raghavachari, K.; Foresman, J. B.; Ortiz, J. V.; Cui, Q.; Baboul, A. G.; Clifford, S.; Cioslowski, J.; Stefanov, B. B.; Liu, G.; Liashenko, A.; Piskorz, P.; Komaromi, I.; Martin, R. L.; Fox, D. J.; Keith, T.; Al-Laham, M. A.;

Peng, C. Y.; Nanayakkara, A.; Challacombe, M.; Gill, P. M. W.; Johnson, B.; Chen, W.; Wong, M. W.; Gonzalez, C.; and Pople, J. A.; Gaussian 03, Revision B.05; Gaussian, Inc., Wallingford CT, 2004.

(319) Lowry, T. H.; Richardson, K. S. *Mechanism and Theory in Organic Chemistry*, 3rd ed.; Harper & Row: New York, 1987.

(320) Salyi, S.; Kritikos, M.; Åkermark, B.; Sun, L. *Chem.--Eur. J.* **2003**, *9*, 557–560.

(321) Lawrence, J. D.; Li, H.; Rauchfuss, T. B. *Chem. Commun.* **2001**, 1482–1483.

(322) Jones, A. K.; Sillery, E.; Albracht, S. P. J.; Armstrong, F. A. *Chem. Commun.* **2002**, 866-867.

(323) Vincent, K. A.; Cracknell, J. A.; Lenz, O.; Zebger, I.; Friedrich, B.; Armstrong, F. A. *Proc. Natl. Acad. Sci. U. S. A.* **2005**, *102*, 16951-16954.

VITA

Jesse Wayne Tye graduated from the University of Kentucky in May 2001 with a B. S. degree in chemistry. He moved to Texas A&M University in August 2001 and worked under the direction of Professors Michael B. Hall and Marcetta Y. Darensbourg. He graduated with a Ph.D. in chemistry in May 2006, and accepted a postdoctoral position with Professor John F. Hartwig at the University of Illinois Urbana-Champaign. The author can be contacted at Dr. Jesse W. Tye (c/o Dr. Michael B. Hall or Dr. Marcetta Y. Darensbourg), Department of Chemistry, Texas A&M University, PO Box 30012, College Station, TX 77842-3012.